352

# CAPACITOR COMMUTATED CONVERTERS (CCC) HVDC INTERCONNECTIONS

## Digital modeling and Benchmark circuit

**Working Group**
**B4.34**

**June 2008**

# CIGRE WG B4.34

# Capacitor commutated converters (CCC) HVDC interconnections

# Digital modeling and benchmark circuit

**WG Members:**
Azevedo, R.M. (BR), Secretary
Campos Barros, J.G. (BR), (Convener)
Carvalho, A.R. (BR)
Brandt, D. (CA)
Espírito Santo, S. (BR)
Gomes Jr. S. (BR)
Kuisti, H. (FI)
Lírio, F. L. (BR)
Macedo, N.J.P. (BR)
Menzies, D. (SE)
Pahalawaththa, N.(NZ)
Peixoto, C.A.O. (BR)
Ping, W. W. (BR)
Sarcinelli Luz, G. (BR)



**ISBN: 978- 2- 85873- 038-4**

INDEX

1 INTRODUCTION....3

2 SCOPE....6

2.1 Main topics....6

2.2 Studies performed by WG B4-34 and included in this report....6

3 GENERAL CHARACTERISTICS OF CONVERTER INSTALLATIONS WITH COMMUTATION CAPACITORS....8

3.1 Definition and basic characteristics of CCC converters....8

3.2 General control characteristics....17

3.3 Criterion for reactive power exchange at converters AC buses....20

3.4 Modeling Characteristics of Converters with Commutation Capacitors, for Steady-State and for Electromechanical Stability....20

3.5 Steady-State Performance....22

3.6 Dynamic performance....26

3.6.1 Tests on the CCC Control Systems....27

4 THE PROPOSAL OF A BENCHMARK....37

4.1 Premises for obtaining the benchmark model....37

4.2 Systems connected to the AC buses of Converter Stations....38

4.2.1 Equivalent AC Networks....38

4.2.2 Simplified AC Networks....47

4.2.3 Short-circuit Ratios....48

4.3 Modeling in the Programs PSCAD/EMTDC and ATP....49

5 CONCLUSIONS....51

6 BIBLIOGRAPHICAL REFERENCES....54

ANNEX A - SPECIFIC CONSIDERATIONS FOR DEFINING THE MAIN CHARACTERISTICS OF MAJOR EQUIPMENT IN THE PRINCIPAL CIRCUIT OF CCC CONVERTERS....56

ANNEX B - CCC INSTALLATIONS IN COMMERCIAL OPERATION....60

ANNEX C - PSCAD/EMTDC BENCHMARK MODEL....64

ANNEX D - VALIDATION OF THE CCC LINK MODEL – COMPARISON OF SIMULATIONS ON ATP x PSCAD....89

ANNEX E - CONSIDERATIONS ON THE IMPACT OF THE TRANSFORMER SATURATION CHARACTERISTICS UPON THE POST-FAULT RECOVERIES....112

ANNEX F - ATP CASES: COMPARISON OF LINK PERFORMANCE AND MODELING WITH AND WITHOUT DC FILTERS....122

ANNEX G - ELECTROMECHANICAL STABILITY STUDIES....135

ANNEX H – DATA USED FOR ELECTROMECHANICAL STABILITY STUDIES....170

ACRONYMS

| |
|---|
| ALFA, ALFA DASH - firing angle (α), firing margin (α') |
| ANAFAS – Fault Analisys Program |
| ANAREDE – Power Flow Analisys Program |
| ANATEM – Transient Stability and Dinamic Analisys Program |
| ATP – Alternative Transients Program |
| BM – Benchmark |
| CCA – Current Control Amplifier |
| CCC – Capacitor Commuted Converters |
| GAMMA, GAMMA DASH - extinction angle (γ), commutation margin (γ') |
| Graetz Bridge – 6-pulse thyristor valves for conversion from AC to DC or vice versa |
| GTO – Gate Turnoff Thyristor |
| HVDC – High Voltage Direct Current |
| IGBT – Insulated Gate Bipolar Transistor |
| MTDC – Multi-terminal DC System |
| μ – Overlap (commutation) angle |
| PLL – Phase Locked Loop |
| PSCAD/EMTDC - Power Systems Computer Aided Design / ElectroMagnetic Transients including DC |
| SCR, ESCR - Short-Circuit Ratio, Effective Short-Circuit Ratio |
| SEPOPE – Electrical Power Systems Planning and Operation Symposium (Brazil) |
| VCO - Voltage Controlled Oscillator |
| VDCOL - Voltage Dependent Current Order Limiter |
| VSC - Voltage Source Converters |
| Statcom - Static Synchronous Compensator |

**ANAREDE – POWER FLOW ANALISYS**

ANAREDE is a tool for analysis and simulation of power system featuring power flow analysis, static network equivalent, contingency analysis, voltage stability and voltage sensibility analysis. Other tools added recently includes PxQ capability diagram, voltage control via capacitor / reactor switching, algorithm for identification of voltage control conflicts within the input data and tools to help restoration studies. Its usability is enhanced by a graphical interface that includes one-line diagram. ANAREDE is largely used by power utilities, the Brazilian system operator, and the company responsible for system planning. Over the last two decades its algorithms have proven to be extremely efficient and reliable.

**ANATEM – TRANSIENT STABILITY & DINAMIC ANALISYS**

ANATEM is an advanced simulation tool for power system transient stability and dynamic analysis. It is able to model all relevant equipment in the power system for electromechanical stability assessment, such as synchronous generators, AVRs, speed governors, inductor motors, HVDC links (including CCC-type), FACTS devices, OLTC, protective relays, etc. Its user defined control (CDU) feature is of an unique flexibility allowing the representation of controllers of any topology associated with any power system equipment. The recent development of the most prevalent types of wind generators met the urgent needs of the Brazilian electrical power sector related to grid performance studies involving new wind power projects (wind penetration studies).The initial operating conditions are read from a file produced by the ANAREDE power flow program. There are some auxiliary programs for pre and pos-processing, such as PlotCepel for graphical visualization of the results. ANATEM is currently the reference program for stability simulations in most Brazilian power utilities, the Brazilian system operator and the company responsible for system planning.

CEPEL Contact:
Phone: +55-21-2598-6100
Email: anarede@cepel.br ; anatem@cepel.br
www.cepel.br/anarede ; www.cepel.br/anatem

# 1 INTRODUCTION

HVDC transmission based on Graetz bridges with conventional thyristors, although efficient, reliable and economical, requires a considerable expense for filters on the AC side. It also presents, at the inverter terminal, some sensitivity to those faults which produce voltage magnitude reduction, or abrupt changes in the voltage phase angles on the AC side – especially in receiving systems with low short-circuit ratio (SCR). Such events often lead to commutation failures resulting, in most cases, in transitory voltage loss for a maximum duration of tens of milliseconds, similarly to what happens upon the occurrence of scintillation or flicker. In a few rare cases, they may lead even to energy interchange interruption. In both instances, provided the problem is not associated to a permanent fault, recovery is automatic and fast. Nevertheless, in order to minimize the most significant events, the designer is forced, in many cases and at the cost of a less favorable power factor at the station bus, to oversize the converter transformers, so as to permit a permanent operation with higher extinction angles.

In theory, the replacement of natural by forced commutation would eliminate the problem of commutation failures while allowing, at the same time, the operation as an inverter even if the receiving bus were entirely passive (without voltage sources, either local or remote). In this respect, during the last 20 plus years a great effort was employed to develop new devices (GTO's, IGBT's etc.) capable to apply grid control and to suppress conduction current even when the device is positively polarized. Voltage Source Converters (VSC) using such devices have been applied and are working satisfactorily in several HVDC and Statcom applications. Of course, the higher investment and operation costs limit the number of applications with economic convenience.

The search for means to improve the economic convenience and the operational safety of conventional thyristor converters led to the discussion of arrangements considering the inclusion of series capacitors in HVDC systems, either inside the commutation circuit, or in series with the AC systems or lines which feed the converters. Figure 1.1, below, presents three configurations studied and mentioned in the literature.

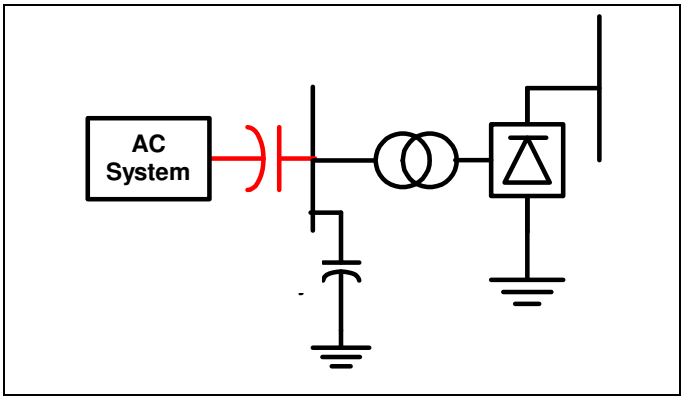


Configuration (a)

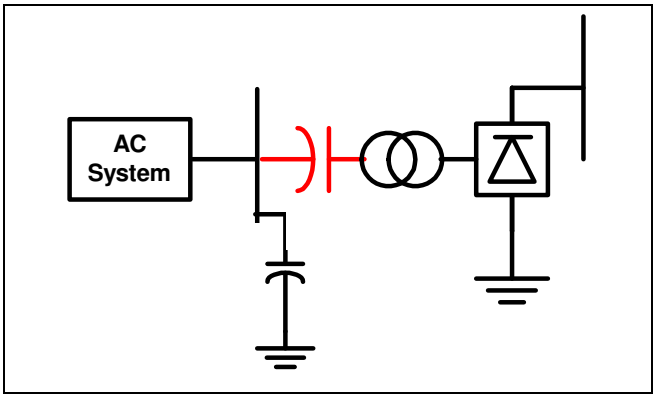


Configuration (b)

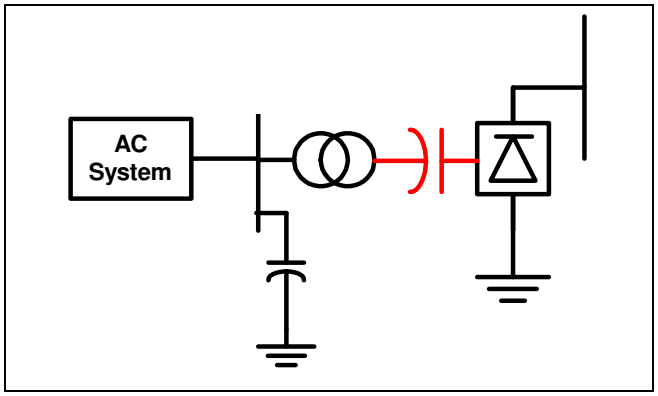


Configuration (c)

Figure 1.1 - Series Capacitors in HVDC converter stations. Only in configurations (b) and (c) is the series capacitor included in the commutation circuit.

In configuration (a), the series capacitor is located on the AC line side, similarly to conventional series compensation. In this case, the capacitor is not included in the commutation circuit and, therefore, it does not influence the internal operation of the converter station. This kind of arrangement is entirely conventional as far as converter stations and HVDC interconnections are concerned.

In the next two arrangements, the series capacitor is inserted into the commutation circuit and, consequently, it affects the internal operation of the converter station. The capacitor is placed between the converter transformer and the commutation bus in configuration (b), while in (c) it is placed between the transformer and the Graetz bridge. Among these options, the most widely accepted up to now is that shown in Figure 1.1 (c), with the series capacitor located between the converter transformer and the valves.

Therefore, it is the configuration (c), having the capacitor between the transformer and the valves, that will be studied in this work. It has become widely known as CCC, an acronym that will be adopted in this work, since it is adequate both in English and in Portuguese (“Capacitor Commutated Converter” or “Conversor com Capacitor de Comutação”). The system proposed in Chapter 4 as a benchmark has been adapted to this arrangement.

The number of installations with CCC arrangement in commercial operation is still small and, therefore, their features are relatively little known. The largest converter plant having such an arrangement – Garabi, located at the Brazil-Argentina border – has two Back-to-Back converters, and operates integrated into the Basic Network of the Brazilian Southern System. For this reason, CIGRÉ Brazilian National Committee decided, through its Study Committee B4, to constitute Working Group B4-34, in order to prepare a report presenting the state of the art in digital studies of HVDC connections with CCC converters; if possible, it should also propose a benchmark circuit, which may serve as a simplified guide of application / specification for converter stations using that arrangement. As the first outcome of the work of WG B4-34, the article "Series Capacitor Commutated (CCC) HVDC Converter Stations: Benchmark for Digital Simulation Studies" was presented at the IX SEPOPE, held in May 2004, in Rio de Janeiro, under FURNAS coordination.

Before dealing particularly with the proposed equivalent networks, some specific comments on the characteristics, advantages and disadvantages of the configurations shown in Figure 1.1 should be given; also, it should be noted that, in either of the three alternatives mentioned, the amount of installed reactive power is basically the same, and it is approximately equal to that required for the conventional configuration. The main reasons which led to a better acceptance of the alternative shown in Figure 1.1 (c) are given next, by means of a brief analysis of technical benefits and disadvantages of these three alternative configurations.

1. Arrangement (b) of Figure 1.1: commutation capacitor on the AC system side that is, between the commutation bus and the transformer. This arrangement has some disadvantages, such as:

- There is a possibility of ferroresonance occurring in the circuit formed by the AC system, series capacitors and converter transformers;

- The circuit formed by the capacitors and converter transformers allows the circulation of zero-sequence current. Single-phase faults in the system may produce very high current stresses on the capacitor;
- Currents resulting from faults at the capacitors terminals will not be limited by the converter transformer reactance. This leads to higher stresses on the surge arresters;
- Capacitor banks platforms insulation levels will be necessarily higher in back-to-back schemes, as the voltage on the valve side is generally lower than that at the commutation bus side. This may not be the case, however, in ultra high voltage overhead line DC links.

2. Arrangement (c) of Figure 1.1: commutation capacitor between the converter transformer and the valves. Among the main advantages of this configuration, the following may be pointed out:

- Converter transformers capacity may be smaller, since the reactive power flowing through them is minimized;
- There is no circulation of zero-sequence current through the capacitors, thus reducing the stresses;
- Capacitor banks platform insulation levels are lower in back-to-back schemes as the voltage on the valve side is generally lower than that at the commutation bus side;
- There is no risk of ferroresonance.

As to the disadvantages of this arrangement, the following stand out:

- The need for a larger number of capacitor banks per 12-pulse bridge (each 6-pulse bridge requires, in this case, a separate set);
- Although the total reactive power is practically the same, some additional expenditure may be expected, mainly because of its greater complexity, due to the presence of individualized banks for each 6-pulse bridge in the arrangement.
- In extra and ultra high DC voltage overhead line transmission links, the series capacitor banks for the upper bridges will be installed, at some additional cost, on increased insulation level platforms.

# 2 SCOPE

The market availability of a new configuration for HVDC converter stations – Stations with Series Capacitor Commutated Converter – CCC, or Converter with Commutation Capacitor, as discussed above in the Introduction – created the need for developing models for the digital studies of such converters, both in steady-state and in transient conditions. These tools should be able to work as additions to the more usual programs, such as: ANAREDE, ANATEM, EMTP/ATP and EMTDC.

As to HVDC system configurations, multi-terminal (MTDC) will not be broached in this work. The studies described below were based on HVDC applications in Brazil, and on its associated modeling experience. So, the work has been focused on point-to-point overhead line transmission. In applications of this kind the inverter is normally controlling the extinction angle and the rectifier the dc current. In cable applications the inverter will likely need to operate in dc voltage control or in dc current control for very long cables. These additional control modes have been modeled in this work as part of the VDCOL and in response to transient situations. Normal operation is a different matter. It requires another set of control parameter adjustments and possibly some modification in the control circuit arrangement.

## 2.1 Main topics

The main items presented in this work are:

- Definition and basic characteristics of CCC converters, including – for a basic configuration – the steady-state performance equations, the waveforms, the rectifier firing margin and the inverter commutation margin;
- General control characteristics – discussion of control philosophies for rectifier and inverter, of those for rectifier and inverter taps, of control system dynamic characteristics, and of the study of performance under special conditions;
- Development of characteristic curves, V x I curves and maximum power curves;
- Discussion of reactive power balance as a function of DC power or current;
- Criteria and procedures for the definition of the major characteristics of the main circuit equipment (Annex A);
- Steady-state performance: having in mind the adaptation of the usual power flow programs, the general equations are presented, with the required simplifications and the control modes. With the program adapted to a system with CCC converter, maximum power curves and reactive power curve as a function of DC current and power are developed;
- Performance under dynamic conditions: discussion of the CCC converters modeling characteristics, for analysis of the dynamic performance, having in mind the adaptation of the modeling into the existing programs, such as: digital simulation with three-phase representation (EMTDC and EMTP/ATP) and program for electromechanical stability analysis (ANATEM). For a sample case, performances of systems with different short-circuit ratios (SCR) are presented, for single-phase and three-phase faults, and for alterations in the orders of DC current and power. The effect of capacitors in asymmetric disturbances is also studied;
- Brief description of existing installations under commercial operations, Annex B;
- Presentation of the Benchmark developed for CCC system studies in steady state, dynamic and transient conditions.

Whenever possible, the differences in performance between CCC converters and systems with conventional converters are shown for steady state or dynamic conditions. Lastly, conclusions are presented, with a proposal for future work and the reference list.

## 2.2 Studies performed by WG B4-34 and included in this report

- Steady-state Performance: Item 3.5 presents the results obtained with the ANAREDE program for the survey of the steady-state behavior of CCC converters. Several features of the operation are evaluated, as

a function of the transmitted power or current, and comparisons are also made with a conventional HVDC link.

- Performance under Dynamic Conditions: Chapter 3 describes the tests for the control system of the CCC link in an AC system with infinite buses, using the ANATEM program; comparisons with results obtained with more precise three-phase models, developed for the ATP and EMTDC programs, are also presented.
- Development of equivalent networks to be used as a benchmark: the elaboration of a network with a HVDC/CCC system is described in Chapter 4. It contains the definition of the AC networks chosen for the converter and rectifier sides, the definition of the DC line, and the discussion of adjustments of power flow and of short-circuit ratios at the converter buses (SCR and ESCR).
- Electromechanical stability studies. In order to evaluate the adequacy of the network to the purposes of a benchmark[1], different simulations were performed, described in Chapter 4 and Annexes G and H, such as the complete and partial blocking of the link, reductions of the power order, and fault applications.
- Three-phase modeling. Chapter 4 also describes the elaboration of a simplified network for electromagnetic transients studies, with three-phase modeling, using the ATP and EMTDC programs, as well as tests of the CCC link control systems, comparing results with those of ANATEM program.
- Implementation of the benchmark in the ATP and EMTDC programs: technical data, characteristics of the controls, evaluation of dynamic performance, Annex C.
- Validation of the modeling for electromechanical stability studies. Analyses were made aiming to compare the studies performed on the complete and on the simplified network. Divergences were noted, suggesting the relevance of including in the simplified network the effect of the dynamical characteristics of machines. Therefore, dynamic modeling was included in the equivalent network utilized with ATP. This work is described in Annex G. The relevant data used for these studies is also included as Annex H.
- Simulations with variation of SCR and ESCR. In Annex G, are described studies performed with the ANATEM, ATP and EMTDC programs, where faults were applied with the values of SCR and ESCR being altered after a change in topology due to line isolation (circuit-breaker operation), so that the system is directed to promote recovery under conditions of a significant reduction of ESCR values. This way, it is attempted to have an indication of the minimum values of short-circuit capacity that would still ensure a robust operation.
- Validation of the influence, on the CCC link performance, of filters in the DC line. Annex F.

[1] It should permit operation under realistic conditions, but without excessively high safety margins, in order not to conceal problems.

# 3 GENERAL CHARACTERISTICS OF CONVERTER INSTALLATIONS WITH COMMUTATION CAPACITORS

## 3.1 Definition and basic characteristics of CCC converters

The following three-phase arrangement is intended to represent a twelve-pulse CCC, including the converters' snubber circuit:

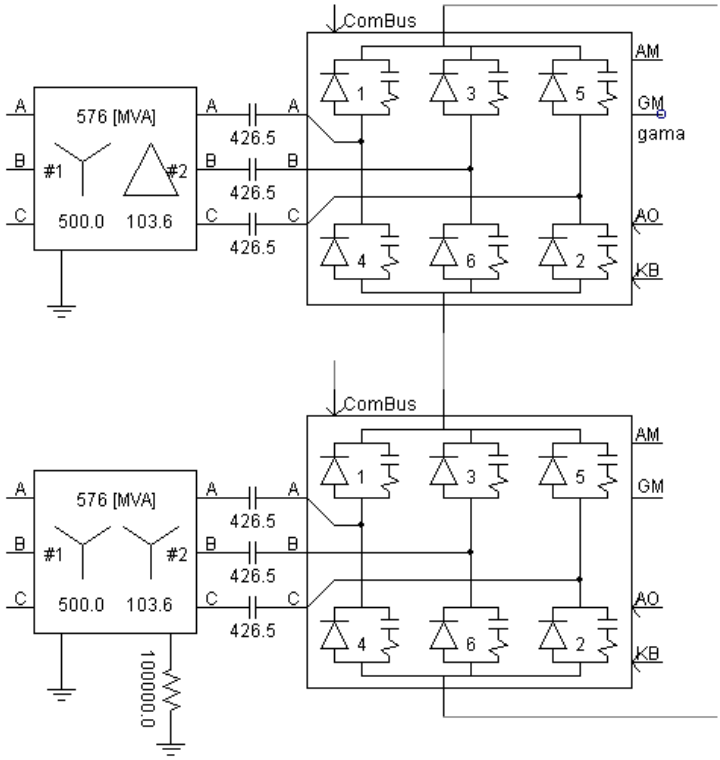


Figure 3.1 - Three-phase diagram of 12-pulse CCC in PSCAD program representation

Each six-pulse bridge may be represented by the diagram below, where numbers within the valves indicate the firing sequence:

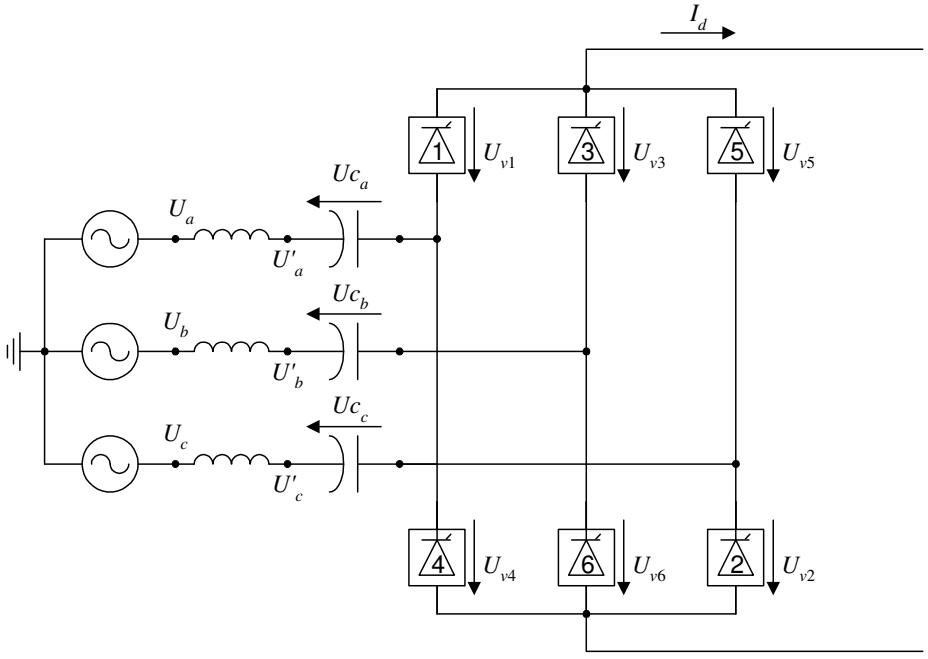


Figure 3.2 - Circuit with CCC converter

In Figure 3.2, the source phase voltages correspond to the transformer primary voltages referred to the secondary, i.e., they are the voltages ahead of the drop produced by each transformer leakage reactance multiplied by a factor equal to the transformer ratio.

Shortly before the firing of valve 3, valves 1 and 2 would be conducting, as shown below in Figure 3.3, where the conducting valves are shown in black.

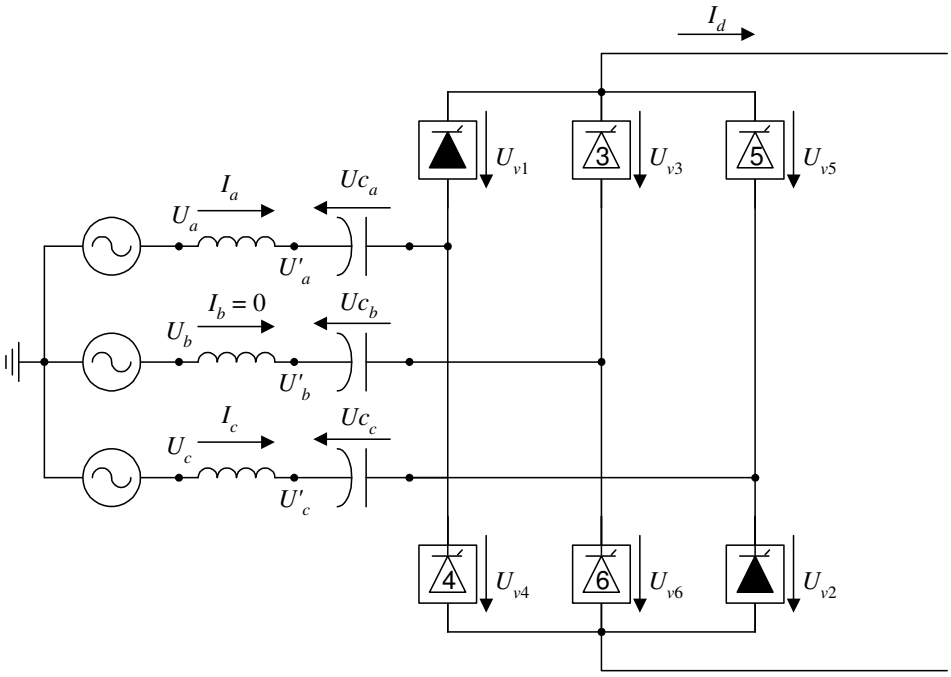


Figure 3.3 - Circuit indicating conduction of valves 1 and 2, shortly before the firing of rectifier valve 3

Figure 3.4 and 3.5 show the steady-state current and voltage waveforms, in the commutation capacitor of phases A and B, for the case of the CCC converter operating as rectifier. It is emphasized that, during the non-conducting period, the capacitor voltage is constant. Figure 3.6 shows the voltage on valve 3, together with the terminal voltage between phases B and A. It can be noted that the section of the valve voltage sinusoid before firing is advanced in relation to terminal voltage. This voltage advance is caused by the commutation capacitor, as explained next.

In the case of a conventional converter, without commutation capacitors, the voltage across valves 1 and 3 is given by:

$$U_{v3} - U_{v1} = U'_b - U'_a \tag{3.1}$$

As valve 1 is conducting, its voltage is ideally equal to zero and, in consequence:

$$U_{v3} = U'_b - U'_a \tag{3.2}$$

As the DC line current is approximately constant, and it passes entirely through phase A and C, respectively, when valves 1 and 2 are conducting, there would be no voltage drop in transformer inductances, since $L.\mathrm{d}I_d/\mathrm{d}t$ would be equal to zero. Also, as there is no current in phase B, voltage $U_b$ would be equal to voltage $U'_b$. Therefore, shortly before the valve 3 firing:

$$U_{v3} = U_b - U_a \tag{3.3}$$

On the other hand, in the case of the CCC, there is a voltage contribution from the capacitors, as follows:

$$U_{v3} - U_{v1} = (U'_b - Uc_b) - (U'_a - Uc_a) \tag{3.4}$$

During valve 1 conduction, its voltage drop is ideally equal to zero:

$$U_{v1} = 0 \tag{3.5}$$

Similarly to the conventional converter, voltage drop in phase A leakage inductance is approximately equal to zero, since the current circulating through valves 1 and 2 is approximately constant. In addition, voltage drop in phase B inductance is equal to zero, because valve 3 is not yet conducting. Therefore:

$$U_b - U_a = U'_b - U'_a \tag{3.6}$$

Replacing (3.5) and (3.6) in (3.4), valve 3 voltage, shortly before the firing of that valve, is obtained:

$$U_{v3} = U_b - U_a - Uc_b + Uc_a \tag{3.7}$$

Comparing (3.3) to (3.7), the main difference verified between the conventional and the CCC converter is that the latter has an increase in the voltage of the valve 3 (next valve to be fired), caused by the commutation capacitors. Note that the firing instant of valve 3 is indicated in these figures. Phase B capacitor voltage is maximally negative because, previously, thyristor 6 of the same phase had conducted negative current, loading the capacitor with the maximum negative voltage and, after the current blocking of thyristor 6, the current flowing through the capacitor is zero and, as a consequence, the capacitor voltage remains fixed at the same maximum negative value till the beginning of valve 3 condution. On the other hand, Phase A voltage is almost maximally positive, as valve 1 conducted positive current during almost all the conduction period, before valve 3 fires. This causes a voltage increment in the valve – produced by the negative voltage of phase B capacitor and by the positive voltage of phase A capacitor – of a value a little lower than twice the value of commutation capacitors steady-state maximum voltage. Its effect is to cause a significant advance in valve 3 voltage sinusoid section, in relation to the terminal voltage between phases B and A, as mentioned before, thus increasing the margin for valve firing. This effect is noted in Figure 3.6 and in Figure 3.7.

In Figure 3.7 are jointly presented the voltages $U_b$-$U_a$ (voltage between phases ahead of leakage reactance, equal to transformer primary voltage referred to the secondary), $U'_b$-$U'_a$ (voltage between phases of transformer secondary), $U_{v3}$-$U_{v1}$ (voltage between valves 3 and 1) and the voltages of commutation capacitors $Uc_a$ and $Uc_b$. Before the instant of valve 3 firing, voltage $U'_b$-$U'_a$ is approximately equal to voltage $U_b$-$U_a$, as the voltage drop in the leakage reactance is really negligible, since current is approximately constant before commutation starts. When valve 3 firing occurs, valve 1 current begins to decrease approximately according to a ramp function, while valve 3 current increases, similarly according to a ramp function, but in opposite direction of variation. This makes a difference between voltages $U'_b$-$U'_a$ and $U_b$-$U_a$ appear only during the current commutation period, when the current shifts from valve 1 to valve 3. It may be verified that voltage between valves 3 and 1 is equal to the sum of the voltages $U'_b$-$U'_a$ and the contribution of phases A and B capacitors, causing this voltage to increase and shifting the voltage zero crossing to the left (phase lead of valve voltage) related to zero crossing of voltage $U_b$-$U_a$ in the semi-cycle when valve 3 is fired. An interesting observation is that, with a current increase, this displacement also increases, promoting a higher valve voltage and, as a consequence, a higher firing margin. Note that a minimum firing margin is needed to avoid a firing failure, when the thyristor 3 would not start conducting due to insuficient positive valve voltage at the firing instant.

Curve $U_{v3}$-$U_{v1}$ permits to check simultaneously the voltage values of valves 1 and 3. Prior to valve 3 firing, valve 1 voltage is equal to zero and, therefore, voltage $U_{v3}$-$U_{v1}$ will be simply equal to the value of valve 3 voltage. Once valve 3 fires, both valve voltages become equal to zero during the whole commutation period, i.e., $U_{v3}$-$U_{v1}$ = 0. After commutation, valve 3 voltage continues to be equal to zero, so that $U_{v3}$-$U_{v1}$=-$U_{v1}$. In short, voltage $U_{v3}$-$U_{v1}$ is equal to $U_{v3}$ before commutation and equal to -$U_{v1}$ after commutation, being equal to zero during the whole commutation period.

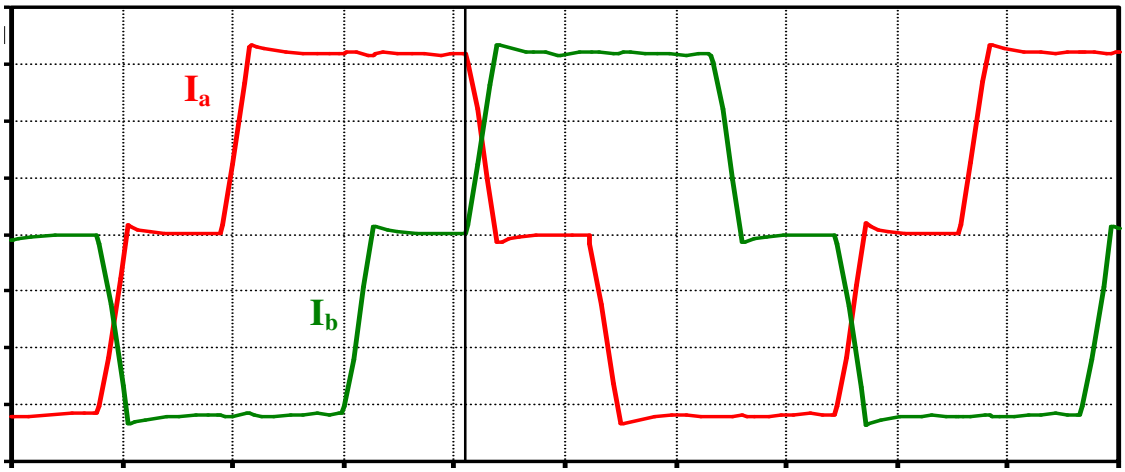


Figure 3.4 - Current in rectifier phases A and B

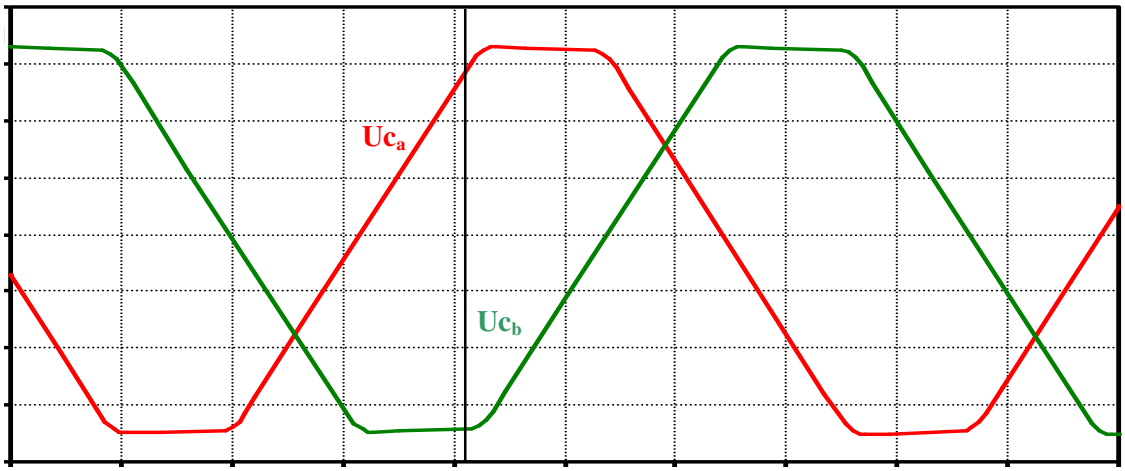


Figure 3.5 - Voltage at rectifier phases A and B capacitors

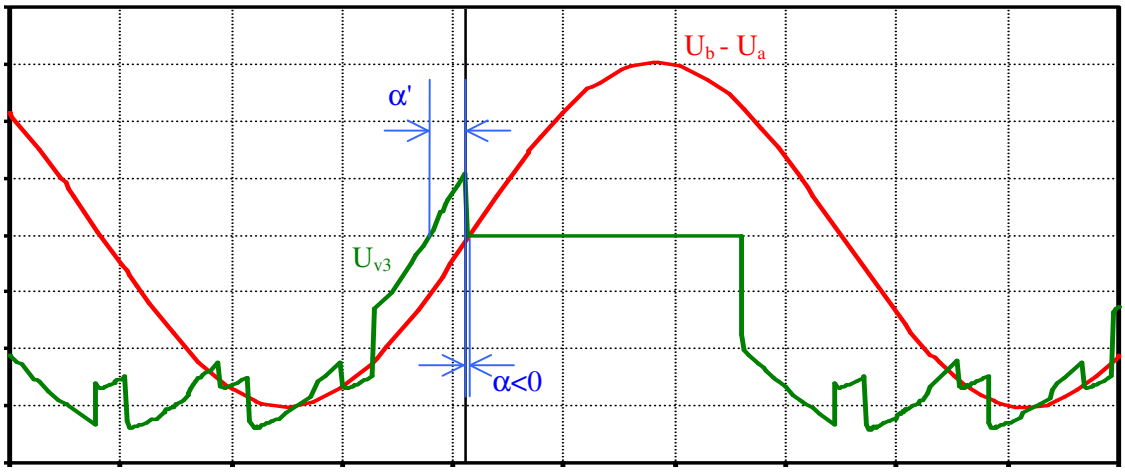


Figure 3.6 - Terminal voltage between phases B and A, and rectifier valve 3 (phase B) voltage.

When the valve fires, the angle between the instant of zero terminal voltage and the firing instant is called firing angle (**α**). With the voltage contribution from the commutation capacitor, that introduced an advance in valve voltage, that angle may even be negative (as in the presented case), allowing that, even with a negative terminal voltage at the firing instant, a positive voltage may exist in the valve for firing. At the firing moment, the valve voltage of course drops to zero, supposing that thyristors are ideal. The angle between the instant of zero valve voltage and the firing moment is called "firing margin" and is represented by the symbol (**α'**). Therefore, with the introduction of the commutation capacitor, it is possible to operate with firing angles (**α**) quite lower (or even negative), leading to an inherently lower reactive power

consumption by the converter station. If that angle takes negative values, there may be even a production of reactive power, that is, the converter would act as a capacitive load for the AC system at the rectifier side. However, given the minimum limits that need to be observed in relation to the firing margins (α'), in practice it may be unadvisable to operate with rated negative firing angles. Furthermore, similarly to a conventional converter, as the firing angle is normally employed to control current or power in the link, the rated operating value to be used should be such as to allow a margin for control sufficient to perform this control action during system operation. It should be noted that for small negative values of firing angle the sensitivity of dc voltage does not change or, in other words, the dc voltage will increase with the reduction of the firing angle. A minimum firing angle limit in the control system will avoid the inversion of this sensitivity that would cause loss of stability.

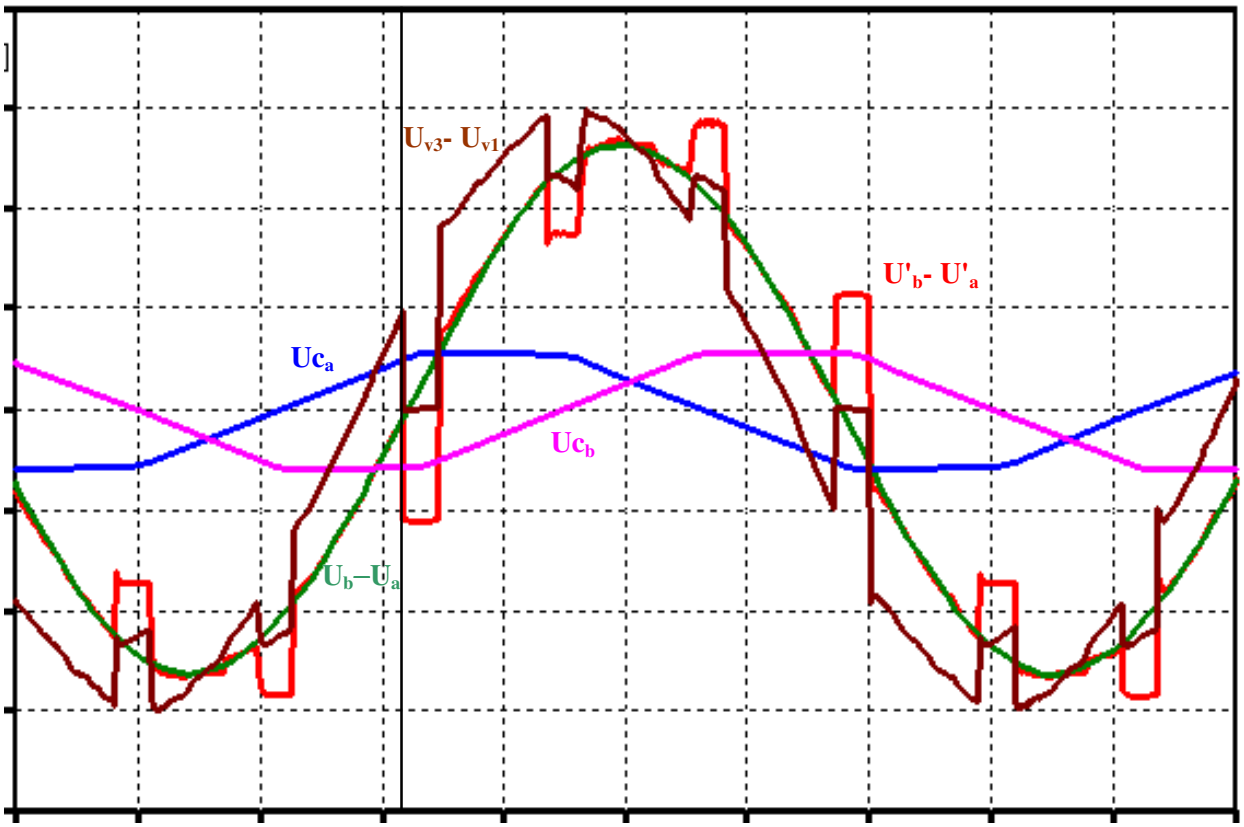


Figure 3.7 - Capacitor contribution in the rectifier commutation process

As in the case of the rectifier, shortly before the firing of inverter valve 3, valves 1 and 2 would be conducting, as shown in Figure 3.8 below, where the conducting valves are represented in black:

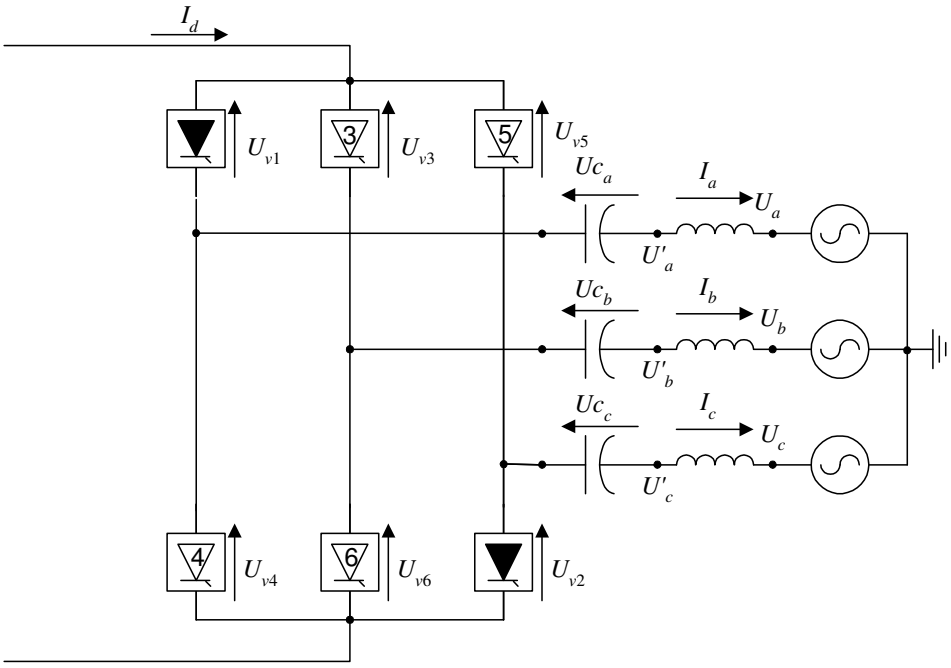


Figure 3.8 - Circuit indicating conduction of valves 1 and 2, shortly before the firing of inverter valve 3

In a similar way, the waveforms of the same variables are shown next, but now for a CCC converter operating as an inverter. The variables on the inverter side, compared with those on the rectifier side; show an analogous behavior; capacitors voltages and currents have the same characteristics, but with opposite directions. In the case of the inverter, the extinction angle (γ) is defined as that between the zero crossing instant of phase-to-phase terminal bus voltage and the moment of extinction of valve conduction. The instant of extinction in valve 1 is indicated in the figures. Similarly to the firing angle in the case of the rectifier, the extinction angle in respect to terminal voltage may be negative, since the capacitor contributes to a delay in valve voltage, meaning that, for a positive terminal voltage, there may be a negative voltage in the valve, that makes possible the extinction of the conduction. As in the case of the rectifier, the commutation margin (γ') is defined as the angle between the zero crossing instant of valve voltage and the instant when conduction is extinguished. The introduction of the series capacitor results in a smaller extinction angle (γ), maintaining the commutation margin (γ') in the safe region, with a consequent lower consumption of reactive power by the inverter, or even a possible generation of reactive power. The extinction angle (γ) and the commutation margin (γ') are shown in Figure 3.11.
In the case of inverter the following formulas are used:

$$U_{v1} - U_{v3} = (U'_b + Uc_b) - (U'_a + Uc_a) \tag{3.8}$$

At the extinction instant, valve 1 stops conducting and valve 3 conducts the whole current. In this case the current in valve 1 is zero ($U'_a$=$U_a$) and current in valve 3 is constant ($U'_b$=$U_b$). Additionally voltage at valve 3 is zero. Then, voltage at valve 1 at the extintion instant is given by:

$$U_{v1} = U_b - U_a + Uc_b - Uc_a \tag{3.9}$$

The voltage $Uc_b$ is very negative and $Uc_a$ is very positive. Therefore, the capacitors contribute significantly to the current extinction in valve 1 and consequently improving behavior against commutation failures and allowing the use of small or negative values of extinction angle.

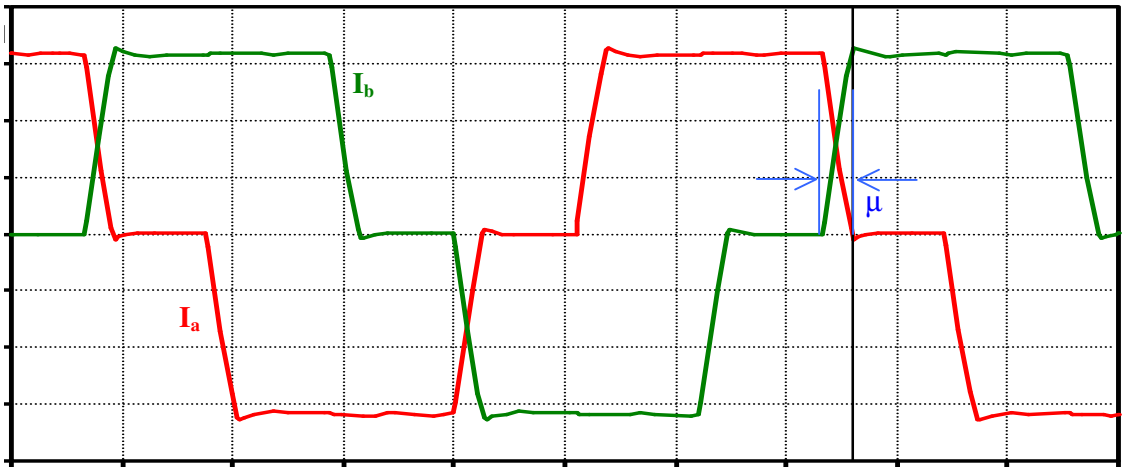


Figure 3.9 - Current in phases A and B of the inverter

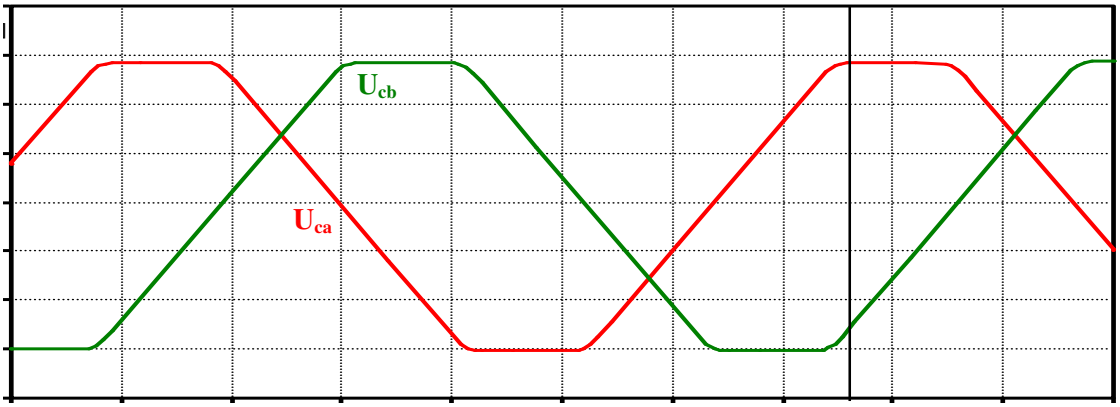


Figure 3.10 - Voltage of capacitors in phases A and B of the inverter

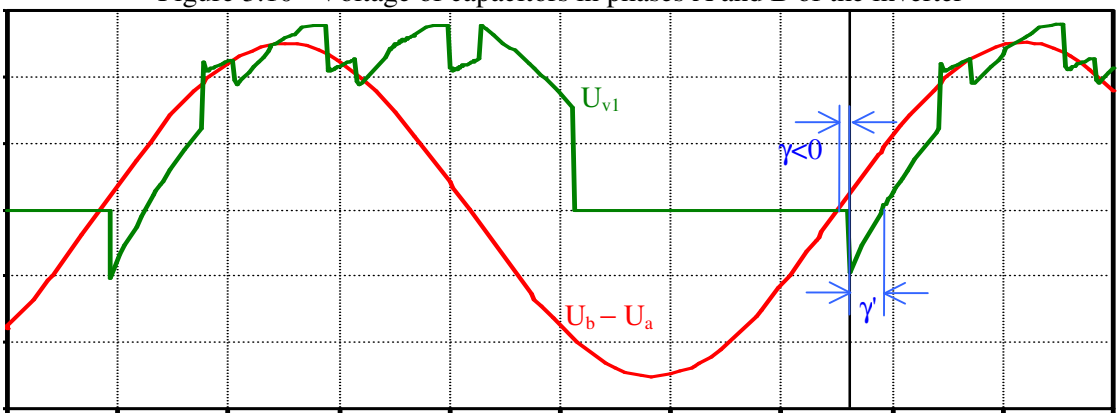


Figure 3.11 - Terminal voltage between phases B and A, and inverter valve 3 (phase B) voltage

Alike to the case of the rectifier, the following voltages are jointly presented in Figure 3.12: $U_b$-$U_a$ (voltage between phases ahead of leakage reactance, equal to transformer primary voltage referred to the secondary), $U'_b$–$U'_a$ (voltage between phases of the transformer secondary), $U_{v1}$–$U_{v3}$ (voltage between valves 1 and 3) and the commutation capacitor voltages $Uc_a$ and $Uc_b$. Similarly to the case of the rectifier, voltage $U'_b$-$U'_a$ coincides with voltage $U_b$–$U_a$ except in the instants of commutation, when $U'_b$–$U'_a$ experiences a difference in level due to the voltage drop in phase A leakage reactances, caused by current variation during the commutation periods. Inversely to the case of the rectifier, the contribution of the inverter capacitors is made in the direction promoting current blocking by valve 1, when commutation to valve 3 occurs.

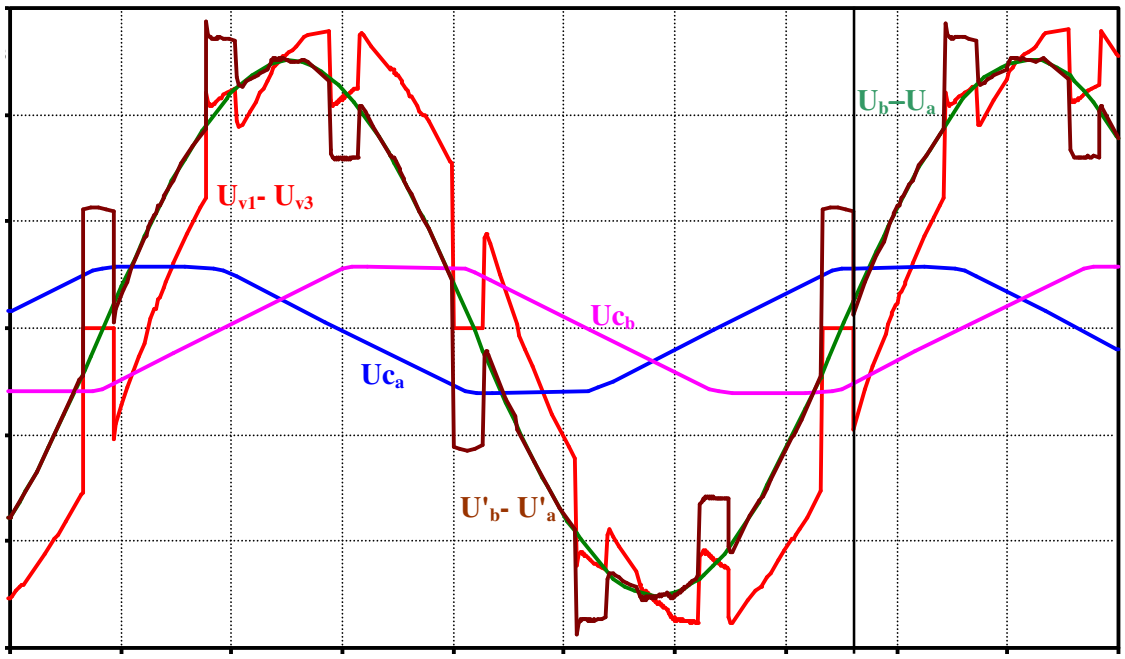


Figure 3.12 - Contribution of the capacitor in the inverter commutation process

Figure 3.13 shows the current in the same chart as the valve voltage. In order to avoid a superposition, the voltage curve was placed below the valve current curve. It is noted that, during the whole conduction period, including the commutation phase, the valve voltage is practically equal to zero, when current is reduced, at approximately constant rate, until the instant of valve 1 current blocking. At this blocking instant, valve voltage changes suddenly to a negative value. If the voltage were not negative, a commutation failure would occur, i.e., valve 3 will not conduct current during this cycle, that would continue to be conducted by valve 1. In practice, a minimum negative area for the integral of valve voltage, up to its zero crossing instant, should always be assured in normal operation, in order to avoid a commutation failure. In fact, the smaller that area is, the higher will be the probability of occurring a commutation failure. In case of a commutation failure, a short-circuit will occur on the DC side when valve 4 fires, due to the simultaneous conduction of valves 1 and 4, while on the AC side current falls to zero, since DC current starts circulating wholly by the short-circuited valves.

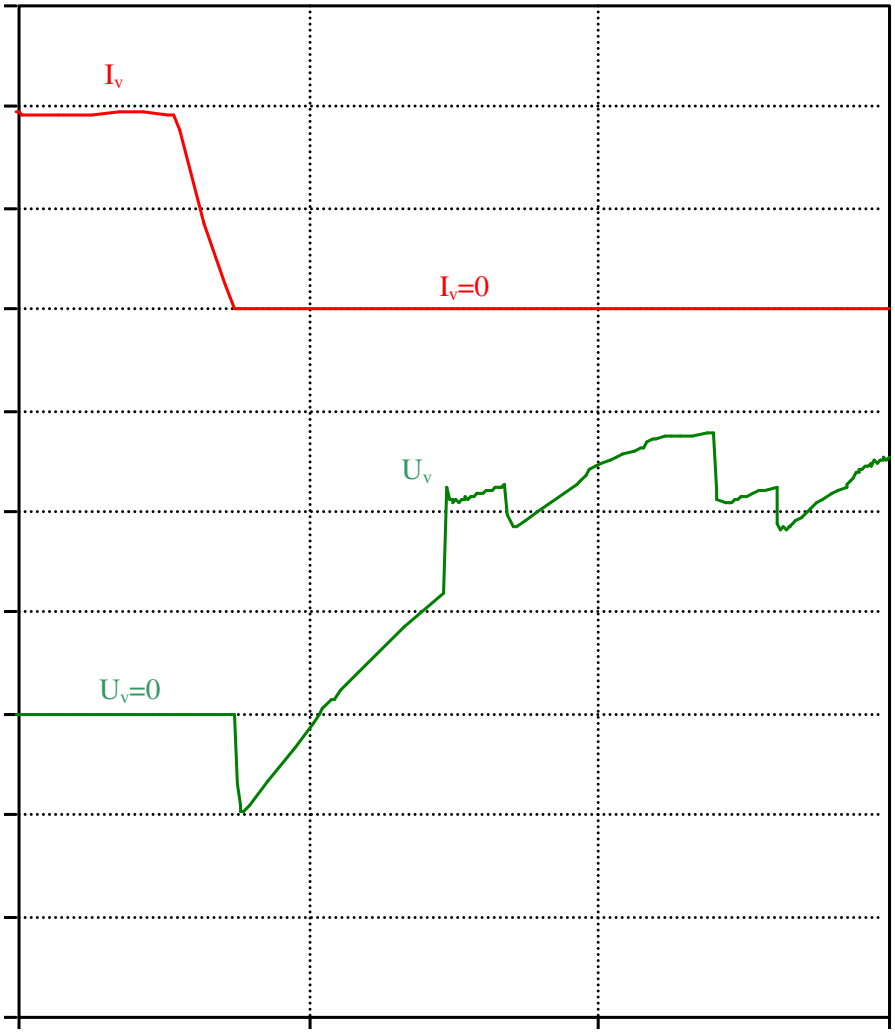


Figure 3.13 - Current and voltage in valve 3

Alike to the conventional converter, overlap angle (μ) is defined by the angle corresponding to the difference between the firing instant of the new valve that will take over the current, and the instant when the valve that is conducting will block the current. This definition is valid both for the operation as a rectifier and that as an inverter. That angle is shown in following figure.

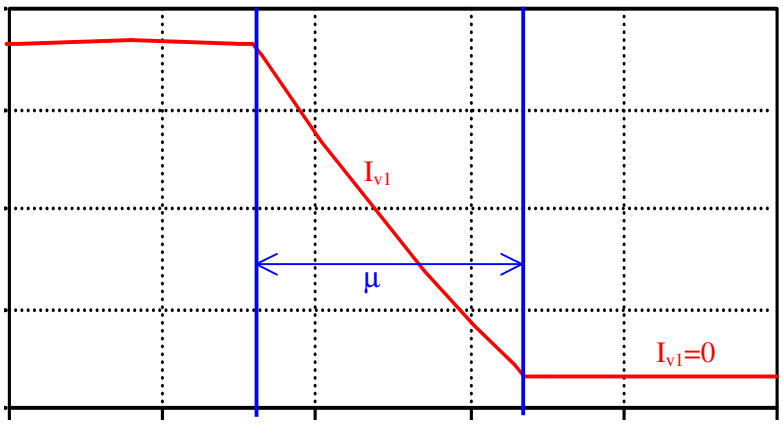


Figure 3.14 - Definition of the commutation angle as a function of valve current

## 3.2 General control characteristics

The main components of the CCC control are basically the same as those for a HVDC conventional converter, i.e.: VDCOL (Voltage Dependent Current Order Limiter – responsible for the decrease and gradual increase of the current order and, consequently, of the link power, as a function of the DC side voltage in case of faults in general), CCA (Current Control Amplifier – responsible for the calculation of the firing angle required to reach the current order, and for the dynamics of DC voltage or current control between inverter and rectifier) and FIRING (responsible for the valve pulse generation based on the order of the firing angle and a reference calculated in respect to the converter station bus voltages).

The block diagram of the rectifier control is presented below, in a simplified form, as in [15]. This block diagram shows the PI (Proportional-Integral) current control of CCA, the power control, the limit $I_o$ imposed by the VDCOL and the minimum and maximum limits of the firing angle. The complete implementation of the control is described in detail in Annex C. Complementary theoretical aspects are presented in [15].

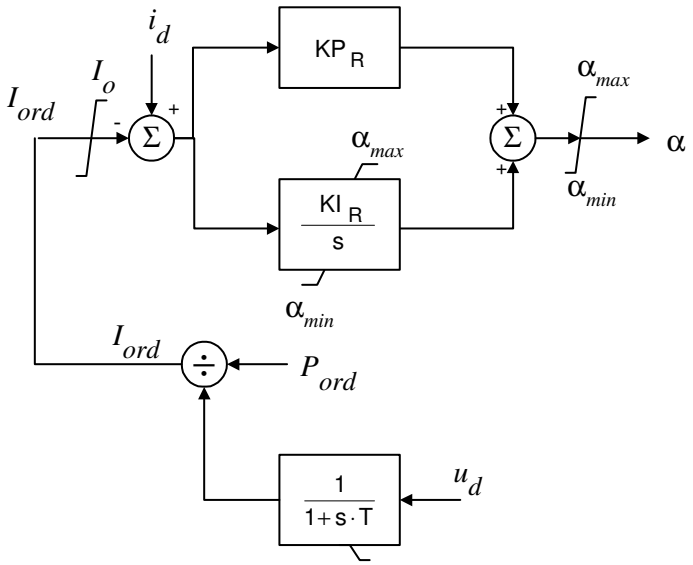


Figure 3.15 - Rectifier Control

The block diagram of the inverter control is shown next, as in [15]. As in the case of the conventional inverter, the CCC inverter works saturated in $\alpha_{max}$, by the inclusion of the current margin signal in the CCA summation block, that angle being calculated as a function of the desired commutation margin $\gamma'_{ref}$.

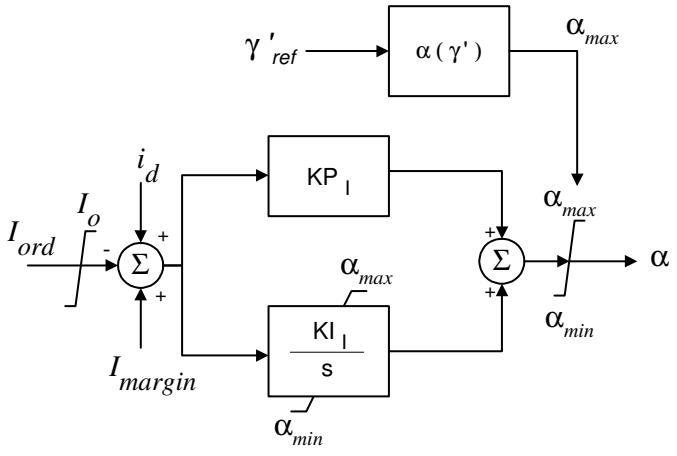


Figure 3.16 - Inverter Control

As well as in conventional converters, some additional devices (such as: correction of firing angle limits, increase of the commutation margin or increase of the current margin in the inverter) have been introduced

into the controls, aiming to provide a greater operational robustness. These actions are taken as a result of the identification of:

- fault occurrence
- presence of commutation failure
- unbalance in capacitors voltage.

In a similar way as in conventional HVDC converters, the CCA of the inverter is programmed with a current margin, so as to operate always with a maximum firing angle (maximum alpha) corresponding to a minimum extinction angle (minimum gamma). The rectifier maintains current control as long as the firing angle is able to change within its range of action, always limited by the minimum firing angle (minimum alpha). The tap of the rectifier transformer is used for adjusting the rectifier firing angle within a range centered in the rated value, while the tap of inverter transformer is usually used for controlling DC voltage. This control scheme may be different, e.g., the inverter firing angle may be used for DC voltage control and the tap of inverter may be used for firing angle control.

In the case of the CCA, some modifications were included in the calculation of minimum and maximum angles, since the presence of the series capacitor produces a voltage phase displacement on the valves, in relation to the converter bus voltage. This characteristic increases the control margins, allowing the firing angle to be lower than the conventional one in the rectifier, and higher in the inverter. This makes the CCC more robust, and endows it with a satisfactory recovery in such situations where conventional converter stations do not achieve it. Thus, the CCC can be used in systems with ESCR (effective short-circuit ratio) values around 1.0, as it will be shown farther on with respect to the proposed benchmark system..

The presence of commutation capacitors introduces a difference of behavior upon a fault occurrence because, in this case, the higher the current is, the greater will be the effect caused to the voltages on the valves, increasing the commutation margin in the inverter and, consequently, improving control stability during recovery. On the other hand, the capacitors present voltage unbalance after asymmetrical faults (single-phase or double-phase), caused by the magnitude difference between the currents of each phase during the disturbance. This unbalance is very important, especially for the inverter, because, by altering the voltage upon the valve, it may cause commutation failures. However, as the current on the DC side returns to its pre-fault value, the balance is re-established naturally. To avoid this occurrence, the margin of commutation during recovery is increased for a certain time, then reduced to its normal value after recovery reaches a specified value, thus ensuring that phase currents will balance without risk of commutation failures. The adjustment of this additional protection function may be made by trial and error, with the assistance of programs such as PSCAD/EMTDC or ATP.

In the representation of FIRING, in both PSCAD/EMTDC and ATP programs, a generic control was used, called “phase vector”, utilized in the model of 6-pulse converter bridge (“HVDC Valve group model” - G6P200) available in the PSCAD model library. Figure 3.17 shows the block diagram corresponding to the PLL (Phase Locked Loop)[1], as presented in [18]. The firing pulses are generated based on the calculated angle ( $\theta$ ), considering, for the two 6-pulse bridges in each 12-pulse group, the respective 30º phase differences. This model has given a very satisfactory performance.

[1] It should be noted that PLL is also frequently indicated as PLO (phase locked oscillator).

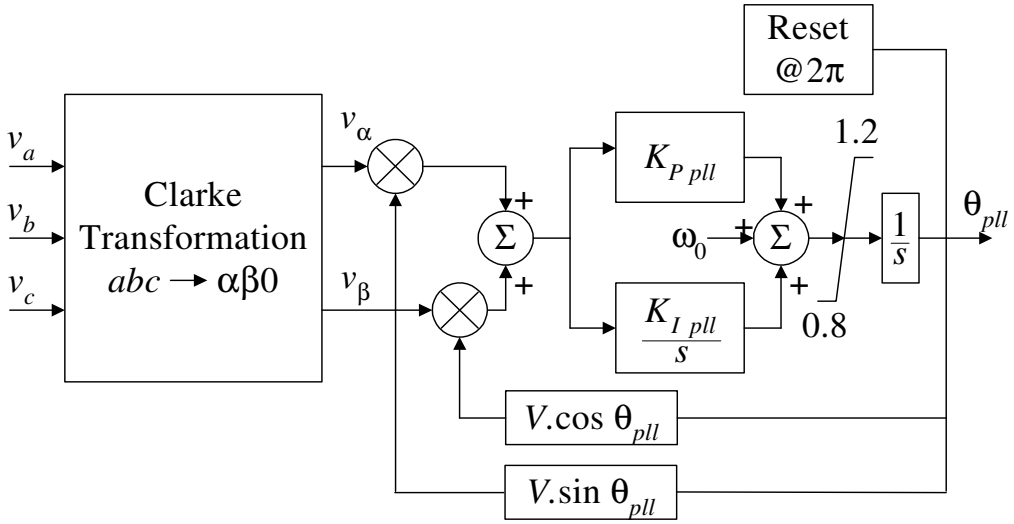


Figure 3.17 – "Phase Vector Phase Locked Loop" Generic Control

Figures showing the PLL outputs are given below. The first presents Phase A voltage ($U_a$), used by PLL as a reference for measuring the angle ($\theta_{pll}$)**.** Phase A voltage angle, measured by the PLL, varies from zero – when phase A voltage crosses zero value – up to 360 degrees, returning to zero at each 360 degree cycle, as the figure shows. It also shows voltage between phases A and C ($U_{ac}$) and currents in phases A ($I_a$) and C ($I_c$). The variables are graphically represented in different scales for better visualization and, for this reason, the ratio of $\sqrt{3}$ between amplitudes of $U_{ac}$ and $U_a$ is not apparent.

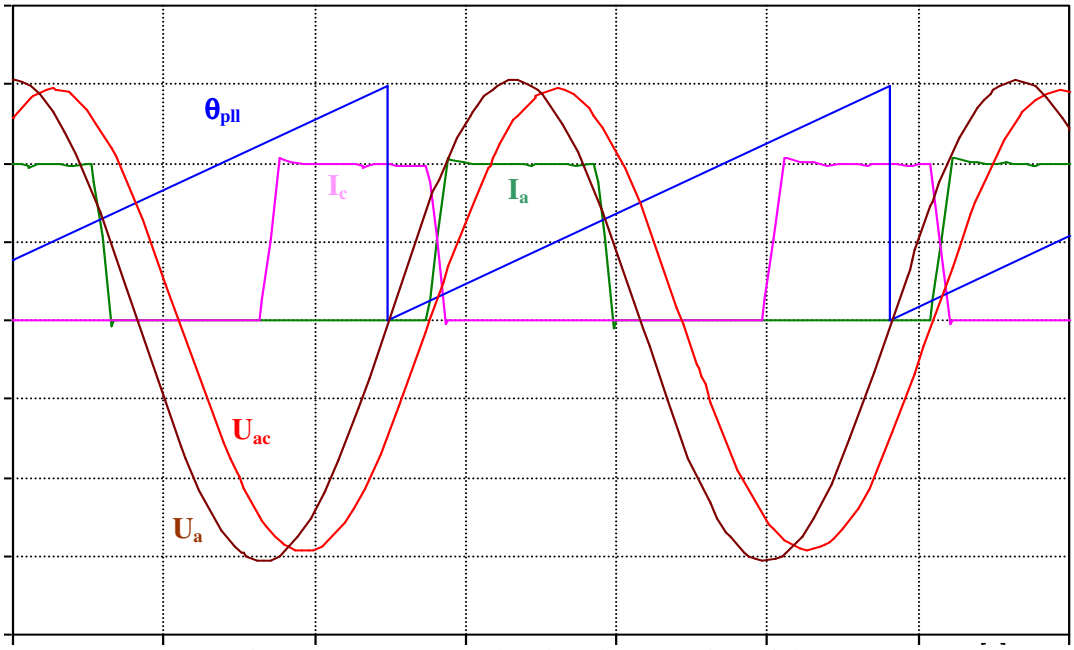


Figure 3.18 - Curves showing the operation of the PLL

The previous figure is shown next in an enlarged scale. It is possible to observe current commutation from phases C to A, when the firing angle, increased by 30 degrees (corresponding approximately to the angle of the voltage between phases A and C) coincides with the angle given by the PLL. It is noted that, in the specific operational situation here indicated, the firing angle measured in relation to the commutation voltage (voltage at the station AC bus) is about $-3^o$ , i.e., it is negative. In such situations, the CCC converter station, instead of consuming, supplies reactive power to the AC system.

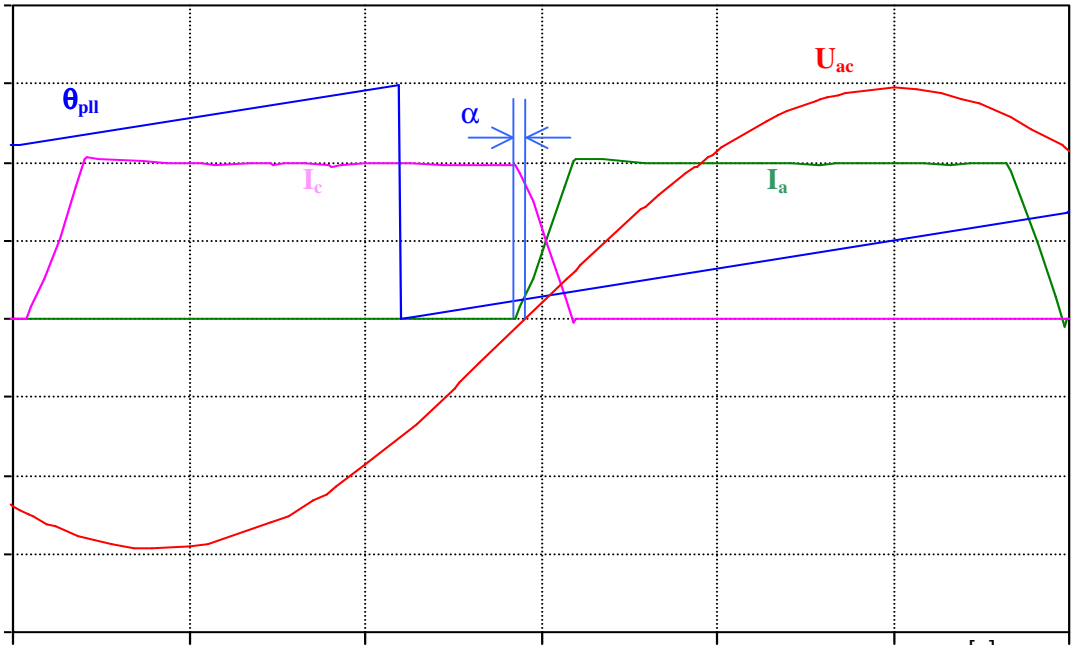


Figure 3.19 - Detail of the curves demonstrating the operation of the PLL

### 3.3 Criterion for reactive power exchange at converters AC buses

The two main advantages of the configuration using converters with commutation capacitors regard the aspects associated to the reduction of shunt reactive compensation[2] at the converters, and to a greater robustness in respect to commutation failures.

On account of the commutation capacitors contribution, filter banks are, in general, already sufficient to provide the reactive power support. For the dimensioning of filters, in addition to their adequacy to the levels of harmonic currents produced during the AC-DC conversion process, other features should be considered, such as the value of the commutation capacitor and the desired commutation margin (or firing angle).

The most significant impact is due to the reduction in the switching of shunt banks, for different DC power transmission levels.

### 3.4 Modeling Characteristics of Converters with Commutation Capacitors, for Steady-State and for Electromechanical Stability

The mathematical model of the CCC converter was initially presented in reference [1], and some alterations were introduced in reference [15]. The basic equations are transcribed below, for the case of a CCC converter operating as a rectifier.

$$u_{dio} = \frac{3\sqrt{2}}{\pi} \cdot V_{ss}\,; \quad d_{xl} = \frac{3X_t}{\pi}\,; \quad d_{xc} = \frac{3}{\pi\omega C}\,; \quad \omega_0 = \sqrt{\frac{d_{xc}}{d_{xl}}}$$

$$u_{cN} = \frac{\pi^2 d_{xc}}{9}\,; \quad K = \frac{1}{2}\frac{1}{d_{xc} - d_{xl}}\,; \quad E = -K u_{dio}\cos(\alpha) - \frac{i_d}{2}$$

$$F = K u_{dio}\omega_0 \sin(\alpha) + \frac{\pi\omega_0}{3} i_d - \frac{3\omega_0}{2\pi d_{xc}\omega}\Delta V_1$$

$$\beta = \arctan\left(\frac{F}{E}\right) \qquad Y = \sqrt{E^2 + F^2}$$

[2] It is important to keep in mind that, constructively, the total capacitive compensation (series plus shunt) is practically the same in both conventional and CCC arrangements.

where $u_{dio}$ is the no-load DC voltage; $V_{ss}$ is the converter transformer phase-to-phase voltage on the valve side; $i_d$ is the DC current; $\alpha$ is the firing angle in relation to the terminal bus voltage; $\mu$ is the commutation angle (overlap); $C$ is the capacitance of the commutation capacitor; $\omega(= 2\pi f)$ is the angular speed corresponding to system frequency; $X_t$ is the transformer reactance; $\Delta V_1$ and $\Delta V_2$ are variations of the voltage upon the series capacitor during a commutation, when the phases stop and start to conduct, respectively.

The average DC voltage is given by:

$$u_d = u_{dio} \cdot \frac{\cos(\alpha+\mu)+\cos\alpha}{2} + \left(1 - \frac{3}{4\pi}\mu\right) \cdot (\Delta V_1 - \Delta V_2) \tag{3.10}$$

Variations $\Delta V_1$ an $\Delta V_2$ are calculated by the following expressions:

$$\Delta V_1 = \frac{2\pi d_{xc}}{3[1+\cos(\omega_0 \mu)]} \left[ \frac{i_d \mu}{2} - K u_{dio} \sin(\alpha+\mu) + \frac{1}{\omega_0} \left( K u_{dio} \cos(\alpha) + \frac{i_d}{2} \right) \sin(\omega_0 \mu) \right. \tag{3.11}$$

$$\left. + K u_{dio} \sin(\alpha) \cos(\omega_0 \mu) + \frac{\pi}{3} i_d (\cos(\omega_0 \mu) - 1) \right]$$

$$\Delta V_2 = \frac{\pi}{3} i_d \ \mu \ d_{xc} - \Delta V_1 \tag{3.12}$$

The overlap angle ($\mu$) is calculated by:

$$\frac{i_d}{2} - K u_{dio} \cos(\alpha+\mu) - Y \cos(\omega_0 \mu - \beta) = 0 \tag{3.13}$$

The equations above form a set of transcendental equations, therefore variables $\mu$, $\Delta V_1$ e $\Delta V_2$ have to be obtained by iterative processes (e.g., by the Newton-Raphson method).

For a given $u_{dio}$, the DC voltage $u_d$ has a higher value in the case of the CCC, when compared to the conventional converter, for two reasons: the smaller value of $\alpha$ and the difference $(\Delta V_1 - \Delta V_2)$ in equation (1).

The same formulas may be applied to the CCC converter when operating as an inverter, considering that the same is a rectifier, except that it is physically inverted and operating at firing angles greater than 90 degrees.

From the point of view of the DC network, the model for a DC link composed of two converters connected by a DC line may be represented by the diagram below. It is noted that, in this diagram, DC filters are not shown, as it would be usual in electromechanical stability studies.

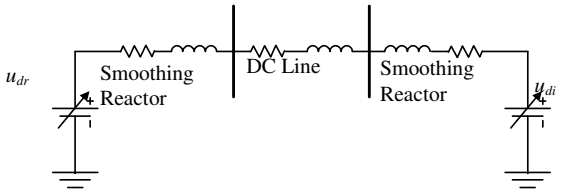


Figure 3.20 - Diagram of the DC network model

The average DC voltage of each converter is a function of its firing angle, DC current, commutation angle, and the parameters $d_{xl}$ and $d_{xc}$ (that are respectively functions of the transformer and of the series capacitor reactances). The DC line and the smoothing reactors may be modeled by first order differential equations describing a RL circuit. However, in case of a connection by a long underground or submarine cable, the shunt capacitance of the cable should also be considered.

From the AC network point of view, the CCC converter drains an apparent power given by:

$$S_{dc} = P_{dc} + j\, Q_{dc} = 3\, U_1\, I_1^* \tag{3.14}$$

where $\boldsymbol{U_1}$ is the phase-to-ground voltage and $\boldsymbol{I_1}$ the AC transformer current on the bridge side. Taking as a reference the phase angle of $U_1$, the relations involving $U_1$, $I_1$ and the DC variables are described by the equations:

$$U_1 = \frac{\pi}{3\sqrt{6}} u_{dio} \tag{3.15}$$

$$I_1 = \frac{\sqrt{6}\, e^{-j\alpha}}{\pi}\left\{\frac{i_d}{2}\left(1+e^{-j\mu}\right)+\frac{K u_{dio}}{2}\left[\frac{e^{-j\alpha}}{2}\left(1-e^{-j2\mu}\right)+ j\,\mu\, e^{j\alpha}\right]\right. \tag{3.16}$$

$$\left.+\frac{Y}{\omega_0^2-1}\left[e^{-j\mu}\left[\cos(\omega_0\mu-\beta)+ j\omega_0\sin(\omega_0\mu-\beta)\right]-\cos(\beta)+ j\omega_0\sin(\beta)\right]\right\}$$

These equations were used in the implementation of the DC model in the ANAREDE program, for the calculation of power flow, as described in [8]. In this steady-state calculation, the following assumptions were considered:

- The filters eliminate ideally the current and voltage harmonics on the AC and DC sides.
- The effect of the converter valves waveform, including the contributions of the commutation capacitor, is considered on the basis of the formulas for DC average voltage and fundamental-frequency AC current introduced into the network.
- In a power flow program, depending on the control mode, the values of some variables are set as specified by the user, while the values of the other variables are calculated in order to comply with basic equations.
- During the iterative process (which utilizes, for instance, Newton's method), control modes are switched automatically.

### 3.5 Steady-State Performance

The ANAREDE program was used to survey the steady-state behavior of the CCC, as a function of the transmitted power or current, and to compare it to a DC link with conventional converter stations, in a system having SCR equal to 2 on the inverter side.

The system is a simplified version of Itaipu HVDC system with a dc transmission line of about 800 km and the converters connected to infinite buses by simple reactances. The commutation capacitor was included and the shunt ac filters were modified to compensate the reactive power generated by the commutation capacitor.

The objective of this section is to present some differences on behaviors of CCC and conventional converters, noting that these differences are highly dependent on the system parameters, including dc transmission line length and SCR at both sides.

Figure 3.21 shows the PV curve (voltage as a function of power), indicating that the voltage stability margin is greater for the CCC, and demonstrating the need for switching capacitor banks in the case of conventional converter station, which may not occur for the CCC.

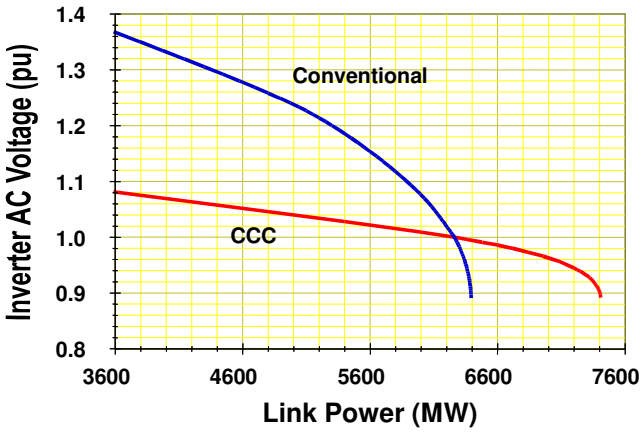


Figure 3.21 - PV curves of the conventional converter and of the CCC

Next, the steady-state curves for active power, reactive power, transformer tap and commutation angle are shown, for the rectifier and the inverter, respectively, as a function of the current. In these curves, it was considered that the firing angle ($\alpha$) was utilized to control the current, and the commutation margin ($\gamma'$) was kept fixed at 21°. The tap changer on the rectifier side acted towards keeping the firing angle at the desired value (15°), while the inverter side tap changer acted towards keeping the DC voltage level constant.

As the DC voltage was maintained by the variation of the tap on the inverter side, active power is proportional to the current, as shown in the figure below.

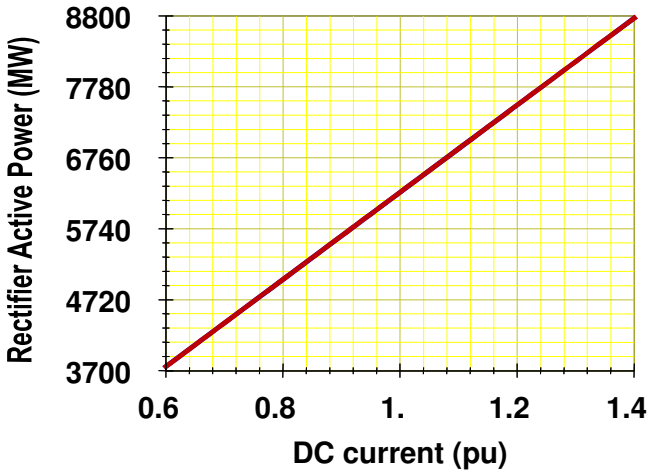


Figure 3.22 - Rectifier active power as a function of current, for the conventional converter and for the CCC

Reactive power is shown in the following figure. It is seen that reactive power variation is much larger in the case of the conventional converter.

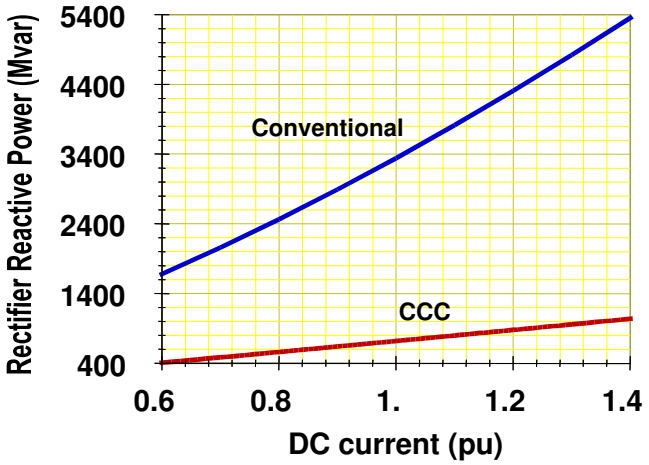


Figure 3.23 - Rectifier reactive power as a function of current, for the conventional converter and for the CCC

The variation of rectifier transformer taps is shown on Figure 3.24. It is noted that, in the case of the CCC, there is practically no need to change taps on the rectifier side, which is an advantage in relation to the conventional converter.

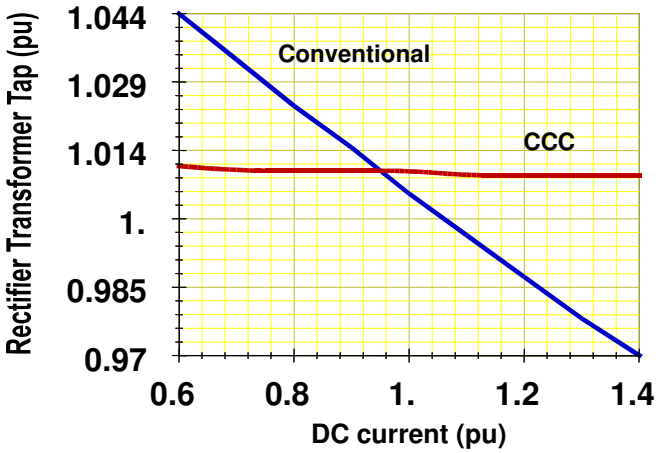


Figure 3.24 - Rectifier transformer tap as a function of current, for the conventional converter and for the CCC

Figure 3.25 shows the overlap angles for both cases. It can be noted that the variation is much larger for the conventional converter, thus explaining in part the greater variation in reactive power.

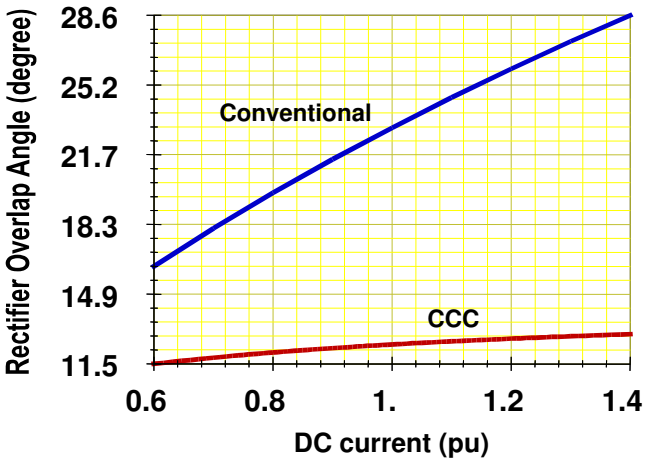


Figure 3.25 - Rectifier overlap angle as a function of current for the conventional converter and for the CCC

Next, the curves for the inverter are presented. Active power is equal to rectifier power minus line losses.

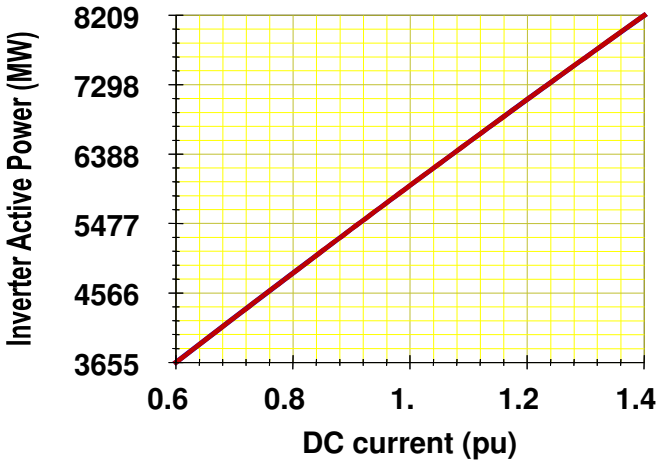


Figure 3.26 - Inverter active power as a function of current, for the conventional converter and for the CCC

Reactive power shows an opposite behavior in the two types of converters, as indicated on the next figure. While in the conventional converter reactive power increases when current increases, in the CCC reactive power decreases, inasmuch as the current increase causes a greater generation of reactive power by the commutation capacitor, which exceeds the increase of the reactive power consumption by converter and transformer.

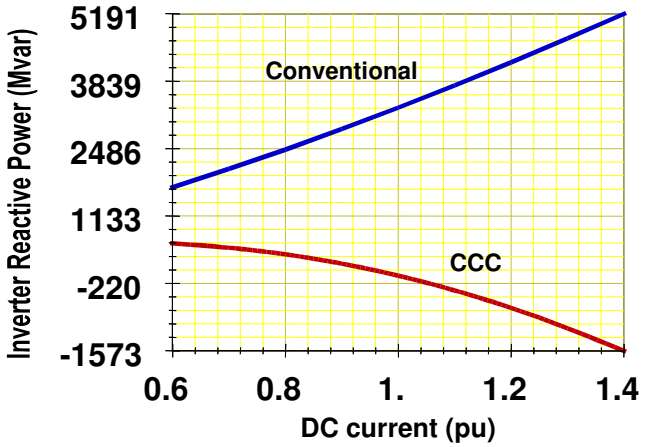


Figure 3.27 - Inverter reactive power as a function of the current, for the conventional converter and for the CCC

Inverter transformer tap variation with DC current is shown next. It is noted that the variation of the CCC curve is not monotonic, as that of the conventional converter.

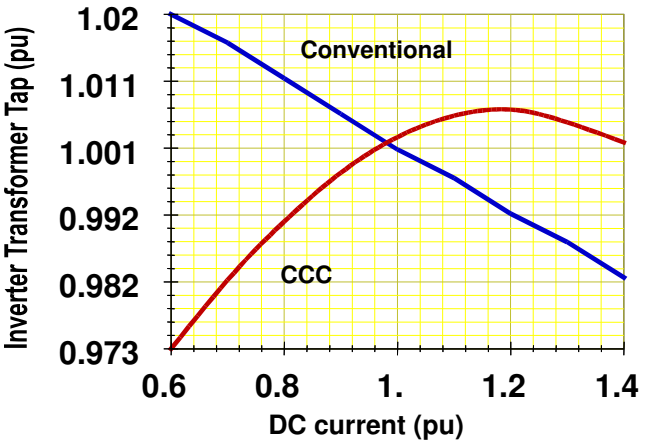


Figure 3.28 - Inverter transformer tap as a function of current, for the conventional converter and for the CCC

Below, it is shown the overlap angle, that is greater for the conventional converter, in the whole range of operation.

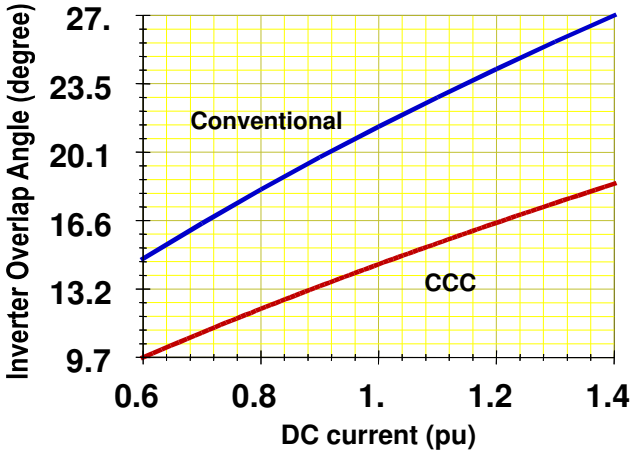


Figure 3.29 - Inverter overlap angle, as a function of current, for the conventional converter and for the CCC

### 3.6 Dynamic performance

The detailing of models of a DC link and its controls, in electromechanical stability programs, aims to make possible the analysis of the different operation modes, and the evaluation of the influence of emergencies, occurring close to that link, on the dynamic performance of the associated AC systems.

The introduction of series capacitors, in the valve commutation circuit, augments the difficulty of representing events which lead to significant current or voltage unbalances upon these capacitors. Despite persistent efforts to improve the representation of DC Transmission Systems in electromechanical transients programs, special procedures are generally required, in order to reproduce adequately their behavior in the simulation of certain events, on account of the limitations inherent to single-phase modeling of DC links.

The models of the controls for the CCC link, represented in the ANATEM electromechanical stability program [19], were prepared on the basis of the more precise three-phase models developed for the ATP and PSCAD/EMTDC electromagnetic transients analysis programs. Ref. [8] presents details of the implementation of the models utilized in the feasibility studies, performed on ANAREDE and ANATEM, for the commencement of the Garabi CCC link. The models utilized in this CIGRÉ Report are more generic, and do not present some of the specific features of the models used in ref. [8]. Refs [7] and [9] present comparisons between conventional and CCC links, from the dynamic and static points of view. Ref. [15] presents complementary results of the CCC dynamic performance in stability programs.

#### 3.6.1 Tests on the CCC Control Systems

The tests for the validation of the CCC modeling were carried out gradually in this study, starting from a simpler representation of the AC network, up to a more complex one, attempting to identify the differences in the dynamic performance of the CCC control, and trying to improve its representation in the ANATEM electromechanical stability program.

In order to eliminate any possible discrepancy, derived from differences in the AC network modeling in the ATP and ANAREDE programs, during the validation tests of the controls for the CCC link, represented in ANATEM, in the first stage it was used an AC system with infinite buses on the rectifier and inverter sides, as shown in Figure 3.30. In this system, the DC shunt filters were not included, because it is irrelevant to represent or not such equipment in electromechanical stability studies. However, they were considered in the benchmark described in the next chapter. It should be noted that, in practical studies using electromagnetic transients programs, DC filters should be included, in order to make possible the identification of adverse interaction problems among the AC network, the DC link and its control system. Usually, DC shunt filters

are present in DC transmission using aerial lines, in order to decrease electromagnetic interferences caused by DC voltage harmonics.

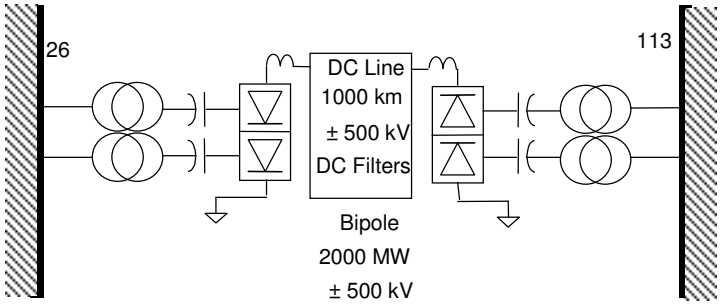


Figure 3.30 - Test system with infinite buses at the rectifier and at the inverter

The events analyzed for the evaluating the behavior of the models for the control of the CCC link, using the test system of Figure 3.30, were the following:

- -/+ 2% step in the order of the CCC link current;
- -/+ 50% step in the order of the CCC link current;
- -/+ 90% step in the AC voltage on the rectifier side;
- -/+ 90% step in the AC voltage on the inverter side.

The results obtained with the stability program (ANATEM), compared to those obtained with the ATP (Alternative Transients Program), are shown next.

### 3.6.1.1 -/+ 2% steps in the order of CCC link current

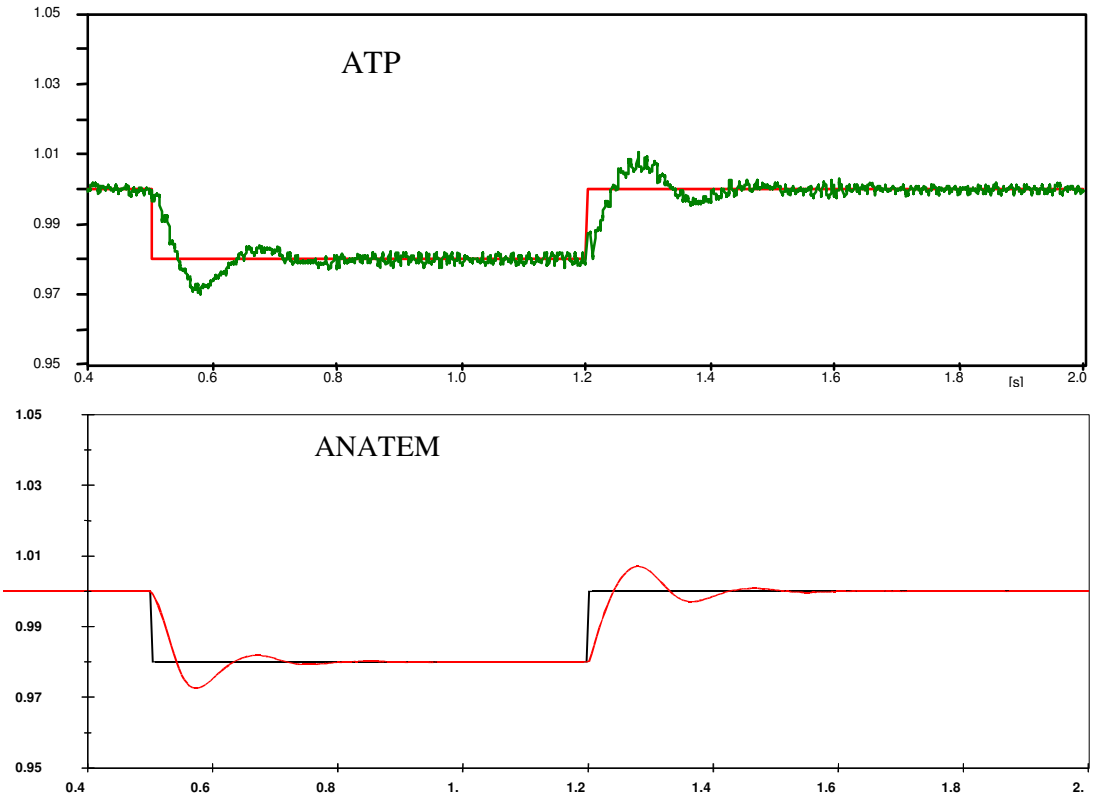


Figure 3.31 - DC current (pu)

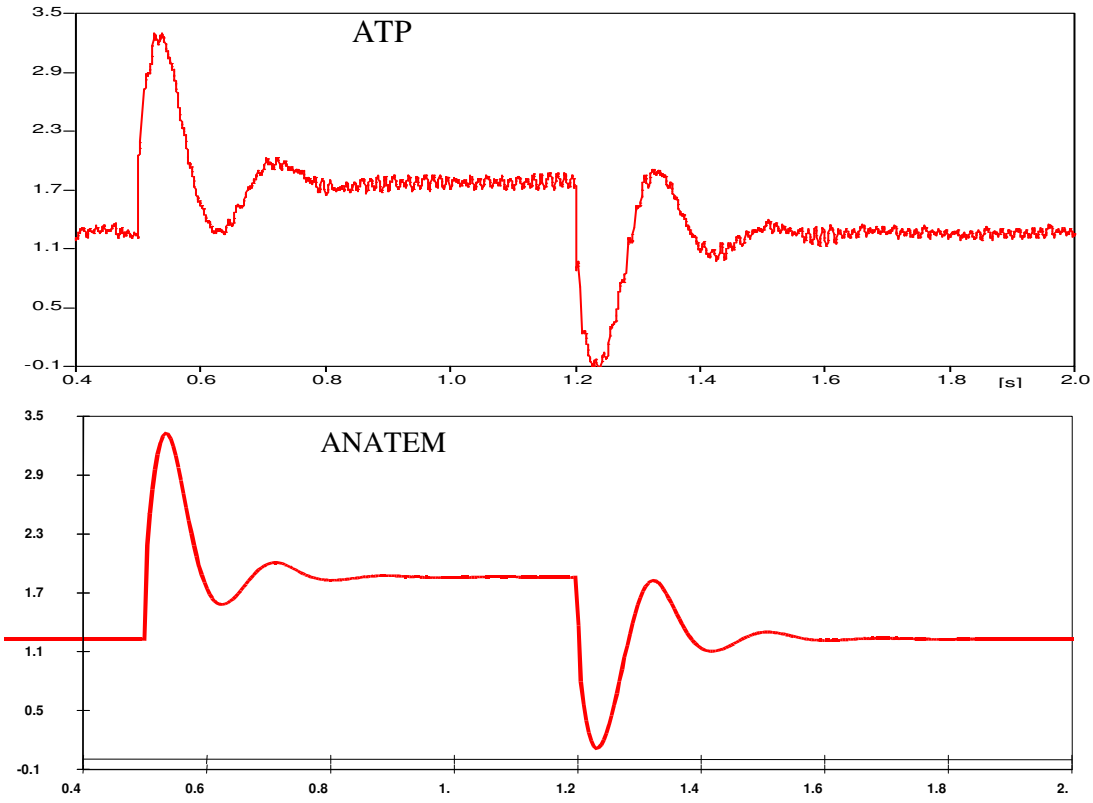


Figure 3.32 - Rectifier firing angle (α rect - degrees)

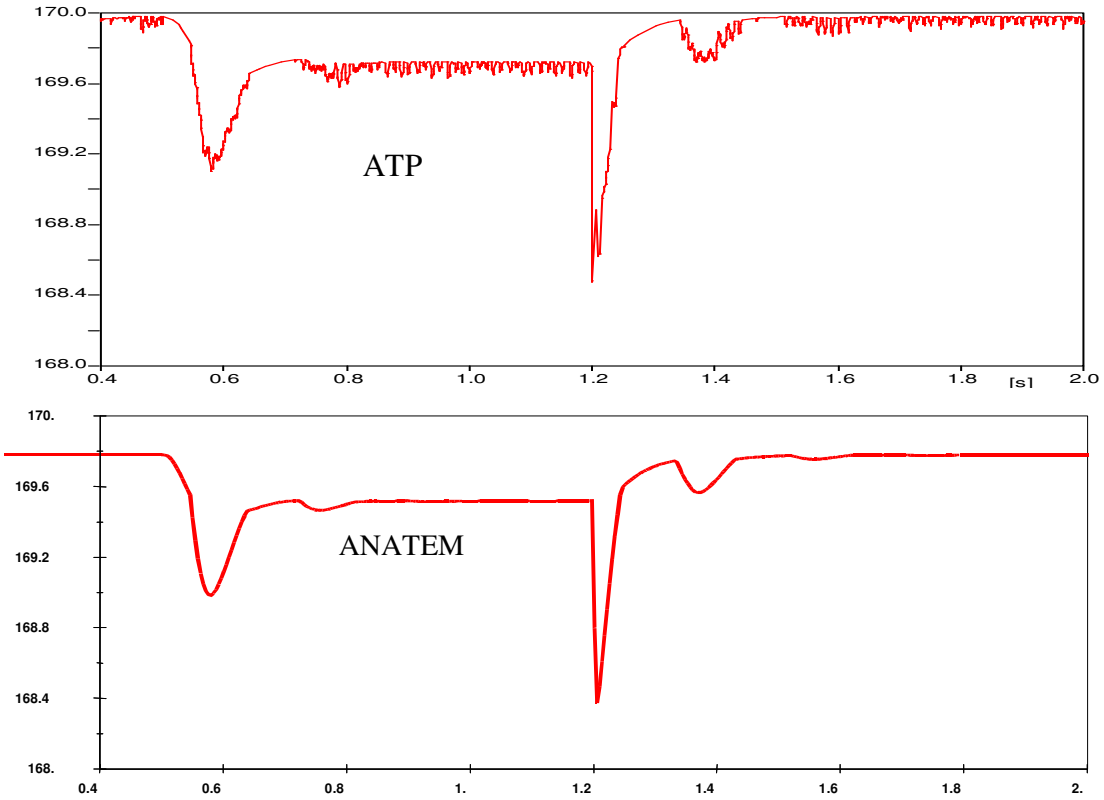


Figure 3.33 - Inverter firing angle (α inv - degrees)

### 3.6.1.2 -/+ 50% steps in the order of the CCC link current

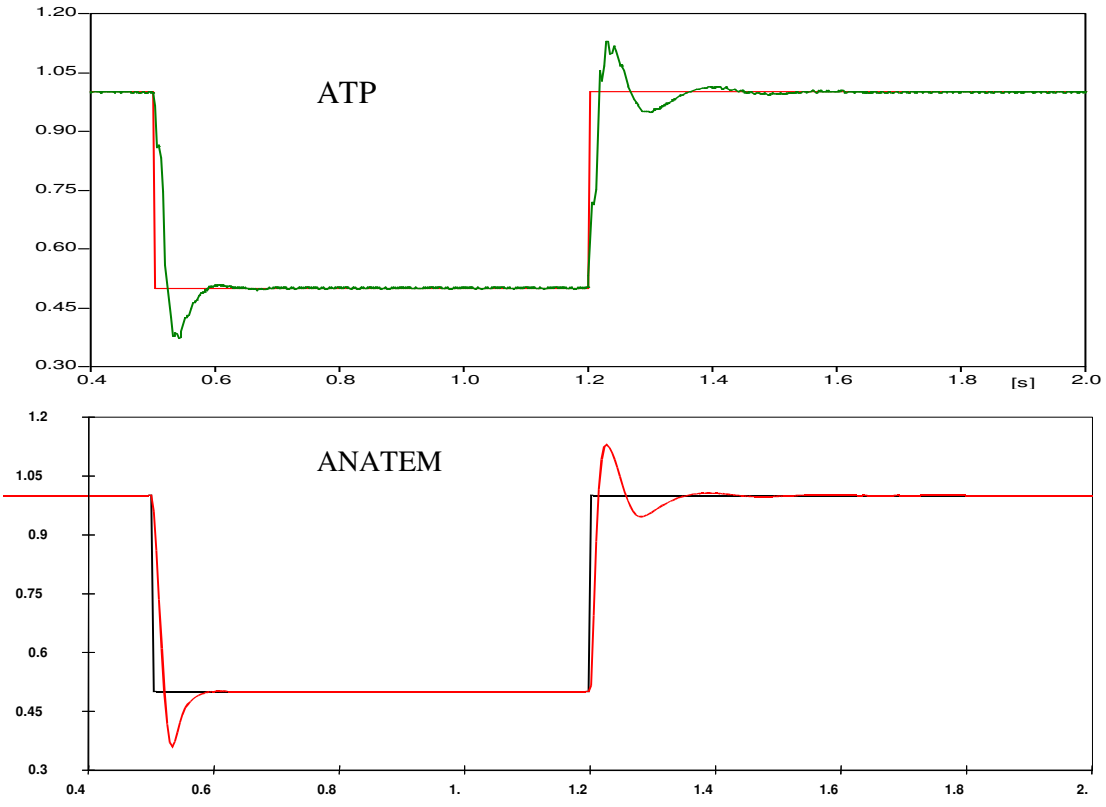


Figure 3.34 - DC current (pu)

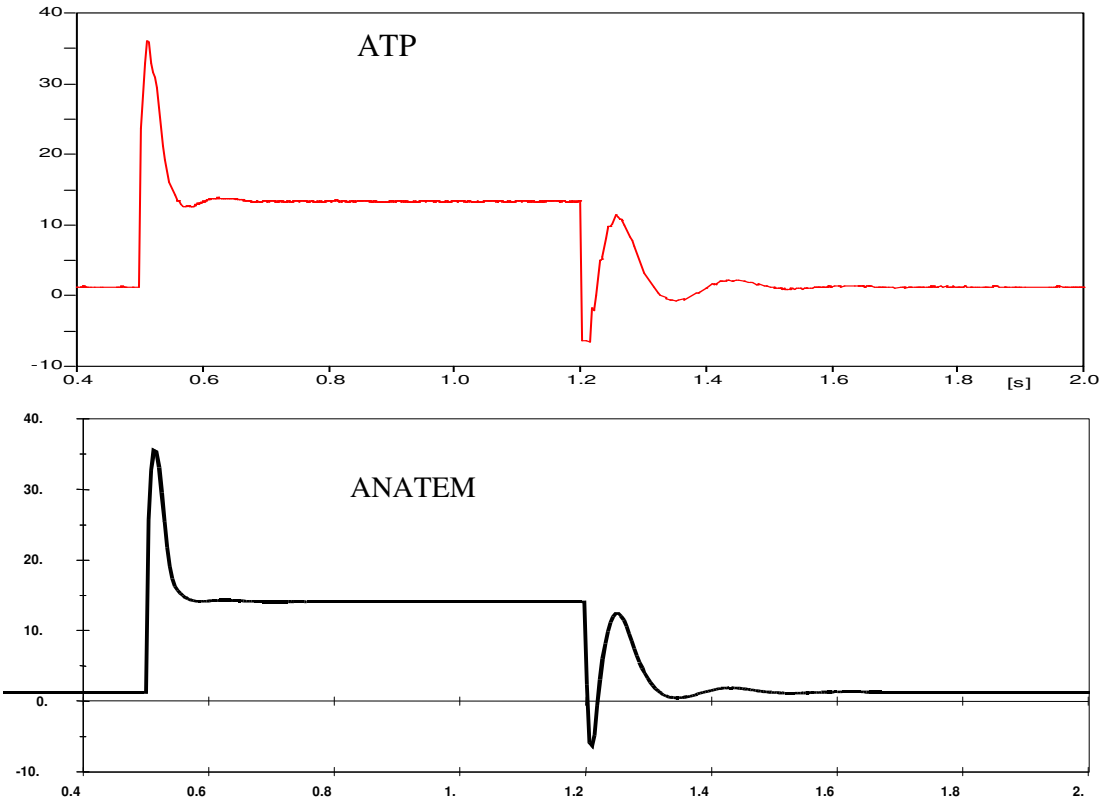


Figure 3.35 - Rectifier firing angle (α rect - degrees)

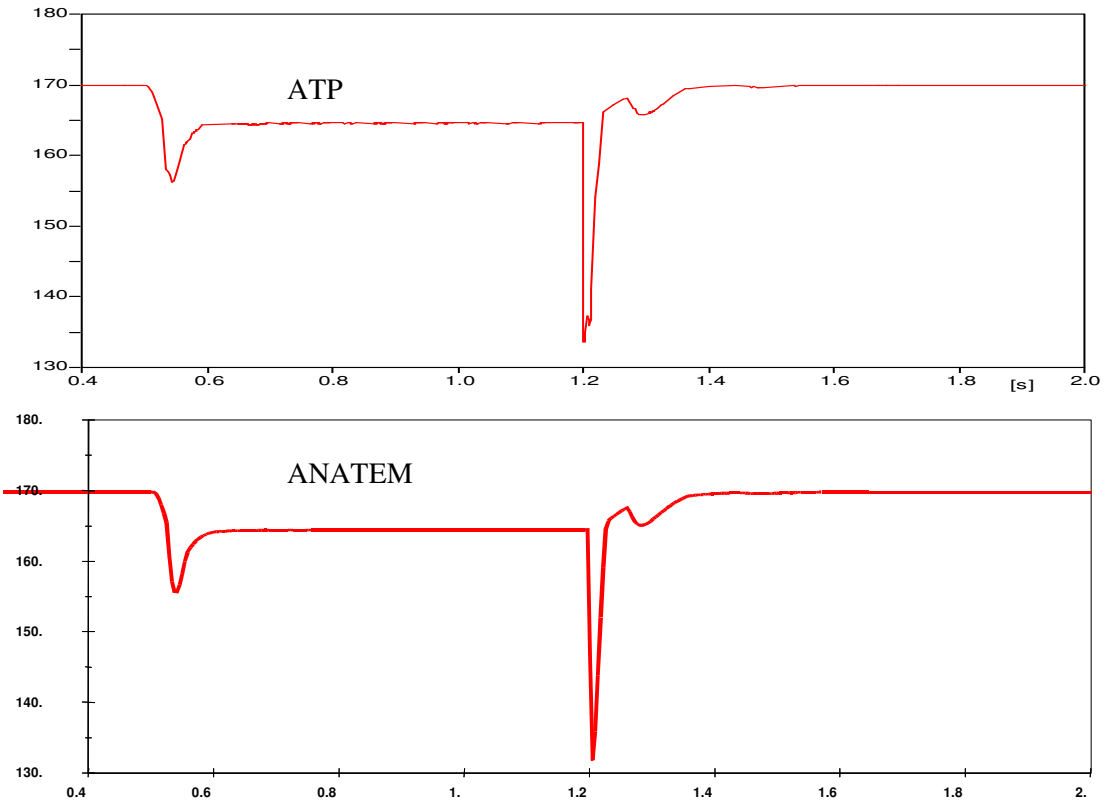


Figure 3.36 - Inverter firing angle (α inv - degrees)

### 3.6.1.3 -/+ 90% variation in rectifier AC voltage

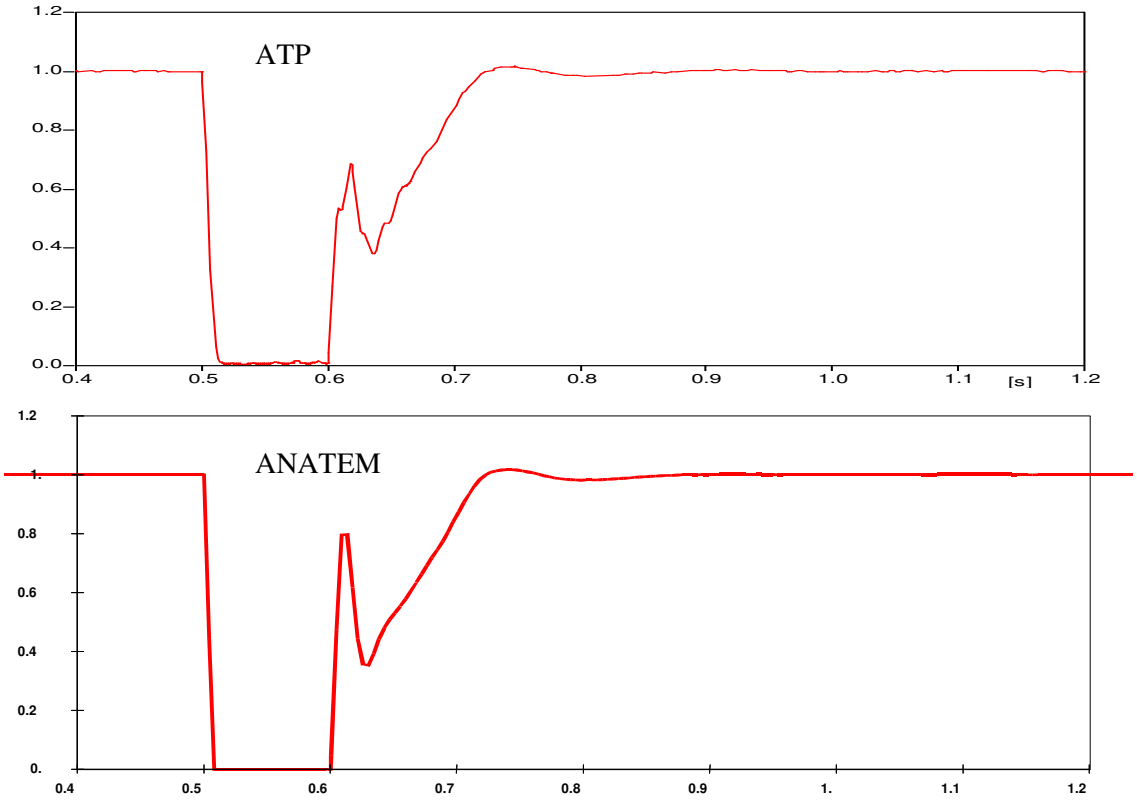


Figure 3.37 - DC current (pu)

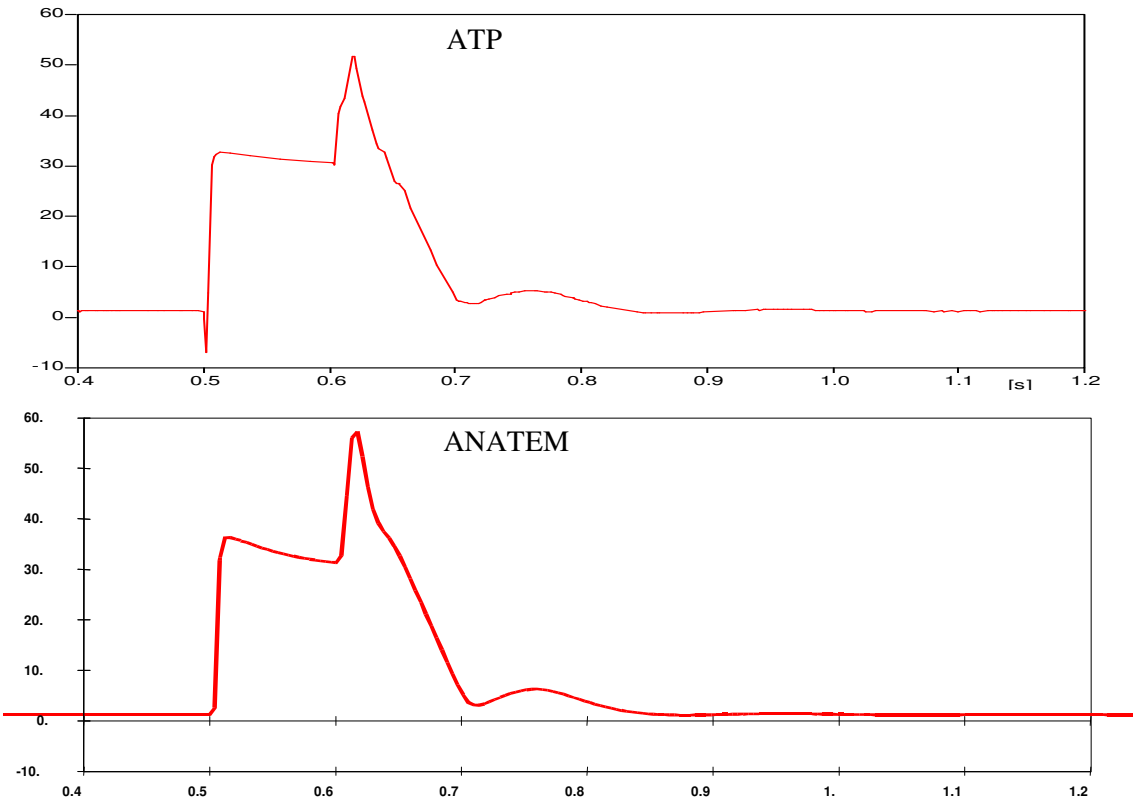


Figure 3.38 - Rectifier firing angle (α rect - degrees)

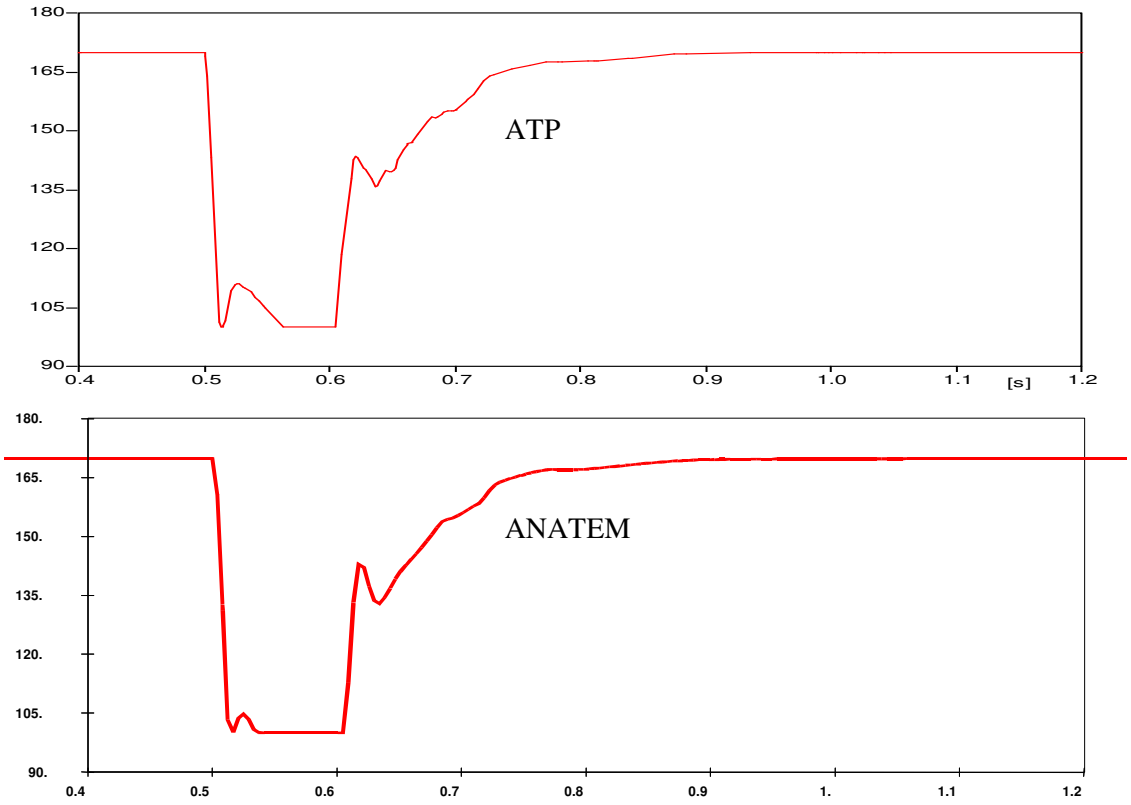


Figure 3.39 - Inverter firing angle (α inv - degrees)

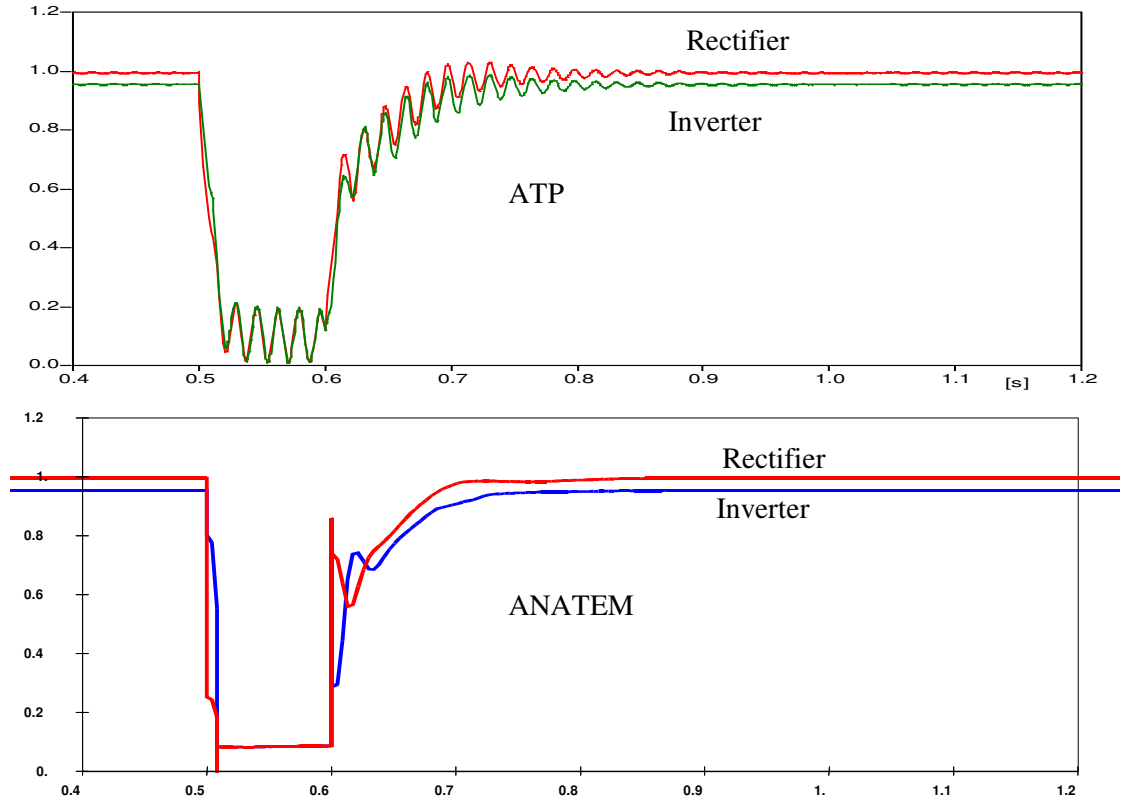


Figure 3.40 - DC Voltage at Rectifier and Inverter (pu)

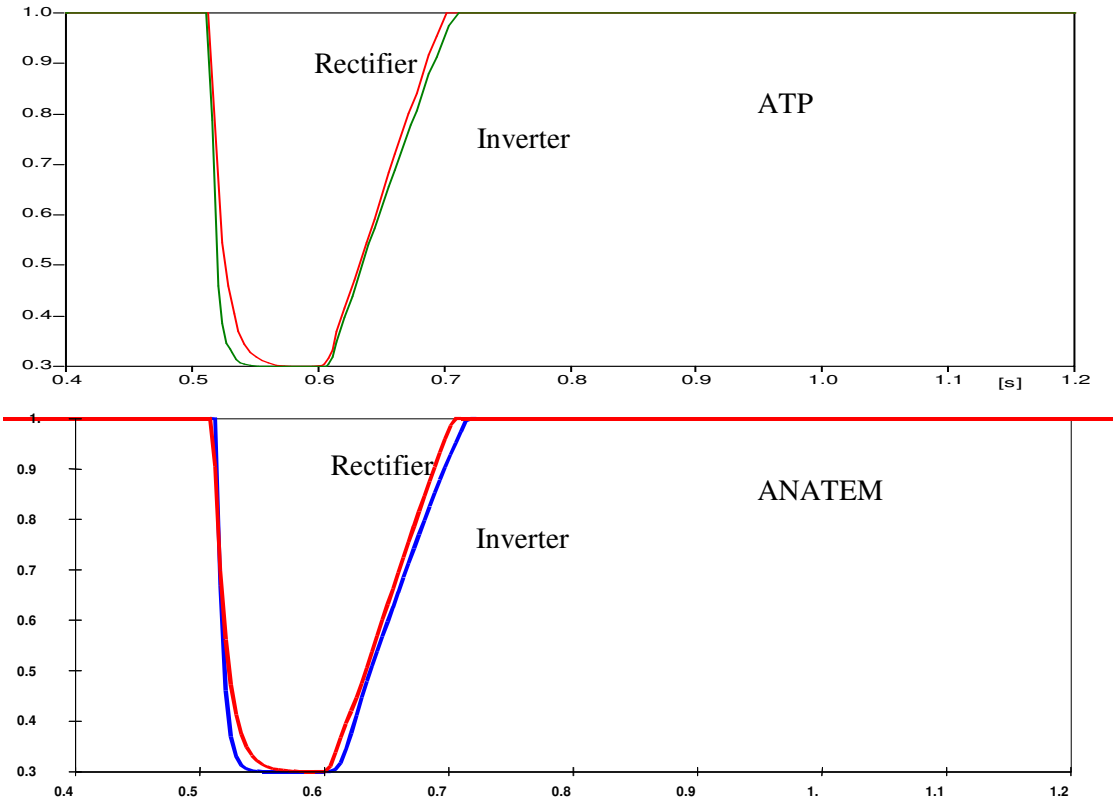


Figure 3.41 - Rectifier and Inverter VDCOL output (pu)

### 3.6.1.4 -/+ 90% variation in inverter AC voltage

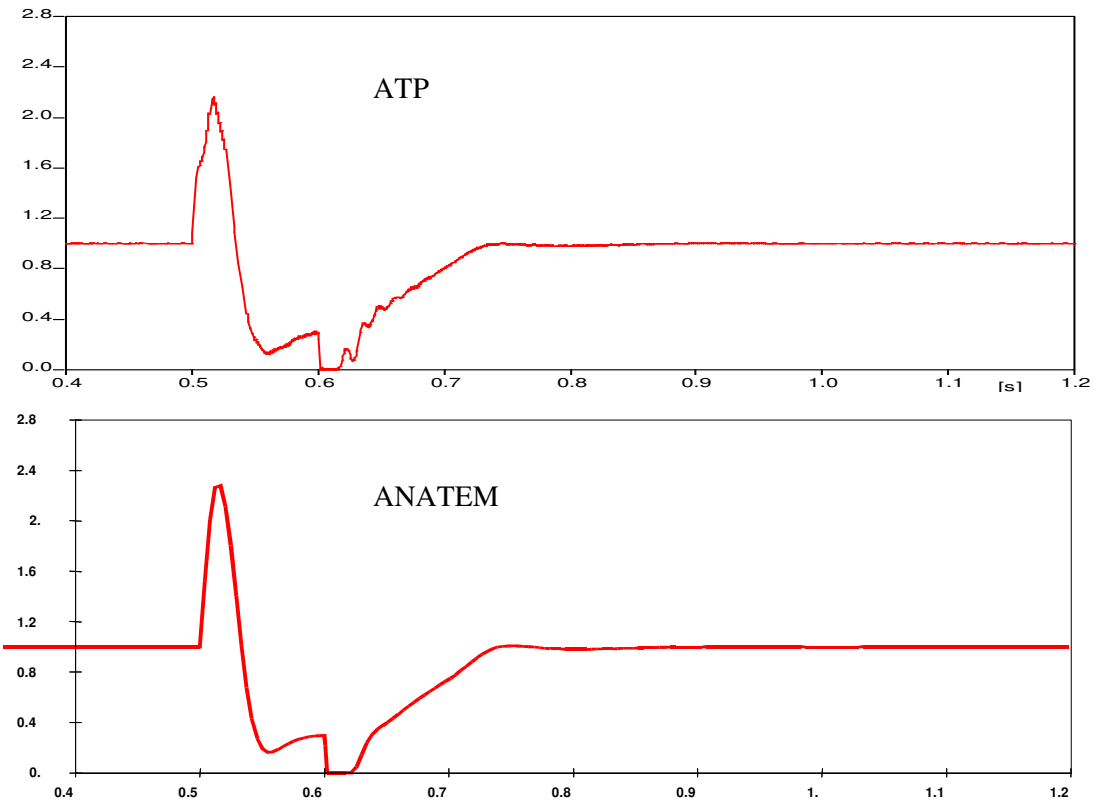


Figure 3.42 - DC current (pu)

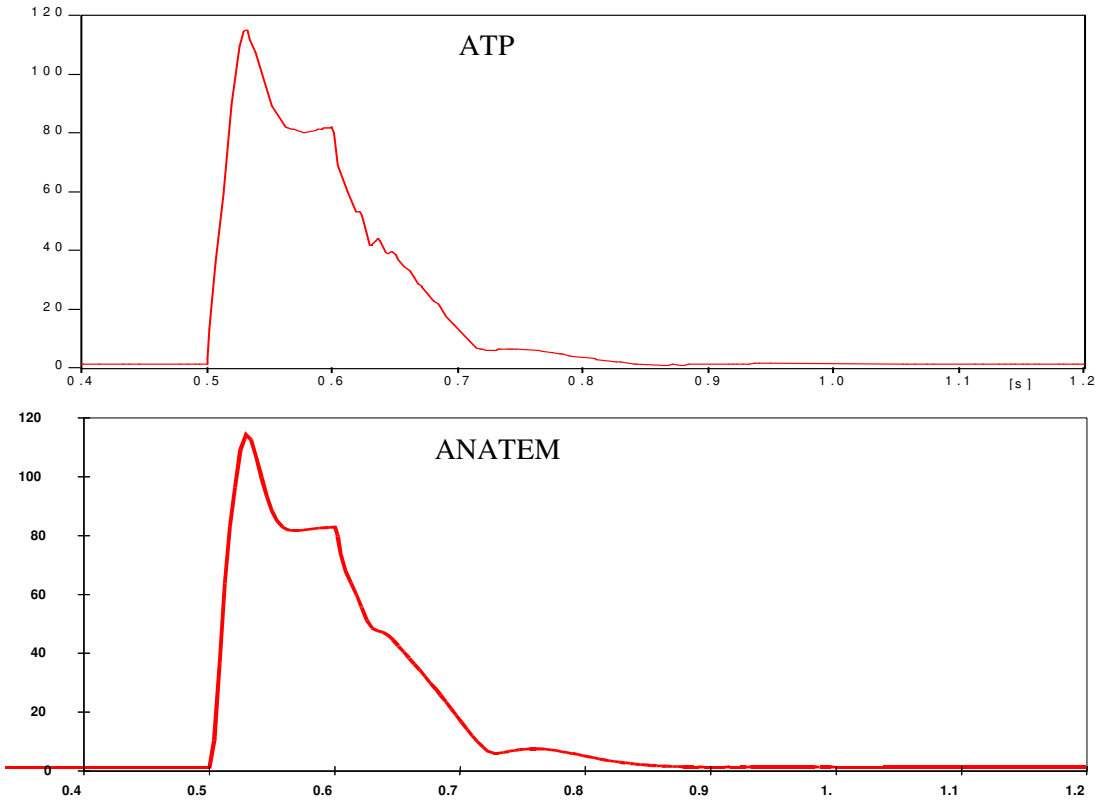


Figure 3.43 - Rectifier firing angle (α rect - degrees)

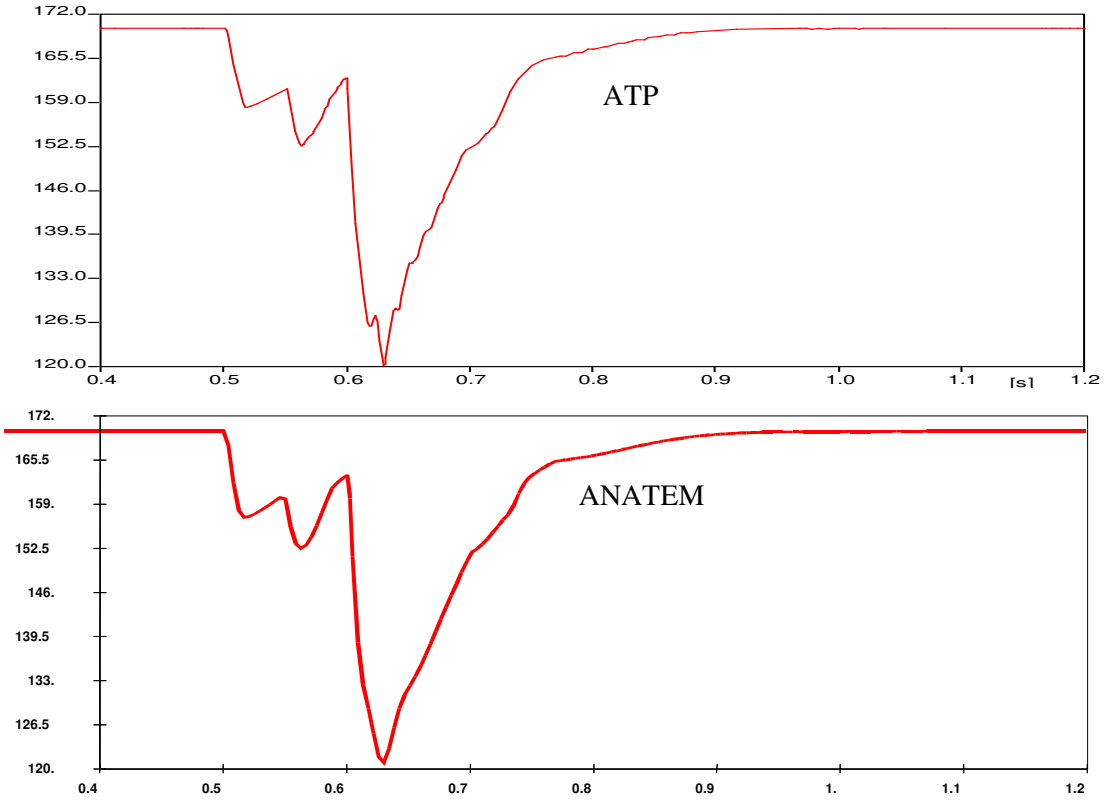


Figure 3.44 - Inverter firing angle (α inv - degrees)

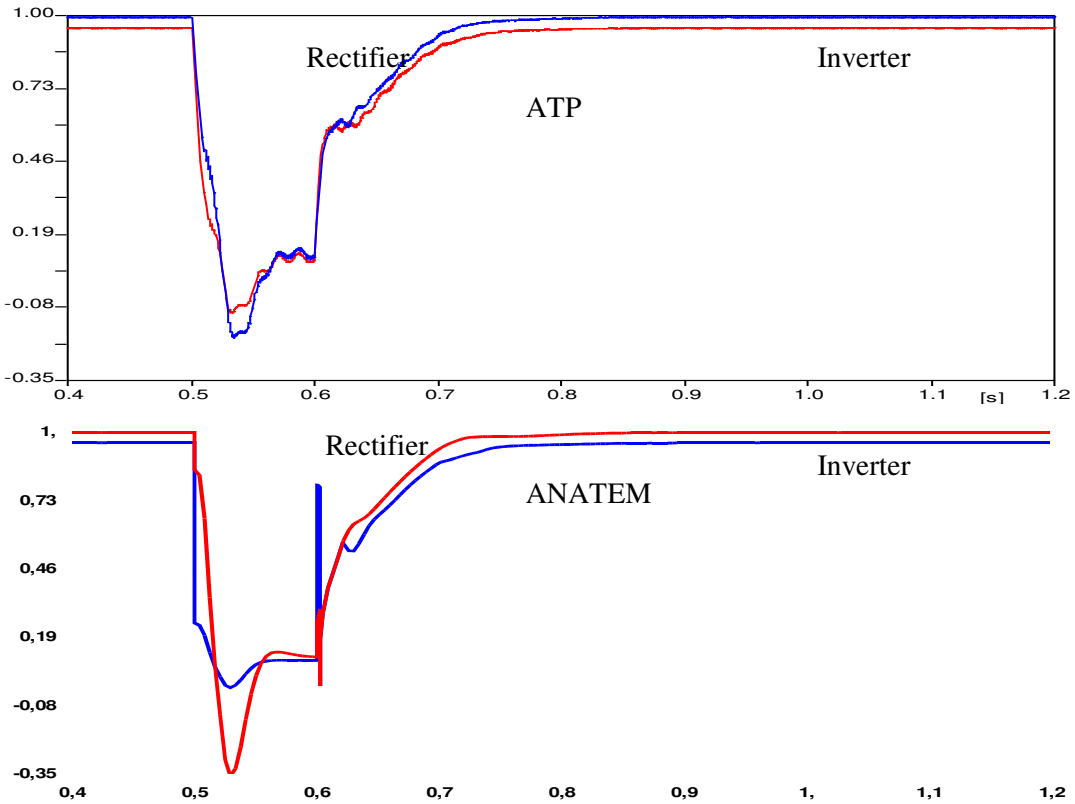


Figure 3.45 - DC voltage at Rectifier and Inverter (pu)

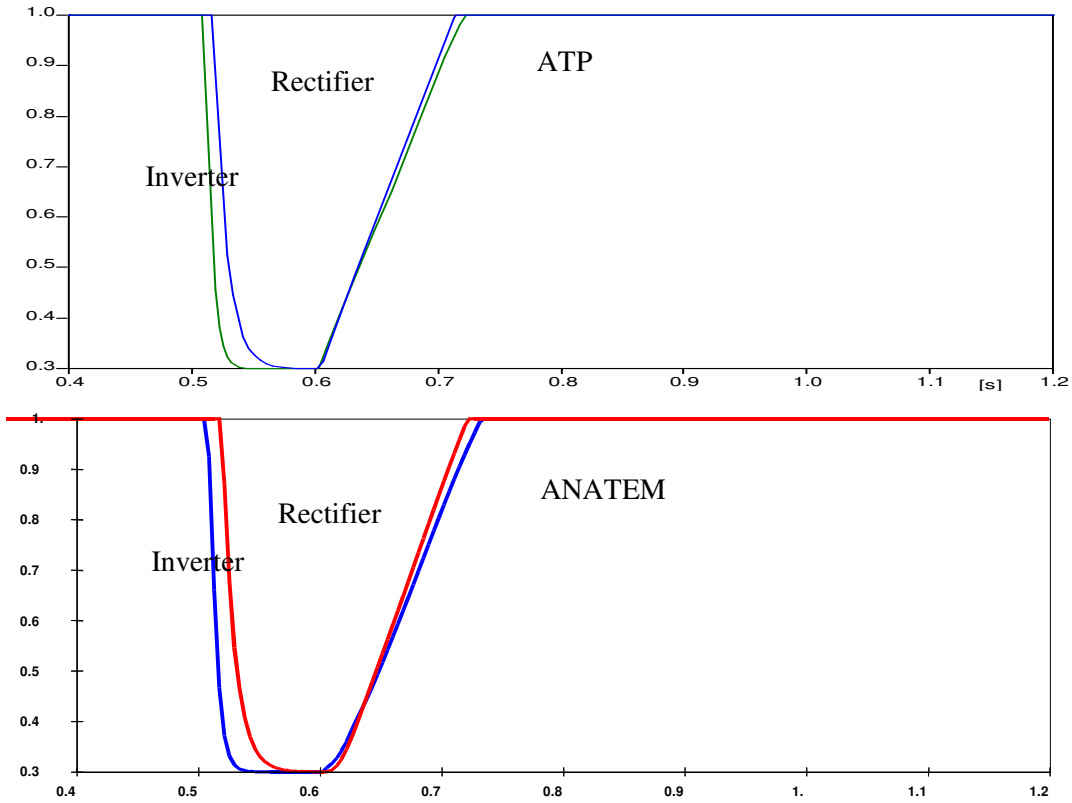


Figure 3.46 - Rectifier and Inverter VDCOL output (pu)

### 3.6.1.5 Analysis of the results of tests on System 1:

- The dynamic performance of the controls for the CCC link, represented in ANATEM, was very close to that obtained in ATP, thus indicating that the models developed for both analytical tools show compatible results, for variations in the current order and balanced variations in the AC voltage on the rectifier and inverter sides.

- In order that results from ANATEM and ATP should be compatible, it was necessary to replace the simpler VCO (Voltage Controlled Oscillator) model in ANATEM program, represented by a 1st order filter with a time constant of about 0.0014 s, by a more elaborate model, that took into consideration the variation of angular phase displacement of converter buses [22]. Figure 3.47 presents the block diagram of this new model, for representation in electromechanical stability programs.

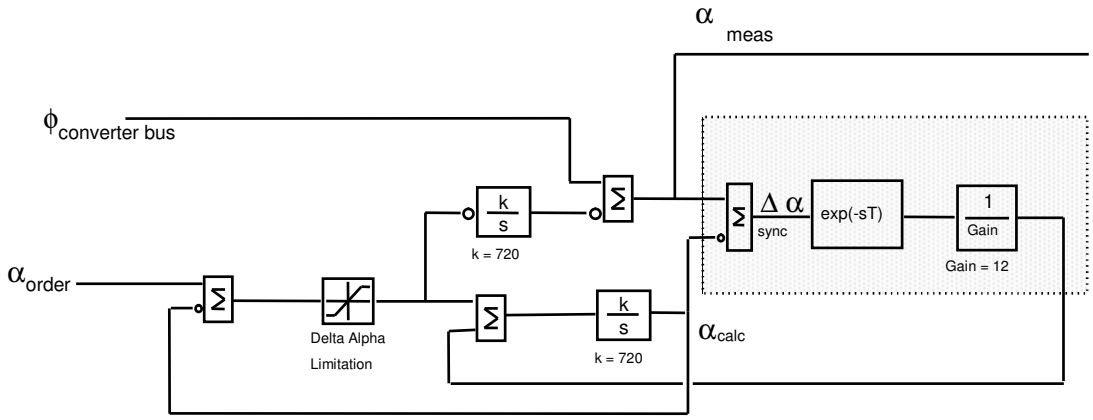


Figure 3.47 - Block diagram of the new model for VCO

# 4 THE PROPOSAL OF A BENCHMARK

Among the objectives of Working Group B4-34, of CIGRÉ Brazilian National Committee Study Committee B4, an outstanding one is the proposal of a benchmark circuit, which may serve as a reference for the study of converter stations utilizing the CCC arrangement.

In such context, the purpose of this chapter is to present the development of that benchmark circuit, characterized as follows.

*Equivalent Network:* The process of obtaining the benchmark circuit produced an AC equivalent network connected to the inverter terminal, with a total load of about 5000 MW, 4 generating units, 1 synchronous condenser and 12 transmission lines at 500 kV and 230 kV. For the AC system at the rectifier terminal, a simplification was made to the equivalent proposed for the inverter side, resulting in a network composed of 3 generating units and nine 500 kV transmission lines.

Further, in order to increase the degree of flexibility for the users, it was decided to develop a second, more simplified benchmark circuit, derived from the *Equivalent Network* and called *Simplified Network*. For this purpose, the transmission lines connecting the converter stations to the first next bus in the AC network were maintained, and equivalent circuits calculated at the fundamental frequency were connected to that bus.

With such procedure, the utilization of one or the other network is an option for the user, and depends on the purposes of his study.

In the scope of this Report, the *Equivalent AC Networks* (rectifier and inverter) were modeled only in the tools for analysis of steady-state and electromechanical stability (ANAREDE and ANATEM programs, both developed by CEPEL), while the *Simplified AC Networks* (rectifier and inverter), in addition to those programs, were also modeled in the electromagnetic transients programs ATP and PSCAD / EMTDC.

## 4.1 Premises for obtaining the benchmark model

The following features guided the definition of the AC networks which compose the benchmark circuit :

- Power transmitted by the DC link corresponding to 2000 MW.
- Considering that one of the main advantages of the CCC configuration is the application of HVDC converters in weak networks, it was sought to define the networks having approximately the following values of short-circuit ratio (SCR) at the HVDC link terminals:

  Rectifier: 1.7
  Inverter: 1.3

Since two reference networks are being proposed, it was deemed necessary that a minimum consistency be preserved between the dynamic behaviors of these *Networks* during the process of their development. Therefore, in addition to the description of the procedures involved in their definition, it was also attempted to present in this chapter the actions taken to assure such consistency.

Still, it should be noted that, purposely, there was no excessive concern in this chapter as to the optimization of the dynamic response of the HVDC/CCC link employed in the studies herein performed.

## 4.2 Systems connected to the AC buses of Converter Stations

### 4.2.1 Equivalent AC Networks

As a first step towards achieving the benchmark model, it was attempted to focus on the aspects directed to steady-state operation and to dynamic performance.

Taking into account the operating experience of the Garabi Back-to-Back Interconnection, located in the Southern Region of Brazil – which employs the CCC technology – the receiving system on the Brazilian side was used as an initial reference in this process; a few modifications were made to adapt it to the purposes of the work. Figure 4.1 presents a map of the system which was then used as a reference.

Initially, it was attempted to preserve some of the Region's main generating plants and transmission trunks. The representation of the Southeast System, connected to the Southern System mainly by 500 kV and 765 kV transmission lines, was very simplified. It was also attempted to fulfill the following requirements:

- Steady-state operation with voltages within acceptable limits, and power flows compatible with the transmission lines utilized.
- Compliance with the planned SCR values.
- Stable dynamic performance, with positive damping, during the occurrence of system disturbances.

A procedure based on the grouping of coherent machines was adopted, aiming to reduce system dimensions. It should be pointed out that there was no concern as to fully preserve the local modes of oscillation of the Southern System. Some adjustments to the controllers were made, in order to adapt the network to the purposes of this work, as indicated farther on.

This process resulted in an equivalent network, for the inverter side, with a total load of some 5000 MW, 4 generating units, 1 synchronous condenser and 12 transmission lines, at 500 kV and 230 kV. For the rectifier side, a simplification of the equivalent proposed for the inverter was made, obtaining a network composed of 3 generating units and nine 500 kV transmission lines.

The *Equivalent AC Networks* thus envisaged, as well as the adjusted power flow, are shown in Figures 4.2 and 4.3, for the inverter and the rectifier sides, respectively. It should just be noted that it was represented at the commutation buses, as a simplification, the net value of reactive compensation, i.e., AC filters minus shunt compensation of the transmission lines converging to those buses. The amount of AC filters is 280 Mvar per terminal. The data utilized for the power flow adjustment are found in Table H.1 and Table H.2 in the Annex H.


Figure 4.1 – Map of Brazil's Southern Region electrical system

*500 kV lines*

*230 kV lines*

*138 kV lines*

*Garabi Back-to-Back connection point*

*Hydroelectric plants*

*Thermoelectric plants*

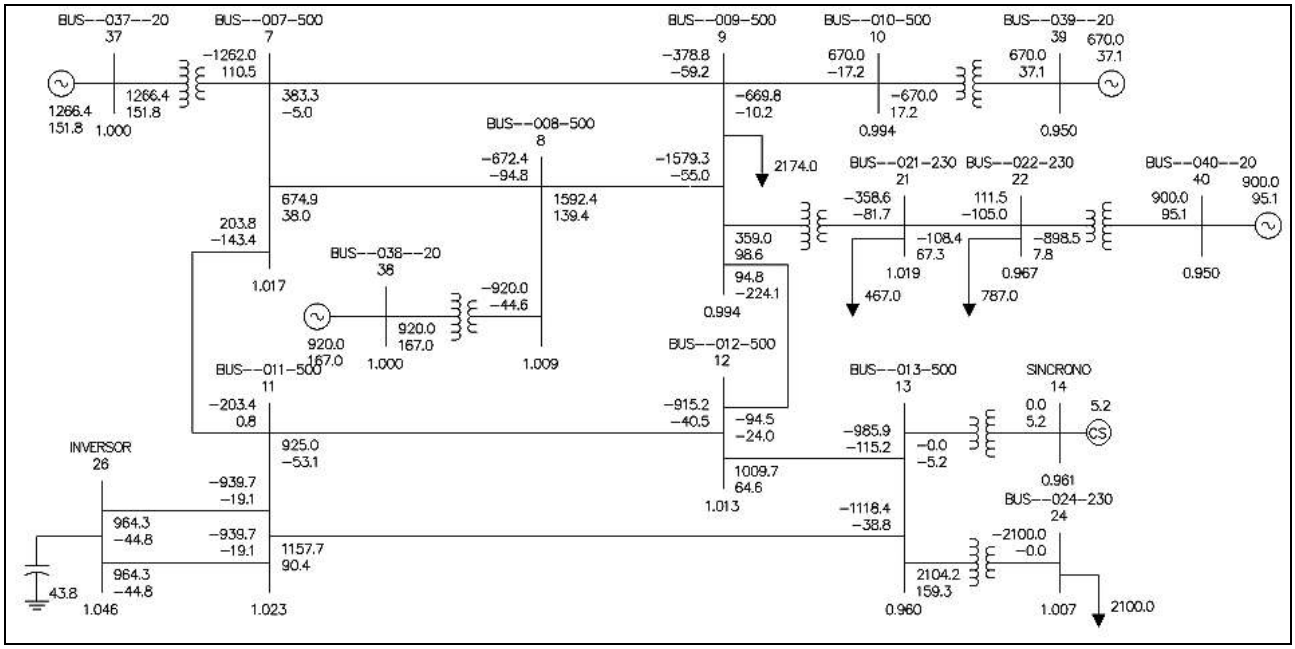


Figure 4.2 – Power flow adjusted on the *Equivalent Network* (inverter AC network)

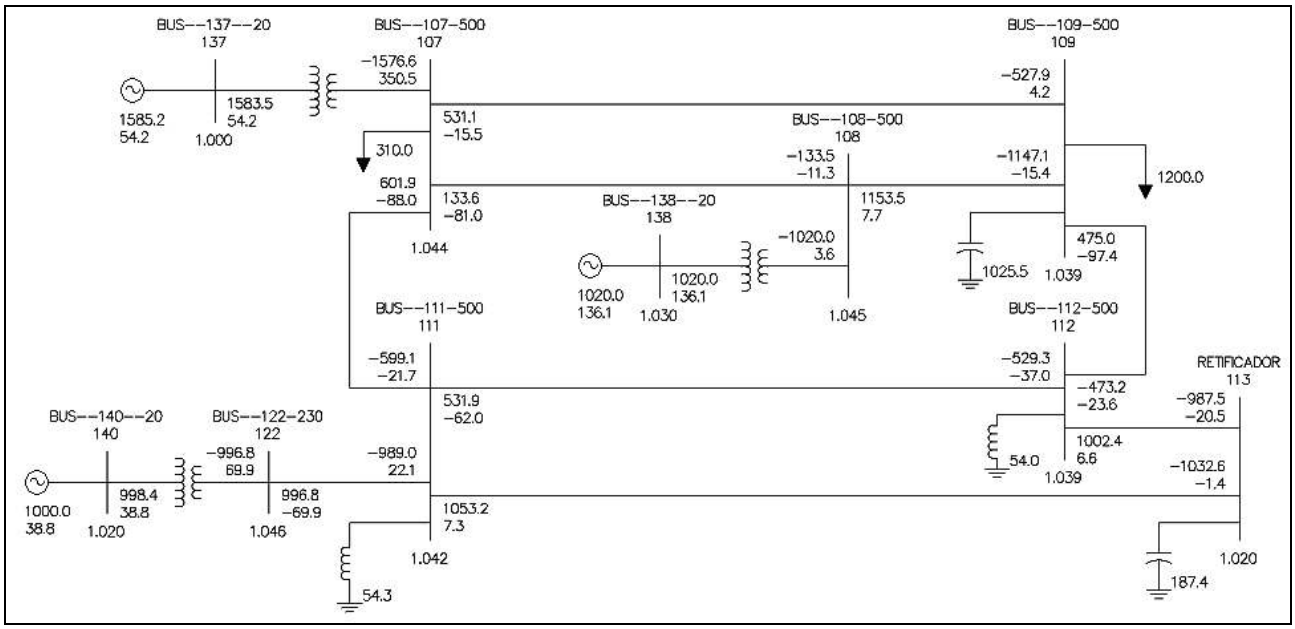


Figure 4.3 – Power flow adjusted on the *Equivalent Network* (rectifier AC network)

Still associated to the *Equivalent Network* design procedure, for what concerns issues related to electromechanical stability, and for purposes of machine grouping, dynamic performance evaluations were performed. These simulations had also the purpose to promote the adjustment of machine regulators parameters, in order to provide the system with a damped behavior. Having in mind the purpose of the benchmark, the degree of damping was not optimized for all the generators, in order to maintain potential sources of disturbances in the network.

Several simulations were carried out, comprising the application of different disturbances. The loads were modeled by constant impedances, and some of the results obtained are pointed out below.

The data required to carry out these simulations are present in the Table H.3 to Table H.7 in the Annex H. The models and the corresponding adjustments of synchronous machines regulators are also included in the Figure H.1 to Figure H.3 in the Annex H.

The CCC data model and the associated controller parameter are presented respectively in the Table H.8 and Table H.9 in the Annex H. The associated controllers of the and rectifier inverter are presented respectively in the Figure H.4 and Figure H.5 of the Annex H.

Figures 4.4 (a), (b) and (c) present the behavior of the *Equivalent Network* for the full blocking of the HVDC link. Figure 4.4(a) shows the frequency in the inverter and rectifier AC networks. On the inverter side, a significant reduction of the frequency in relation to its rated value is observed, followed by its recovery. In the rectifier terminal AC network, the overfrequency attains 62.3 Hz.

In the inverter AC network, an oscillatory behavior at a frequency of 0.6 Hz stands out, with low damping, between the machine connected to bus #40 and machine #37 (taken as a reference), as shown in Figure 4.4(b), which presents the angular variation between them. On the rectifier side, these variations are much smaller (the machine connected to bus #137 was taken as a reference).

Figure 4.4(c) depicts the power generation of each machine on the inverter side. Low-damped oscillations are observed. Machines #37, #38 e #39 do so in a coherent manner, in phase opposition to machine #40.

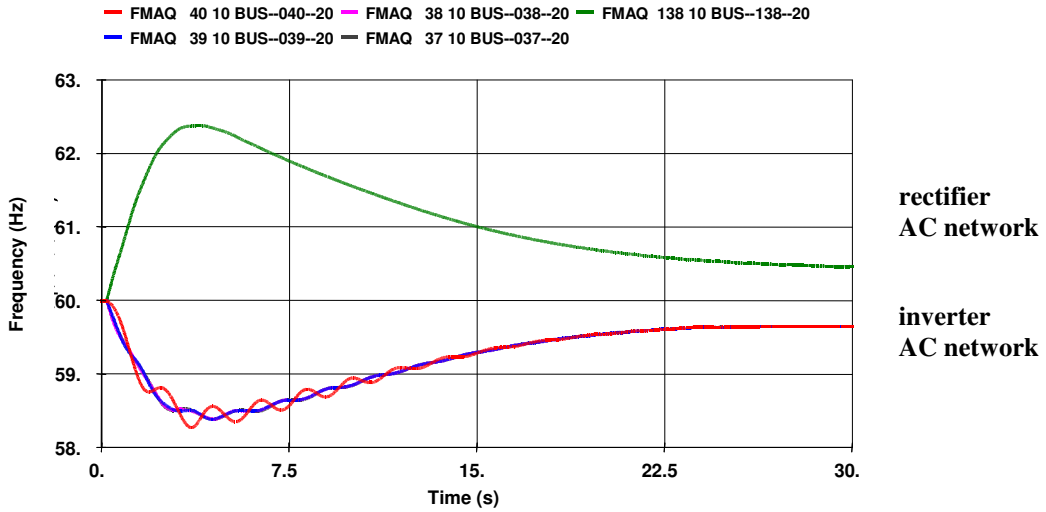


(a) Frequency of the machines in the rectifier and inverter AC networks

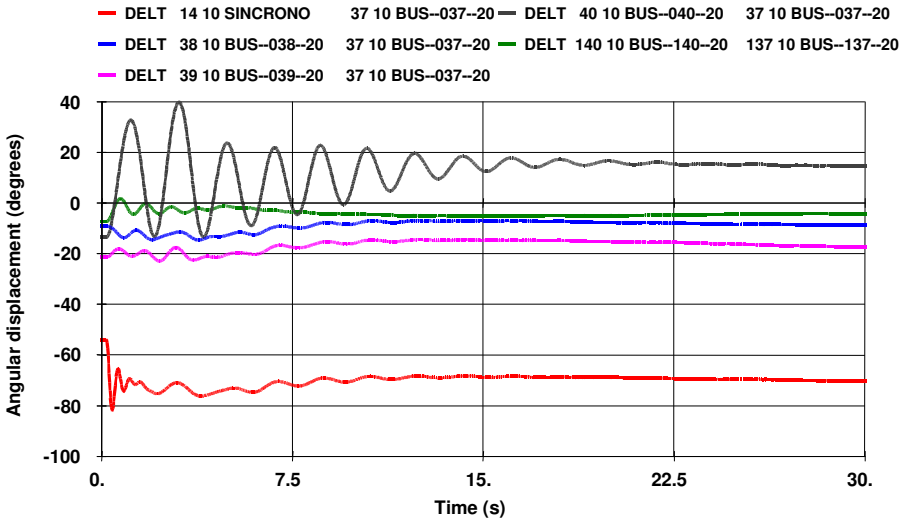


(b) Angular displacements between machines (rectifier and inverter AC networks)

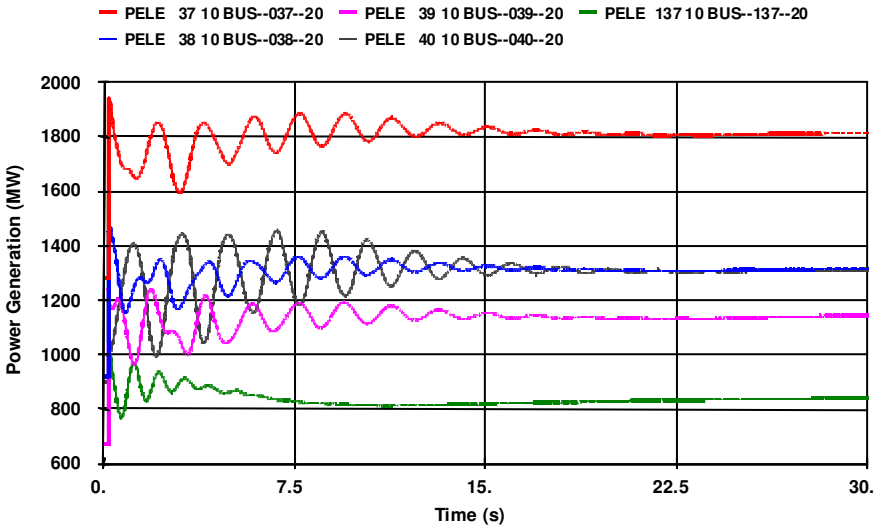


(c) Machines Power generation

Figure 4.4 – HVDC link full blocking

Another simulation was performed, considering the application of a solid three-phase fault, for 100 ms, on #11 bus of the inverter AC network. In this case, frequency variations in the AC network were not relevant. Figures 4.5 (a), (b) and (c) present other quantities of importance for the analysis of the *Equivalent Network* faced by that disturbance.

In Figure 4.5 (a), angular displacements may be noted, of the machines in the inverter AC network, in relation to machine #37, and between machines #138 and #137, on the rectifier side. Except for the synchronous condenser connected to bus #14, the other machines do not present significant oscillations. On the rectifier side, these variations have smaller amplitudes. Figure 4.5(b) indicates the machines power generation on the rectifier and the inverter sides. As a result of the disturbance, significant oscillations are observed, but they tend to be damped quickly. Figure 4.5(c) shows the behavior of voltages at several buses of the rectifier and of the inverter AC networks. After fault extinction, machines power generation and bus voltages both return to their original values.

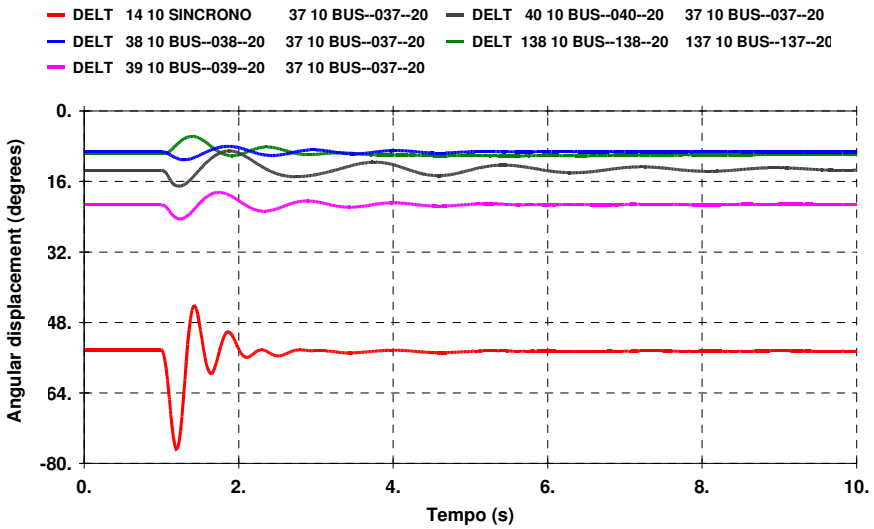


(a) Angular displacements between machines (rectifier and inverter AC networks).

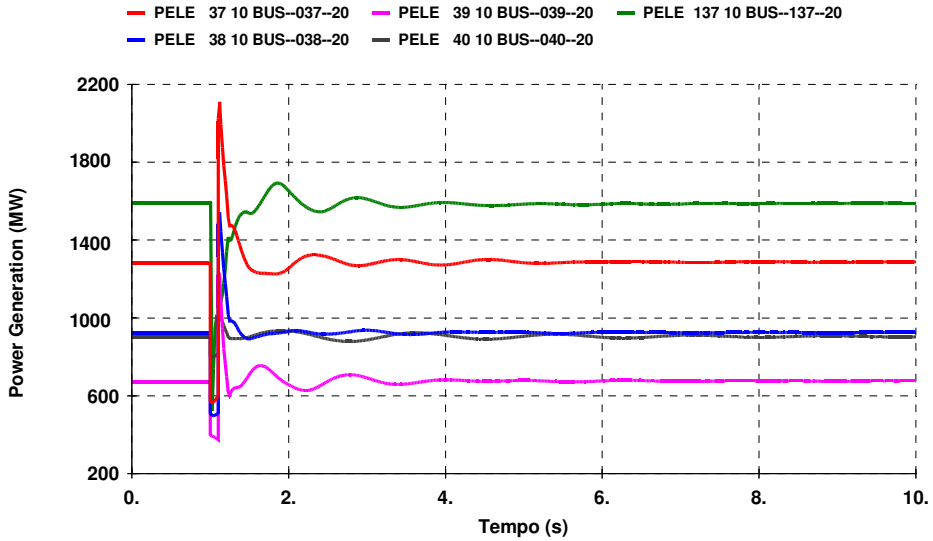


(b) Machines Power generation of in the rectifier and inverter AC networks

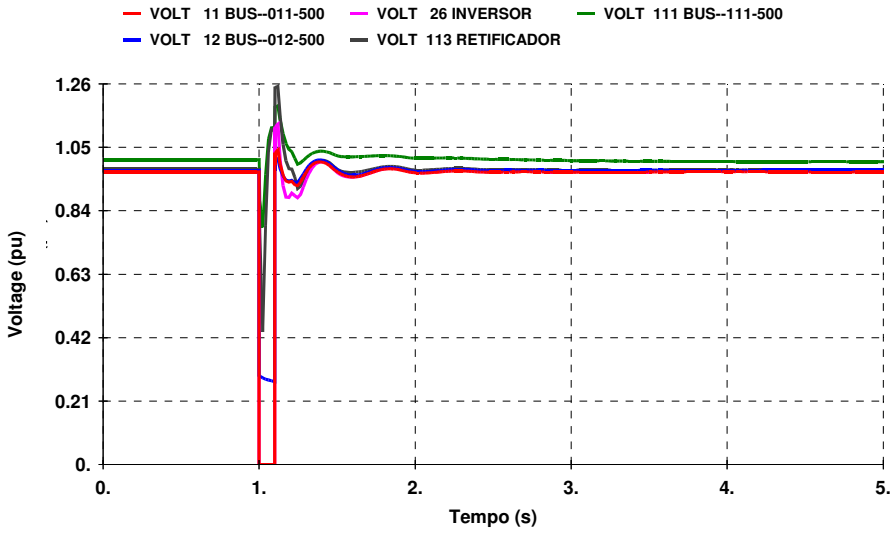


(c) Voltages in the rectifier and inverter AC networks

Figure 4.5 – Three-phase solid fault, during 100 ms, at bus #11 of inverter AC network

Also, a solid three-phase fault was applied for 100 ms, at bus #112 of rectifier AC network. The behavior of the *Equivalent Network* is illustrated in Figures 4.6 (a), (b) and (c).

Figure 4.6 (a) indicates the behavior of the DC power, measured at the rectifier terminal, and the curves of reactive power consumption of rectifier and inverter. Figure 4.6 (b) shows the firing angles at the rectifier ($\alpha$', $\alpha$), and the extinction angles at the inverter ($\gamma$).

In Figure 4.6 (c), it may be observed the angular displacements of machines in the inverter AC network, in relation to machine #37, and of those of the rectifier AC network in relation to machine #137. Again, the machine connected to bus #40 presents a low-damping oscillatory behavior. On the rectifier side, these variations have smaller amplitude.

In this case, AC network frequency variations were not significant.

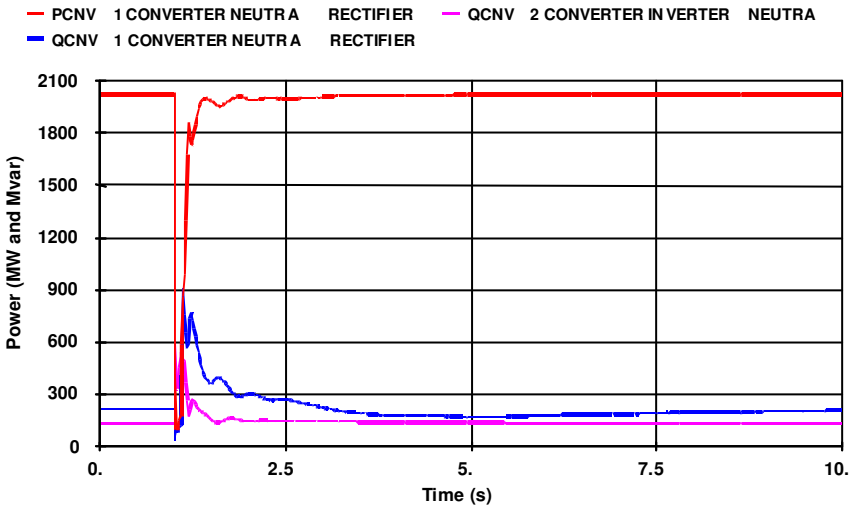


(a) DC power at rectifier and Reactive power consumption in the converters

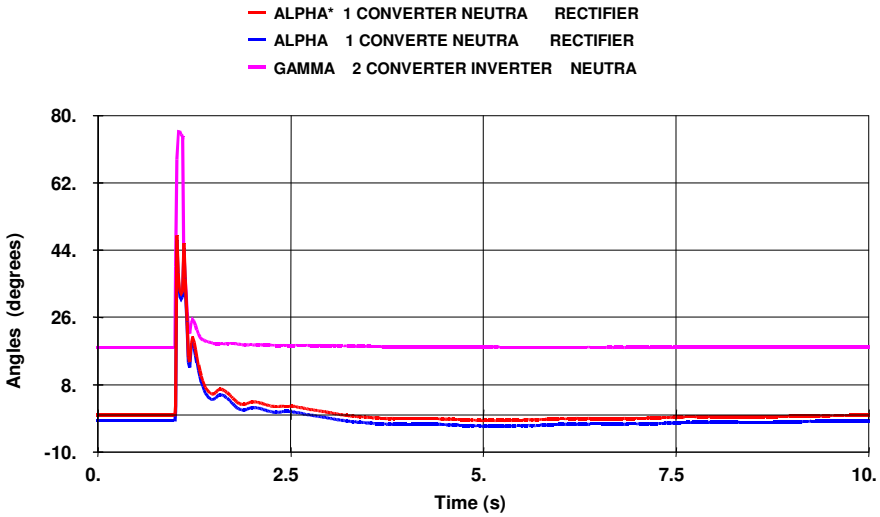


(b) Firing angles at rectifier (α', α) and extinction angles at inverter (γ)

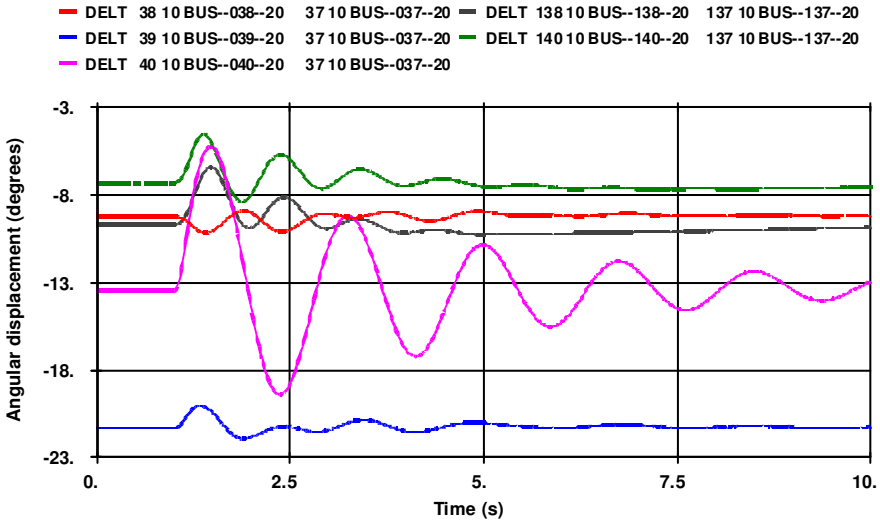


(c) Angular displacements between machines (rectifier and inverter AC networks)

Figure 4.6 – Three-phase fault, during 100 ms, at bus #112 of rectifier AC network

### 4.2.2 Simplified AC Networks

Besides having defined the *Equivalent Network*, as previously presented, a more reduced model, called *Simplified Network*, was also conceived.

In an initial stage, very simplified AC systems were considered, both at rectifier and inverter terminals, composed only of equivalent impedances as seen from the converter buses, complying with the premises defined in item 4.1. In the electromagnetic transients programs, however, such equivalents proved to be inadequate because the system presented, during recovery after disturbances, inrush currents in the inverter converter transformers which, despite their relatively low values, were sufficient to cause the appearance of commutation faults. These faults were avoided by the implementation of a control action, which resulted in a delay of the link recovery, thus significantly impairing its performance. However, when the transmission lines connected to the converter station buses were included – that is, making the connection of the equivalents of AC systems to a subsequent bus – those currents did not appear any longer. Annex E presents the results processed in the EMTDC/PSCAD program, in which this analysis was made.

In brief, the following procedure was adopted:

- Transmission lines connecting the converter stations to the next bus were preserved (bus # 11 on the inverter side, buses #112 and #111 on the rectifier side).
- The equivalents calculated at the fundamental frequency were connected to these border buses.
- In a first stage, constant-amplitude ideal voltage sources were connected to the equivalents. Later on, the dynamic representation of the equivalent machines was added.

Then, using ANAREDE program, the respective power flow adjustments were made to both AC networks, so that they should keep similarity to the adjustment adopted in the *Equivalent Network*. Figure 4.7 presents the single-line diagrams of the *Simplified Networks* for the rectifier and for the inverter, in which it is outlined (dashed lines) the position of the equivalents which were then calculated. In Tables H.10 and H.11 of Annex H the listing with the respective data is presented.

The procedure adopted for the calculation of the equivalent circuits, as well as the values obtained for the same, are outlined in item 4.3.

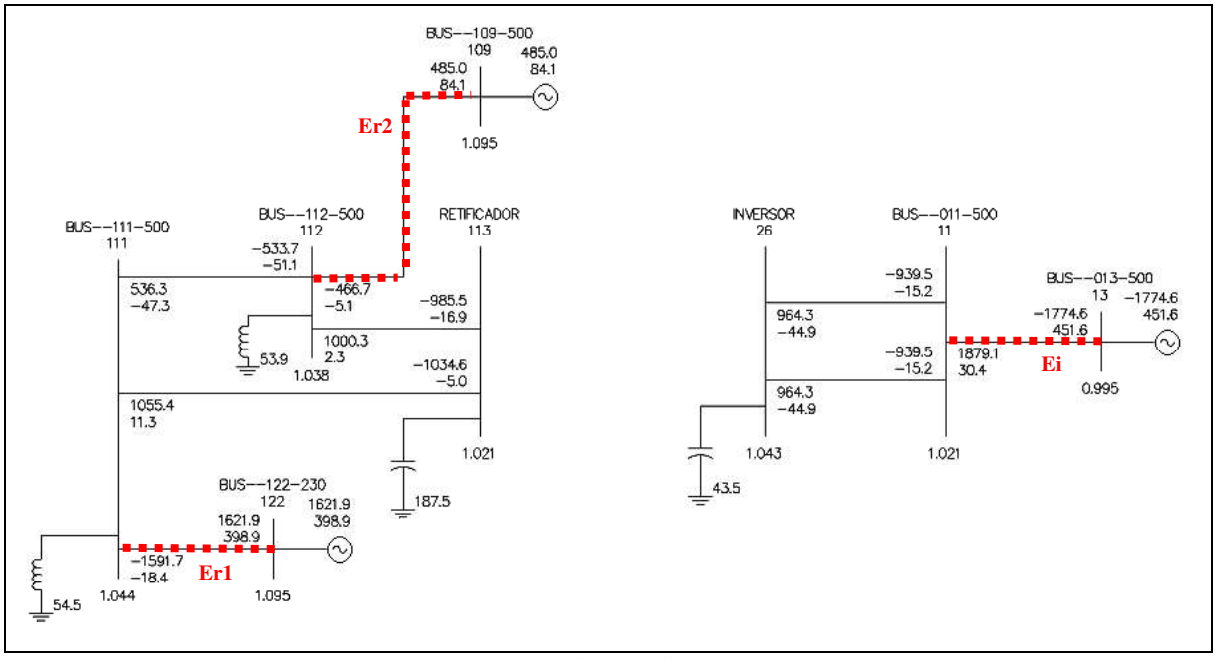


Figure 4.7 – Power Flow adjusted for the *Simplified Network*

### 4.2.3 Short-circuit Ratios

The results of the calculations of short-circuit capacities at the commutation bars of both converters are listed on Table 4.1, indicated in terms of *Short Circuit Ratio* (SCR) as well as in those of *Effective Short Circuit Ratio* (ESCR). These values are very close for the *Equivalent* and for the *Simplified Network*, and are approximately equal to those initially planned.

Table 4.1 – Short-circuit ratios at the converters commutation buses

| SYSTEM | SCR Planned Values | SCR Obtained Values | ESCR Obtained Values | THREE-PHASE SHORT-CIRCUIT CAPACITY (MVA) |
|---|---|---|---|---|
| Inverter | 1.30 | 1.42 | 1.28 | 2840. |
| Rectifier | 1.70 | 1.86 | 1.73 | 3710. |

The principal qualitative information expected to be obtained from those two indices regards the relation between the robustness of the AC system and the anticipated performance of the HVDC link. Whereas the SCR mirrors the relationship between the short-circuit capacity at the commutation bus and the DC power, in the calculation of the ESCR the AC filter power is deducted from the short-circuit one. As the amount of AC filters is usually much smaller in CCC configurations than in the case of conventional converters, the SCR and ESCR for this new type of converter will then take values close one to the other. In order to evaluate the consequences of this evidence, a sensitivity analysis was performed.

Table 4.2 is an example of a first comparison between those two indices, for the same AC network at the inverter, assuming the use of a link in two converter configurations: conventional and CCC. It is noted that, while the values of ESCR indicate that the HVDC link in the conventional configuration should present greater difficulty for its performance, if compared to the CCC configuration, the values of SCR point to very similar performances. At first sight, this indicates that the ESCR supplies more adequate information, since a better performance is expected with the CCC arrangement.

Table 4.2 – Short-circuit ratios at the inverter commutation bus

| CONFIGURATION | SCR | ESCR | THREE-PHASE SHORT-CIRCUIT CAPACITY (MVA) |
|---|---|---|---|
| Conventional | 1.42 | 0.92 | 2840. |
| CCC | 1.42 | 1.28 | 2840. |

Considering that, in order to have similar performances, the SCR for the conventional configuration should be greater than that for the CCC configuration, Table 4.3 shows a second example where, taking respectively the values of 1.78 and 1.42 for the SCR, the same value of 1.28 is obtained for the ESCR. Under these conditions, it is again noted that the ESCR would indicate a similar performance for both configurations.

Table 4.3 – Short-circuit ratios at the inverter commutation bus

| CONFIGURATION | SCR | ESCR | THREE-PHASE SHORT-CIRCUIT CAPACITY (MVA) |
|---|---|---|---|
| Conventional | 1.78 | 1.28 | 3560. |
| CCC | 1.42 | 1.28 | 2840. |

These examples indicate that, in a preliminary analysis for comparison of the expected performance of HVDC systems utilizing conventional and CCC configurations, if only short-circuit ratios are considered, the ESCR is a more adequate index than the SCR.

## 4.3 Modeling in the Programs PSCAD/EMTDC and ATP

In order to analyze the performance of the HVDC/CCC link, the work was begun by modeling, in the PSCAD/EMTDC program, the *Simplified AC Networks* of rectifier and inverter, the DC line, the DC filters and the smoothing reactors, the converter transformers of the valves, as well as a basic control. After adjusting that control and implementing some additional controls, a satisfactory recovery performance of the link was obtained, under several fault conditions, both in the rectifier and in the inverter. Next, the whole set was modeled in the ATP program, utilizing for the representation of controls both TACS and MODELS routines (facilities existing in the ATP program, for modeling control systems). Finally, the results obtained from those programs were compared, as presented in Annex D. The option for the implementation in the ATP program was made because it is a free program and, therefore, of more widespread use, making the benchmark representation available to a greater number of users.

### a) The DC Bipole

The DC bipole, composed of a 2-pole line, with 4 sub-conductors, 1351 MCM each, with a total length of 1000 km, was modeled in both programs considering its electric parameters to be frequency-dependent. In Table H.17 (Annex H) the data utilized to obtain the model of the DC line is presented, containing its configuration and its dimensions. Figure H.9 (Annex H) shows the structures and parameters of the DC filters in both terminals, tuned to the 12th and the 24th harmonic. The value of smoothing reactors is 270 mH.

Figure 4.8 (a) presents the frequency response (impedance in ohms) of the DC line with the presence of only the smoothing reactors, while Figure 4.8(b) illustrates the influence of the addition of DC filters. In both cases, it was not detected a series resonance occurrence in frequencies corresponding to characteristic harmonics, but series resonance close to the 2nd harmonic (100 Hz) should be pointed out.

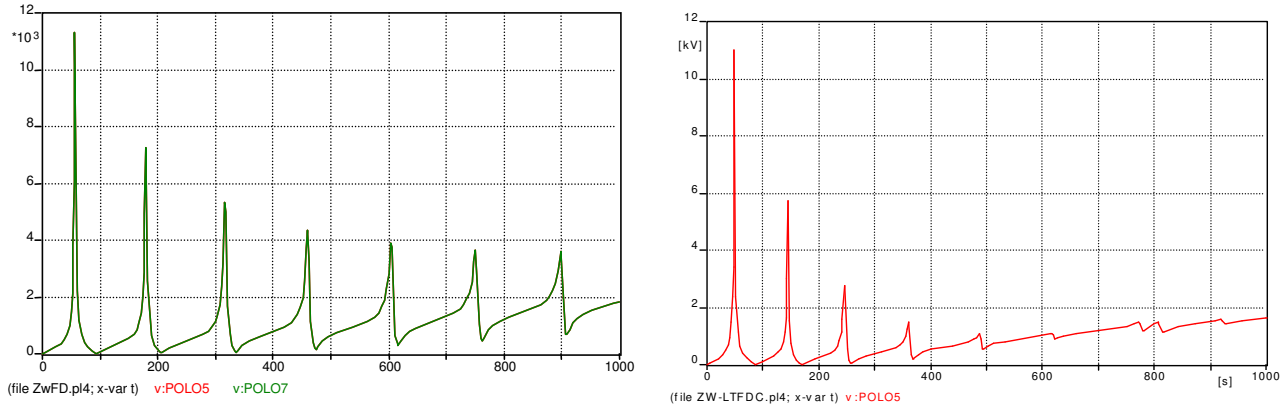


(a) Without DC Filters (b) With DC Filters

Figure 4.8 – Frequency Response of the DC line

### b) The AC networks

The *Simplified Network* was utilized to represent the AC systems connected to the converter stations, taking into account the purpose of this stage. Nevertheless, the following considerations were made:

- the transmission lines connecting these stations to the next external bus (bus # 11 on the inverter side, buses #112 and #111 on the rectifier side), were represented including the frequency dependence of their parameters, by adopting the configuration of the Garabi 500 kV line (Brazilian side).
- In these border buses, in addition to the positive-sequence components, the zero-sequence components of the equivalents' impedance were considered.

The file with data employed in the calculation of line models (specifically for line #11 - #26) – including its configuration and the respective dimensions – is presented in the Table H.18 (Annex H). In Table H.19 (Annex H) are also pointed out the lengths attributed to each circuit in question.

For the calculation of the modal equivalents connected to the border buses, the ANAFAS program, developed by CEPEL, was used. The circuits constituting the *Equivalent Network* were of course used as the source of data for the positive sequence. The zero-sequence circuits were obtained as follows: the transmission lines, included in that part of the network to be replaced by the modal equivalents, were separately modeled in the ATP program, employing the same typical configuration previously mentioned. This way, it was possible to obtain the zero-sequence impedances of each line, at the fundamental frequency, and then the zero-sequence networks were composed for the rectifier and for the inverter sides.

On the inverter side, the zero-sequence and positive-sequence equivalent impedances, as seen from bus #11, were calculated, starting from the values of the three-phase and single-phase short-circuit capacities at that bus. For the rectifier AC network, the own and mutual impedances at buses #111 and #112 were calculated (positive-sequence and zero-sequence). Since a transmission line exists between these buses, and the equivalent impedance between them resulted a value four times greater, this one was disregarded. The values of positive-sequence and zero-sequence equivalent impedances thus obtained are given below (in % on a 100 MVA basis). The location of those equivalent circuits may be visualized on Figure 4.7.

| | | Positive-seq. | | Zero-seq. | | | |
|---|---|---|---|---|---|---|---|
| BUSES | | R1 | X1 | R0 | X0 | | |
| **112** | **0** | **.90783** | **3.9117** | **2.6783** | **7.3773** | **Rectifier** | **(Er2)** |
| 111 | 112 | .13919 | 4.8962 | 16.788 | 65.378 | *(disregarded)* | |
| **111** | **0** | **.12983** | **1.6354** | **.65441** | **2.9996** | **Rectifier** | **(Er1)** |
| **11** | **0** | **.30861** | **1.423** | **.94085** | **2.7777** | **Inverter** | **(Ei)** |

After concluding the modeling of transmission lines and the calculation of modal equivalents, the power flow adjustment previously presented was utilized to finalize the representation of the *Simplified Network*. In order to simplify it and make its visualization easier, the models of the AC and DC lines were removed. It is emphasized the presence, on both sides, of the 11th and 13th orders AC filters (24th and 36th order AC filters were also considered, to absorb the 23rd/25th and 35th/37th harmonic pairs).

Subsequently, a survey was performed of the frequency response of the positive-sequence impedance, as seen from the converter buses of rectifier and inverter; results are presented in Figures 4.9 and 4.10. On the inverter side, a resonance very close to the 2nd harmonic is noted and, on the rectifier side, a parallel resonance close to the 3rd harmonic, which may be a source of overvoltages in case of unbalanced faults in that AC network.

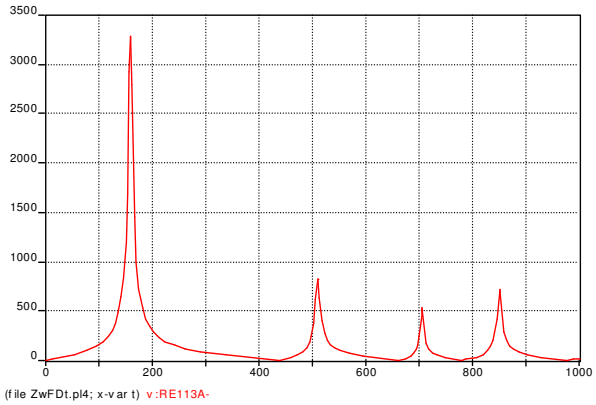


Figure 4.9 – Frequency Response, rectifier AC network - Positive-sequence impedance

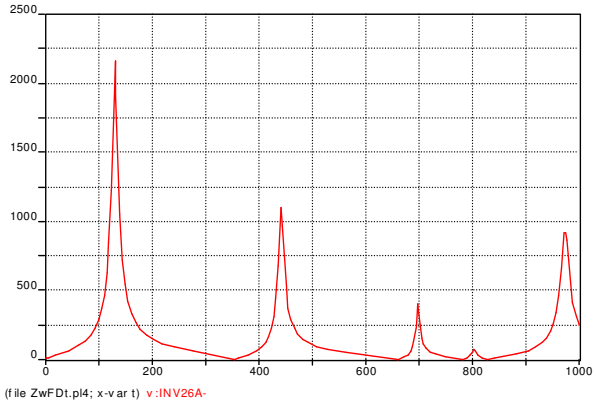


Figure 4.10 – Frequency Response, inverter AC network - Positive-sequence impedance

Table 4.4 summarizes, for the purpose of comparison, the 60 Hz positive-sequence impedances values obtained from the ATP and ANAFAS programs, disregarding the presence of AC filters. A very good consistency between results is noted.

Table 4.4 – 60 Hz positive-sequence impedances at the commutation buses of the converters

| | **ANAFAS Program** | **ATP Program** |
|---|---|---|
| Inverter | 89.00 ∠81.46° Ω | 87.27 ∠81.54° Ω |
| Rectifier | 62.25 ∠83.74° Ω | 63.38 ∠83.73° Ω |

The structures and parameters of the AC and DC filters are presented in the Figure H.9 (Annex H).

# 5 CONCLUSIONS

1. The technology of direct current transmission (HVDC), in the natural commutation type (LCC – Line Commutated Converter), has experienced important improvements in the last years, aiming chiefly to obtain a better performance and a better economic convenience of the different possibilities of application. Among these improvements, the use of series capacitors in the converters main circuit stands out. The configuration of the main circuit with capacitors between the six-pulse bridges and the secondary of the converter transformers (commonly denominated CCC), has been preferred by the industry, due to some of its specific advantages. At present, two important CCC back-to-back installations, one in Brazil and the other in the U.S.A. (Annex B) are in commercial operation.

   1.1. The series compensation may be installed in one or in both terminals of the HVDC link, using the same or different capacitor values in the rectifier and the inverter, especially in the case of links between a generation plant and a load center.

   1.2. The new features of the CCC converters main circuit, introduced by the series capacitors, provide them with an extremely favorable behavior when installed in AC systems having an ESCR equal to at least 1 at the inverter. In addition to this important performance feature, that impacts favorably the economics of the link, such converters present a very robust behavior regarding commutation failures, as it can be concluded from the simulations presented and discussed in this report.

   1.3. The above mentioned features are provided by new firing and extinction margins, defined in this report as alpha dash – rectifier firing margin, and gamma dash – inverter commutation margin. These new margins are due to the phase anticipation undergone by the phase-to-phase voltages that are actually seen by the valves, in relation to the commutation bus voltage, as explained in item 3.1 and indicated in Figures 3.6 and 3.11 of Chapter 3.

   1.4. The presence of the capacitors in the main circuit also brings about lower commutation angles (overlap) and, consequently, somewhat higher values of AC and DC harmonics, as compared to the values presented in HVDC links with conventional converter stations.

2. Components of the main circuit are dimensioned according to the basic principles that guide the definition of equipment parameters for conventional stations. The following additional points should, however, be observed:

   2.1. Dimensioning of AC filters for CCC converters should be developed considering the smallest filter capacitance needed to satisfy harmonic correction requirements, in accordance with the criteria established for inductive coordination. The additional reactive power required for the operation of the converter should be then allocated to the series capacitor, given the favorable implications of larger series capacitors on station performance.

   2.2. Converter transformers, in addition to the usual requirements considered in their dimensioning for conventional stations, should also comply with additional requirements deriving from the installation of the series capacitor, such as that of a higher steady-state maximum voltage, due to the composition with the voltage drop in the capacitor, of higher voltage variation rates (dv/dt) and of a higher proportion of current and voltage harmonics.

   2.3. The dimensioning of the series capacitor is defined considering the reactive power balance in the station, of which the following portions should be taken into account: (a) AC filter power, (b) reactive power exchange with the AC system, as defined in the station design criteria, and (c) reactive power consumption of the station itself, in the conditions stated for nominal operation, and also in order that it may have a good performance regarding commutation failures. In the case of rectifier stations supplied directly by generating plants, the possibility of having a substantial portion of the reactive power balance supplied by the generators themselves should also be considered, because of its generally favorable economic convenience.

   2.4. The control system for CCC converters is structured based on the same basic philosophy used in DC links with conventional converters, but considering the new margins, alpha dash and gamma dash. Conceptually, the only major difference is the need to include a new function, intended to monitor the symmetry of currents in the phases of the series capacitor. This is due to the fact that,

during asymmetric faults, unbalanced currents flow and lead to an asymmetric loading of each capacitor phase and, consequently, to voltage unbalance. Fortunately, this unbalance is transient, and tends to disappear as soon as current symmetry is recovered. Nevertheless, just after asymmetric faults, the decreasing but still present unbalance may lead to commutation failures during recovery. A possible solution to reduce the eventual problems caused by that unbalance is to have extinction angles increased transitorily (by some 25-30%), as indicated in this work.

3. In order to investigate the new arrangement of converters, and to establish the characteristics of new HVDC links using CCC converters, it becomes necessary to provide the existing digital simulation programs with models of this type of converter, so as to make possible planning and operational studies for such links, both in steady-state and during electromechanical and electromagnetic transients.

   3.1. For such purposes, WG B4-34 developed models, as described in this report, based on the means already available in the programs ANAREDE (load-flow), ANATEM (electromechanical transients), EMTDC and ATP, which were used for structuring and adjusting a benchmark circuit (BM), with complex equivalents representing the AC networks connected to the converter stations at the rectifier and inverter terminals, as well as simplified equivalents of the AC networks with detailed representations of the converters controls, for electromagnetic and electromechanical transients studies.

   3.2. The developed benchmarks allow performing studies, to define and/or to optimize parameters for new links using CCC converters, to compare studies performed with different tools and/or investigations performed by different bodies.

   3.3. Bearing in mind that the possible applications of CCC configurations are those interconnecting AC systems with low short-circuit ratios, the BM's were defined for AC systems with ESCR equal to 1.73 in the rectifier and 1.28 in the inverter. During parametric studies, as shown in Chapter 4, it was noted that applications with ESCR around 1 (1.01 in our case) in the inverter probably represent the lower limit for an acceptable performance of this arrangement.

   3.4. When defining simplified equivalent circuits, it was verified that it was not adequate to merely use infinite busbars in the equivalent representation, as it is conventionally done. This happens because the absence of a dynamic representation of the machines, even if only a simplified one, distorts significantly the results, as shown in item G.1 of the Annex G of this Report.

   3.5. In addition, the need to include smoothing reactors, DC filters and AC filters should be observed, especially in the most critical cases. It should be noted, also, that the inclusion of smoothing reactors should be considered relevant, not only for studies of resonance of the link with CCC converters, but also as a part of DC filters.

   3.6. It was verified that, in spite of the limitations inherent to the AC network equivalents, it was possible to observe resonances upon the occurrence of asymmetric faults, especially at the inverter terminal.

   3.7. The simplified equivalents (simplified networks) may also be used in the ANATEM program, provided that a detailed dynamic representation of the machines is included. It must not be forgotten, however, that results of studies using simplified equivalents are not representative with respect to the behavior of the different oscillation modes of a large-size system.

   3.8. In order to obtain a correct response of studies to be carried out utilizing simplified equivalents as discussed in this Report, it should be observed that the border buses of these equivalents should never be the converter AC buses themselves, but others connected to the former by actual transmission lines of the simulated systems. In this context, moving just one line away (that is, including the next removed node from the converter station) in the equivalent appears to lead to satisfactory results.

   3.9. This Report presents, in item G.1.3 of the Annex G, important considerations – and also proposes procedures to be adopted – regarding the correct representation of commutation failures in studies of transient stability (of electromechanical transients), where the basic algorithms only represent only low-frequency phenomena in the range of oscillations between machines and between areas (a few Hertz, or a fraction). This point is very relevant, especially in system planning and in

preliminary system design studies, where proper detailed electromagnetic transient studies might not be performed and substituted for very crude and inaccurate assumptions (such as just assuming DC link blocking at certain arbitrated voltage reduction levels after AC faults).

3.10. The occurrence of asymmetrical disturbances, in systems with series compensation in the commutation circuit (CCC), originates unbalanced voltages in the capacitors. The schedule of studies on the performance of transmission systems with CCC converter stations should therefore include the investigation of the effects of those unbalances in the system performance, in addition to the usual electromechanical stability studies. Such studies should be done with detailed equivalents (including bridge control and valve firing representation) using digital electromagnetic transients programs of the ATP type, as electromechanical stability programs, including ANATEM, are not appropriate for this type of study.

# 6 BIBLIOGRAPHICAL REFERENCES

[1] John Reeve, John A. Baron and G. A. Hanley, "A Technical Assessment of Artificial Commutation of HVDC Converters with Series Capacitors", IEEE Trans on PAS, vol. PAS-87, No. 10, October 1968.

[2] A. M. Gole, R. W. Menzies, "Analysis of Certain Aspects of Forced Commutated HVDC Inverters", IEEE Trans on PAS, vol. PAS-100, No. 5, May 1981.

[3] S. Nyati, S. R. Atmuri, D. Gordon, V. Koschik and R. M. Mathur, "Comparison of Voltage Control Devices at HVDC Converter Stations Connected to Weak AC Systems", IEEE Trans on Power Delivery, vol. 3, No. 2, April 1988.

[4] Bradley K. Johnson, "HVDC Models Used in Stability Studies", IEEE Trans on Power Delivery, vol. 4, No. 2, April 1989.

[5] Tomas Jonsson, Per-Erik Björklund, "Capacitor Commuted Converters for HVDC", IEEE/KTH Stockholm Power Tech Conference, Stockholm, Sweden, June 1995.

[6] J. R. Diago, F. J. Bugallo, M. Baleeiro, G. Biledt, J. Graham, "GARABI - A Interligação de 1000 MW Argentina - Brasil", VIII ERLAC, Ciudad Del Este, Paraguay, May1999.

[7] A. R. Carvalho, S. Gomes Jr., W. W. Ping, N. Martins, "Comparação do Desempenho Dinâmico de Conversores Convencionais e Conversores com Capacitor de Comutação", VIII ERLAC, 1999.

[8] S. Gomes Jr., H. J. Pinto, N. Martins, R. D. Rangel, A. R. Carvalho, R. Ljungqvist, T. Jonsson, "Modeling ABB's HVDC/CCC into the CEPEL Simulation Package", VI SEPOPE, 1998.

[9] S. Gomes Jr., N. Martins, W. W. Ping, A. R. Carvalho, "Vantagem da Utilização do Conceito CCC nos Esquemas em HVDC", XVI SNPTEE, 1999.

[10] CIGRÉ WG 14.22, "New Circuit Concepts for HVDC", summary 5/99.

[11] M. Meisingset, A.M. Gole, R. Burton, T.R. Time, P.O.Eide, R. Fredheim, "Impact of Capacitor Commutated Converters in AC-Systems with Multiple DC Infeed", 13rd PSCC, 1999.

[12] M. Szechtman, T. Wess, C.V. Thio, et. al., CIGRÉ WG 02, "First Benchmark Model for HVDC Control Studies", Electra n°. 135, pp. 54- 73, April 1991.

[13] CIGRÉ WG 14.02, "The CIGRE HVDC Benchmark Model - a New Proposal with Revised Parameters", Electra n°. 157, pp. 60-66, December 1994.

[14] M.M. Babu Narayanan, S. Parameswaran, "Study of control strategies for New CIGRE HVDC Benchmark Model", Report 14-113, CIGRÉ 1998 Session, Paris, France, August 1998.

[15] S.Gomes Jr., N.Martins, T. Jonsson, D. Menzies, R. Ljungqvist, "Modeling Capacitor Commutated converters in Power system Stability Studies", IEEE Trans. On Power Systems, Vol. 17, No. 2, May, 2002.

[16] L. Carlsson, A. Persson, T. Jonsson, G. Liss, P. Ebjörklund, "New Concepts in HVDC Converter Station Design", Report 14-102, CIGRÉ 1996 Session, Paris, France, 1996.

[17] Barros, J. G. C., et. al., CIGRÉ GT B4-34, "Series Capacitor Commutated (CCC) HVDC Converter Stations: Benchmark for Digital Simulation Studies", IX SEPOPE, Rio de Janeiro, Brazil, May 2004.

[18] "PSCAD/EMTDC User´s Manual ", Manitoba HVDC Research Center, Canada, 2004.

[19] "Manual do Usuário do Programa ANATEM", CEPEL, Brazil, 2004.

[20] Dommel, H. W., "Electromagnetic Transients Program Reference Manual (EMTP Theory Book)", Bonneville Power Administration, Portland, Oregon, August 1986.

[21] "Alternative Transients Program (ATP) Rule Book", Leuven EMTP Center (LEC), July 1987.

[22] Donald F. Menzies – "Estudo de Desempenho Dinâmico do Elo de Corrente Contínua" – Nota Técnica DEE.O 02/98 – FURNAS CENTRAIS ELÉTRICAS S.A - April 1998.

[23] ABB Utilities AB, SE-771 80 Ludvika, Sweden.

[24] ABB Power Technologies AB, Power Systems / HVDC, SE-771 80, Ludvika, Sweden.

[25] John Graham, Don Menzies, Geir Biledt, Antônio Ricardo Carvalho, Wo Wei Ping, Acacio Wey; "Electrical System Considerations for the Argentina-Brazil 1000 MW Interconnection", CIGRE Biennial, Paris, 2000.

[26] Don Menzies, Hans Eriksson, Fabiano Uchoas Ribeiro, "Commissioning The Garabi I Back-to-Back Converter Station"`, ERLAC 2001.

[27] Torbjörn Karlsson, Mats Hyttinen, Lars Carlsson and Hans Björklund, "Modern Control and Protection System for HVDC", ABB Power Systems, S-771 80 Ludvika, Sweden.

# ANNEX A - SPECIFIC CONSIDERATIONS FOR DEFINING THE MAIN CHARACTERISTICS OF MAJOR EQUIPMENT IN THE PRINCIPAL CIRCUIT OF CCC CONVERTERS

In the definition of the characteristics of major equipment of a CCC converter, the features that will be discussed below should be considered, in addition to the points normally covered in the specification of such equipment for a conventional converter. As a general guidance, it can be said that the commutation capacitor major influence is on the physical ratings of the AC filters and converter transformers, on account of its role on minimizing converter reactive power absorption during normal operation. Converter transformers, as well as AC filters fundamental frequency ratings, can be significantly reduced. Valve design is also affected, mostly on account of higher valve snubber losses and higher valve voltage stresses during normal operation. However, this must be treated as a secondary consideration because the increases are small and also because other effects, especially valve short circuit duties, tend to be significantly favorable.

## A.1 Filters

1. AC filters and their Mvar capacity are defined as in conventional converter stations, so as to control AC side harmonics and their effects within the limits established in the converter design criteria.
2. Harmonic values for conventional arrangements with similar steady state operating parameters can be taken as a first approximation. It must be realized, however, that the establishment of the definitive filter parameters is dependent on the final definition of the basic electric circuit parameters, such as AC system short circuit level, converter transformer reactance, series capacitor rating and extinction/firing angles. Thus, it is only after the definition of all these that actual steady state harmonic values can be estimated.
3. Conventional HVDC converter AC filters are normally designed to produce the major part or, at least, a large proportion of the reactive compensation required at nominal frequency. In CCC converters, however, operation improves if the major part of the reactive power compensation is allocated to the commutation capacitor. Hence, it is beneficial to design the AC filters with reduced nominal frequency reactive compensation capacity (typically 10 to 15%) that is, with just enough capacity for the performance of their harmonic reduction duties. In this context the use of high Q, narrow bandpass filters has been proposed as advantageous given that such filters require far less capacitance.
4. At a final dimensioning stage improved estimates of the actual steady state harmonic values can be obtained with EMTP/ATP type programs using the converter station electrical circuit parameters (operating angles, series capacitor and transformer reactance) determined as indicated in A.2 below. Optimized filter parameters can then be determined.
5. DC filters are also dimensioned similarly as for a conventional arrangement. An adjustment will be required, as well, at the final stage of station design after the choice of a definite value for the extinction/firing angles and for the series capacitor physical rating.

## A.2 Dimensioning of the Series Capacitor

**A.2.1 Series Capacitor Physical rating.** The definition of the series capacitor capacity involves aspects connected to the station reactive compensation and to its control. It should also be kept in mind that, given the automatic adjustment of the series capacitor compensation effect as load current varies, it is preferable to maximize the amount of series compensation and minimize the shunt AC filters contribution to the converter station fundamental frequency reactive compensation. Another important consideration is to assure that the series capacitor physical rating is effective in reducing commutation failures in inversion mode on the occurrence of AC faults that lead to sudden voltage drops of specified values. With this in mind, a simple iterative procedure, such as indicated below, can be performed.

1. Considering the requirements for reactive power exchange with the AC system, established in the station design criteria, the total reactive power that should be available in the station may be computed. Select a series capacitor Mvar corresponding to this total reactive power minus the AC filter capacity defined above in item A.1 (typically 10 do 15% of Pdc).
2. To obtain initial values to start the process up, assume the inverter operating with typical values of extinction angle (say gamma = $19^{o}$) and typical values of transformer converter reactance (say 10%).

3. Specify converter performance in respect to commutation failures (say voltage drops of 15% to 20% in the inverter station AC bus without occurrence of commutation failures during remote AC faults).[1]
4. Run cases in the ATP/EMTP or similar programs, using as initial nominal parameters the ones previously defined and make small adjustments, by trial and error, searching for a combination of gamma angle and adequate basic parameters that allows normal operation of the inverter satisfying the specified commutation failure restrictions.
5. After each adjustment of gamma angle, a new value of reactive power required for steady-state operation of the converter is defined and the capacitor Mvar modified correspondingly. The process ends when satisfactory convergence is achieved.
6. In principle, it may be adopted in the rectifier the same capacitor defined for the inverter terminal. In case the rectifier is fed by a generating plant, the capacitor may be optimized, considering that a portion of the required reactive power will be supplied by the generators, which should be specified with an appropriate power factor.

**A.2.2. Overvoltages and overcurrents.** The series capacitor should be protected from overvoltages by metal-oxide varistors (MOV, usually zinc oxide ones). The withstand voltage (voltage rating) of the series capacitors and, consequently, the varistors (MOV) characteristics are defined considering that:

1. The capacitor shall be dimensioned so as to withstand any overcurrent and any overvoltage resulting from all faults in the AC network, in the absence of the varistors (MOV) themselves.
2. The maximum overcurrent level is a function of the short-circuit levels at the rectifier, of the characteristic of the current control amplifier (CCA) and of the location and type of fault. Usually, converter station internal zero impedance faults at valve bridges terminal connections are likely to provide maximum stresses. However, when investigating the most critical fault location, a detailed study of the actual converter station arrangement and construction characteristics, such us the use of metal clad bus bar arrangements or the use of GIS bus bars and breakers, etc, is of fundamental importance.
3. Typical values of overcurrents and of the associated overvoltages, resulting from external faults, are of the magnitude of 2.0 to 2.5 pu.

### A.3 Converter transformers

1. Current derivative. The presence of the capacitor reduces the effective inductance seen during the commutation process. For this reason, the commutation angles are smaller. This is favorable from the standpoint of power factor at the bus, a systemic parameter. From the equipment point of view, however, it means operating with slightly higher values of di/dt during commutations and, possibly more serious, during faults. The inter-turn voltage should be carefully evaluated, in order to define the need, or not, of an increase in the insulation, especially in the initial parts of the coils.
2. Voltage derivative. The speed of voltage application upon the windings (dV/dt) may increase, depending on the magnitude and polarity of the charge of the capacitor at the actual firing instant. So, this is also a parameter to be carefully verified.
3. Voltage peaks. As it may be seen from the simulations, the maximum values are not excessive Even so, they should be checked, similarly to what is done for the conventional arrangements.
4. Harmonic losses. Apparently, there is no significant increase in the circulation of harmonics; in principle, the conventional dimensioning practices for this parameter may be maintained.
5. Tap changing. The energy levels ($^1/_2Li^2$) to be dissipated in each operation are associated directly to the instantaneous values of current in the coils that are being switched. In conventional stations transformers, the number of on-load tap changes is statistically much higher than in stations with CCC arrangement, causing a great wear and the need for frequent maintenance, unless thyristor tap changers are used. As shown in Chapter 3, this is an aspect for which the CCC arrangement appears especially advantageous.

[1] When the converter feeds a transmission with underground or submarine cables, the definition of the maximum voltage drop in the AC bus without occurrence of commutation failures requires additional care, because a small variation of that voltage may cause discharges in the cables and also, very probably, a commutation failure. To avoid such occurrence, the inverter control, when feeding cables, should be able to keep the DC voltage constant during sudden AC voltage drops of specified values.

### A.4 Smoothing reactor

This is selected as in conventional arrangements, considering:

- the maximum derivative of the short-circuit current (di/dt),
- the resonance modes of the DC line and, as a part of the DC filter,
- the control of the DC line harmonics.

### A.5 Valves

As described in the literature [Jonsson, T., et al., 1995; Carlsson, L. et al., 1996] there is some increase in peak valve voltage stresses in normal operation on account of higher commutation overvoltages that will result in increased duties for snubber circuits and valve arresters, as well as in somewhat increased valve losses. In the opposite direction, the charging of the commutation capacitors by fault currents tend to establish counter-voltages that are beneficial in limiting both peak current values and the number of short circuit current peaks during converter faults, as well as reducing the blocking voltage of the valve stressed by the fault. In short, some effects are detrimental and some favorable and the overall impact in valve design appears to be of little significance. Valve design should, therefore, be kept in principle dependent on the main parameters choice and be adapted to the final system requirements after the commutation capacitor, the AC filters and the converter transformer parameters have been established.

Similarly to conventional converters, simulation studies must be performed to determine the limiting stresses in normal operation and during faults.

Valve limiting stresses are obtained from the evaluation of:

1. Current derivative. The dimensioning should take into account what is mentioned above (1) for the transformer.
2. Voltage derivative. The most unfavorable conditions should be verified, as a function of observation 2 of item A.3 above.
3. Maximum short-circuit current. The LC series combination in each phase has the effect of reducing the short-circuit impedance. However, once the actual parameters are known, the dimensioning is trivial.
4. Maximum blocking voltage. Similar to the dimensioning for conventional arrangements.

### A.6 Main parameters of control circuit

The control equipment itself is basically the same as for the conventional configuration. The control philosophy of the CCC is similar, in its basic concepts, to that for the control of a conventional HVDC converter station. There are, however, some important differences, that will be described next:

- Firing angle (alpha) measuring ranges, as well as the regions where firing is permitted, are enlarged in order to allow operation in 4 quadrants, differing from the conventional, where the range from 0 to 180 degrees is sufficient. In the rectifier, this occurs because the operation with $\alpha < 0$ degrees is allowed. In the same way, in the inverter the operation with $\alpha > 180$ degrees is also allowed.
- The minimum limit (alpha min) of firing angle in rectification (normally of the magnitude of 5 degrees), and the maximum limit (alpha max) of the firing angle in the inversion (normally about 162 degrees, for operation with normal extinction angle gamma zero equal to 18 degrees), are calculated dynamically as a function of $Udi_0$ and $I_d$. In order to minimize the complexity of the control circuits themselves, the calculations are carried out separately (off line) and an approximation, in the form of expansion in a Taylor series of second order, is used in the controls. Such approximation has shown to be sufficiently precise for the studies already completed.
- During asymmetrical disturbances, current unbalance leads to unbalanced voltages in the series capacitor phases. This voltage unbalance results in a firing asymmetry, with a risk of commutation faults in inversion if the controls try to re-establish operation with rated extinction angles - gamma zero equal to 18 degrees - while significant unbalance levels in the phases of the series capacitor are

still present. Therefore, to reduce the risk of commutation failures, the unbalance in the series capacitor is checked by measuring phase voltages and, if the filtered value of the combination of this voltage differs from zero by more than a specified tolerance, the reference value for gamma zero in the inversion is transiently increased from 18 to 23 degrees[2]. As a consequence, this additional function delays the final part of recovery, given the small reduction of DC voltage in the inverter. It was noted that the elimination of the unbalance depends on the load, being slower at light load. Yet, slower recoveries at light load are normally not considered to be a problem.

Other control functions, conceptually similar to those of conventional converter station controls, are also included, as described below:

- Asymmetric faults on the AC side are detected by the presence of the 2nd harmonic in the rectified voltage $U_{di0}$. In rectification, severe symmetric faults (3-phase) are detected by the AC voltage drop in the three phases. AC fault detection is used to increase the alpha minimum limit in rectification, or to reduce the alpha maximum limit in inversion. The changes to these limits are made immediately, but with a slow return to the rated values.
- The value of current margin affects the recovery speed after some types of faults on the AC side. Thus, in order to accelerate recovery after faults, the current margin is transiently increased from 0.1 to 0.2 pu during AC faults. This is done in the Current Control Amplifier (CCA) of the inverter station.
- Recovery after AC faults tends, in general, to be slower under light load. In order to compensate this tendency, the integral gain of the Current Control Amplifier (CCA), in the studies described in this Report, was made load-dependent both in rectification and inversion. It is believed, however, that other, eventually better, solutions may exist.

[2] The "dc offset" effect following asymmetrical faults can be dealt with using an internal loop to offset the valve firing. It has been suggested that in this alternative way the asymmetry can be reduced much more quickly. No such control mode has been implemented in EMTP type models in this work and this method may not be freely available due to patents.

# ANNEX B - CCC INSTALLATIONS IN COMMERCIAL OPERATION

## B.1 INTRODUCTION

Two CCC installations are now in commercial operation [23 to 27]. Both interconnections have "back-to-back" arrangement. Curiously, their rated capacities are in the ratio of about ten to one: Garabi (Rio Grande do Sul, at the Brazil-Argentina border) with 2200 MW and Rapid City (South Dakota, USA) with 200 MW.

## B.2 THE BRAZIL – ARGENTINA INTERCONNECTION AT GARABI

### B.2.1 Historical review and location

In April 1997, the governments of Argentina and Brazil signed an agreement aiming at creating conditions for electric power commercialization between the two countries. On May 5, 1998, the Brazilian Mines and Energy Ministry (by means of Eletrobrás, jointly with Furnas and Gerasul) and the Argentinean Government, signed a 20-year contract with the Power Interconnection Company – CIEN, for the importation of 1000 MW from the Argentinean wholesale power market; this amount was soon increased to 2200 MW. CIEN is an ENDESA Group enterprise. As the Argentinean system operates at 50 Hz and the Brazilian system at 60 Hz, the interconnection is made through HVDC converters in back-to-back configuration, located at Garabi – municipality of Garruchos, State of Rio Grande do Sul, on the left bank of Uruguay river, in the Brazil-Argentina border region. The interconnection was planned and built in two consecutive 1100 MW stages.

The two stages connect the 500 kV Brazilian (60 Hz) and Argentinean (50 Hz) systems through 500 kV lines. The first stage started commercial operation in June 2000, and the second in August 2002, when the full 2200 MW transfer capacity was attained in both directions. The station uses converters with commutation capacitors in the arrangement discussed in this Report and known as "CCC". The Argentinean transmission lines (132 km) connect to the Rincón de Santa Maria substation, close to Yacereta hydro plant, while the Brazilian lines (354 km) connect to Itá hydro plant substation, at the border between the States of Santa Catarina and Rio Grande do Sul, with a tap in Santo Ângelo. The metering of power purchased from Argentina is made in Itá substation. A simplified single-line diagram is shown below in Figure B.1.

It is relevant to note that the first stage has been interconnected to the Brazilian Southern system at 230 kV in a transformer station at Santo Ângelo (the tap mentioned above). Such interconnection was not contemplated in the initial design, and was built by Eletrosul in order to strengthen the system in Rio Grande do Sul. Inversely, the second stage is not interconnected to Santo Ângelo, as it may be seen from Figure B.1. The line routing, however, was purposely designed close so as to make possible a future interconnection, if desired. Among the guarantees, it was included that of an electrical availability above 97%.

### B.2.2 Transmission system

Though both power systems are of a considerable size, their connection is made at relatively weak points. Ríncón de Santa Maria substation is located at the northern end of the Argentinean system and, despite being close to Yaceretá plant, its short-circuit capacity is relatively weak, varying from 3000 to 9000 MVA, depending on the number of generators in operation at Yacereta. This condition remains practically unchanged since the commissioning of the first stage, and so the minimum short-circuit capacity at Garabi, on the Argentinean 50 Hz side, is of about 2000 MVA, falling to 1600 MVA under contingency conditions. At the connection point with the Brazilian Southern/Southeast system (Itá plant), when the first stage started operation, the short-circuit capacity was calculated as 6000 MVA falling to 3500 MVA under the worst contingency conditions. When the second stage started operation, additional generators had been commissioned at Itá, raising those levels to 12,000 and 5000 MVA respectively. Thus, the short-circuit capacities, as seen individually by each of the converters on the 60 Hz at Garabi, present today the same values of the first stage, varying approximately from 1750 and 2160 MVA.

The converters of both stages are designed to operate individually or in parallel[1], resulting in a set of challenging operating conditions, in view of the guarantee of supply of 2000 MW at a relatively weak point.

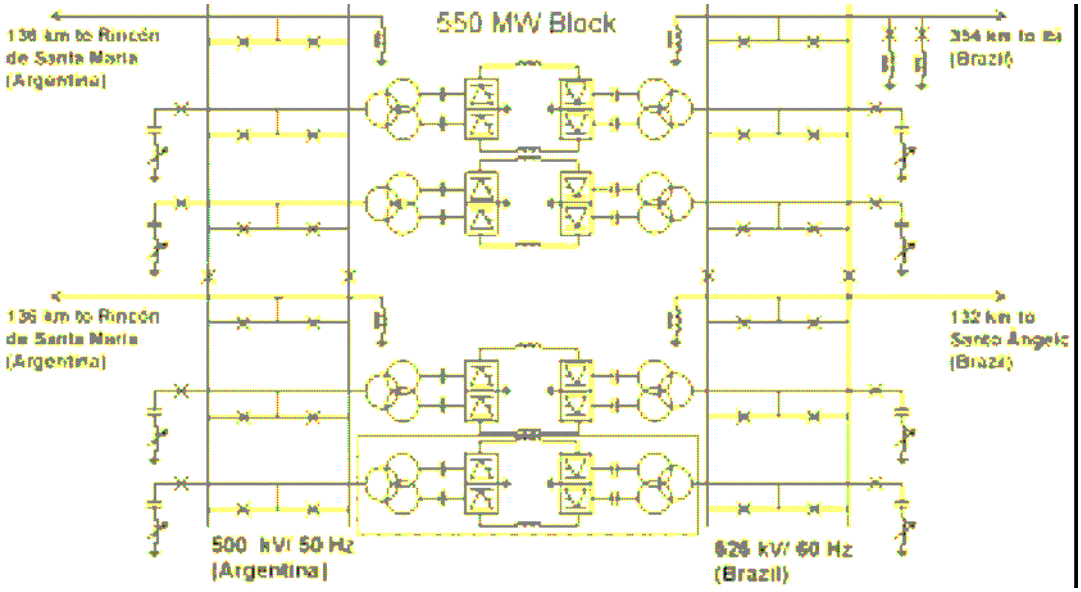


Figure B.1 - Garabi Back-to-back Converter Station, Simplified single-line diagram.

### B.2.3 Garabi station main circuit data

Rated output of Garabi station: 2200 MW

**Capacity per converter block:**

Rated output: 550 MW
DC voltage: ± 70 kV
DC current: 4 kA
CCC capacitor, 50 Hz side: 190 Mvar
CCC capacitor, 60 Hz side: 322 Mvar
(The higher value at the 60 Hz side allows the supply of the reactive power required by the system at full load)

**Voltages, frequencies and AC filters:**

Argentina: 500 kV at 50 Hz
AC filters per converter: 85 Mvar, $11^{th}$ +$13^{th}$, type "Contune" and High-Pass for $24^{th}$ +$36^{th}$

Brazil: 525 kV at 60 Hz
AC Filters per converter: 85 Mvar, $11^{th}$ +$13^{th}$, type "Contune" and High-Pass for $24^{th}$ +$36^{th}$

Guaranteed availability: 97%

## B.3 RAPID CITY INTERCONNECTION

### 3.1 Historical review and location

This is the seventh back-to-back interconnection to be installed at the east-west electrical border in the USA; it is located near Rapid City, in the western part of South Dakota State. Its commercial operation started in

[1] According to information obtained from the operating utilities, both 1100 MW converters have operated, in practice, only in the individual mode.

October 2003, being operated by WAPA – Western Area Power Administration, from its dispatch center in Loveland, Colorado. The owners are Basin Electric Power Cooperative, of Bismarck, North Dakota, and Black Hills Power & Light, of Rapid City.

The arrangement selected was the same as for Garabi, with commutation capacitor, CCC, to prevent the incidence of commutation failures, as the AC networks in that region are relatively weak. The fast controllability typical of DC interconnections will be used, together with additional reactors as described below, in order to improve voltage stability and frequency control on both sides.

The station rated output is 200 MW, with 5% overload capability for 30 minutes at an ambient temperature of 40 ºC. For the sake of redundancy, the station was divided into two 100 MW blocks. The option for the CCC arrangement was due also to the need to make feasible a future expansion of the interconnection to 400 MW, without requiring the construction of additional transmission lines.

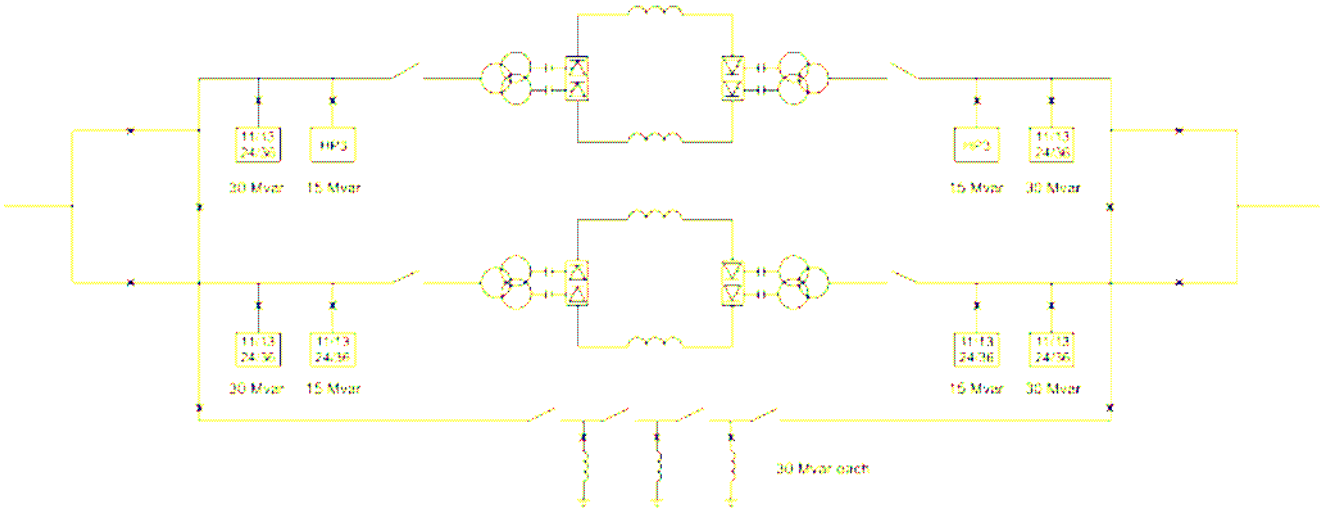


Figure B.2 - Rapid City Interconnection simplified single-line diagram

### B.3.2 Short-circuit capacities in the connected systems

- On the west side: maximum value 1450 MVA and minimum 600 MVA.
- On the east side: maximum value 1180 MVA and minimum 720 MVA.

### B.3.3 Rapid City station main circuit data

Rated output: 2 x 100 MW
Rated DC voltage: 12.85 kV
Rated AC voltage: 230 kV
Overload capability, 30 min: 2 x 105 MW
Maximum DC current: 3974 A

**AC Filters:**

Number of banks, west side: 3 x 30 Mvar + 15 Mvar
Number of banks, east side: 3 x 30 Mvar + 15 Mvar

**Converter bridges and valves:**

12-pulse group in a single structure
Cooling system: water + glycol
Thyristors: 90 $cm^2$
No. of thyristors per valve: 7

Maximum voltage per thyristor: 6.7 kV

**Converter transformers**

Three-phase, three-windings type
Rated output: 109 MVA each

Four filters are available at each side, in order to reduce the harmonics and also for AC systems voltage support. For the same purpose of voltage control, three 30 Mvar shunt reactors were additionally installed, having the possibility of connection to either side of the station.

### B.4 Final Comments

It is interesting to note that the AC filters at Rapid City have fine and fixed tuning, while at Garabi they are of self-adjustable (self-tuning) type (called "ConTune" by their manufacturer).

In both cases, it was successfully used a modular construction and assembly of groups of components (complete DC bridges, in the case of Garabi, and complete converters in that of Rapid City), assembled and tested at the factory, and shipped complete to the site, thus reducing not only the reassembly work but also the number of site tests.

The successful integration of the interconnection between Brazil and Argentina, as well as that of Rapid City, in the operation of their respective systems, has proved an excellent demonstration of the feasibility and of the specific advantages of the CCC arrangement.

# ANNEX C - PSCAD/EMTDC BENCHMARK MODEL

## C.1. Introduction

This annex offers a brief description of the PSCAD/EMTDC benchmark version of an HVDC transmission system using CCC converters at both the rectifier and inverter. The model performance has been examined by applying AC faults at different locations.

## C.2. Description of the Main Circuit

Figure C.1 shows the overall PSCAD layout. The rectifier and inverter are enclosed in their own subsystems shown in Figure C.2 for the inverter only (the rectifier is essentially the same).

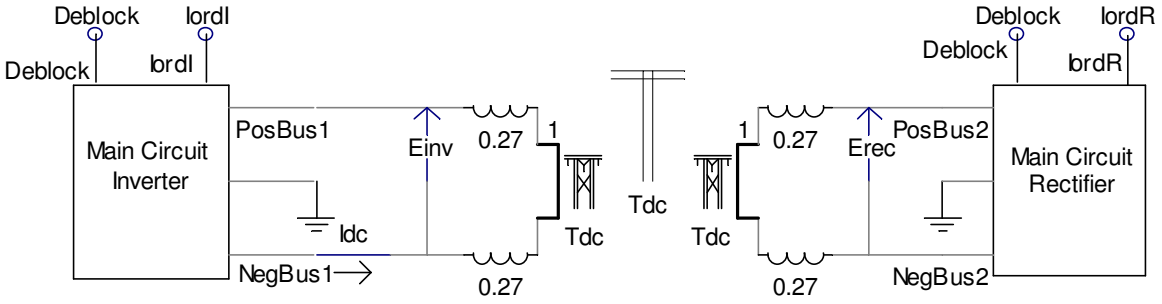


Figure C.1 - Overall PSCAD Layout

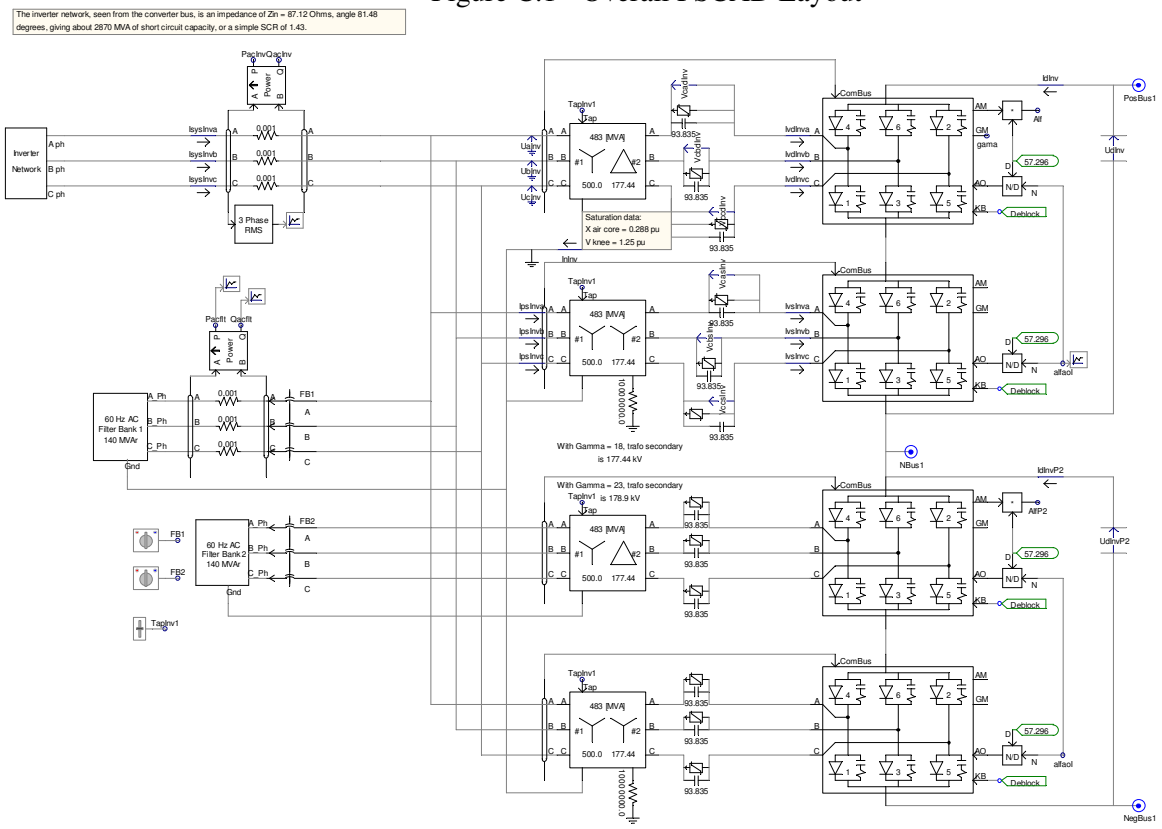


Figure C.2 - ± 500 kV 2000 MW CCC inverter

### C.2.1. HVDC converter dimensions

#### C.2.1.1. Rectifier

- The rating of each 12 pulse pole is 1000 MW, 500 kV, 2 kA, 60 Hz.
- The star-star and star-delta converter transformers are each rated (3-phase rating for one six-pulse converter bridge) at 505 MVA, 500/187.3 kV, X=0.12 pu. Typical saturation characteristics are included with an air core reactance of 0.240 pu and a knee point voltage of 1.25 pu.
- The commutation capacitor is rated at 93.835 μF, (dxc= 0.2235) producing 372 Mvar (for each 12 pulse converter). Peak voltage across each capacitor at rated current is 59.21 kV.
- Arrestors are provided in parallel with each commutation capacitor. The arrestor rated voltage is 140 kV. (No attempt was made to optimize the arrestor characteristics. With the value of rated voltage chosen and the number of parallel columns, the arrestors have no impact on the dynamic performance of the converter during faults.)
- At nominal conditions rectifier alpha is 1.51 degrees and the reactive consumption of each 1000 MW pole is 140.37 Mvar. Assuming one 140 Mvar AC filter bank per 1000 MW pole, the reactive exchange measured at the converter bus is, therefore, essentially zero.
- The maximum DC voltage occurs at alpha = - 9.4 degrees. At this value of alpha, the converter's reactive consumption is zero. Measured at the converter bus, the reactive exchange is now 140 Mvar, injected into the AC system. Operation below alpha = -9.4 degrees is not permitted in this model.
- A tap changer is provided to permit rated voltage to be maintained at reduced load.

#### C.2.1.2. Inverter

- The rating of each 12 pulse pole is 954.4 MW, 477.2 kV, 2 kA, 60 Hz.
- The star-star and star-delta converter transformers are each rated (3-phase rating for one six-pulse converter bridge) at 483 MVA with a 500 kV primary side rating. Depending on the nominal gamma prime selected, the secondary rating will be 178.9 kV (at $\gamma' = 23°$) or 177.44 kV (at $\gamma' = 18°$). The leakage reactance is X=0.12 pu. Typical saturation characteristics are included with an air core reactance of 0.240 pu and a knee point voltage of 1.25 pu.
- The commutation capacitor is rated at 93.835 μF, (dxc= 0.2235) producing 372 Mvar (for each 12 pulse converter). Peak voltage across each capacitor at rated current is 59.21 kV.
- Arrestors are provided in parallel with each commutation capacitor. The arrestor rated voltage is 140 kV. (No attempt was made to optimize the arrestor characteristics. With the value of rated voltage chosen and the number of parallel columns, the arrestors have no impact on the dynamic performance of the converter during faults.)
- The inverter controls permit operation at $\gamma' = 18$ degrees or at $\gamma' = 23$ degrees.
- At $\gamma' = 23$ degrees (alpha = 166.2 degrees), the reactive consumption of each 954.4 MW pole is140.3 Mvar. Assuming one 140 Mvar AC filter bank per pole, the reactive exchange measured at the converter bus is, therefore, essentially zero.
- At $\gamma' = 18$ degrees (alpha = 170.3 degrees), the reactive consumption of the converter is reduced to 58.2 Mvar, allowing 81.8 Mvar to be injected into the AC system. This option of using $\gamma' = 18$ degrees has been used for all of the fault cases.
- A tap changer is provided to permit rated DC voltage to be maintained at reduced load.

### C.2.2. DC transmission line data

A 1000 km bipolar HVDC line, based roughly on the IPP line is used, but with a 4 conductor bundle of 1351 MCM ACSR rather than a 3 conductor bundle. With the 4 conductor bundle, the line resistance is 1000 * 0.04561 / 4 Ohms = 11.4025 Ohms. Line losses are then 45.61 MW per 1000 MW pole. The line topology is shown in Figure C.3 and the line physical parameters are given in Table C.1.

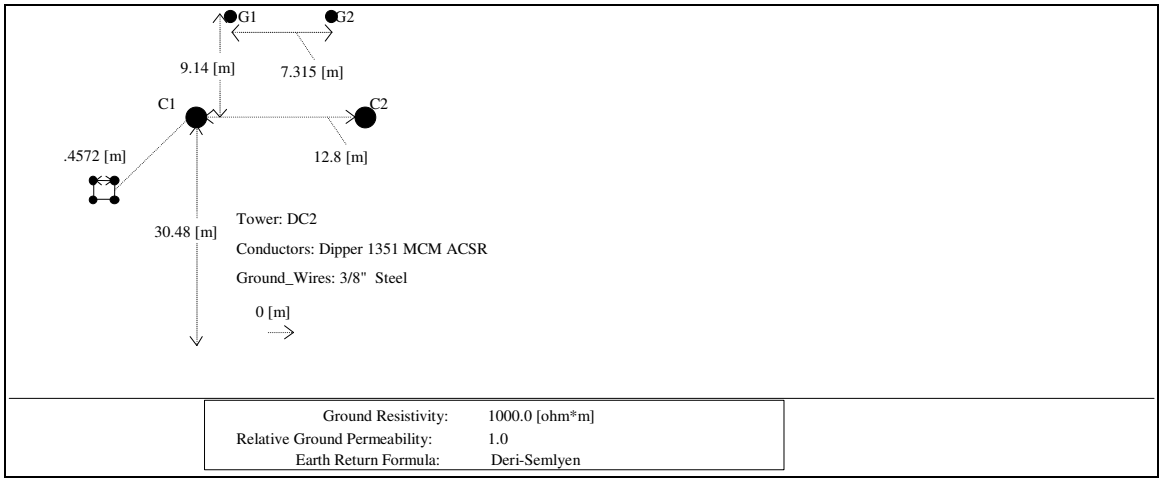


Figure C.3 - HVDC line topology

Table C.1 - HVDC line physical data

| Description | Value |
|---|---|
| Height of all conductors measured at tower | 30.48 m |
| Horizontal spacing between conductors | 12.8 m |
| Is circuit ideally transposed ? | No |
| Eliminate overhead ground wires ? | Yes |
| Conductor type | Bundle of 4x1351 MCM Rook |
| Sub-conductor radius | 0.01760 m |
| DC resistance | 0.04561 Ω/km |
| Sag for all conductors | 12.19 m |
| Number of sub-conductors in bundle | 4 |
| Bundle spacing | 0.457 m |
| Overhead ground wire (OHGW) type | 3/8” EHS |
| OHGW radius | 0.00475 m |
| OHGW DC resistance | 4.164 Ω/km |
| Sag for all ground wires | 12.19 m |
| Height of OHGW above lowest conductor | 9.14 m |
| Spacing between OHGW | 7.315 m |
| Average ground resistivity | 1000 Ω-meters |
| Line length | 1000 km |

### C.2.3. Smoothing reactors

Smoothing reactors of 270 mH are included as shown in Figure C.1. No attempt has been made to optimize this value.

## C.2.4. AC Systems

### C.2.4.1. Introduction

A lot of literature exists on the interaction between the converter (classical or CCC) and the interconnected AC networks, specifically relating to voltage stability, maximum power transfer, etc. This information is based on a three phase, positive sequence, steady state network representation and is not included herein. In this study the focus is on the ability of a converter to return to pre-fault power levels, following an AC fault, within an acceptable time and in a reliable manner. To a great extent, satisfactory fault recoveries depend on the ability of the inverter to return quickly to pre-fault gamma prime values, typically in the region of $\gamma' \cong 18°$, following the removal of the fault, without suffering a commutation failure. Avoiding a commutation failure when operating at small gamma prime values requires that the AC voltages be relatively undistorted.

It is instructive to consider, at least qualitatively, the sources of voltage distortion that can occur during and after AC faults. Transformer inrush currents are a major cause. Upon removal of a close-in AC fault, the converter transformer is re-energized, without the benefit of pre-insertion resistors and different levels of inrush current will occur each phase. Depending on the residual flux in the transformer's core, the inrush currents contain a DC component, 2nd and 3rd harmonics as well as smaller values of higher harmonics. The inrush currents decay at a rate determined by the X/R ratio of the AC network. Load taken by the converter may also provide a source of damping. The magnitude of the inrush currents is proportional to the strength of the AC system, with stronger AC systems providing higher levels of inrush currents. However, the amount of voltage distortion created by the inrush currents is inversely proportional to the strength of the AC system and increases as the AC system becomes weaker. Additionally the AC system's frequency response becomes important as natural resonances between the AC filters (plus line shunt capacitance) and the AC lines series reactance may coincide with the inrush current harmonic components, producing high levels of voltage distortion at these specific frequencies. This latter topic will be addressed in the following paragraphs.

### C.2.4.2. Low frequency resonances

Low frequency resonances between the AC filter (and line) capacitance and the AC system series reactance can be estimated as follows.

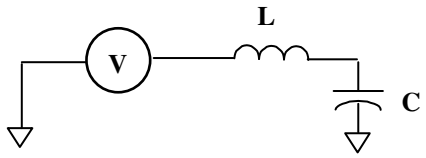


Figure C.4. LC circuit

For the system illustrated in Figure C.4, the natural resonant frequency is given by:

$$\omega_r = \frac{1}{\sqrt{LC}} \qquad \text{(C.1)}$$

If we express L as a function of the system short circuit MVA at the converter bus then:

$$L = \frac{V^2}{\omega_o MVA_{system}} \qquad \text{(C.2)}$$

Similarly, expressing C in terms of the filter MVA then

$$C = \frac{MVA_{filter}}{\omega_o V^2} \qquad \text{(C.3)}$$

Substituting equations C.2 and C.3 into C.1 gives:

$$\frac{\omega_r}{\omega_o} = \sqrt{\frac{MVA_{system}}{MVA_{filter}}} \qquad \text{(C.4)}$$

In CCC applications where the MVA of the AC filters is small, being of the order $0.1P_d < MVA_{filter} < 0.2P_d$ it may be important to include the AC line charging in $MVA_{filter}$ as the line charging may be similar in size to the AC filter MVA rating. Table C.2 shows the results for the rectifier and inverter of the benchmark system described later in this report:

Table C.2 - Low order resonances at rectifier and inverter

| | $MVA_{system}$ | $MVA_{filter}$ | Line Charging MVA | $f_r$ (Hz) |
|---|---|---|---|---|
| Rectifier | 3952 | 280 | 227 | 168 ($\cong 3^{rd}$) |
| Inverter | 2870 | 280 | 353 | 128 ($\cong 2^{nd}$) |

As mentioned earlier, transformer inrush currents contain significant amounts of 2nd and 3rd harmonics so high levels of voltage distortion can be expected upon fault clearing.

It is interesting to note that the low order resonances referred to above for the CCC benchmark, are not much different than those observed in classical HVDC projects. In classical HVDC projects the minimum SCR is typically > 2 and the AC filter capacity is typically $0.5P_d$.

### C.2.4.3. AC system representation

Both the rectifier and inverter AC system representations used herein are simplifications of more complex networks used in the flow and stability studies. The simplifications involved the creation of equivalents for the parts of the AC networks not directly connected to the converter busses. AC lines connected to the converter busses are represented by frequency dependent models. Figure C.5 is a single line diagram of the complete AC/DC system.

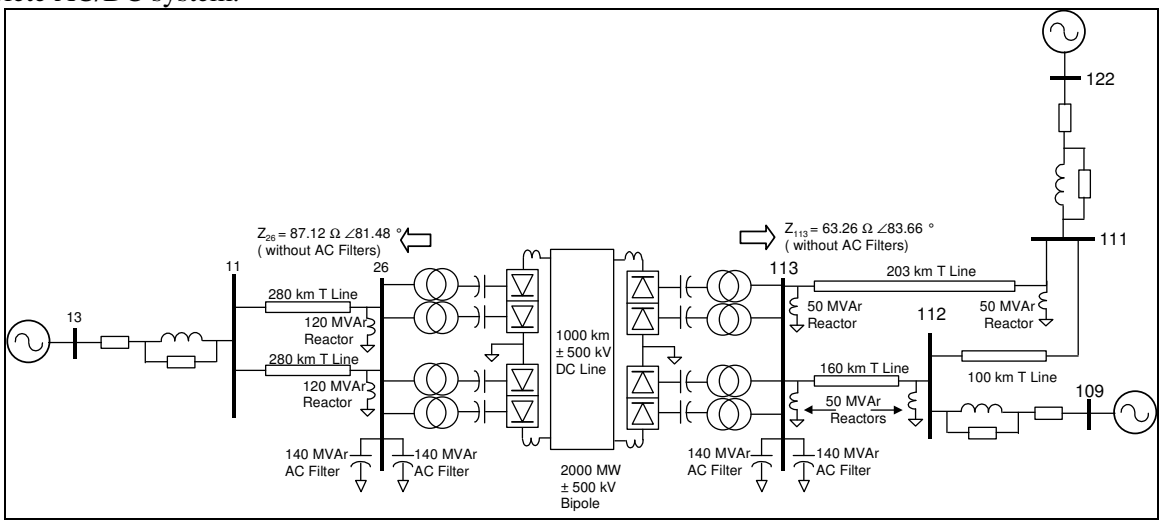


Figure C.5 - Single line diagram of complete AC/DC system

The following paragraphs give the detailed parameters for the AC lines and the equivalent networks.

### C.2.4.4. AC lines

All AC lines utilize the same tower structure (Figure C.6) and have the same per kilometer electrical parameters. The line lengths differ. Table C.3 summarizes the physical data.

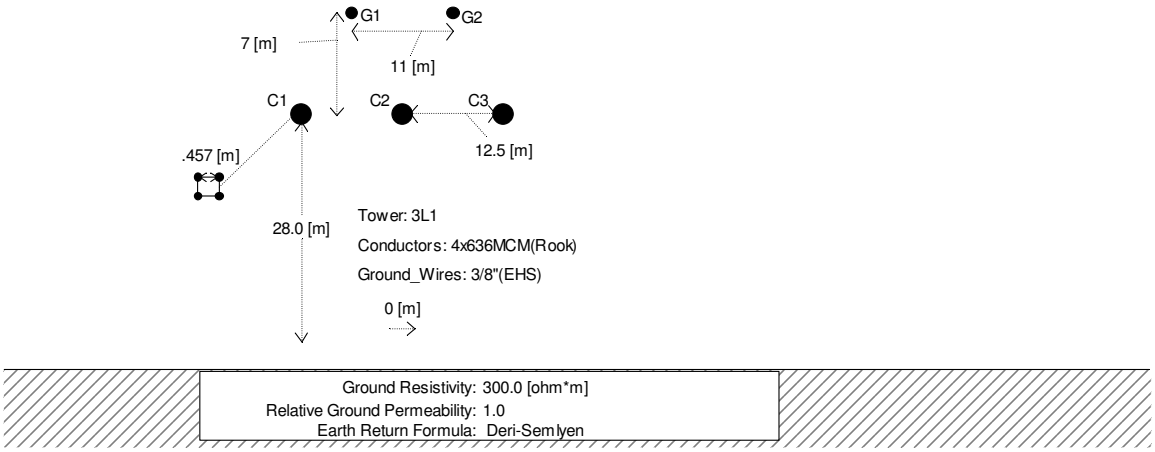


Figure C.6 - AC line topology

Table C.3 - AC line physical data

| Description | Value |
|---|---|
| Height of all conductors measured at tower | 28 m |
| Horizontal spacing between conductors | 12.5 m |
| Is circuit ideally transposed ? | Yes |
| Eliminate overhead ground wires ? | Yes |
| Conductor type | Bundle of 4x636 MCM Rook |
| Sub-conductor radius | 0.01242 m |
| DC resistance | 0.0989 Ω/km |
| Sag for all conductors | 17 m |
| Number of sub-conductors in bundle | 4 |
| Bundle spacing | 0.457 m |
| Overhead ground wire (OHGW) type | 3/8” EHS |
| OHGW radius | 0.004763 m |
| OHGW DC resistance | 3.81 Ω/km |
| Sag for all ground wires | 15.3 m |
| Height of OHGW above lowest conductor | 7 m |
| Spacing between OHGW | 11 m |
| Average ground resistivity | 300 Ω-meters |
| Line length L11-26 | 280 km |
| Line length L113-111 | 203 km |
| Line length L113-112 | 160 km |
| Line length L112-111 | 100 km |

Using the above line data, the PSCAD line constants program generated the following data shown in Table C.4:

Table C.4 - Positive and zero sequence per km AC line parameters

| Description | Value |
|---|---|
| Positive sequence impedance | 0.0254412 + j 0.333059 Ω/km |
| Positive sequence capacitive susceptance | 0.498225E-5 mhos/km |
| Zero sequence impedance | 0.356981 + j 1.261466 Ω/km |
| Zero sequence capacitive susceptance | 0.348418E-5 mhos/km |

### C.2.4.5. Equivalent networks

Network equivalents of the form $R_0 + R_1 // j X_1$ are used to represent the positive sequence impedance for AC systems behind busses 11, 111 and 112. This type of equivalent is commonly used in EMTP type studies and provides a circular locus, with increasing frequency in the Z plane. In EMTDC, this data is specified as a magnitude and phase at fundamental frequency. Additionally, a harmonic frequency at which the phase is the same as at fundamental frequency is also specified (set to the 3rd harmonic herein). Zero sequence values are input as a magnitude and phase at fundamental frequency. Table C.5 gives the positive sequence component values (in rectangular and polar form) and the zero sequence component values (in polar form) used in the equivalents.

Table C.5 - Component values used in equivalents

| Bus | Positive Sequence | | Zero Sequence |
|---|---|---|---|
| 11 | $R_0$ | 5.80 Ω | 73.32 Ω ∠71.29° |
| | $R_1$ | 665.0 Ω | |
| | $X_1$ | 35.70 Ω | |
| | $Z_{11\ (see\ Note\ 1)}$ | 36.42 Ω ∠77.78° | |
| 111 | $R_0$ | 2.435 Ω | 76.75 Ω ∠77.69° |
| | $R_1$ | 2055.0 Ω | |
| | $X_1$ | 40.90 Ω | |
| | $Z_{111\ (see\ Note\ 1)}$ | 41.01 Ω ∠85.46° | |
| 112 | $R_0$ | 17.10 Ω | 196.21 Ω ∠70.05° |
| | $R_1$ | 1710.0 Ω | |
| | $X_1$ | 98.116 Ω | |
| | $Z_{112\ (see\ Note\ 1)}$ | 100.40 Ω ∠76.93° | |

Notes: 1) The impedance of the equivalent is calculated with the rest of the AC network **disconnected**.

Line shunt reactive compensation is provided as shown in table C.6:

Table C.6 - Line shunt reactor values

| Location | Value |
|---|---|
| Line 112-113 | 50 Mvar at each end |
| Line 111-113 | 50 Mvar at each end |
| Line 11-26, circuit 1 | 120 Mvar at bus 26, 0 Mvar at bus 11 |
| Line 11-26, circuit 2 | 120 Mvar at bus 26, 0 Mvar at bus 11 |

Determining the "equivalent π" representation of the AC lines (valid at steady state, fundamental frequency only) and including the AC network equivalents described previously, results in the networks shown in Figures C.6.a and C.6.b.

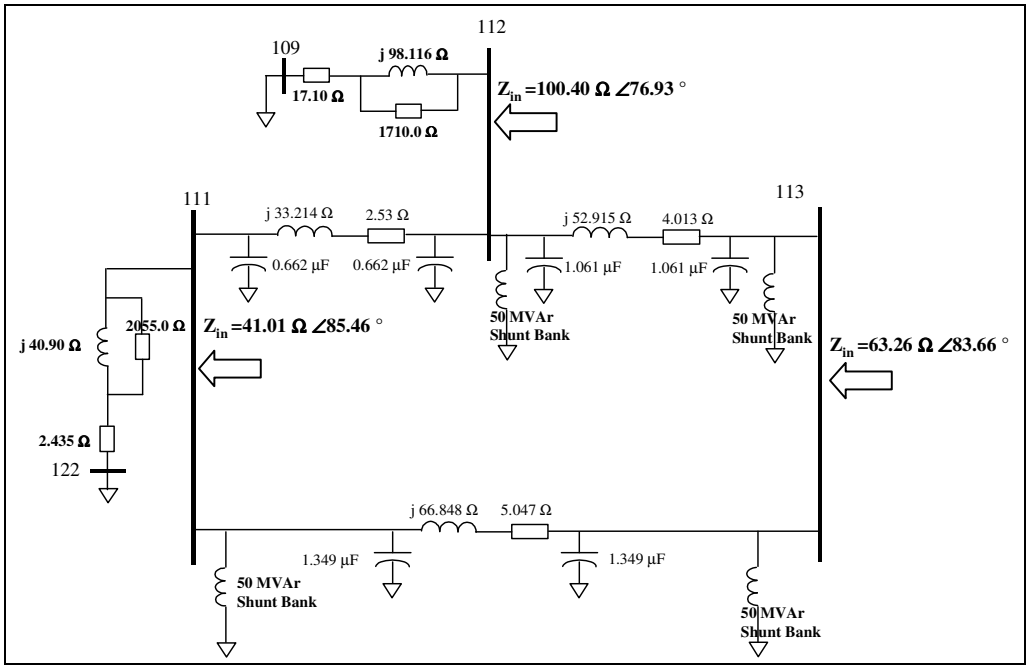


Figure C.6.a - Steady state positive sequence rectifier AC network

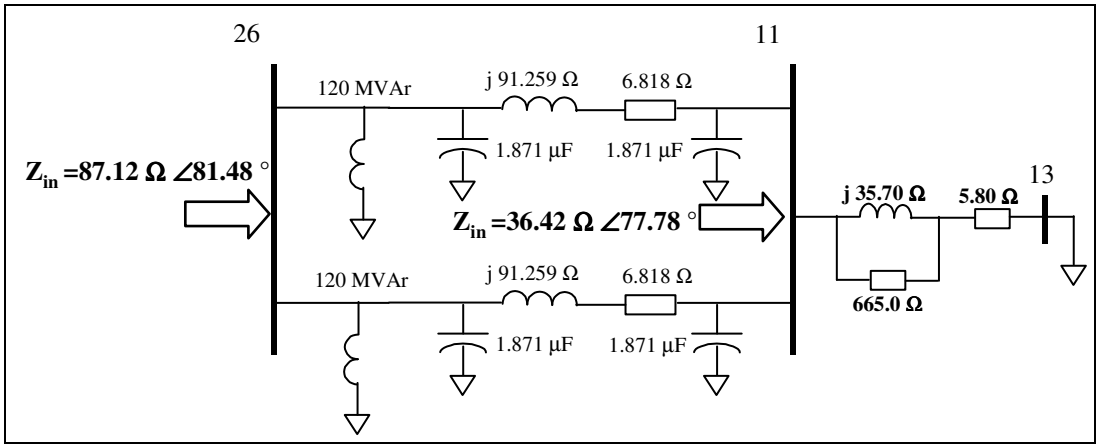


Figure C.6.b - Steady state positive sequence inverter AC network

From the impedances calculated at bus 113 (the rectifier) and bus 26 (the inverter), the simple SCR can be determined as shown in Table C.7.

Table C.7. Converter bus 3-phase short circuit levels and SCR values

| **Bus** | **Impedance** | **Short Circuit Level** | **Simple SCR (Short Circuit Ratio) at $P_d$ = 2000 MW** |
|---|---|---|---|
| **113 (Rectifier)** | 63.26 Ω ∠83.66 ° | 3952 MVA ∠83.66 ° | 1.98 |
| **26 (Inverter)** | 87.12 Ω ∠81.48 ° | 2870 MVA ∠81.48 ° | 1.43 |

### C.2.5. AC Filters

- Each 1000 MW converter has a 140 Mvar AC filter bank and identical ratings are used at the rectifier and inverter: Table C.8 gives the filter component values

Table C.8 - AC Filter Bank Component Values

| | **11th** | **13th** | **24th** | **36th** |
|---|---|---|---|---|
| **R (Ohms)** | 4.244 | 4.999 | 3963 | 1218.0 |
| **L (Henries)** | 0.154 | 0.153 | 0.024 | 0.017 |
| **C (µFarads)** | 0.3788 | 0.2721 | 0.5021 | 0.3265 |
| **S (Mvar)** | 36 | 25.8 | 47.4 | 30.8 |
| **Q factor** | 150 | 150 | 18 | 5.4 |

- The 11th and 13th branches are series tuned RLC filters (R+L+C) while the 24th and 36th are damped branches (C+L//R).

Using the AC networks described previously (using frequency dependent line models) and the AC filter values from Table C.8, the frequency response as seen from the converter busses has been calculated using ATP. Figures C.7.a and C.7.b show the results at the rectifier and inverter respectively.

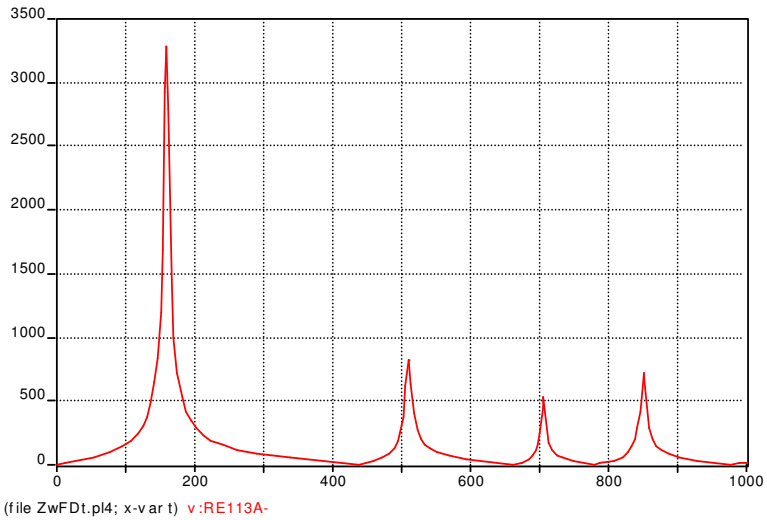


Figure C.7.a - Impedance of AC filter and rectifier AC network seen from converter bus

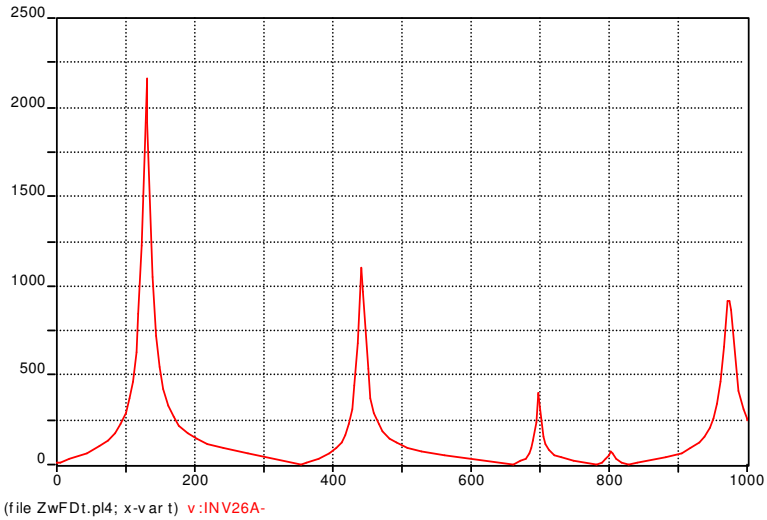


Figure C.7.b - Impedance of AC filter and inverter AC network seen from converter bus

Note that both the rectifier and inverter AC networks, including the AC filters, exhibit low order resonances in the region approximately from the 2nd harmonic (at the inverter) to the 3rd harmonic (at the rectifier).

## C.3. Description of Controls

### C.3.1. Rectifier VDCOL and CCA (Voltage Dependent Current Order Limiter and Current Control Amplifier)

Figures C.8, C.9 and C.10 illustrate the rectifier's VDCOL and CCA. Not all inputs shown in the figures are used.

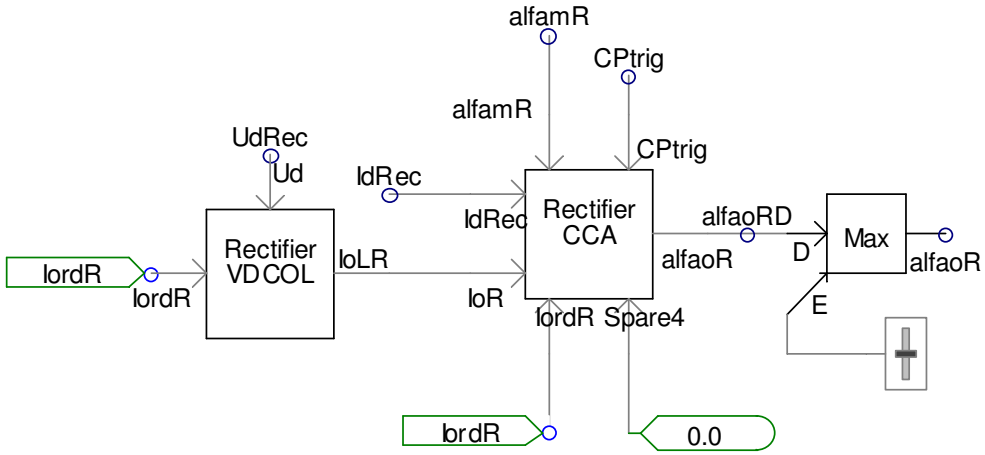


Figure C.8 - Rectifier VDCOL and CCA

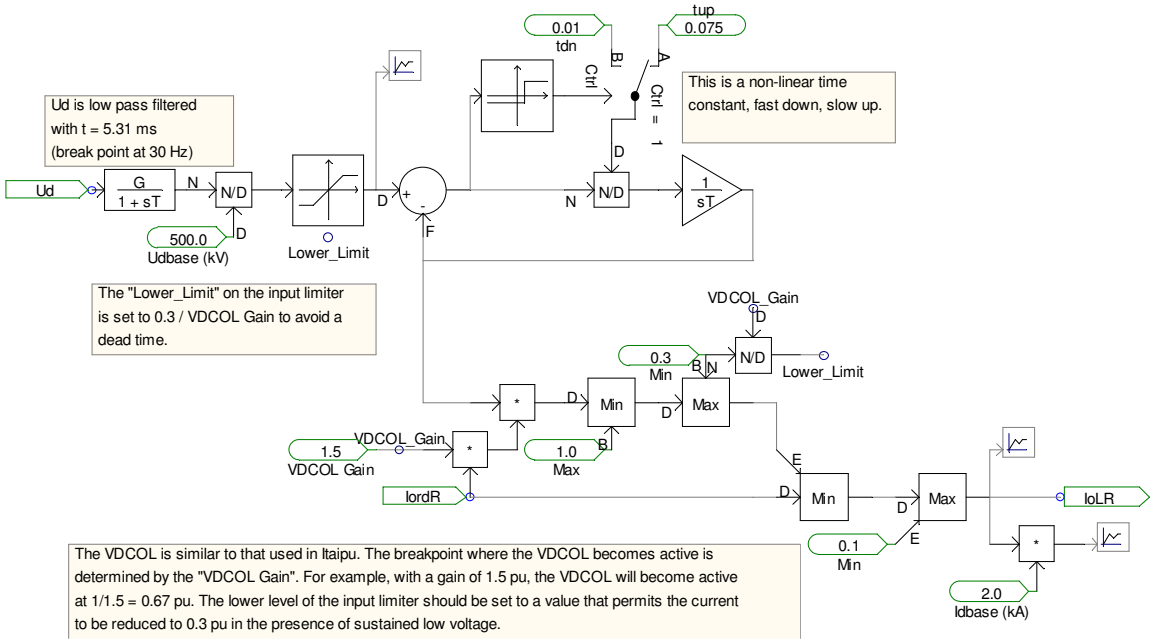


Figure C.9 - Voltage Dependent Current Order Limiter (VDCOL)

The VDCOL produces a current order limit based on measured DC voltage. In early projects, the intent of this function was to limit current to 0.3 pu during disturbances where commutations were not occurring and the DC current would flow continuously through the same valves. By reducing current order in response to low DC (usually resulting from low AC) voltage, the VDCOL is also useful in reducing the converter's reactive power consumption during AC network faults which helps restore the AC voltage. However, this type of VDCOL which makes the current order a sensitive function of measured DC voltage, introduces a

positive feedback path in the current control loop, when the VDCOL is active. This reduces the stability margin and may produce low frequency oscillations during some very long AC faults.

As shown in Figure C.9, a non linear (fast down, slow up) time constant is used to filter the measured voltage. This filtered voltage is then scaled by a gain factor "VDCOL Gain" and used as a current limit. The voltage level at which the VDCOL becomes active is (1 / VDCOL Gain). Settings are determined by experimentation.

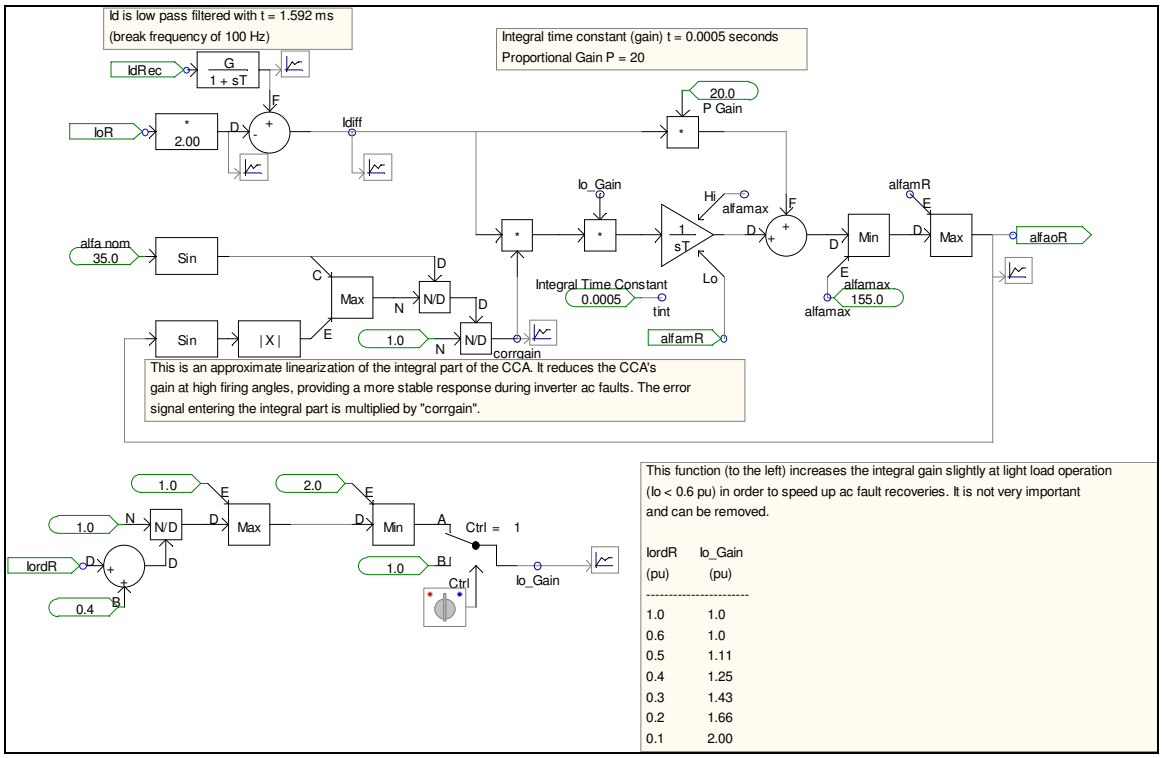


Figure C.10 - Rectifier Current Control Amplifier (CCA)

The current control amplifier is a conventional PI regulator. Of special interest at the rectifier is the alpha minimum limit which is calculated as described in the next section. Note that the HVDC control process is inherently nonlinear with DC voltage being a function of cos(alpha). Consequently at firing angle extremes (near 0 or near 180 degrees) the incremental gain of the CCA is much lower than at values near 90 degrees. During inverter AC faults the rectifier may be required to operate at near 90 degrees firing angles during the fault , resulting in an oscillatory current response due to the high incremental CCA gain. This non-linearity can approximately compensated for by multiplying the current error signal by a factor [sin ($\alpha_{nom}$) / sin ($\alpha$)] where $\alpha_{nom}$ is the value at which the correction factor equals 1 pu and $\alpha$ is the output of the CCA. It is sufficient to apply the correction factor to the current error signal entering the integral part of the current regulator, at the rectifier only.

During operation at low current order, recoveries from AC faults tend to become slower. Although slower recoveries at low power are probably quite acceptable in most projects, a correction factor has been added to minimize this tendency. Similar to the $\alpha$ linearization function mentioned in the previous paragraph, the current error signal entering the CCA's integral term is multiplied by a factor proportional to (1 / $I_{order}$).

### C.3.2. Rectifier Alpha Limit Calculation

In order to ensure reliable firing, a sufficiently high forward voltage should exist across a valve before firing. In this model no valve voltage measurements are used for control purposes and an estimation is used to determine an alpha minimum limit that will provide the required valve forward voltage. Figure C.11 illustrates the relationship between alpha, Udio and Id at the rectifier. In this figure alpha measured at the converter bus produces the minimum alpha prime across the valve (5 degrees nominally).

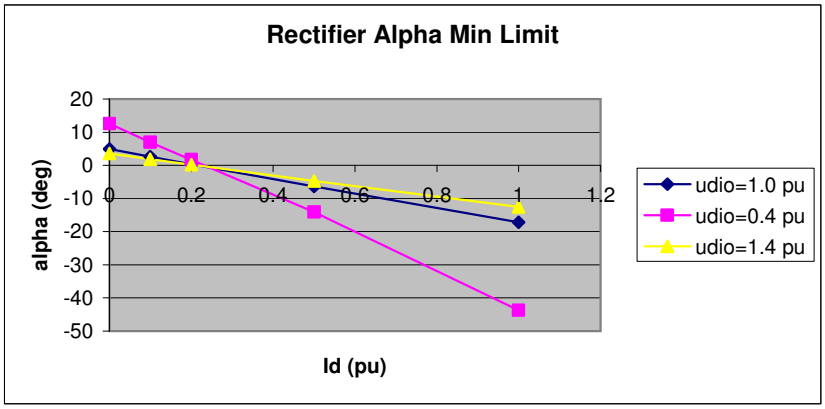


Figure C.11 - Rectifier Alpha Minimum, Udio and Id Curves

A second order approximation of the following form can be made:

$$\alpha_{minimum} = k_{u2}\{(I_d - k_1)/u_{dio}\}^2 + k_{u1}\{(I_d - k_1)/u_{dio}\} + k_{u0}$$

By choosing 3 points from the above curves, the unknown coefficients $k_{u0}$, $k_{u1}$ and $k_{u2}$ can be determined The value $k_1$ is the displacement in the Id curves where the 3 curves intersect (estimated at $k_1$= 0.248). For the main circuit values used, the coefficient values are calculated to be:

$$k_{u0} = -0.76$$
$$k_{u1} = -21.971$$
$$k_{u2} = 0.056$$

Figure C.12 illustrates the details of the rectifier's alpha minimum calculation.

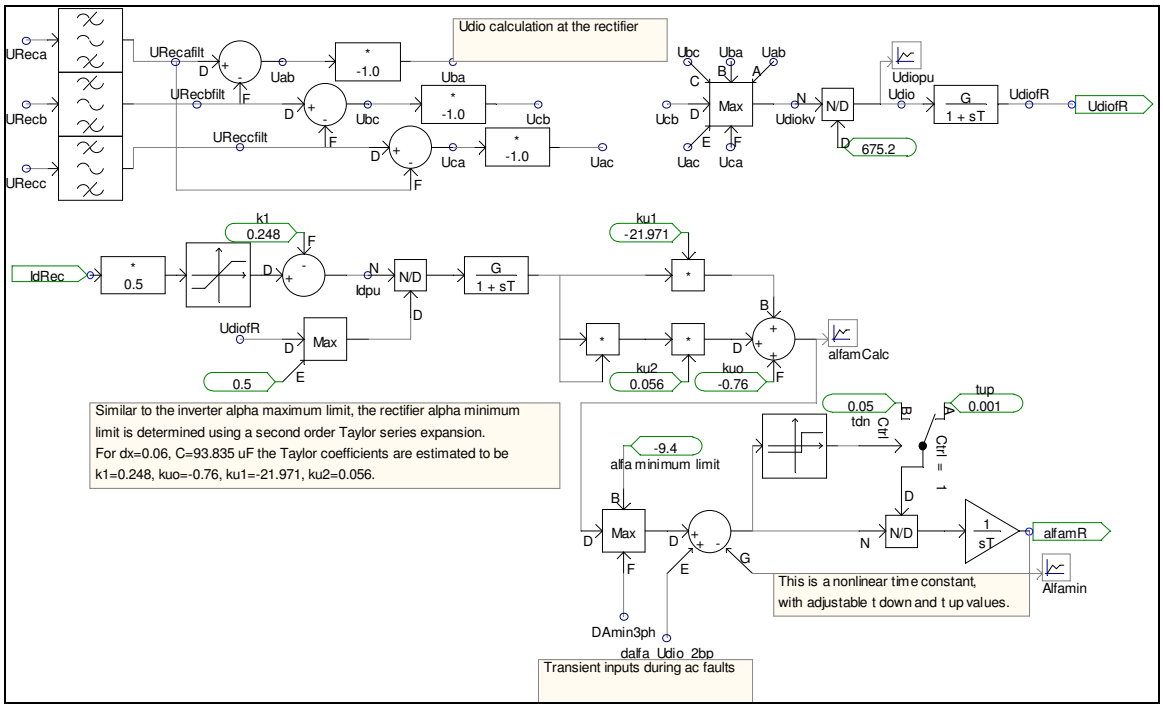


Figure C.12 - Rectifier Alpha Minimum Limit Calculation

In the upper part of the Figure, Udio is measured by full wave rectifying and scaling the 500 kV bus voltages. The remainder shows the 2nd order approximation.

The alpha minimum calculation assumes that that network is in steady state conditions. During rectifier AC faults, alpha minimum is increased to improve the fault recoveries. A non-linear filter (fast increase, slow decrease) is provided to avoid sudden reductions in the alpha minimum limit which could cause a sudden increase in current.

During a rectifier AC fault, the inverter goes into current control and the rectifier's CCA saturates on its alpha minimum limit. Upon removal of the fault the rectifier DC voltage reappears in a step (at least for severe symmetrical faults) and causes a rapid increase in direct current and possibly a commutation failure at the inverter. To slow down the recovery, rectifier AC faults are detected and the alpha minimum limit increased.

Negative sequence voltages on the AC side of the converter produce a 2nd harmonic component in voltage and current on the DC side of the converter. Therefore, unsymmetrical AC faults are easily detected by measuring the 2nd harmonic content of the rectifier's Udio and increasing the rectifier alpha minimum limit as shown in Figure C.13.

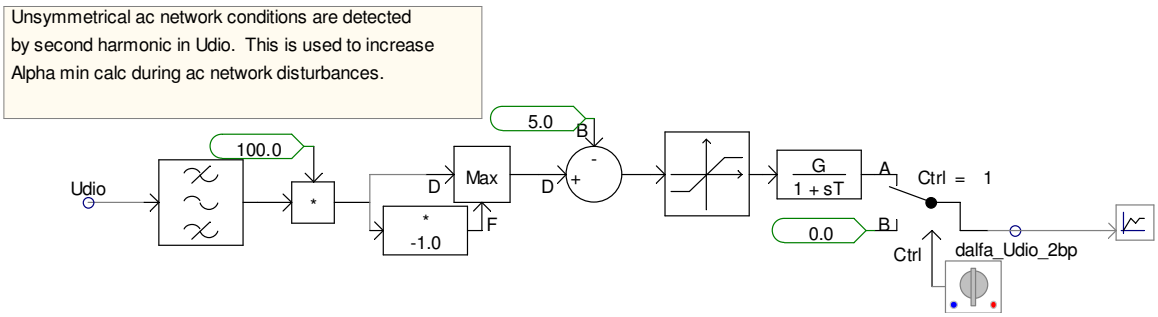


**Figure C.13 - Detection of rectifier unsymmetrical AC faults**

Symmetrical AC faults at the rectifier are detected when all three individual phase voltages fall below a preset level as shown in Figure C.14.

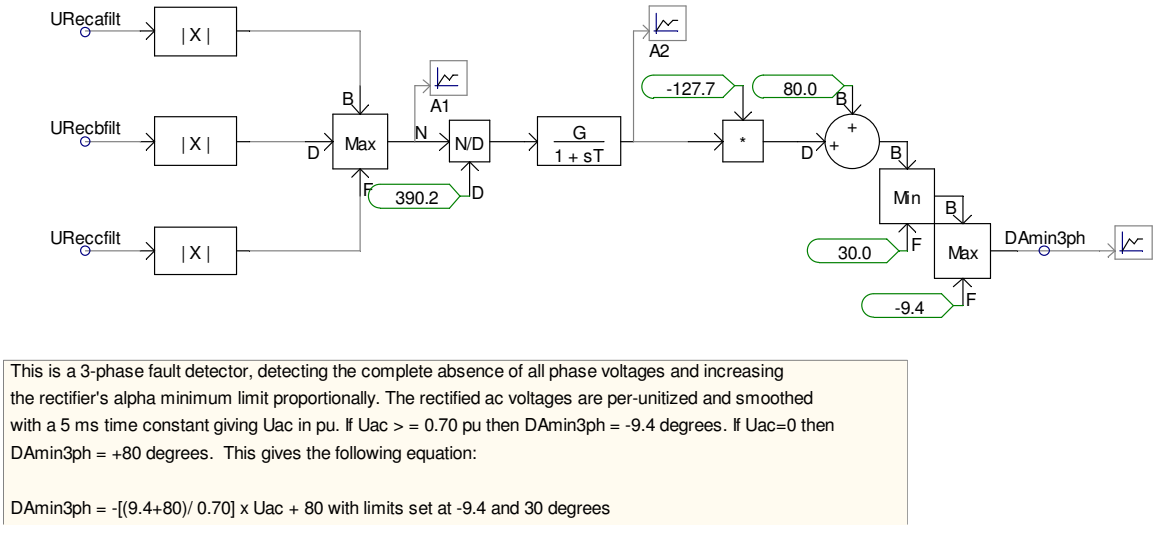


Figure C.14 - Detection of rectifier symmetrical AC faults

Functions that increase the rectifier's alpha minimum limit during rectifier AC fault reduce the power transmitted during such faults. But, they help avoid inverter commutation failures which delay recoveries.

Maximum Ud occurs at alpha = -9.4 degrees. Operation at more negative alpha values could be attractive as it results in the converter actually generating reactive power but is not attempted here as it requires some additional control strategies to overcome the fact that two different alpha values produce the same voltage. To avoid such operation a -9.4 degree limit is included in the alpha minimum calculation shown in the previous figures.

### C.3.3. Firing Controls

Figure C.15 illustrates the concept of the generic "phase vector" firing controls available in PSCAD/EMTDC and used in this model. In general, the performance of the firing controls has been found very satisfactory.

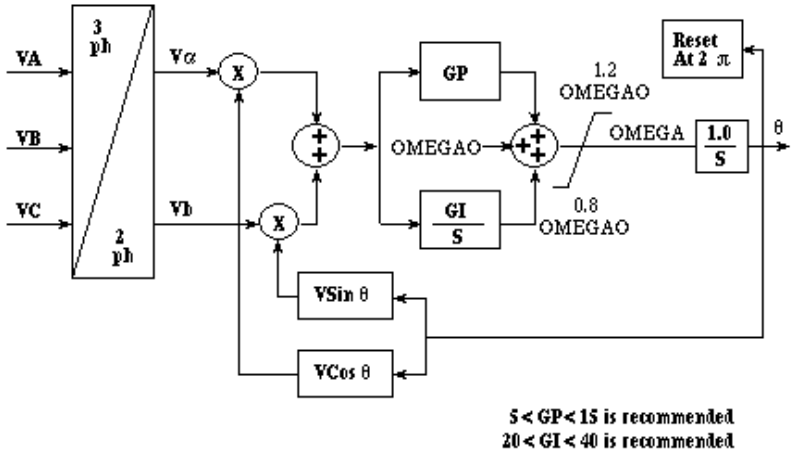


Figure C.15 - PSCAD "Phase Vector" Firing Controls

### C.3.4. Inverter VDCOL and CCA

The inverter's VDCOL and CCA are almost the same as the rectifier's described previously. As shown below in Figure C.16, the inputs to the proportional and integral parts of the CCA are arranged differently to provide the traditional positive resistance characteristic in the inverter's steady state V / I curve. Additionally, the current order margin is subtracted from Id in the inverter's CCA. During disturbances, when the VDCOL is active, the current margin in increased from 10% to 20% in order to speed up some AC fault recoveries. (Note that this also reduces power transmitted during faults).

The inverter's alpha maximum limitation is calculated as described later in this report.

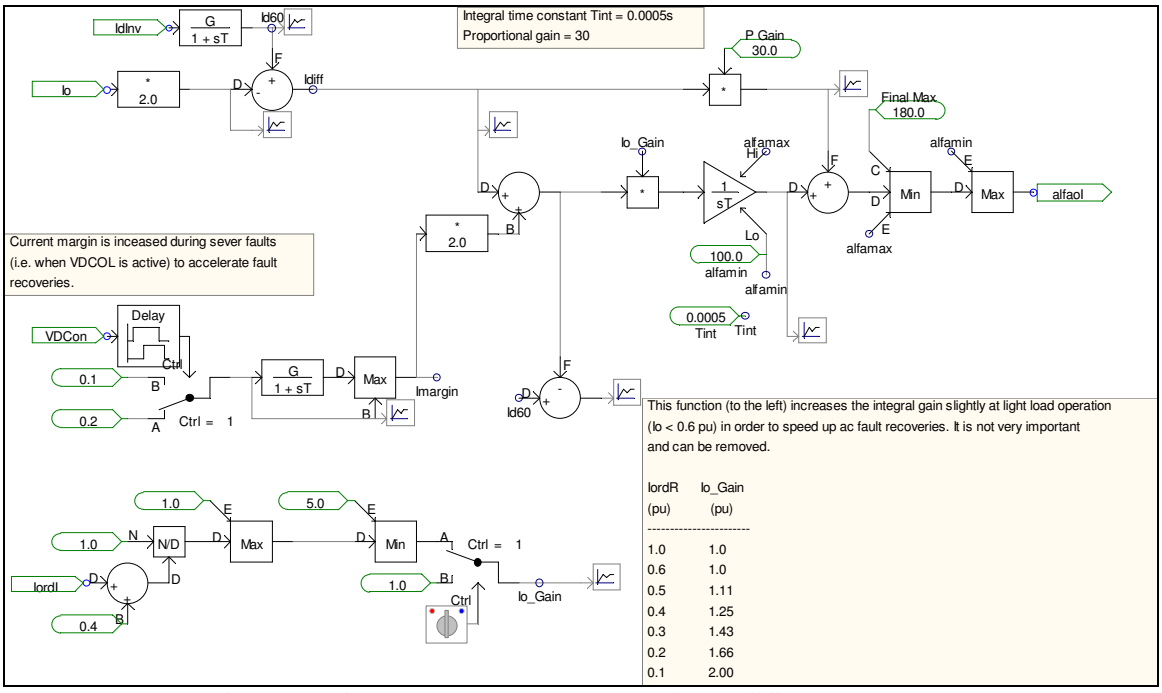


Figure C.16 - Inverter's Current Control Amplifier (CCA)

### C.3.5. Inverter Alpha Maximum Calculation

In the inverter an alpha order is calculated to provide the desired gamma prime value. This calculated value serves as an upper limit for the inverter's CCA and in normal operation the CCA's output is held against this limit. This calculation is based on a second order approximation of the curves shown in Figure C.17 for gamma prime = 23 degrees.

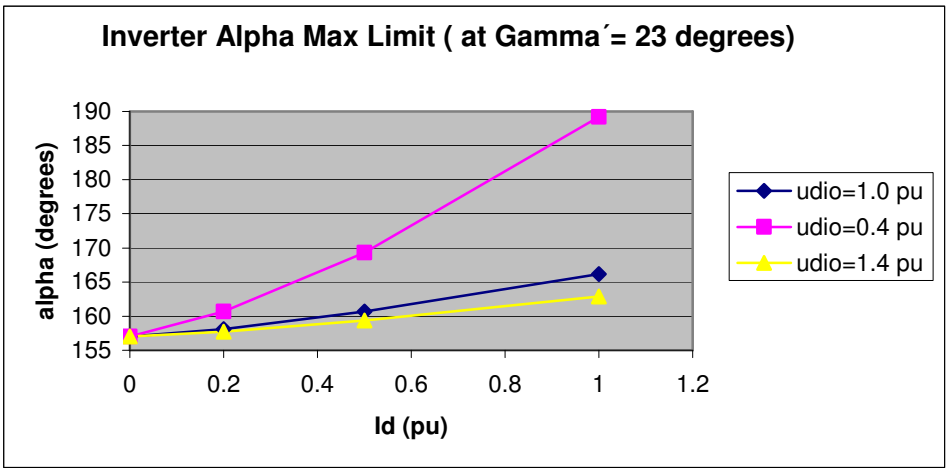


Figure C.17 - Inverter Alpha Maximum, Udio and Id Curves

The approximation, illustrated in Figure C.18, is of the following form:

$$\alpha_{maximum} = a_2(I_d/u_{dio})^2 + a_1\{I_d/u_{dio}\} + a_0$$

where (for gamma prime = 23.0 degrees)

$$a_0 = 157.00;\ a_1 = 5.496;\ a_2 = 3.672$$

For gamma prime = 18 degrees, the calculated coefficients are:

$$a_0 = 162.00;\ a_1 = 3.422;\ a_2 = 4.828$$

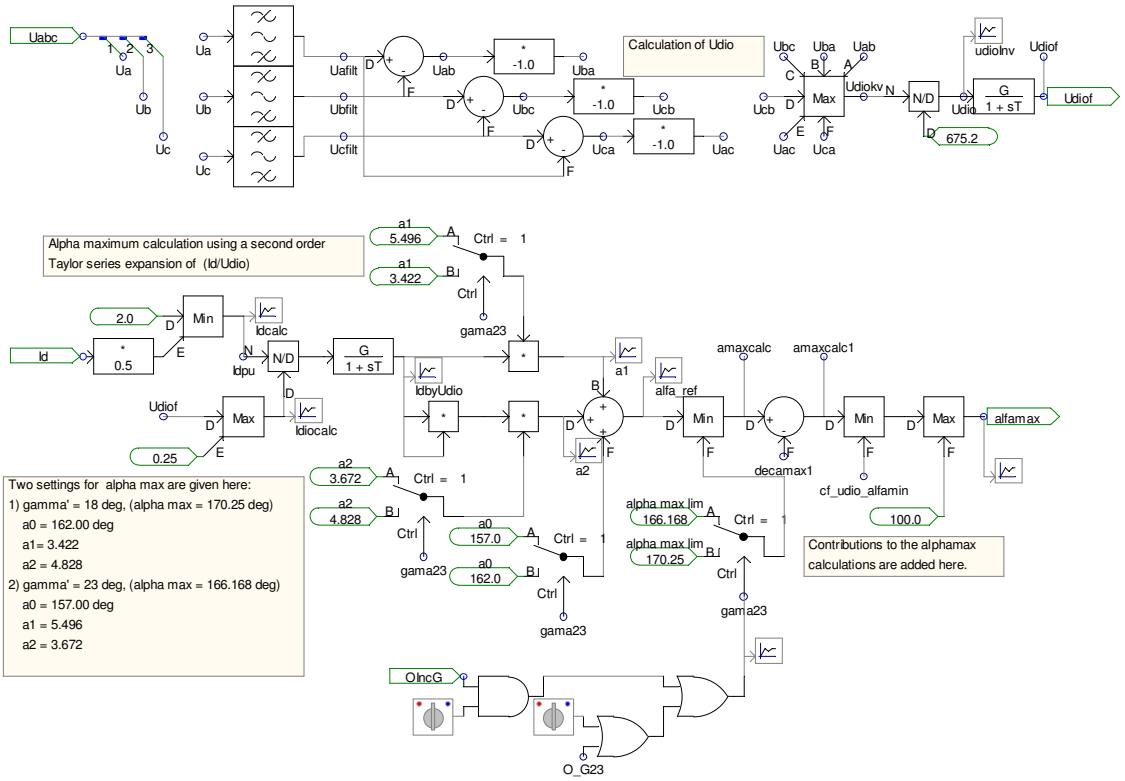


Figure C.18 - Inverter's Alpha Maximum Calculation

Similar to Figure C.12, Udio is measured for use in the calculation. An operator controlled switch is provided to select between gamma prime 23 degree and gamma prime 18 degree operation.

The calculations described above determine an alpha order that will produce a desired gamma prime value. These calculations assume symmetrical steady state operation. Even during symmetrical inverter AC faults the calculations appear adequate. However, there are several cases where additional signals may be useful to transiently reduce the alpha max limit or to transiently select gamma prime 23 degree operation rather than gamma prime 18 degree operation and these are described in the following paragraphs.

- During operation with an unsymmetrical AC network, it should be possible to calculate an alpha to produce a desired gamma prime value on the valves with the lowest AC voltage, but this calculation is not attempted herein. Instead a simple control function is used in which unsymmetrical AC faults are detected by a measurement of 2nd harmonic in Udio. This function is the same as that used in the rectifier. The resulting signal is filtered and used to reduce the inverter's alpha minimum limit. The gain and time constant values are determined by trial and error. This function appears to work well and is illustrated in Figure C.19.

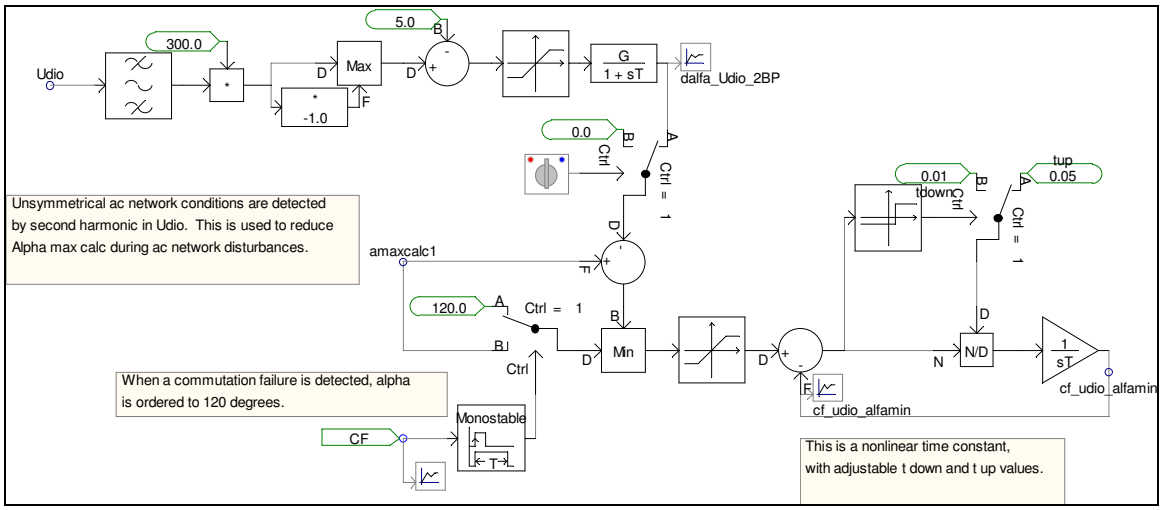


Figure C.19 - Inverter's Alpha Order Reduction due to an Unsymmetrical AC Network or a Commutation Failure

- When a commutation failure is detected, alpha is ordered to 120 degrees as shown in Figure C.19.
- Upon removal of AC faults, the converter transformer is re-energized and transformer inrush currents occur. Inrush currents are typically 2nd , 3rd and 5th harmonic. The current magnitudes are low due to the weak AC network feeding the transformers, but they cause high levels of voltage distortion due to the high values of the network impedance at these frequencies. Inrush currents can last for hundreds of milliseconds, or even seconds depending on the X/R ratio of the network feeding the transformers. Figure C.7.b shows the AC network frequency response as seen from the inverter's AC bus. To reduce the risk of a commutation failure due to transformer inrush currents, the inrush currents are measured and the inverter's alpha minimum limit reduced. The measurement is made by taking the difference between one transformer's primary and secondary currents (corrected for the turns ratio) as shown in Figure C.20. In the last revision of the PSCAD model, with slightly changed AC networks, this function appeared to be unnecessary and was switched off.

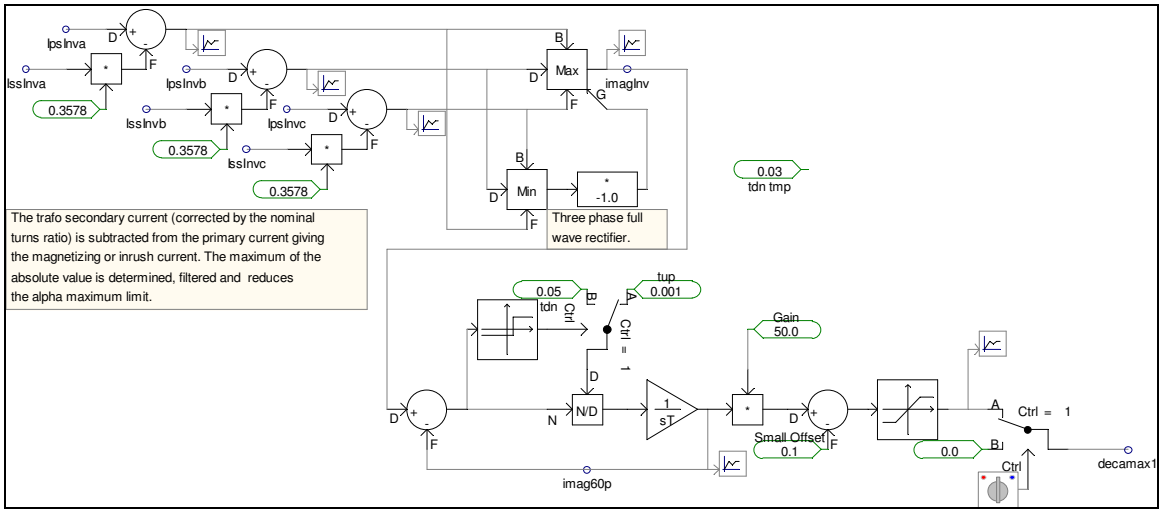


Figure C.20 - Measurement of Transformer Inrush Currents

- After an inverter commutation failure, when the normal sequence of conducting valves is re-established, some of the commutation capacitors may be charged to a high residual voltage. This voltage offset results in unsymmetrical valve firing (some valves fire with an increased value of gamma prime while others fire with a reduced value of gamma prime) and a commutation failure may occur. This phenomenon is most apparent at light load where the DC offset lasts for hundreds of milliseconds. The solution selected was to choose gamma prime 23 degrees whenever a DC offset is measured across the commutation capacitors. This is not a good solution, as it requires measuring the voltages across the capacitors. A less costly solution is to select gamma prime 23 degrees operation whenever light load operation occurs. Figure C.21 illustrates the logic used.

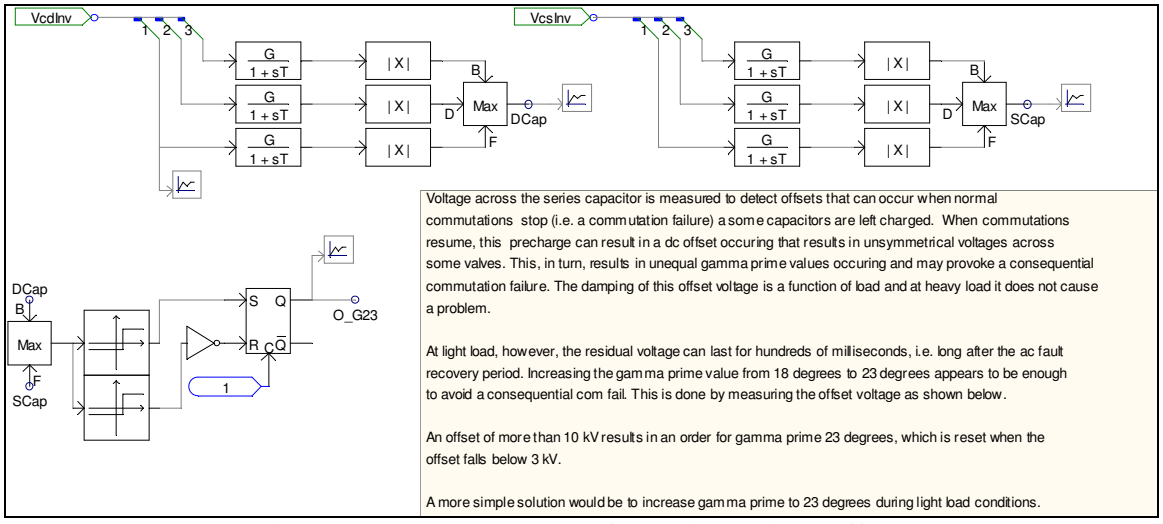


Figure C.21 - Measurement of capacitor voltage offsets

- Gamma prime operation at 18 degrees is the normal mode of operation. However, more reliable fault recoveries occur when gamma prime is 23 degrees. A feature was added that selects gamma prime 23 degrees whenever the VDCOL is active. This slows down the recoveries very slightly.

### C.3.6. Commutation Failure Detection

Commutation failure detection is achieved by comparing the direct current on the converter DC circuit with the rectified currents in the valves (or the rectified currents on the valve side of the converter transformer). Upon detection, the inverter alpha order is set to 120 degrees for a short period of time after which a return to

normal operation is ordered. Without this function, recoveries from inverter AC faults may not be possible in all cases. Figure C.22 illustrates the detection function.

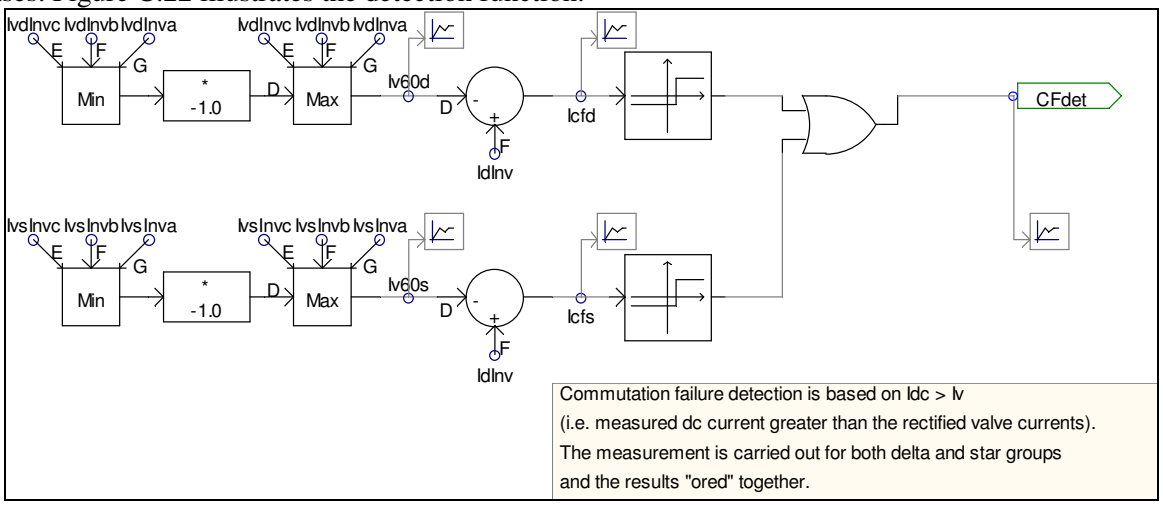


Figure C.22 - Commutation Failure Detection

## C.4. Dynamic Performance Evaluation

The dynamic performance of the transmission system is a measure of its ability to recover from disturbances in a reliable and predictable fashion. The most typical disturbances are AC line faults and these are the only cases include herein. A more complete examination might include starting / stopping of converters, switching AC elements (filter banks, lines, transformers, etc), DC line faults with restart sequences, AC line faults with reclose sequences, etc., but this has not yet been attempted.

A typical HVDC specification could require recovery times of 200 ms from the clearing an AC fault to the restoration of 90% of the pre-fault power. It might also state that commutation failures should not occur during the recovery period, or due to rectifier AC faults. Levels of power transmitted during certain types of AC faults might also be specified.

In this study, to reduce the computing time, one set of controls operate two 12pulse 1000 MW poles.

At the inverter, AC fault recovery times are strongly influenced by the distortion occurring in the AC bus voltages upon removal of the fault. This voltage distortion is mostly due to transformer inrush currents and the impedance of the AC network at frequencies included in the spectrum of the transformer inrush currents. At fundamental frequency, the network impedance is determined by the short circuit level (magnitude and phase). At higher frequencies shunt elements (AC filters, capacitor banks, reactors, etc) and AC transmission lines become important. The network representations used in this report is described in section C.2.4.

Since transformer inrush currents are an important factor in inverter AC fault recoveries, the representation of the transformer saturation is important. In this report “typical” saturation characteristics (default values given in PSCAD) are used and no attempt has been made to determine the correctness of these characteristics. Additionally, transformer inrush depends on the instant of fault application as this determines the flux levels in the transformer that will exist when the fault is removed. Therefore faults must be applied at various time intervals to identify the worst case. Losses are also important in that they determine the duration of the inrush currents.

AC faults are applied by connecting an impedance (R+L), via a circuit breaker, between the converter bus and ground. Impedance values are adjusted to simulate near or remote AC faults. The fault impedance angle is maintained constant at 80 degrees for all cases. Single and 3-phase faults, lasting for 100 ms and 200 ms are used.

Tables C.9 and C.10 below summarize the cases included herein. Plots for these cases, showing typical results, are included in the CD. The fault impedance has been varied to produce converter bus voltages

(during 3-phase faults) of very approximately 0.0, 0.20, 0.40, 0.60, 0.80 pu at loads of Id =1.0, 0.5 and 0.2 pu. The time required to reach 0.80 pu and 0.90 pu of the prefault power is noted for each case. In cases were the power rises above 0.8 pu or 0.9 pu level and then drops below the level for a short time, eventually rising above the level again, the times for each crossing are noted.

For the cases shown herein, the inverter gamma prime was maintained at 18 degrees in the steady state.

Table C.9 - List of Rectifier AC faults.

| Case | Pd (MW) | Type | Duration (ms) | Fault Impedance ( Ω ) | Residual Voltage (pu) | Time to 80% Prefault Power (ms) | Time to 90% Prefault Power (ms) |
|---|---|---|---|---|---|---|---|
| 1 | 2000 | Rec 3-ph | 200 | (0.067+ $j\omega_o$0.001) | ≅ 0 | 105 | 116, 260 |
| 2 | 2000 | Rec 1-ph | 200 | As above | | 47 | 60, 174 |
| 3 | 2000 | Rec 3-ph | 100 | As above | ≅ 0 | 94 | 102, 242 |
| 4 | 2000 | Rec 1-ph | 100 | As above | | 48 | 64, 162 |
| 5 | 2000 | Rec 3-ph | 200 | (3.32+ $j\omega_o$0.05) | ≅ 0.27 | 93 | 100, 176 |
| 6 | 2000 | Rec 1-ph | 200 | As above | | 16 | 27, 123 |
| 7 | 2000 | Rec 3-ph | 100 | As above | ≅ 0.27 | 85 | 97, 161 |
| 8 | 2000 | Rec 1-ph | 100 | As above | | 15 | 18, 110 |
| 9 | 2000 | Rec 3-ph | 200 | (6.64+ $j\omega_o$0.1) | ≅ 0.41 | 73 | 80 |
| 10 | 2000 | Rec 1-ph | 200 | As above | | 10 | 15 |
| 11 | 2000 | Rec 3-ph | 100 | As above | ≅ 0.41 | 70 | 79 |
| 12 | 2000 | Rec 1-ph | 100 | As above | | 7 | 12 |
| 13 | 2000 | Rec 3-ph | 200 | (13.28+ $j\omega_o$0.2) | ≅ 0.59 | 15 | 30 |
| 14 | 2000 | Rec 1-ph | 200 | As above | | 8 | 13 |
| 15 | 2000 | Rec 3-ph | 100 | As above | ≅ 0.59 | 13 | 18 |
| 16 | 2000 | Rec 1-ph | 100 | As above | | --- | 12 |
| 17 | 2000 | Rec 3-ph | 200 | (39.84+ $j\omega_o$0.6) | ≅ 0.80 | 8 | 12 |
| 18 | 2000 | Rec 1-ph | 200 | As above | | --- | 10 |
| 19 | 2000 | Rec 3-ph | 100 | As above | ≅ 0.80 | 8 | 12 |
| 20 | 2000 | Rec 1-ph | 100 | As above | | --- | --- |
| 21 | 1000 | Rec 3-ph | 200 | (0.067+ $j\omega_o$0.001) | ≅ 0.0 | 115 | 130 |
| 22 | 1000 | Rec 1-ph | 200 | As above | | 44 | 65 |
| 23 | 1000 | Rec 3-ph | 100 | As above | ≅ 0.0 | 100 | 120 |
| 24 | 1000 | Rec 1-ph | 100 | As above | | 46 | 79 |
| 25 | 1000 | Rec 3-ph | 200 | (3.32+ $j\omega_o$0.05) | ≅ 0.24 | 94 | 110 |
| 26 | 1000 | Rec 1-ph | 200 | As above | | 17 | 27 |
| 27 | 1000 | Rec 3-ph | 100 | As above | ≅ 0.24 | 90 | 100 |
| 28 | 1000 | Rec 1-ph | 100 | As above | | 19 | 30 |
| 29 | 1000 | Rec 3-ph | 200 | (6.64+ $j\omega_o$0.1) | ≅ 0.39 | 78 | 96 |
| 30 | 1000 | Rec 1-ph | 200 | As above | | 10 | 15 |
| 31 | 1000 | Rec 3-ph | 100 | As above | ≅ 0.39 | 79 | 97 |
| 32 | 1000 | Rec 1-ph | 100 | As above | | 7 | 10 |
| 33 | 1000 | Rec 3-ph | 200 | (13.28+ $j\omega_o$0.2) | ≅ 0.57 | 11 | 15 |

Table C.9 (cont.)- List of Rectifier AC faults.

| Case | Pd (MW) | Type | Duration (ms) | Fault Impedance ( Ω ) | Residual Voltage (pu) | Time to 80% Prefault Power (ms) | Time to 90% Prefault Power (ms) |
|---|---|---|---|---|---|---|---|
| 34 | 1000 | Rec 1-ph | 200 | As above | | 8 | 11 |
| 35 | 1000 | Rec 3-ph | 100 | As above | ≅ 0.57 | 13 | 17 |
| 36 | 1000 | Rec 1-ph | 100 | As above | | 6 | 10 |
| 37 | 1000 | Rec 3-ph | 200 | (39.84+ $j\omega_o$0.6) | ≅ 0.82 | 10 | 13 |
| 38 | 1000 | Rec 1-ph | 200 | As above | | --- | 12 |
| 39 | 1000 | Rec 3-ph | 100 | As above | ≅ 0.82 | 10 | 12 |
| 40 | 1000 | Rec 1-ph | 100 | As above | | --- | 10 |
| 41 | 400 | Rec 3-ph | 200 | (0.067+ $j\omega_o$0.001) | ≅ 0.0 | 127 | 158 |
| 42 | 400 | Rec 1-ph | 200 | As above | | 91 | 110 |
| 43 | 400 | Rec 3-ph | 100 | As above | ≅ 0.0 | 130 | 153 |
| 44 | 400 | Rec 1-ph | 100 | As above | | 97 | 117 |
| 45 | 400 | Rec 3-ph | 200 | (3.32+ $j\omega_o$0.05) | ≅ 0.23 | 138 | 158 |
| 46 | 400 | Rec 1-ph | 200 | As above | | 72 | 100 |
| 47 | 400 | Rec 3-ph | 100 | As above | ≅ 0.23 | 137 | 152 |
| 48 | 400 | Rec 1-ph | 100 | As above | | 77 | 97 |
| 49 | 400 | Rec 3-ph | 200 | (6.64+ $j\omega_o$0.1) | ≅ 0.37 | 130 | 152 |
| 50 | 400 | Rec 1-ph | 200 | As above | | 67 | 91 |
| 51 | 400 | Rec 3-ph | 100 | As above | ≅ 0.37 | 136 | 153 |
| 52 | 400 | Rec 1-ph | 100 | As above | | 61 | 90 |
| 53 | 400 | Rec 3-ph | 200 | (13.28+ $j\omega_o$0.2) | ≅ 0.55 | 80 | 98 |
| 54 | 400 | Rec 1-ph | 200 | As above | | 10 | 15 |
| 55 | 400 | Rec 3-ph | 100 | As above | ≅ 0.55 | 82 | 95 |
| 56 | 400 | Rec 1-ph | 100 | As above | | 10 | 15 |
| 57 | 400 | Rec 3-ph | 200 | (39.84+ $j\omega_o$0.6) | ≅ 0.80 | 11 | 13 |
| 58 | 400 | Rec 1-ph | 200 | As above | | 17 | 30 |
| 59 | 400 | Rec 3-ph | 100 | As above | ≅ 0.80 | 10 | 12 |
| 60 | 400 | Rec 1-ph | 100 | As above | | 13 | 21 |

Table C.10 - List of Inverter AC faults

| Case | Pd (MW) | Type | Duration (ms) | Fault Impedance ( Ω ) | Residual Voltage (pu) | Time to 80% Prefault Power (ms) | Time to 90% Prefault Power (ms) |
|---|---|---|---|---|---|---|---|
| 1 | 2000 | Inv 3-ph | 200 | (0.067+ $j\omega_o$0.001) | ≅ 0 | 143 | 166, 236 |
| 2 | 2000 | Inv 1-ph | 200 | As above | | 177 | 196, 420 |
| 3 | 2000 | Inv 3-ph | 100 | As above | ≅ 0 | 144 | 165, 262 |
| 4 | 2000 | Inv 1-ph | 100 | As above | | 182 | 207, 348 |
| 5 | 2000 | Inv 3-ph | 200 | (6.64+ $j\omega_o$0.10) | ≅ 0.25, average | 170 | 194, 330 |
| 6 | 2000 | Inv 1-ph | 200 | As above | | 147 | 173, 300 |
| 7 | 2000 | Inv 3-ph | 100 | As above | ≅ 0.25, average | 146 | 169, 330 |
| 8 | 2000 | Inv 1-ph | 100 | As above | | 156 | 178, 302 |
| 9 | 2000 | Inv 3-ph | 200 | (13.28+ $j\omega_o$0.20) | ≅ 0.42, average | 66 | 80, 250 |
| 10 | 2000 | Inv 1-ph | 200 | As above | | 106 | 134, 280 |
| 11 | 2000 | Inv 3-ph | 100 | As above | ≅ 0.42, average | 138 | 165, 320 |
| 12 | 2000 | Inv 1-ph | 100 | As above | | 137 | 155, 320 |
| 13 | 2000 | Inv 3-ph | 200 | (26.56+ $j\omega_o$0.40) | ≅ 0.60, average | 155 | 180, 340 |
| 14 | 2000 | Inv 1-ph | 200 | As above | | 72 | 192 |
| 15 | 2000 | Inv 3-ph | 100 | As above | ≅ 0.60, average | 120 | 145 |
| 16 | 2000 | Inv 1-ph | 100 | As above | | 117 | 138, 270 |
| 17 | 2000 | Inv 3-ph | 200 | (59.76+ $j\omega_o$0.90) | ≅ 0.75, average | 25 | 50 |
| 18 | 2000 | Inv 1-ph | 200 | As above | | 42 | 96 |
| 19 | 2000 | Inv 3-ph | 100 | As above | ≅ 0.75, average | 97 | 120 |
| 20 | 2000 | Inv 1-ph | 100 | As above | | 48 | 95 |
| 21 | 2000 | Inv 3-ph | 200 | (93.09+ $j\omega_o$1.40) | ≅ 0.83, average | | 40 |
| 22 | 2000 | Inv 1-ph | 200 | As above | | | 55 |
| 23 | 1000 | Inv 3-ph | 200 | (0.067+ $j\omega_o$0.001) | ≅ 0 | 142 | 175, 259 |
| 24 | 1000 | Inv 1-ph | 200 | As above | | 176 | 235, 300 |
| 25 | 1000 | Inv 3-ph | 100 | As above | ≅ 0 | 147 | 193, 235 |
| 26 | 1000 | Inv 1-ph | 100 | As above | | 181 | 258 |

Table C.10 (cont.) - List of Inverter AC faults

| Case | Pd (MW) | Type | Duration (ms) | Fault Impedance ( Ω ) | Residual Voltage (pu) | Time to 80% Prefault Power (ms) | Time to 90% Prefault Power (ms) |
|---|---|---|---|---|---|---|---|
| 27 | 1000 | Inv 3-ph | 200 | (6.64+ $j\omega_o 0.10$) | ≅ 0.27, average | 105 | 125 |
| 28 | 1000 | Inv 1-ph | 200 | As above | | 150 | 195 |
| 29 | 1000 | Inv 3-ph | 100 | As above | ≅ 0.27, average | 162 | 187 |
| 30 | 1000 | Inv 1-ph | 100 | As above | | 153 | 182 |
| 31 | 1000 | Inv 3-ph | 200 | (13.28+ $j\omega_o 0.20$) | ≅ 0.43, average | 83 | 102 |
| 32 | 1000 | Inv 1-ph | 200 | As above | | 116 | 158 |
| 33 | 1000 | Inv 3-ph | 100 | As above | ≅ 0.43, average | 142 | 164 |
| 34 | 1000 | Inv 1-ph | 100 | As above | | 128 | 167 |
| 35 | 1000 | Inv 3-ph | 200 | (26.56+ $j\omega_o 0.40$) | ≅ 0.60, average | 57 | 79 |
| 36 | 1000 | Inv 1-ph | 200 | As above | | 87 | 150 |
| 37 | 1000 | Inv 3-ph | 100 | As above | ≅ 0.60, average | 117 | 140 |
| 38 | 1000 | Inv 1-ph | 100 | As above | | 117 | 150 |
| 39 | 1000 | Inv 3-ph | 200 | (59.76+ $j\omega_o 0.90$) | ≅ 0.75, average | 48 | 64 |
| 40 | 1000 | Inv 1-ph | 200 | As above | | 44 | 130 |
| 41 | 1000 | Inv 3-ph | 100 | As above | ≅ 0.75, average | 117 | 142 |
| 42 | 1000 | Inv 1-ph | 100 | As above | | 108 | 125 |
| 43 | 1000 | Inv 3-ph | 200 | (93.09+ $j\omega_o 1.40$) | ≅ 0.83, average | 37 | 67 |
| 44 | 1000 | Inv 1-ph | 200 | As above | | --- | --- |
| 45 | 400 | Inv 3-ph | 200 | (0.067+ $j\omega_o 0.001$) | ≅ 0 | 215 | 250 |
| 46 | 400 | Inv 1-ph | 200 | As above | | 248 | 285 |
| 47 | 400 | Inv 3-ph | 100 | As above | ≅ 0 | 227 | 270 |
| 48 | 400 | Inv 1-ph | 100 | As above | | 250 | 310 |
| 49 | 400 | Inv 3-ph | 200 | (6.64+ $j\omega_o 0.10$) | ≅ 0.28, average | 163 | 185 |
| 50 | 400 | Inv 1-ph | 200 | As above | | 207 | 235 |
| 51 | 400 | Inv 3-ph | 100 | As above | ≅ 0.28, average | 220 | 242 |
| 52 | 400 | Inv 1-ph | 100 | As above | | 212 | 236 |
| 53 | 400 | Inv 3-ph | 200 | (13.28+ $j\omega_o 0.20$) | ≅ 0.43, average | 112 | 134 |
| 54 | 400 | Inv 1-ph | 200 | As above | | 150 | 180 |
| 55 | 400 | Inv 3-ph | 100 | As above | ≅ 0.43, average | 213 | 232 |
| 56 | 400 | Inv 1-ph | 100 | As above | | 178 | 202 |
| 57 | 400 | Inv 3-ph | 200 | (26.56+ $j\omega_o 0.40$) | ≅ 0.58, average | 84 | 115 |
| 58 | 400 | Inv 1-ph | 200 | As above | | 105 | 150 |
| 59 | 400 | Inv 3-ph | 100 | As above | ≅ 0.58, average | 186 | 205 |

Table C.10 (cont.) - List of Inverter AC faults

| Case | Pd (MW) | Type | Duration (ms) | Fault Impedance ( Ω ) | Residual Voltage (pu) | Time to 80% Prefault Power (ms) | Time to 90% Prefault Power (ms) |
|---|---|---|---|---|---|---|---|
| 60 | 400 | Inv 1-ph | 100 | As above | | 172 | 194 |
| 61 | 400 | Inv 3-ph | 200 | (59.76+ $j\omega_o 0.90$) | ≅ 0.74, average | 56 | 90 |
| 62 | 400 | Inv 1-ph | 200 | As above | | 64 | 122 |
| 63 | 400 | Inv 3-ph | 100 | As above | ≅ 0.74, average | 163 | 184 |
| 64 | 400 | Inv 1-ph | 100 | As above | | 145 | 168 |
| 65 | 400 | Inv 3-ph | 200 | (93.09+ $j\omega_o 1.40$) | ≅ 0.81, average | 52 | 70 |
| 66 | 400 | Inv 1-ph | 200 | As above | | --- | 70 |

A brief summary of the results follows:

- In most cases it is possible to reach 90% of the prefault power in 200 ms or less. In many inverter faults the power reaches 90% in 200 ms or less, and then rises slowly to 100 %. These recovery times should be adequate.
- Recovery times following all types of rectifier AC faults are extremely fast, (< 125 ms in all cases). For the more severe rectifier AC faults, after reaching 90 % the power may fall very slightly below the 90 % level, rising slowly to 100 %.
- It appears that as long as the inverter AC network is fairly symmetrical, the inverter is quite resistant to commutation failures. For example, a solid 3-phase fault at the inverter AC bus does not always produce a commutation failure. Commutations continue using the voltage across the capacitors. More remote 3-phase inverter AC faults may or may not provoke a commutation failure, depending on the instant of the fault. This appears to be much better than a classical HVDC scheme such as Itaipu.
- Unsymmetrical inverter AC faults cause commutation failures for the more sever faults. Here the performance is rather similar to classical HVDC (with a stronger AC network at the inverter).
- Power transmitted during severe inverter AC faults is rather low, quite similar to classical HVDC. This is at least partially a result of using modern equally spaced firing control systems, which maintain symmetrical firing even with unsymmetrical networks.
- A low frequency oscillation was noted during certain inverter AC faults in which the VDCOL is active during most or all of the fault. This oscillation does not have time to appear if the fault is cleared in 200 ms or less.

### C.5. Remaining Work

The following is a suggestion of additional work that can be done on this model:

- Perform DC line faults;
- Perform AC faults, with or without line tripping (“run backs”), at different locations in the network;
- Investigate the “correctness” of the transformer saturation data used herein;
- Try to increase power transmission during inverter AC faults;
- Examine transfer of disturbances between AC systems due to reactive power variations.

### C.6. Conclusions

- A simple control system (developed using PSCAD/EMTDC) has been developed for a CCC HVDC transmission system and appears to work well, even with a very weak inverter AC network. In this control system complex calculations are required to determine the inverter’s alpha maximum limit and

the rectifier's alpha minimum limit. However, these calculations are done "off line" and only simple approximations are used in the controls.

- The dynamic performance of this system has been evaluated. Fault recovery times to 90 % in about 200 ms or less are achieved for most cases. From 90 % to 100 % is fairly slow for the more severe faults but this is considered acceptable.

# ANNEX D - VALIDATION OF THE CCC LINK MODEL – COMPARISON OF SIMULATIONS ON ATP x PSCAD

## D.1 Introduction

Aiming to obtain a model that may be made available in a more public environment, the CCC model developed in PSCAD/EMTDC was also modeled on the ATP/EMTP program. After the transposition of the models, utilizing the components available in ATP/EMTP, including both TACS and MODELS, several comparisons were made with the purpose of validating it. First, tests with the isolated controls were made and, afterwards, several faults were applied, utilizing the system defined as Benchmark.

## D.2 Validation of basic controls

The following control blocks were analyzed separately: PLL, VDCOL, CCA and the variation of the CURRENT MARGIN during the action of the VDCOL. PLL parameters were adjusted to obtain the same response presented by PSCAD/EMTDC (GP=40 and GI=28). The maximum value of 15 for GP (given in the PSCAD manual) presented a slower response for the control. Figure D.1 shows the PLL response in case of loss and recovery of the AC voltage reference for both programs. Figure D.2 shows the VDCOL response in both programs for a step in the DC voltage. Figure D.3 shows the CCA responses in both programs for a 100 ms step. Figure D.4 shows the responses of the current margin variation in CCA during the action of the VDCOL.

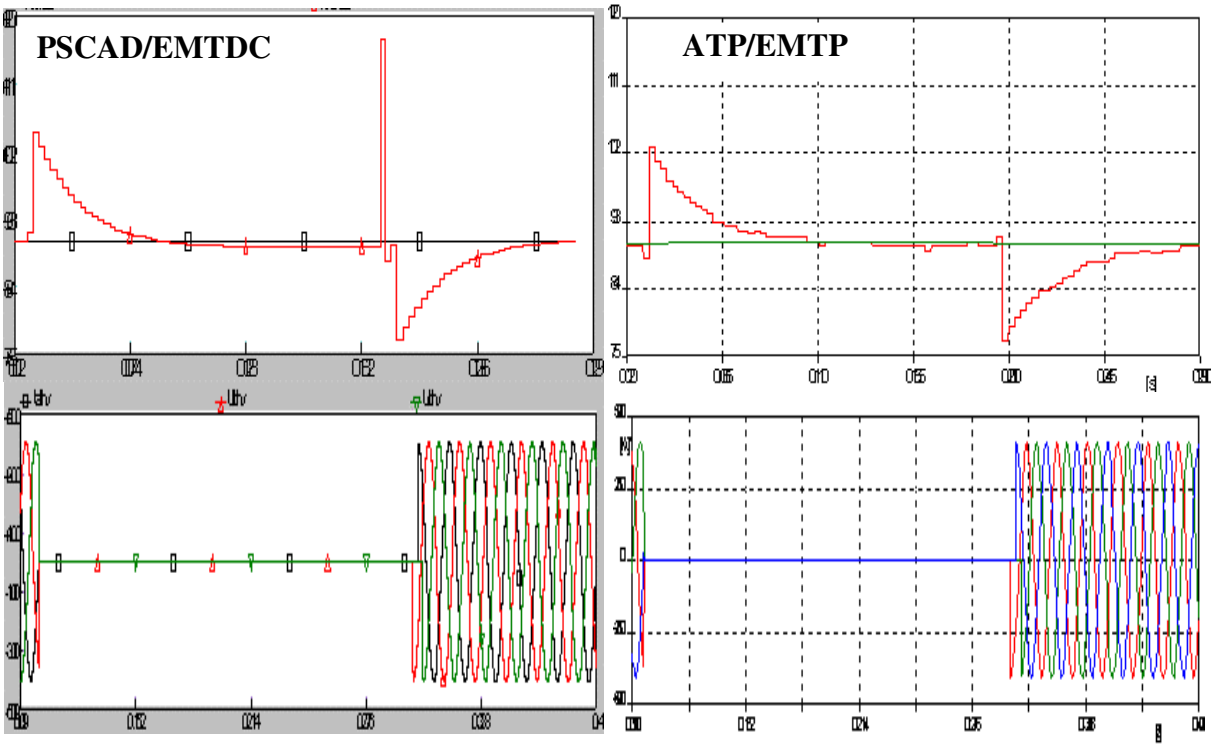


Figure D.1 – PLL response in programs PSCAD and ATP

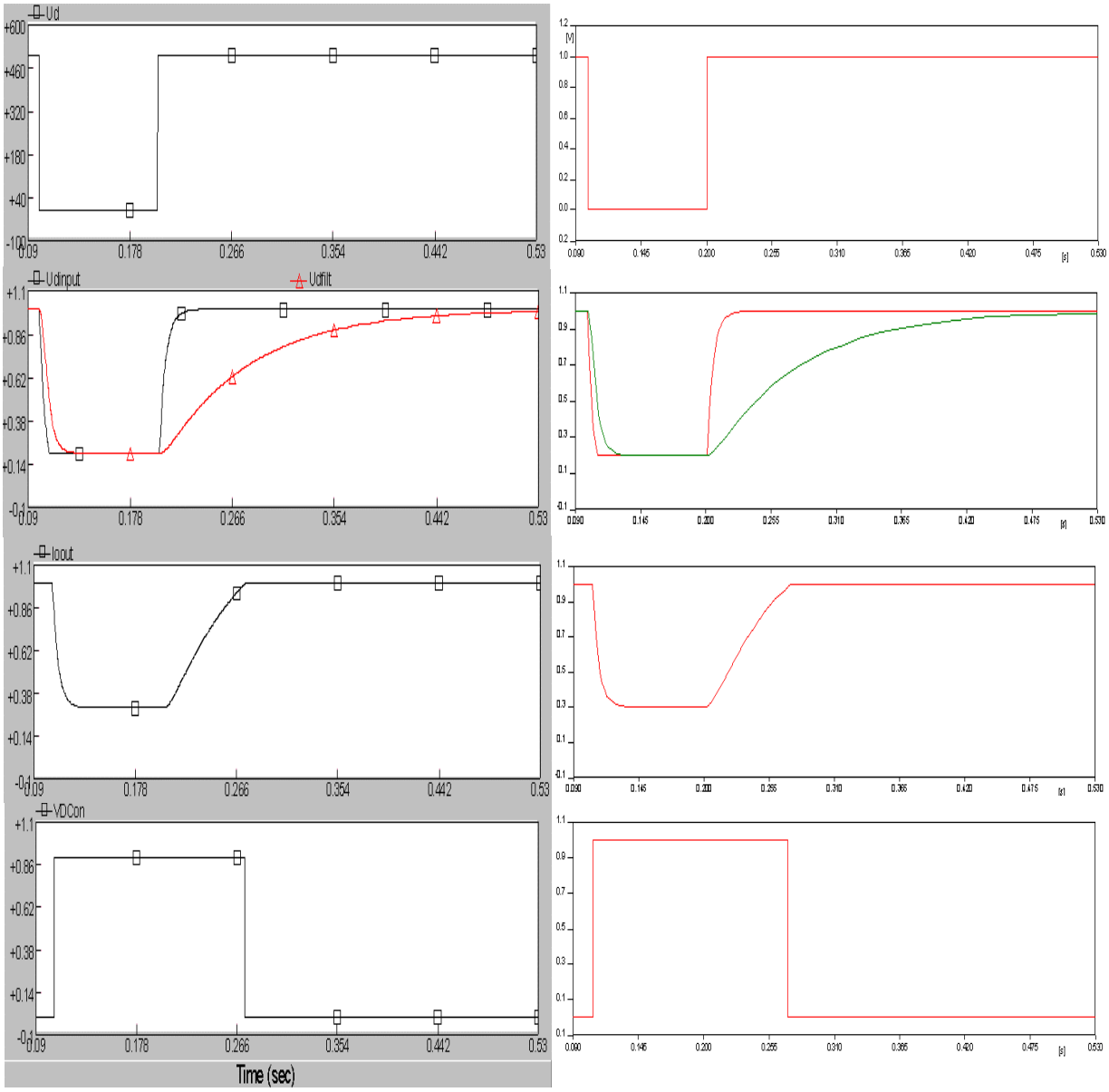


Figure D.2 – VDCOL response in programs PSCAD and ATP

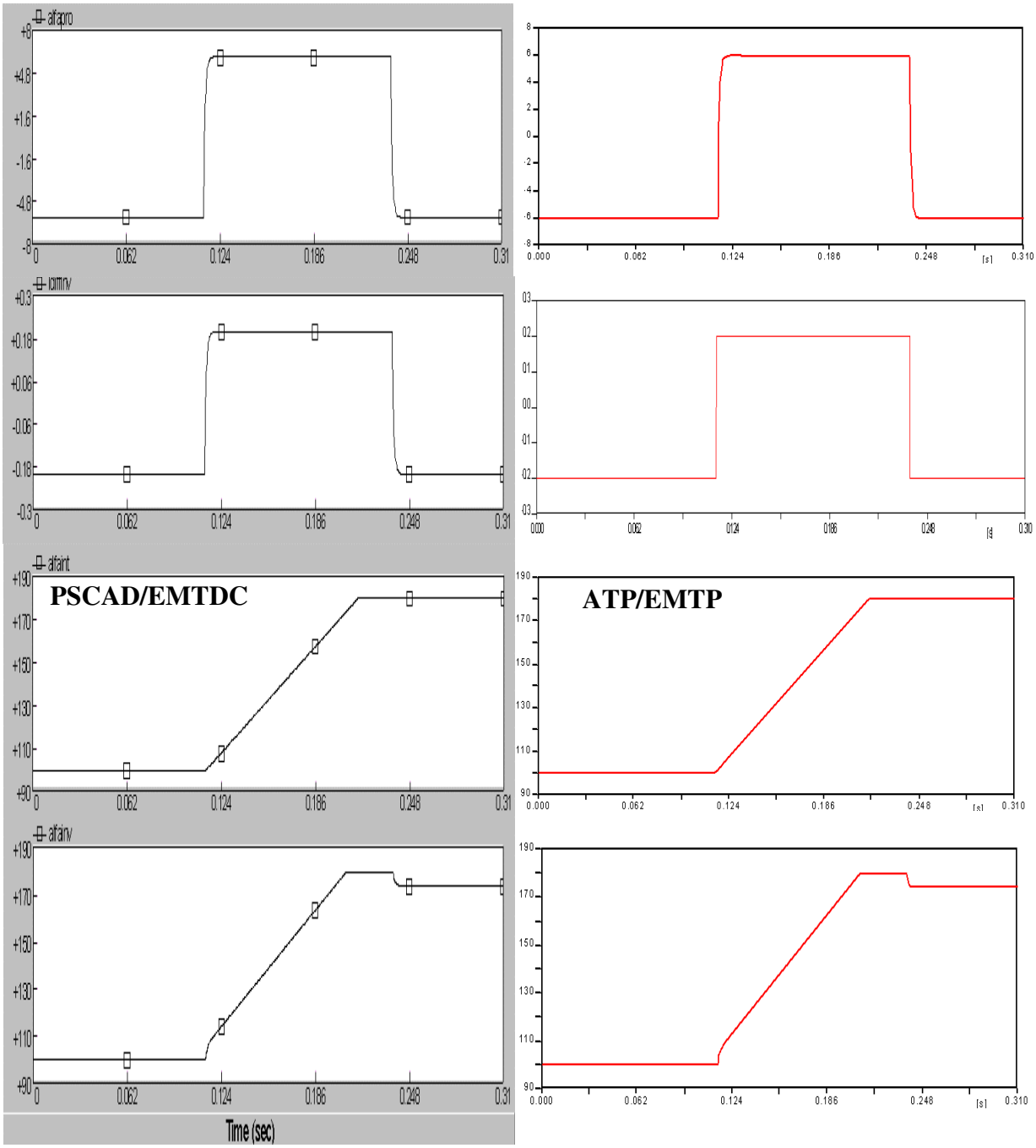


Figure D.3 – CCA response in programs PSCAD and ATP

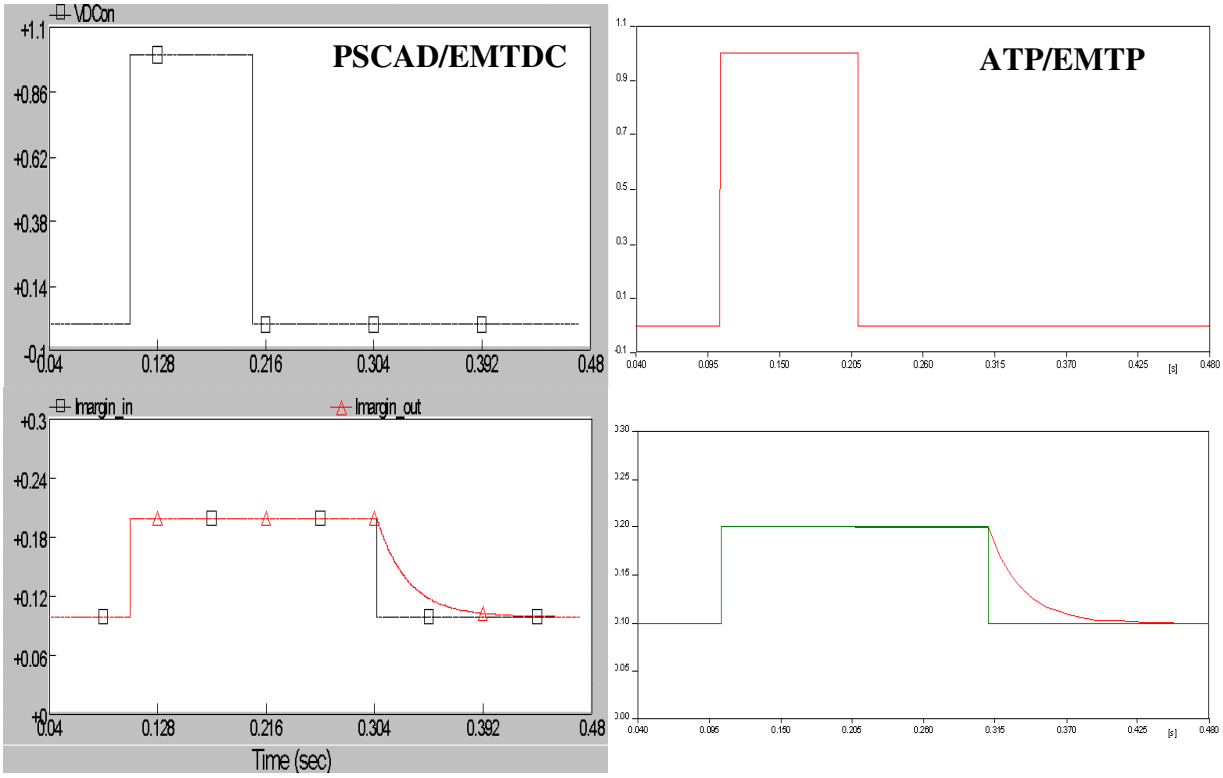


Figure D.4 – Response of the current margin variation in programs PSCAD and ATP.

### D.3 Validation with the Benchmark

Figures D.5 to D.10 present the ATP responses for three-phase and single-phase faults at the rectifier and at the inverter, for three different power levels in the link, and for five different levels of voltage drop. To facilitate the observation, the results of the different levels of voltage drop were grouped in the same chart. As it may be noted, out of 60 processed cases, the following presented commutation faults during fault recovery:

- Three-phase fault at rectifier - 80% voltage drop – Pdc = 1.0 pu
- Three-phase fault at rectifier - 80% voltage drop – Pdc = 0.5 pu
- Three-phase fault at inverter - 0% voltage drop – Pdc = 0.5 pu
- Single-phase fault at inverter - 40% voltage drop – Pdc = 0.2 pu

These faults were not observed in the PSCAD/EMTDC program, although a statistical analysis, varying the fault application point, has not been performed. However, a difference between the programs, which may slightly influence that result, is the interpolation due to thyristor firing made by PSCAD/EMTDC, while ATP maintains invariable the integration interval.

Figures D.11 to D.22 present a detailed comparison between the results of the programs ATP/EMTP and PSCAD/EMTDC, for three-phase and single-phase faults at the rectifier and at the inverter, considering 1.0 pu power level and voltage drops of 0%, 25% and 40%.

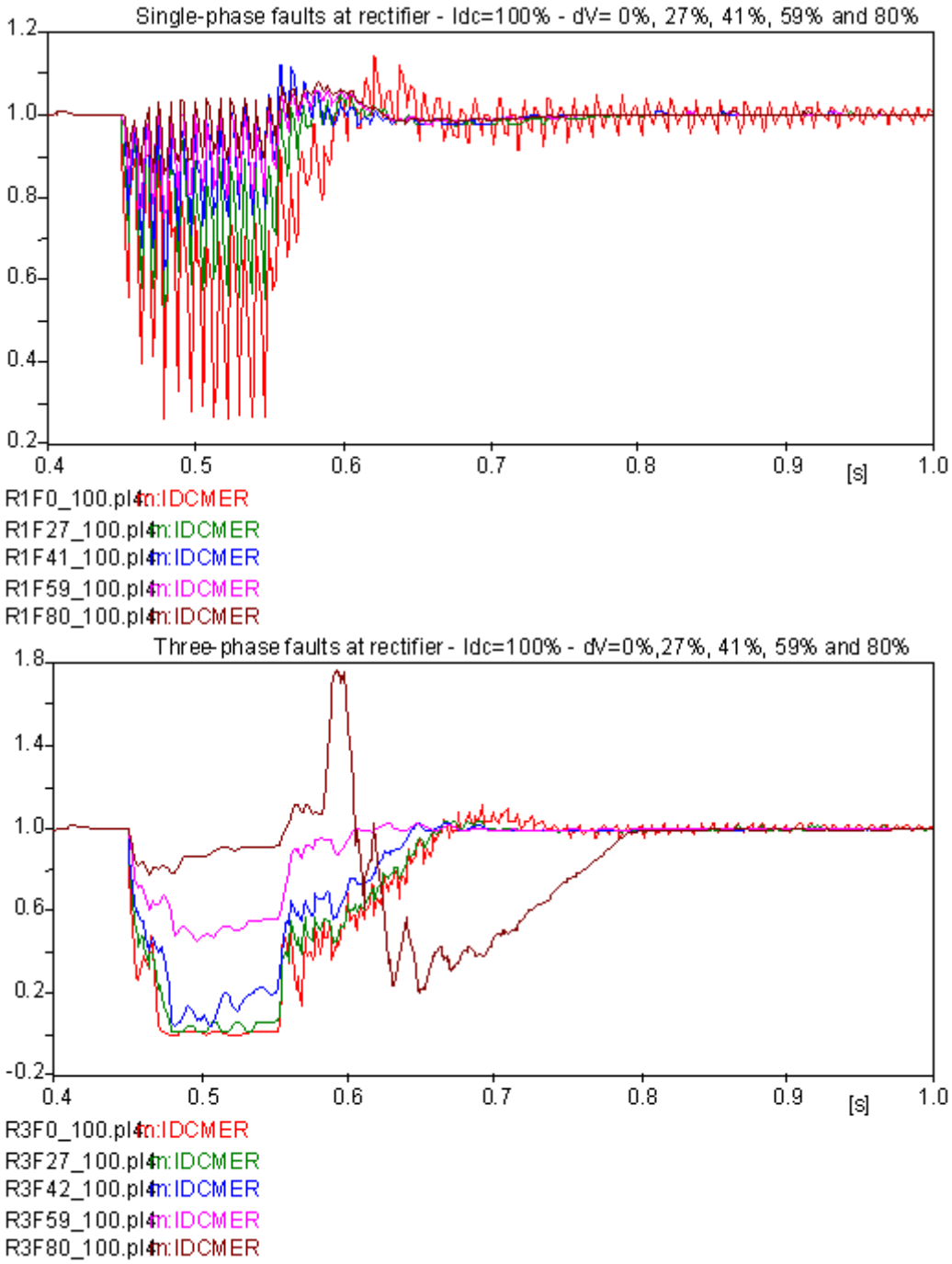


Figure D.5 – Single-phase and three-phase fault at the rectifier for Pdc = 1.0 pu

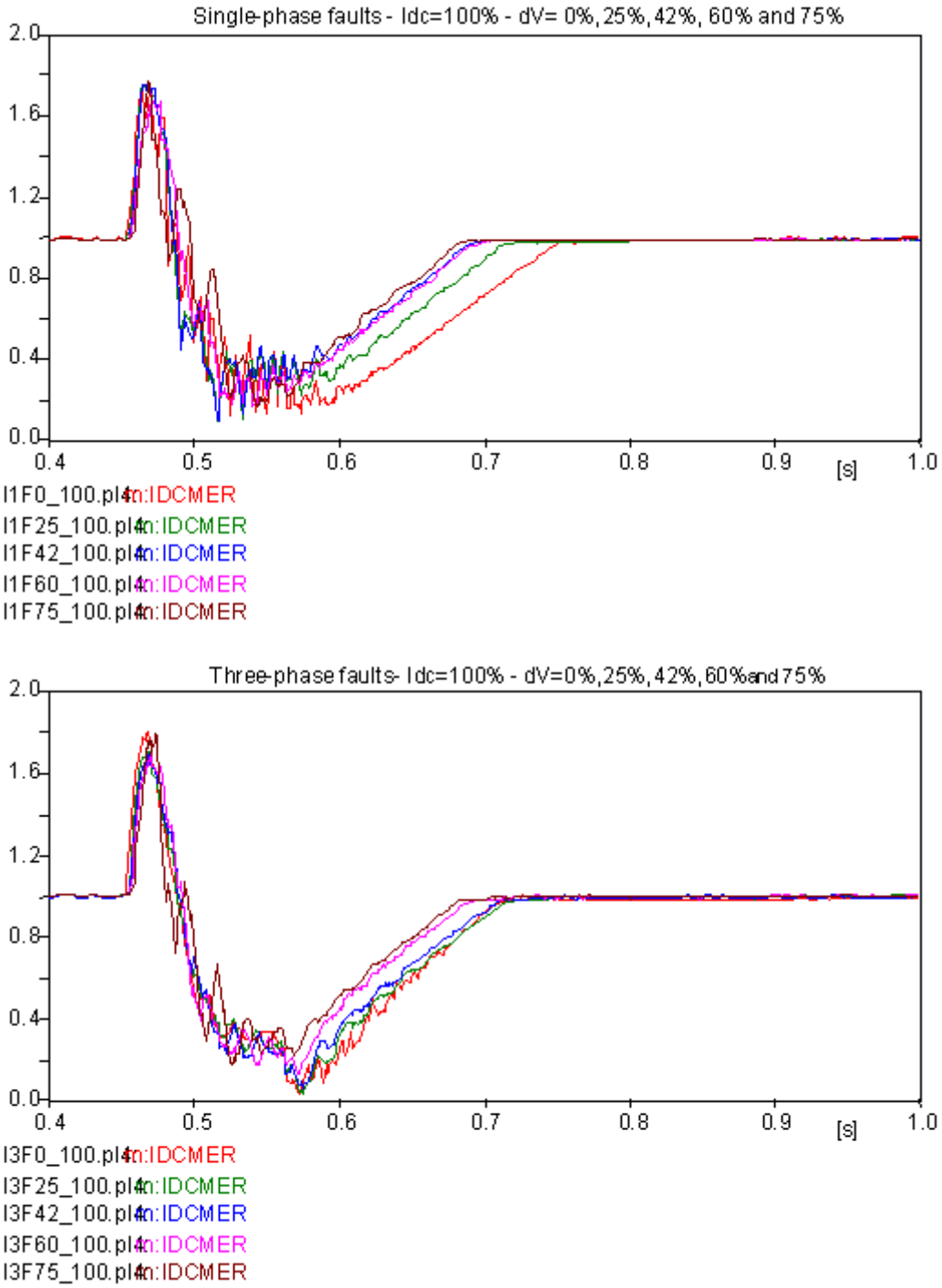


Figure D.6 – Single-phase and three-phase faults at the inverter for Pdc = 1.0 pu

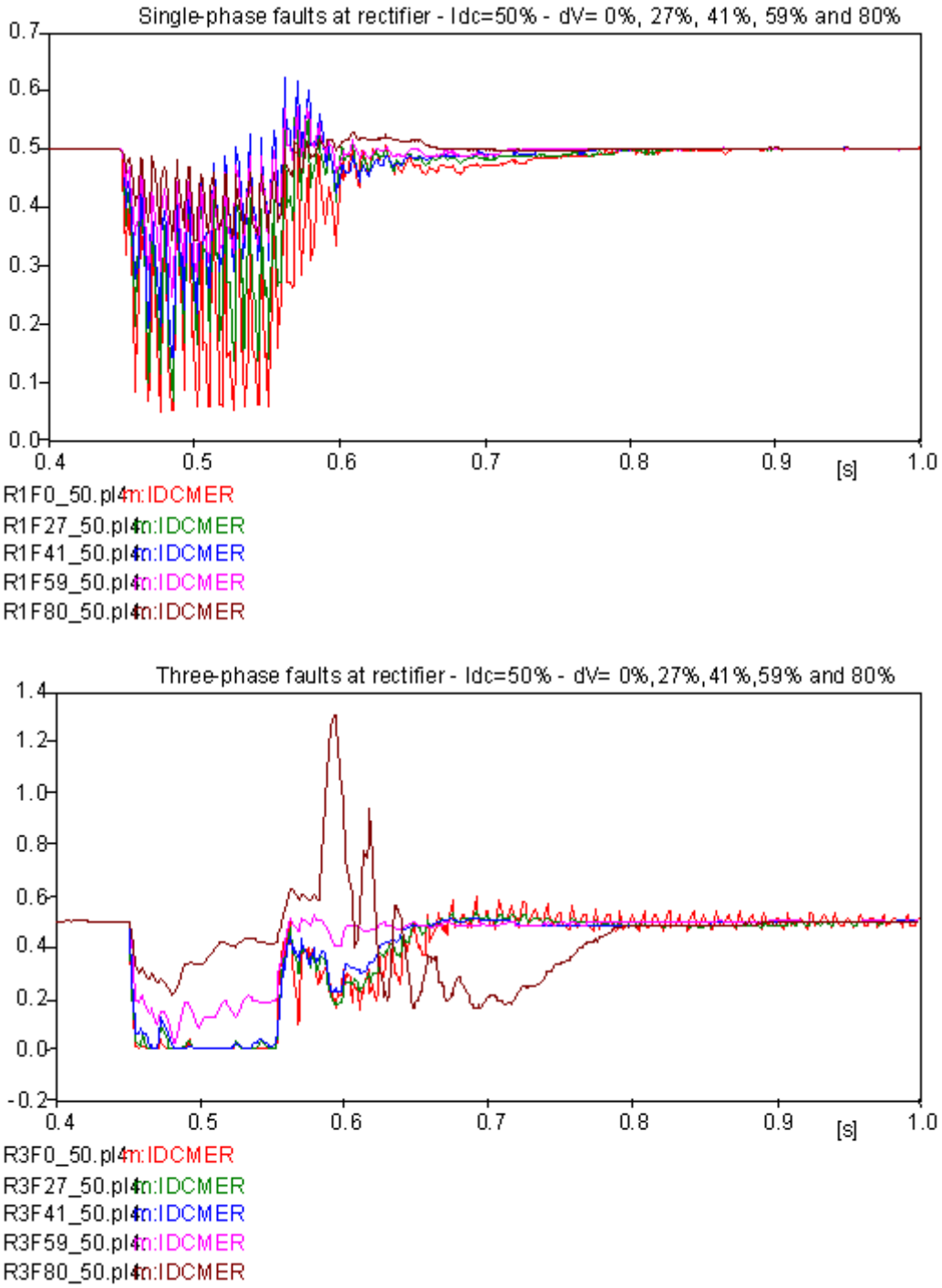


Figure D.7 – Single-phase and three-phase faults at the rectifier for Pdc = 0.5 pu

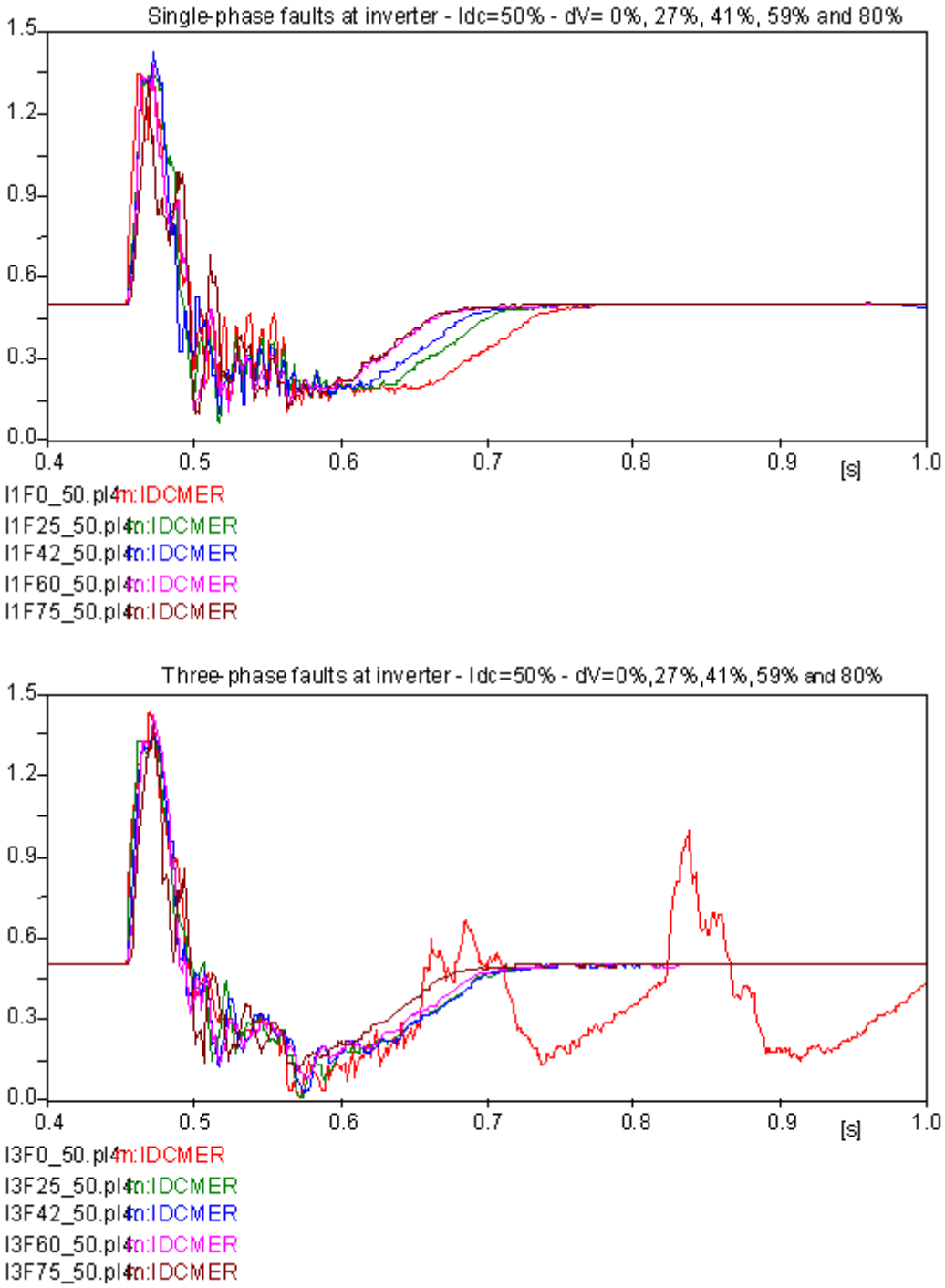


Figure D.8 – Single-phase and three-phase faults at the inverter for Pdc = 0.5 pu

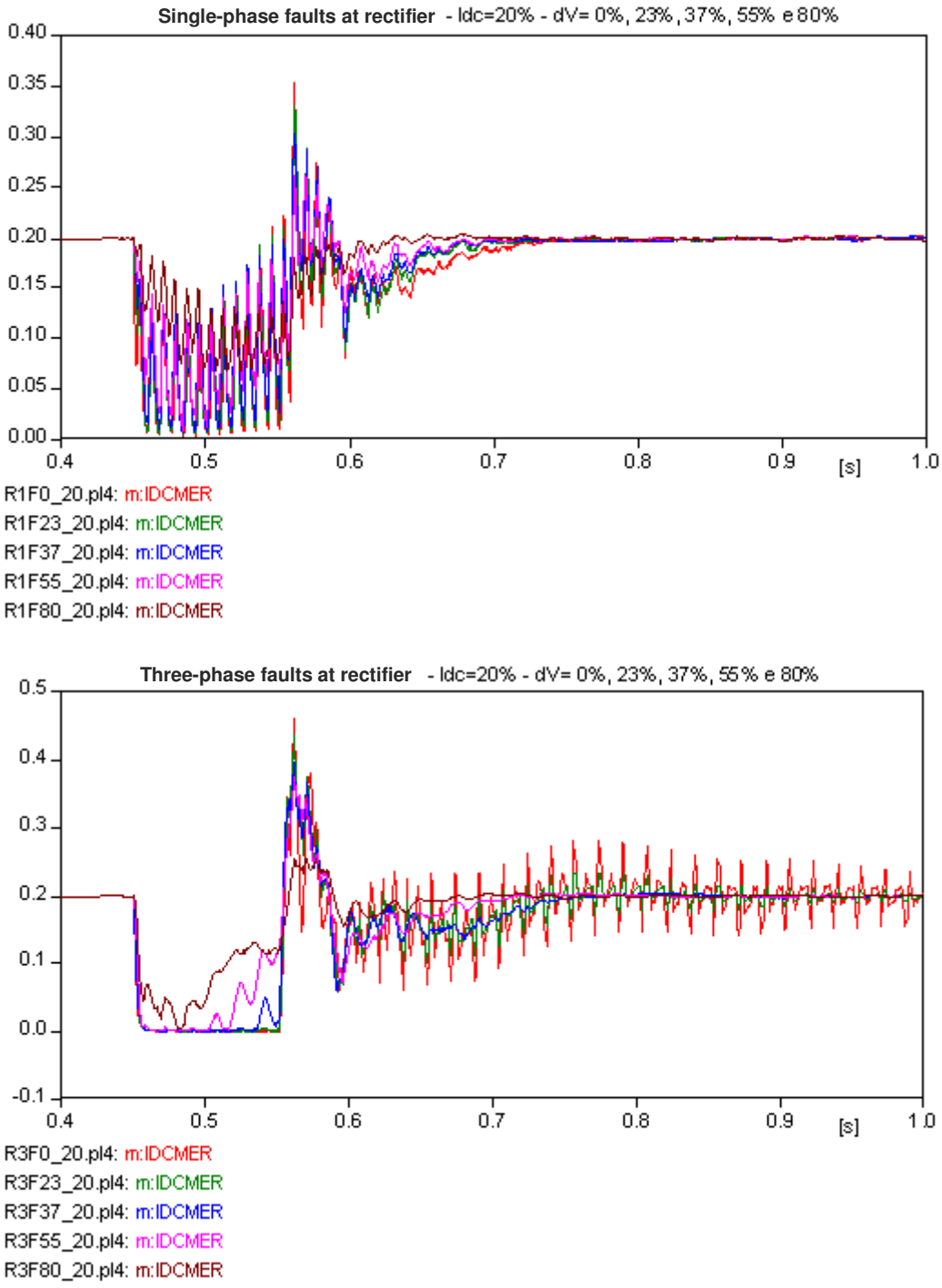


Figure D.9 – Single-phase and three-phase faults at the rectifier for Pdc = 0.2 pu

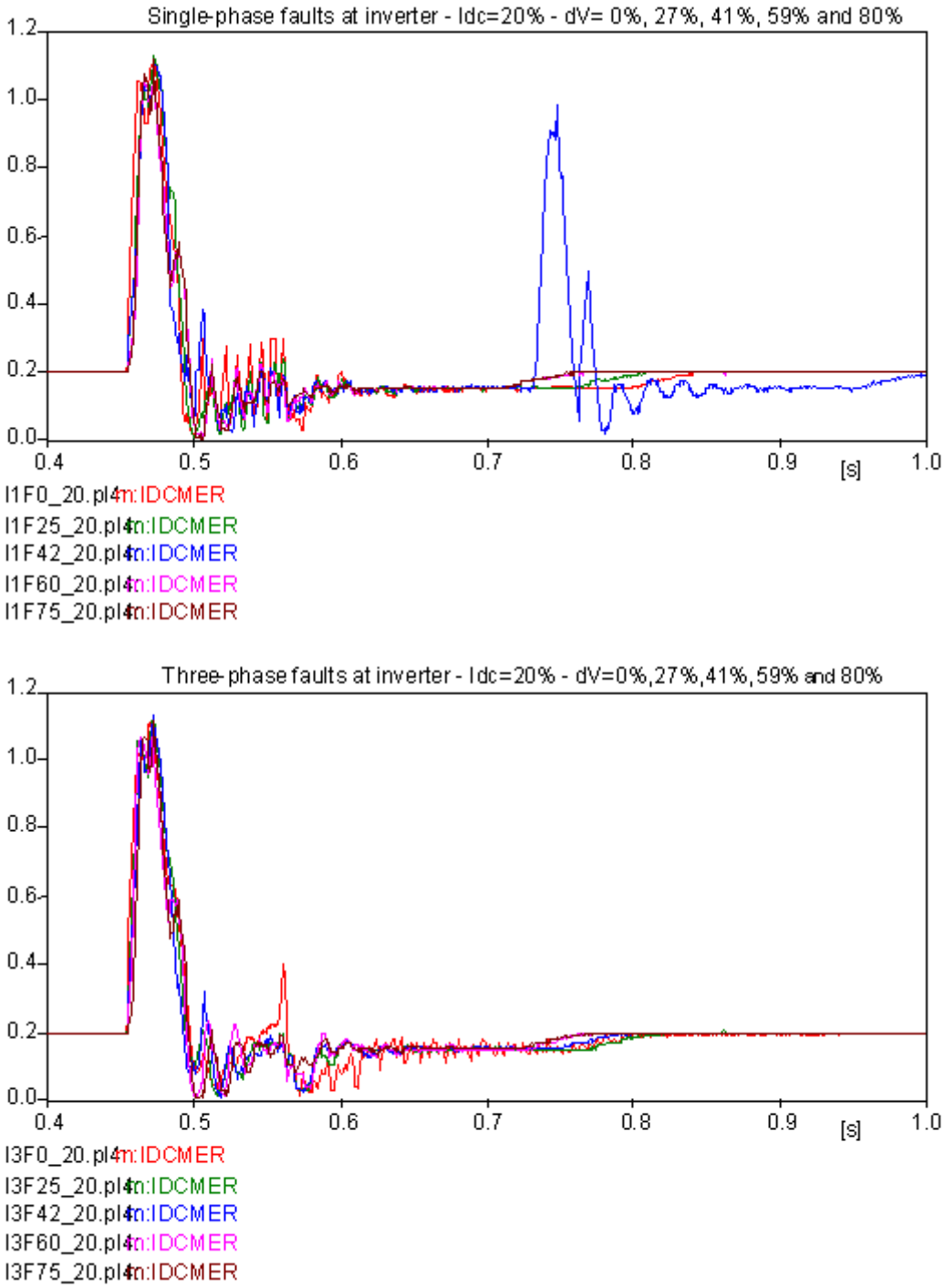


Figure D.10 – Single-phase and three-phase faults at the inverter for Pdc = 0.2 pu

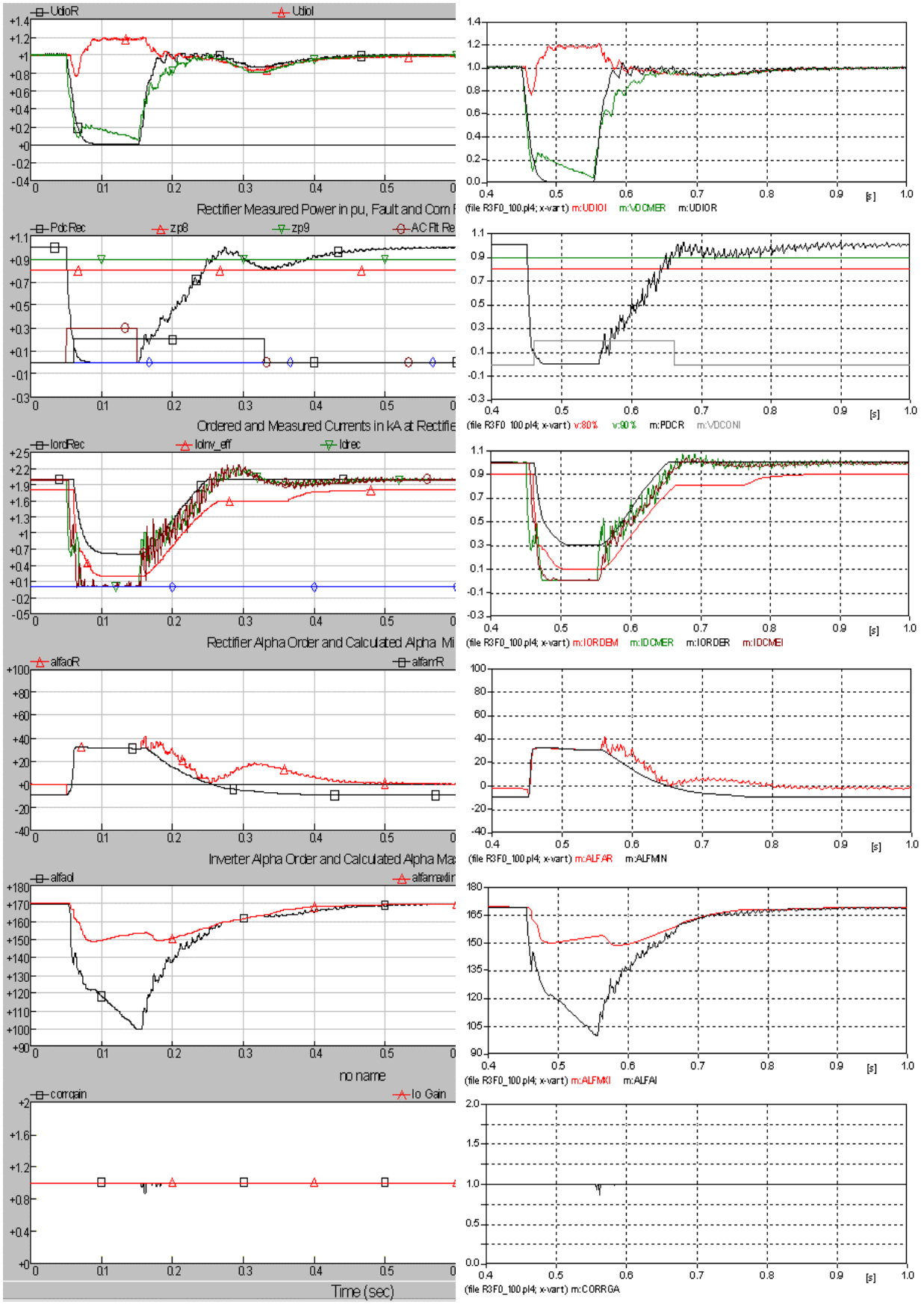


Figure D.11 – Three-phase fault, for 100 ms, at the rectifier – residual voltage 0%

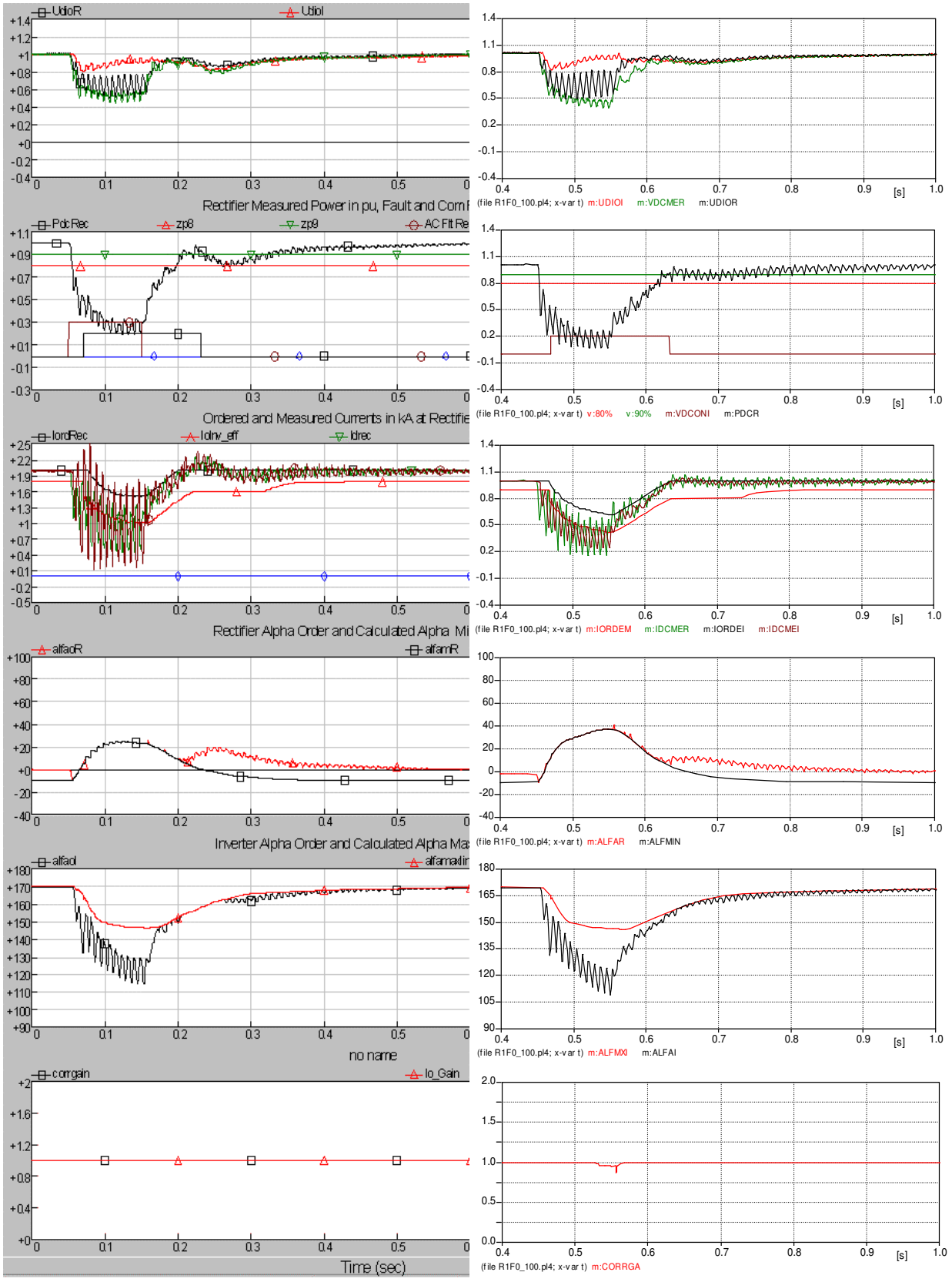


Figure D.12 - Single-phase fault, for 100 ms, at the rectifier – residual voltage 0%

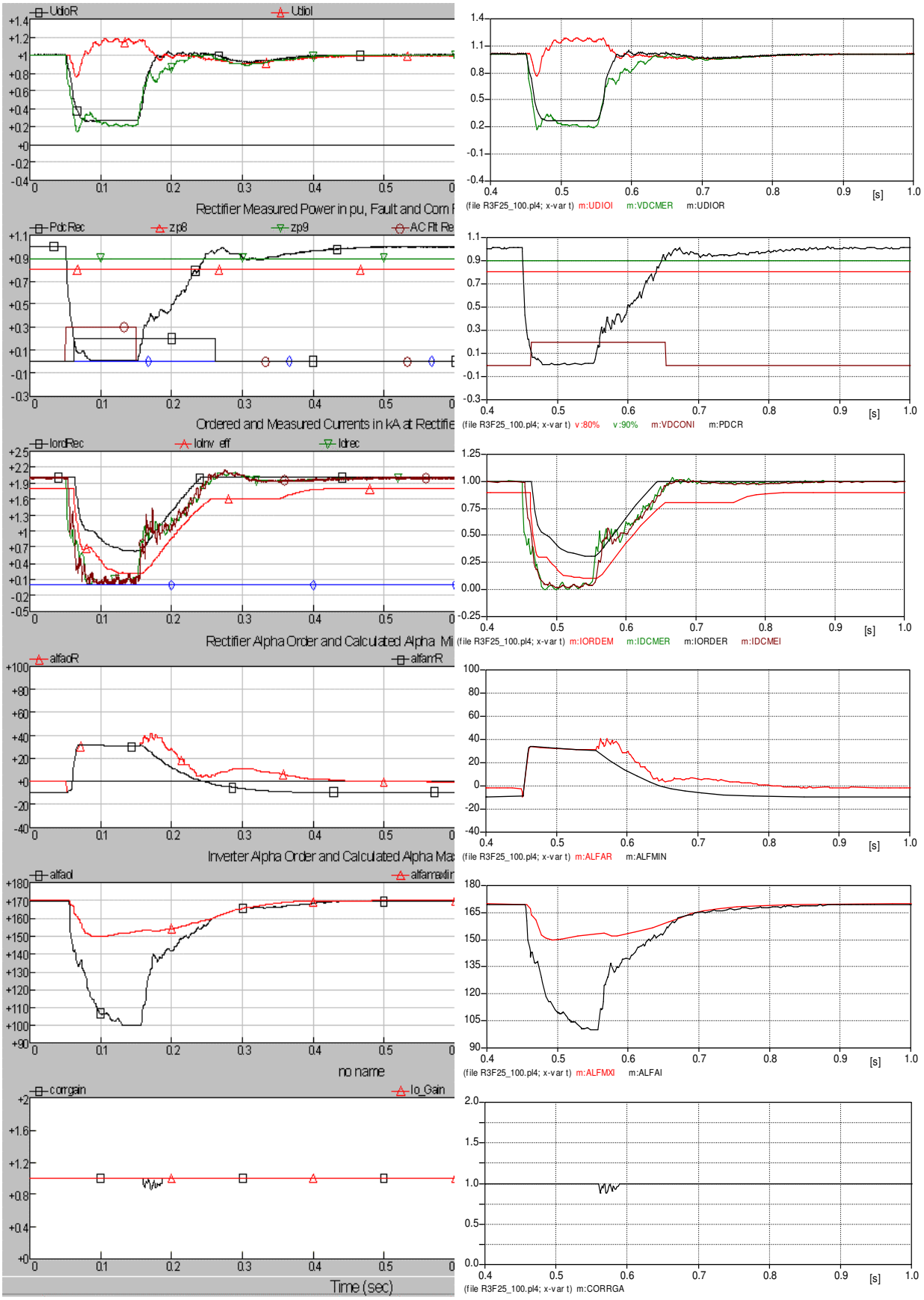


Figure D.13 - Three-phase fault, for 100 ms, at the rectifier – residual voltage 27%

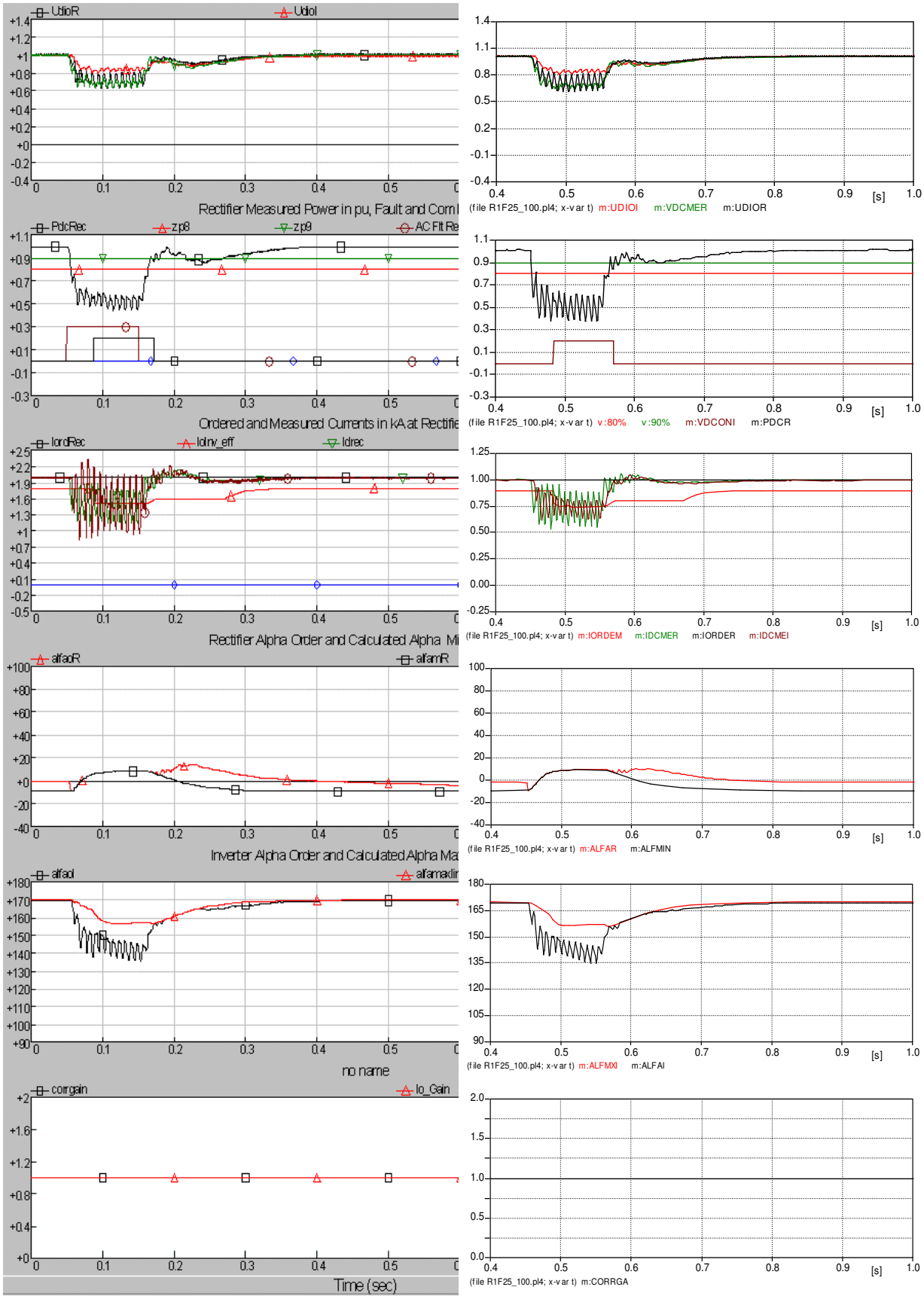


Figure D.14 - Single-phase fault, for 100 ms, at the rectifier – residual voltage 27%

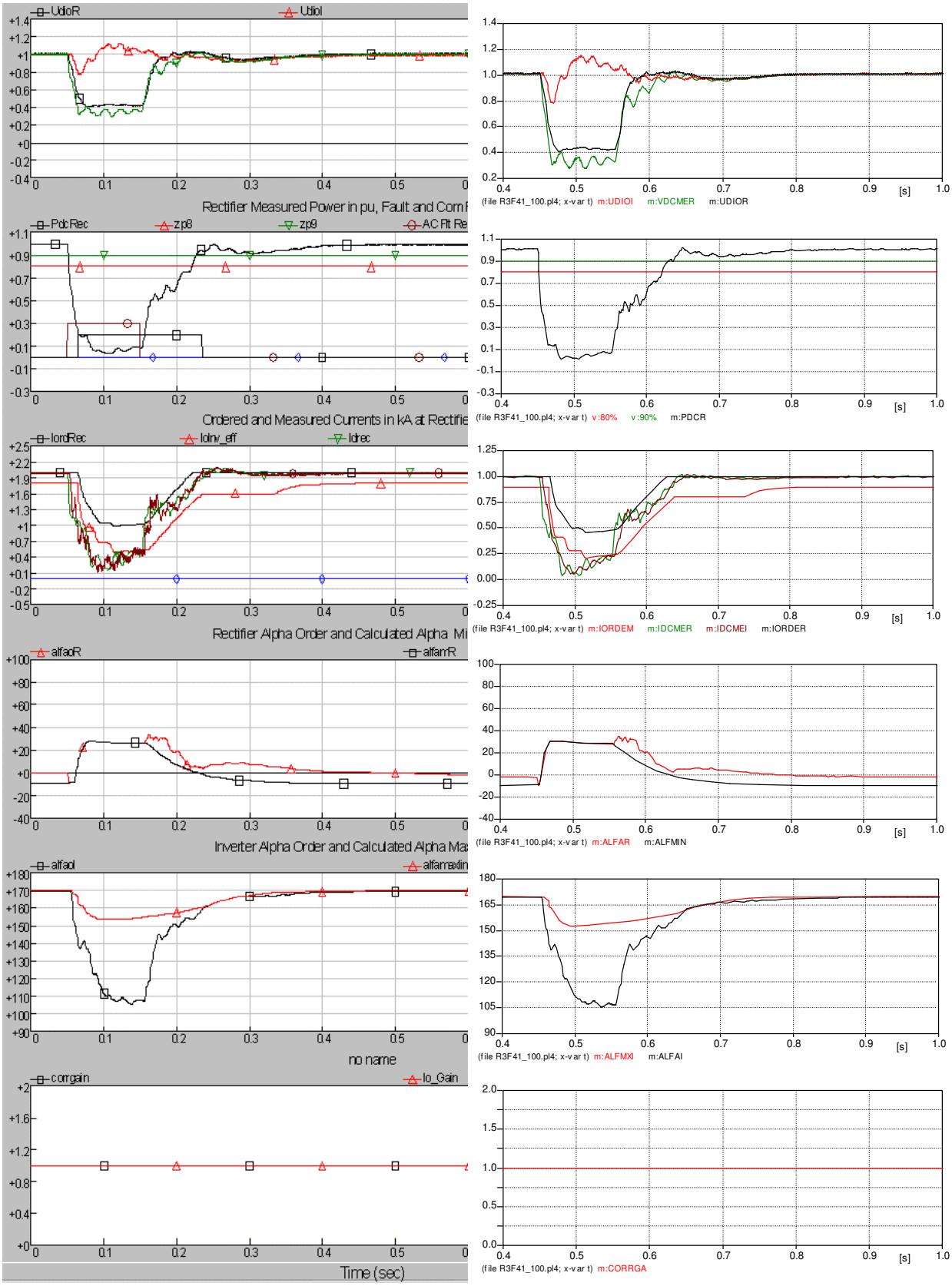


Figure D.15 - Three-phase fault, for 100 ms, at the rectifier – residual voltage 41%

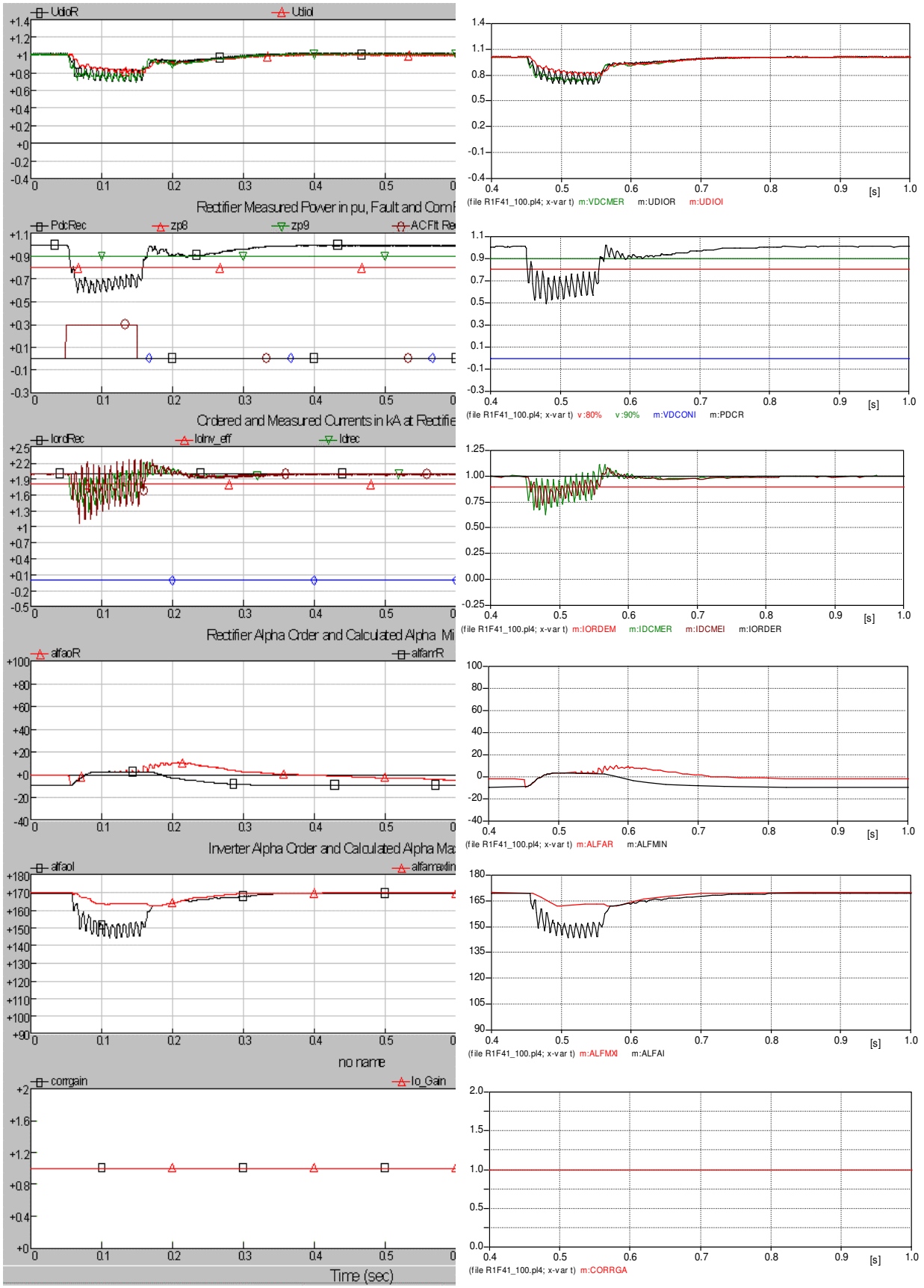


Figure D.16 - Single-phase fault, for 100 ms, at the rectifier – residual voltage 41%

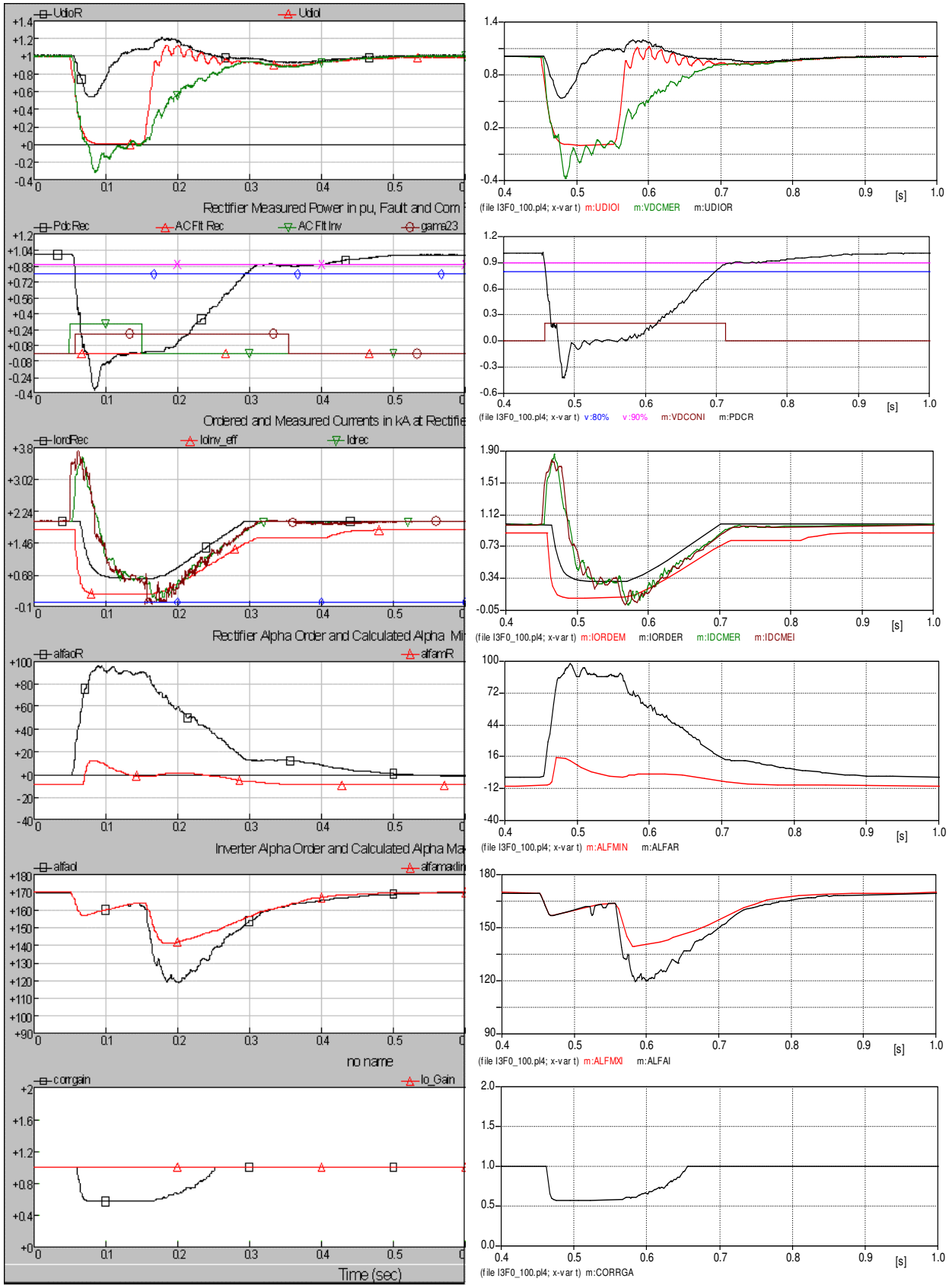


Figure D.17 - Three-phase fault, for 100 ms, at the inverter – residual voltage 0%

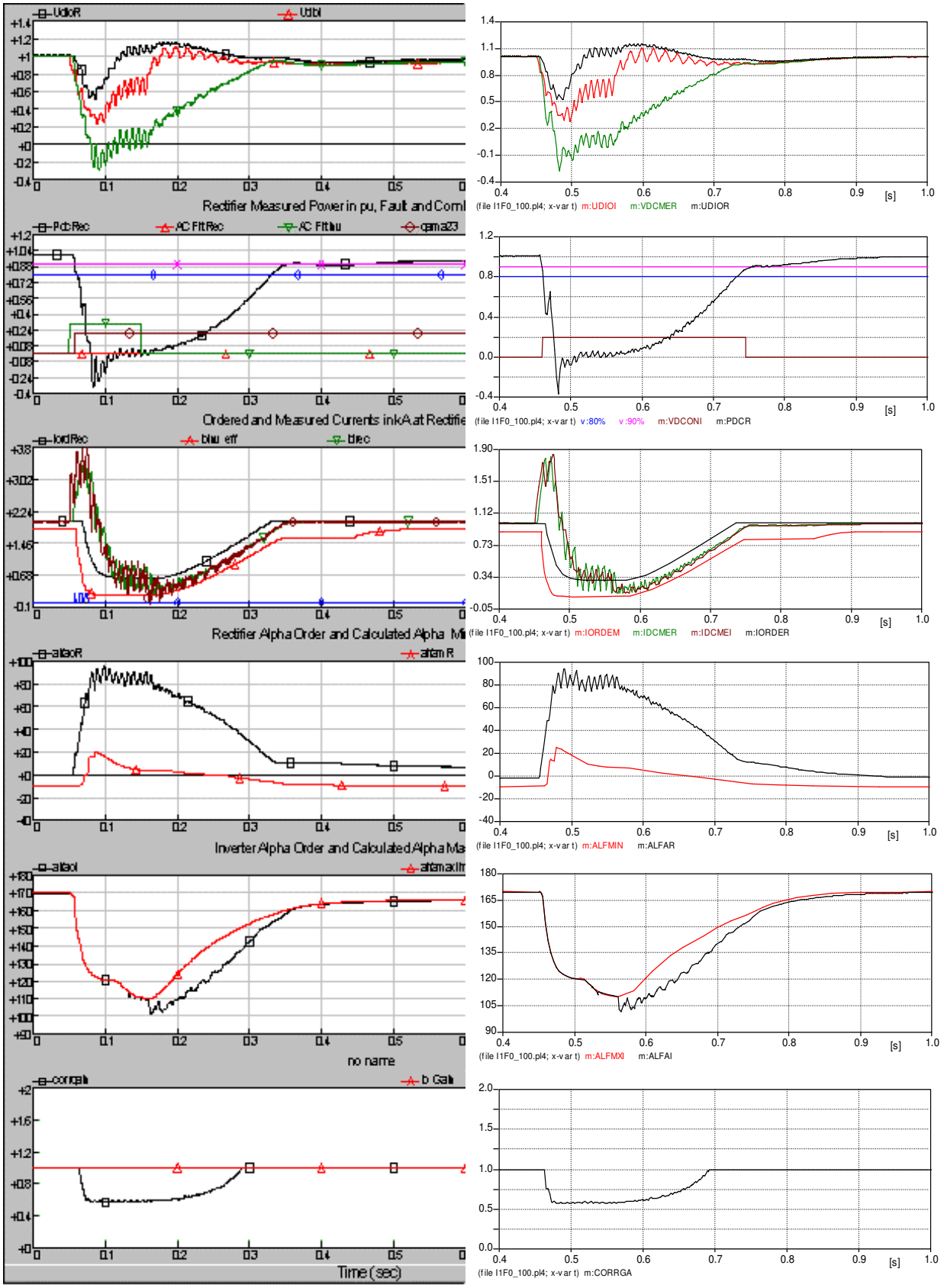


Figure D.18 - Single-phase fault, for 100 ms, at the inverter – residual voltage 0%

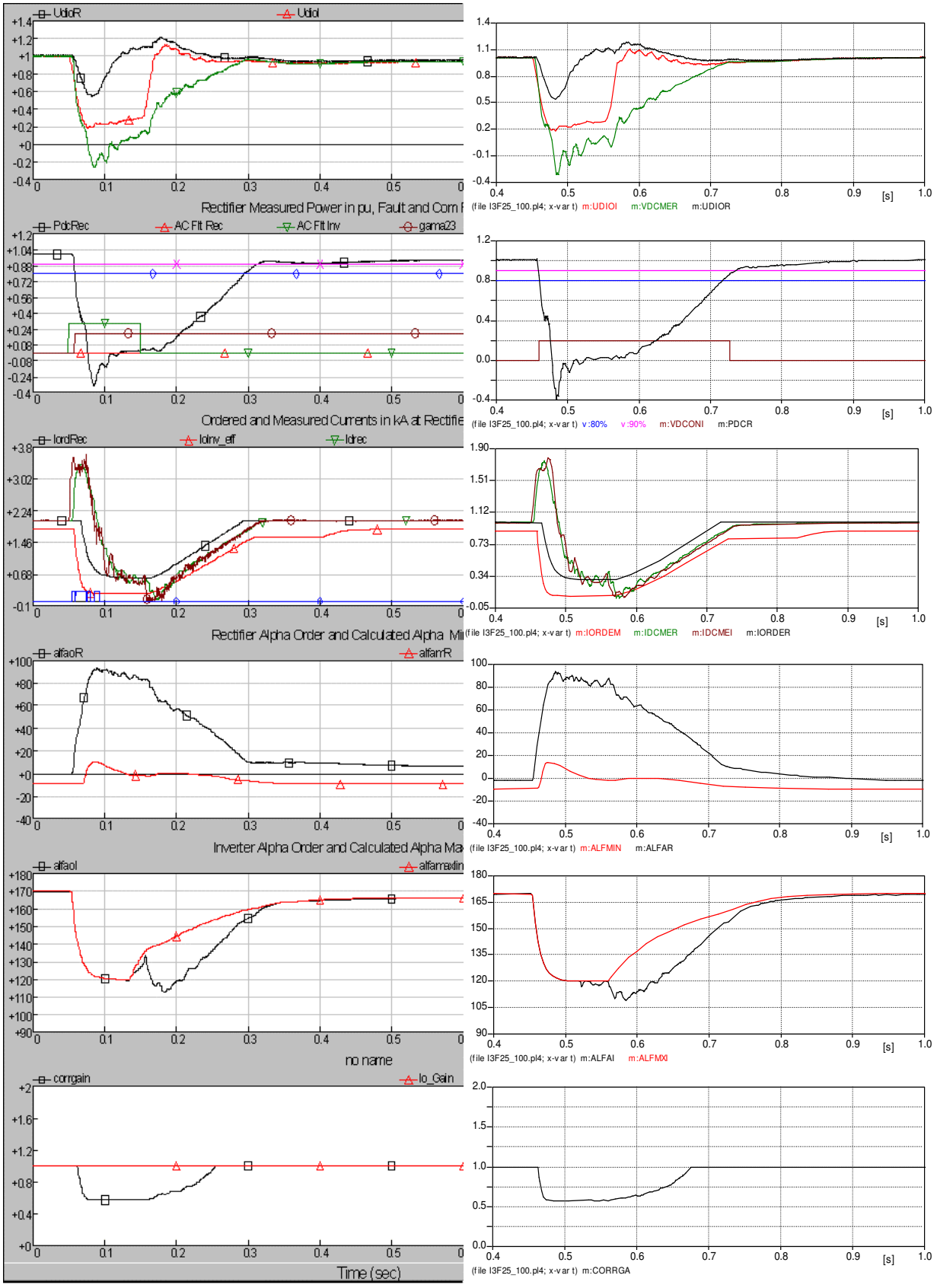


Figure D.19 - Three-phase fault, for 100 ms, at the inverter – residual voltage 25%

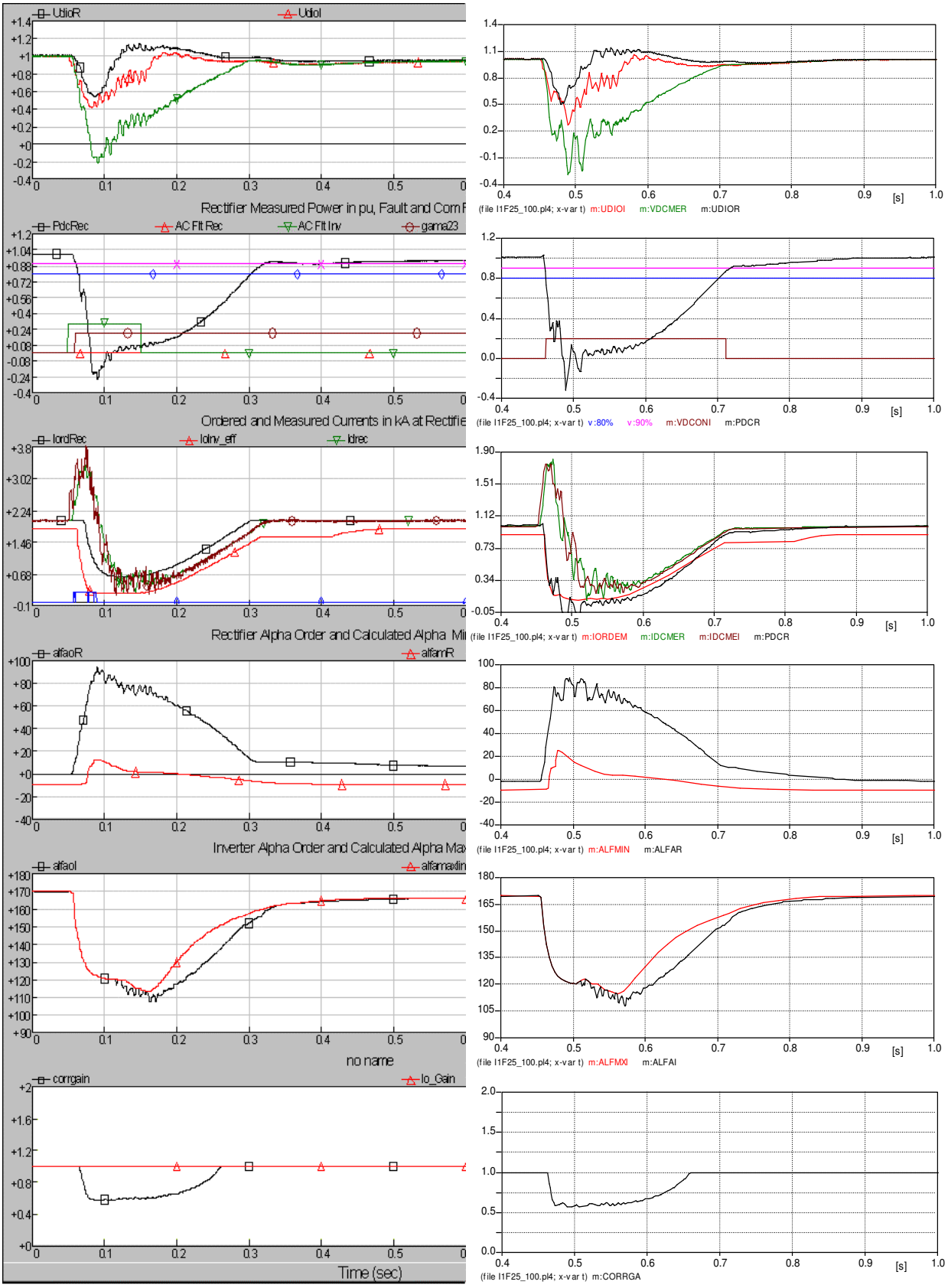


Figure D.20 - Single-phase fault, for 100 ms, at the inverter – residual voltage 25%

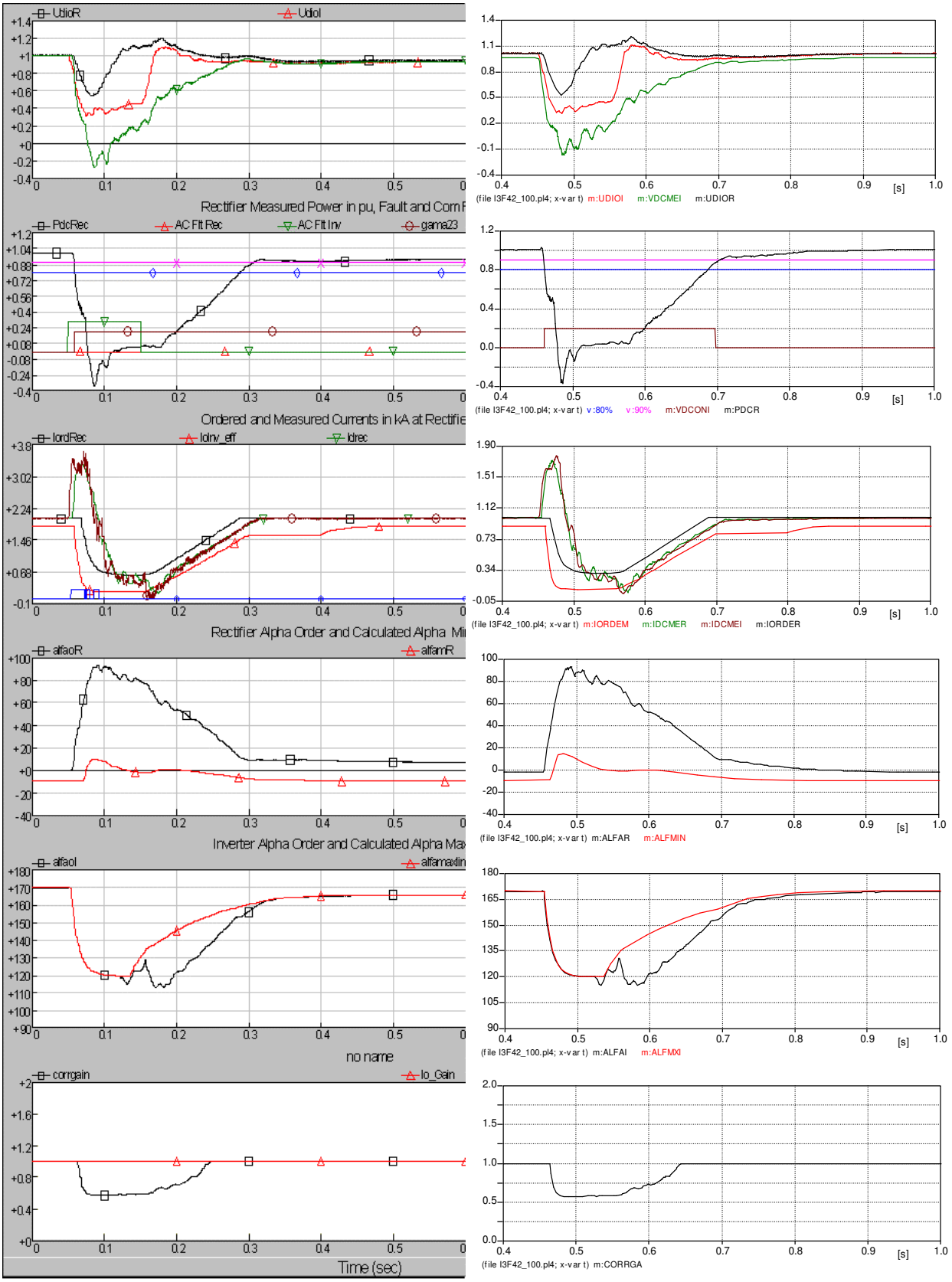


Figure D.21 - Three-phase fault, for 100 ms, at the inverter – residual voltage 42%

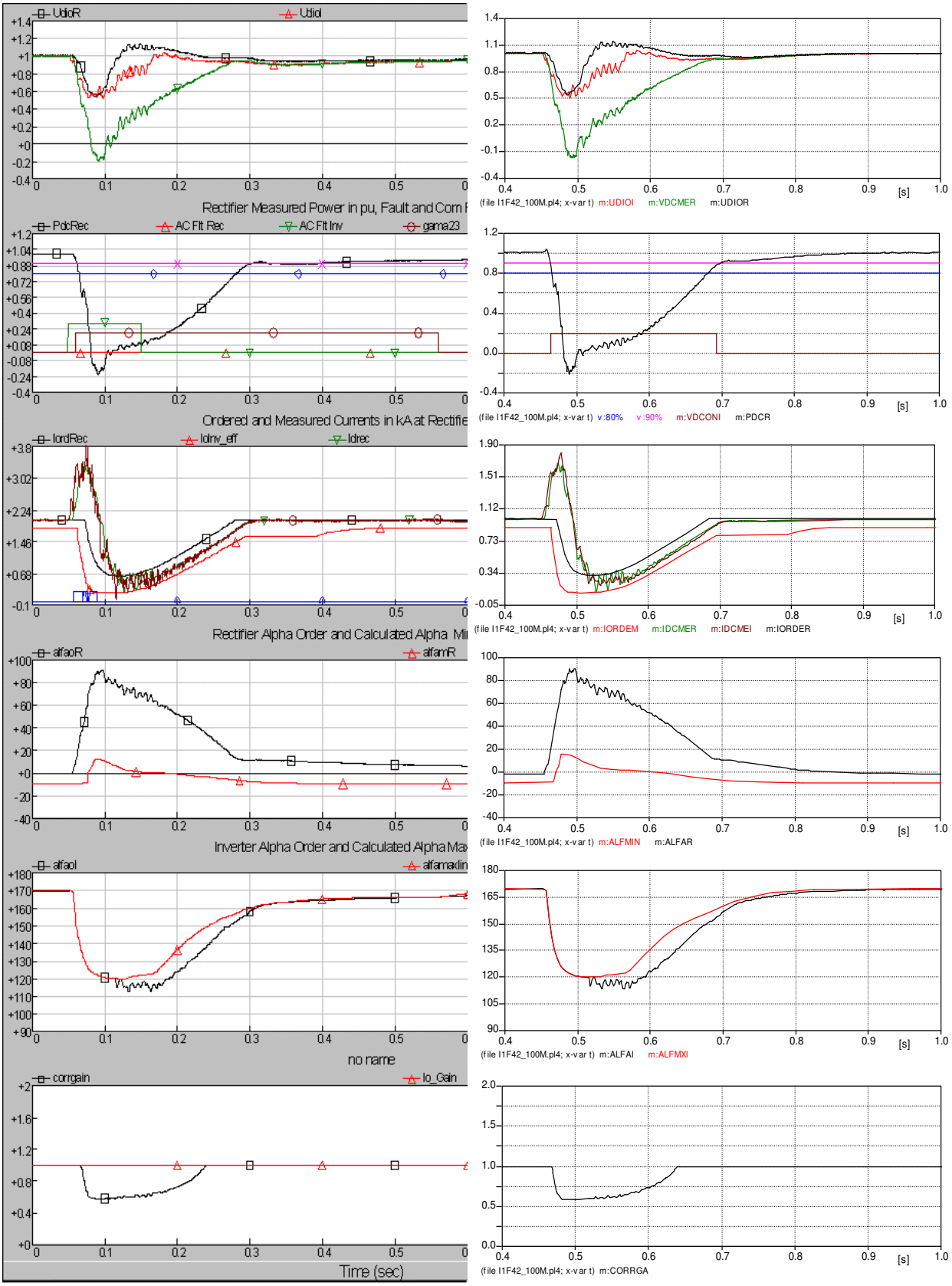


Figure D.22 - Single-phase fault, for 100 ms, at the inverter – residual voltage 42%

## D.4 Conclusions

The comparison with the PSCAD/EMTDC of the results obtained with the ATP model permits to conclude that the latter reproduces in a true and reliable manner the transitory behavior of a CCC link and, thus, that it is adequate for the study of this means for transmission.

It may be observed that the CCC scheme is specially advisable for the insertion of large power blocks in weak receiving systems, where large loads and little generation are present. The differences encountered in relation to PSCAD/EMTDC program are due only to the occurrence, or not, of commutation faults in a small percentage of the various simulated cases.

As the commutation faults have a probabilistic character, it becomes difficult to establish confidently their occurrence; and it is recommended that they should be the object of a separate investigation.

# ANNEX E - CONSIDERATIONS ON THE IMPACT OF THE TRANSFORMER SATURATION CHARACTERISTICS UPON THE POST-FAULT RECOVERIES

## E.1 Introduction

The converter transformer is re-energized upon the removal of an AC fault in the station neighborhood, occasioning the appearance of inrush currents at the transformer. Although these currents are relatively small, in the case of weak AC systems, such as those considered in this work (SCR = 1.3), they may cause a significant distortion of the voltages at the commutation bus (of the AC station bus) and postpone the post-fault recovery of the HVDC link. The distortion levels are dependent on the magnitude of the AC system impedance at the frequency range from the 2nd to the 5th harmonic. On the other hand, the inrush currents decay time is a function of the losses in the AC system.

With low short-circuit ratios (SCR), it is probable that the parallel resonant circuit formed by the shunt equivalent capacitance at the converter station bus (AC lines loading, plus the AC filters capacitance, minus line shunt reactors) and by the impedance of the AC system, may present resonance modes in the region between the 2nd and the 4th harmonic. It is the transformer inrush currents that excite these resonances, producing the high distortion levels observed after fault removal.

In the simulations performed during the development of the PSCAD / EMTDC version of the benchmark, it was opted to measure the transformer magnetizing currents, and to order a decrease of the alpha firing angle (that is, an increase of the gamma extinction angle) so as to avoid commutation faults during the recovery after AC faults. This strategy gave good results, but had the inconvenience to produce slower recoveries than those normally desired, particularly because of an especially slow growth in the final stages of recovery. For instance, in the majority of faults where voltage dropped to levels between 70% and 80% of the pre-fault level, power could be restored in less than 200 ms. Nevertheless, time required to return to the 90% value (the usual measure for recovery times) was often quite longer, attaining from 300 to 400 ms. This being so, it was decided to investigate more deeply the issue of inrush currents, in order to check if it would be possible to reduce recovery times.

This brief report considers two parts:

- The modeling of the AC system on the inverter side, and
- The influence of the transformer saturation characteristics (leakage reactance and saturation curve knee point voltage).

## E.2 Modeling of the inverter AC system.

The frequency response of the positive-sequence equivalent of the inverter AC system was calculated (using Mathcad) for two network topologies, differing but both arriving approximately to the same short-circuit capacity (MVA) at the inverter station bus. The results are presented in the following paragraphs.

### E.2.1 System 1

Figure E.1 shows an equivalent often used in EMTP-type studies. The shunt charging is not represented in this equivalent, possibly because it is generally very small, when compared to the AC filter banks.

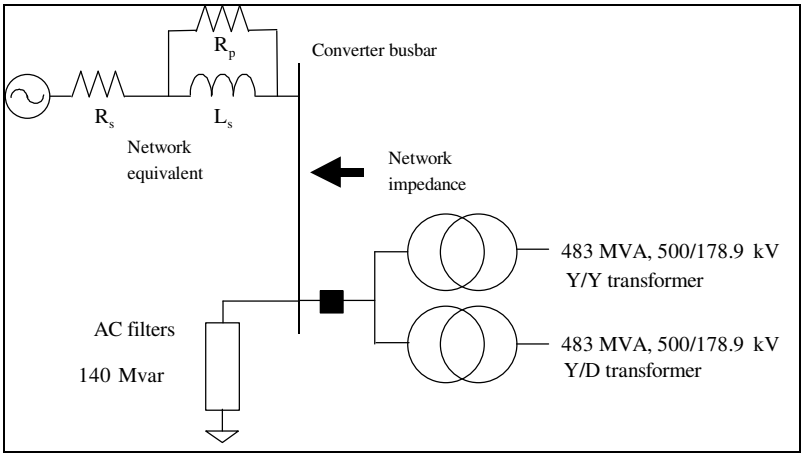


Figure E.1 - Equivalent network, plus AC filters and transformer banks.

Table E.1 shows the value of the discrete parameters utilized in the equivalent, for a 500 kV system (based on 1000 MW transmitted power). Values for a SCR = 2 have been included only as a reference. With a 1.3 SCR, the system impedance, seen from the station bus (without AC filters), is 192.3 Ohms, with an inductive 78 degree angle.

Table E.1 - Values of circuit parameters for the equivalent shown on Figure E.1.

| SCR | $R_s$ (Ohms) | $L_s$ (mH) | $R_p$ (Ohms) |
|---|---|---|---|
| 1.3 | 25.2 | 503.2 | 4400 |
| 2.0 | 16.5 | 327.3 | 2900 |

The frequency response shown on Figure E.2 below was obtained using Mathcad. The calculations were made for the positive-sequence circuit, without the converter transformers.

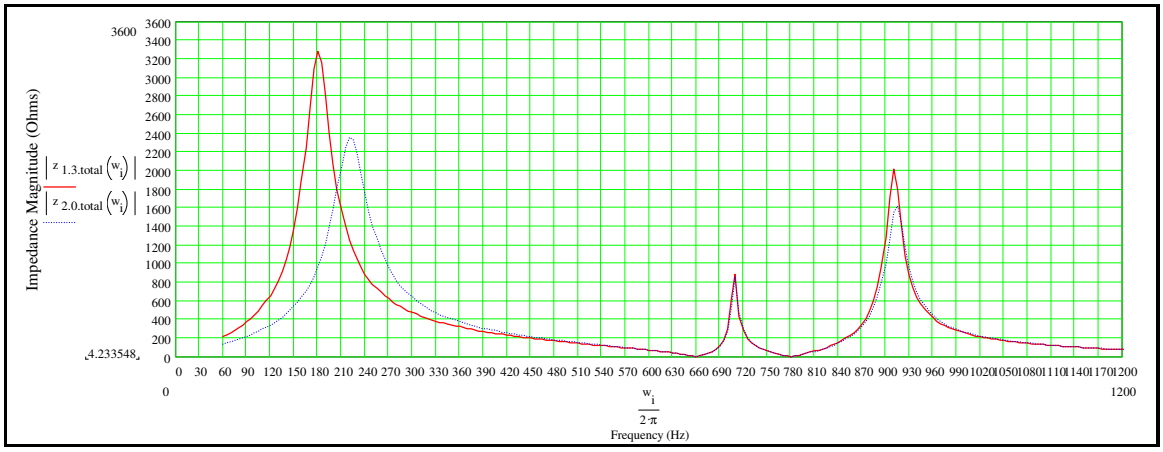


Figure E.2 - Positive-sequence frequency response for the equivalent plus AC filters.

With a 1.3 SCR, a parallel resonance occurs between the AC filter bank and the system, at approximately 180 Hz. With a 2.0 SCR, the resonance shifts to about 215 Hz. In order to verify the effect of the transformer inrush currents with the SCR of 1.3, a solid three-phase fault was applied to the bus of the converter station in the PSCAD version of Figure E.1. In this case, the transformers were included, and the pre-fault voltage adjusted to 1 pu. The bus voltages and the inrush currents (for one transformer only) were submitted to a fast Fourier transform (FFT) and drawn on Figure E.3.

In Figure E.3, the instant of fault clearing was selected so as to leave maximum flow in phase A, which causes a maximum inrush current in phase A. Phase A voltages and currents were submitted to a Fourier fast transform (FFT) and traced in pu values on the basis of $500/\sqrt{3}$ kV for voltages and 0.5577 kA for the

currents. Total distortion values are RSS values, considering the harmonics measured in phase A, between the 2nd and the 5th.

The magnitudes of the inrush currents are not high (Idist < 0.15 pu, maximum), at least if compared to the inrush currents higher than 1 pu that often occur when transformers are energized from strong sources (low impedance sources). The impedance of the circuit amplifies the effect if the distorted currents produce a severe distortion in AC voltages (Udist<0.50 pu maximum). Figure E.4 is an enlargement of voltage tracing in Figure E.3, showing only the first cycles after fault clearing.

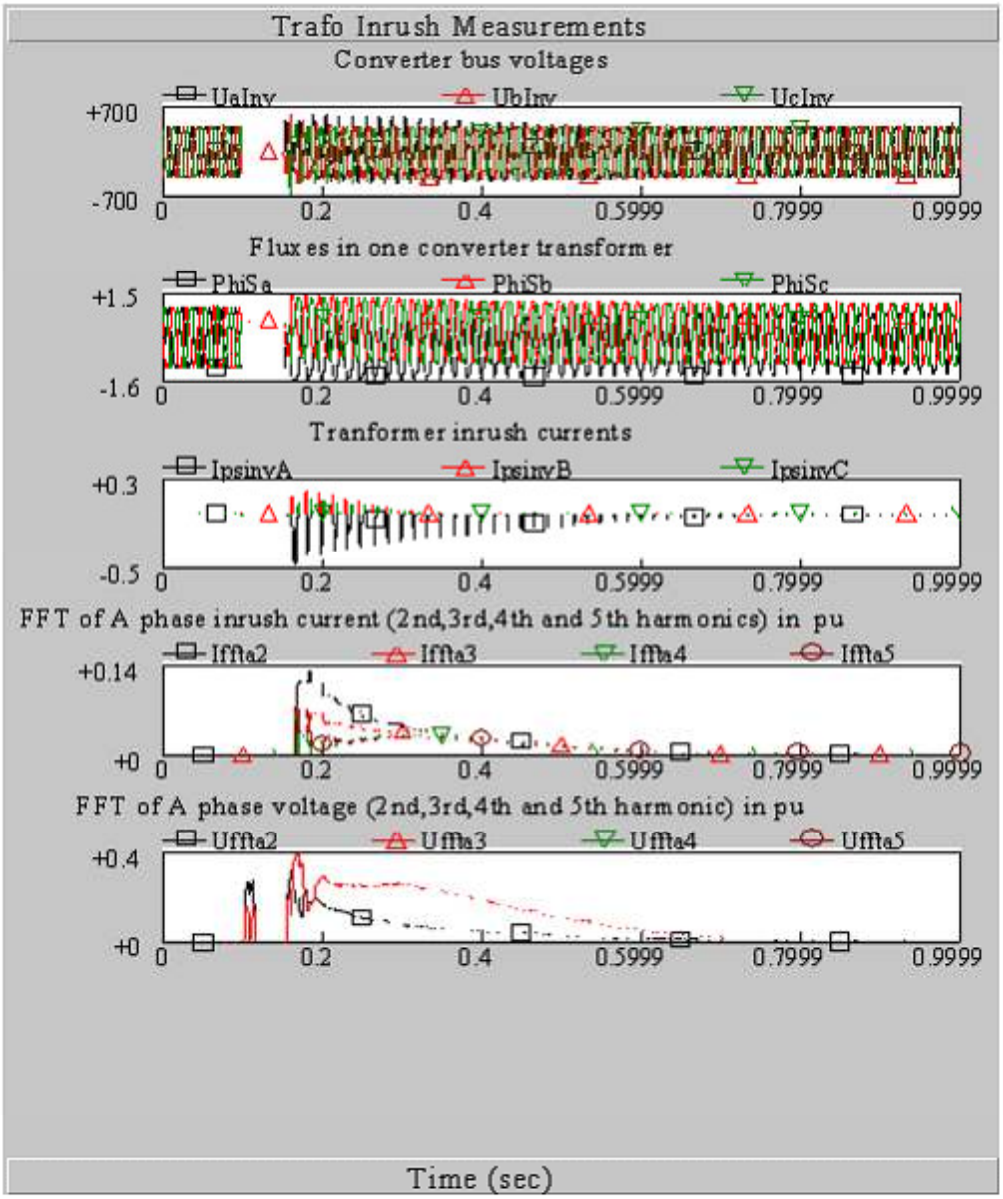


Figure E.3 - Currents and voltages after clearing a three-phase solid fault at the inverter bus (converter blocked)

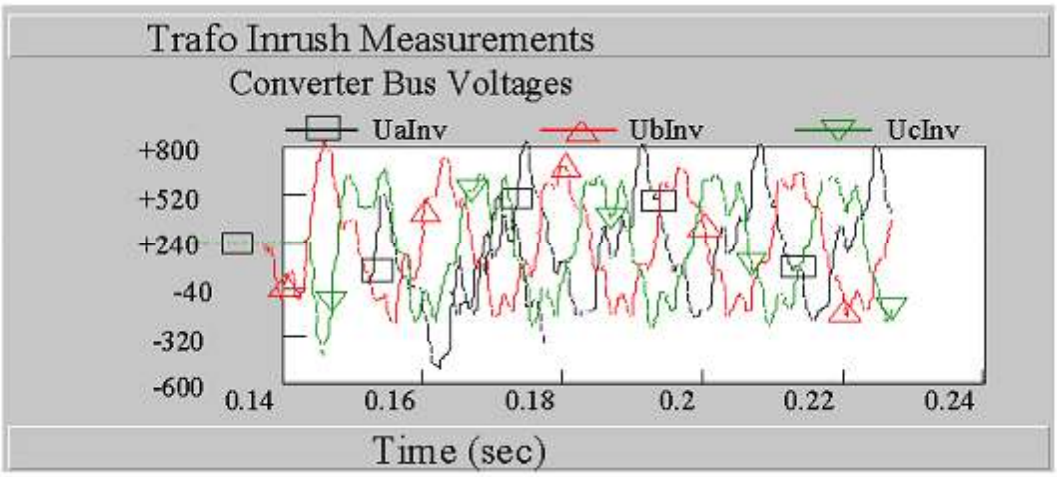


Figure E.4 - Expanded view of the first few cycles of Figure E.3 bus voltages

### E.2.2 System 2

In Figure E.5, a 254 km transmission line was included, thus making the circuit topology more realistic. The line is compensated for about 70% of its loading by shunt line reactors. The total line loading is 349.3 Mvar and each shunt reactor is dimensioned for 120 Mvar. The equivalent circuit was adjusted to present a positive-sequence impedance, seen from the station bus, of a magnitude equal to that of the original circuit shown on Figure E.1. The values of the circuit parameters that were utilized are given in Table E.2.

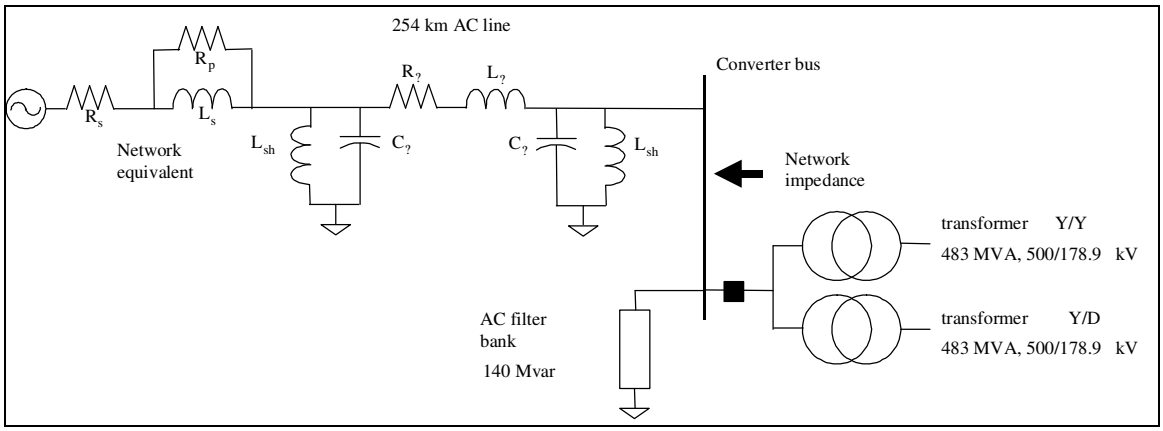


Figure E.5 - Equivalent circuit including AC lines, AC filters and transformer banks

Table E.2 - Values of circuit parameters utilized in Figure E.5

| | |
|---|---|
| $R_s$ | 16 Ohms |
| $R_p$ | 1900 Ohms |
| $L_s$ | 0.26441 H |
| $C_\pi$ | 1.681 µF |
| $R_\pi$ | 6.305 Ohms |
| $L_\pi$ | 0.2222175 H |
| $L_{sh}$ | 5.5262 H |

The frequency response of the positive-sequence equivalent circuit, shown on Figure E.6, was determined using Mathcad. Line loading shifts resonance to a lower frequency (of about 130 Hz), which should reduce the distortion due to transformer inrush currents after fault clearing.

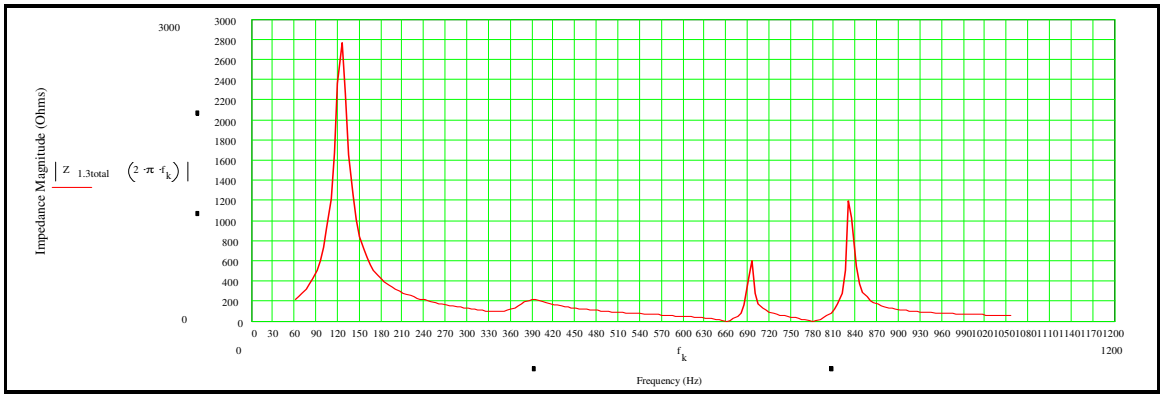


Figure E.6 - Frequency response of the positive-sequence circuit for the equivalent, including AC line and AC filters.

A model of Figure E.5 in PSCAD version was used to examine the response time, after clearing a solid three-phase fault analogous to that of the previous example, using the more simplified circuit given in Figure E.1. In the PSCAD version, the AC line is represented by frequency-dependent parameters. The results are shown on Figure E.7. As expected, with the transmission line reducing the resonance frequency value, the dominant voltage harmonic stays closer to the 2nd than to the 3rd harmonic. The magnitude of voltage peaks and the current distortion are approximately the same, but the inrush currents are damped more quickly.

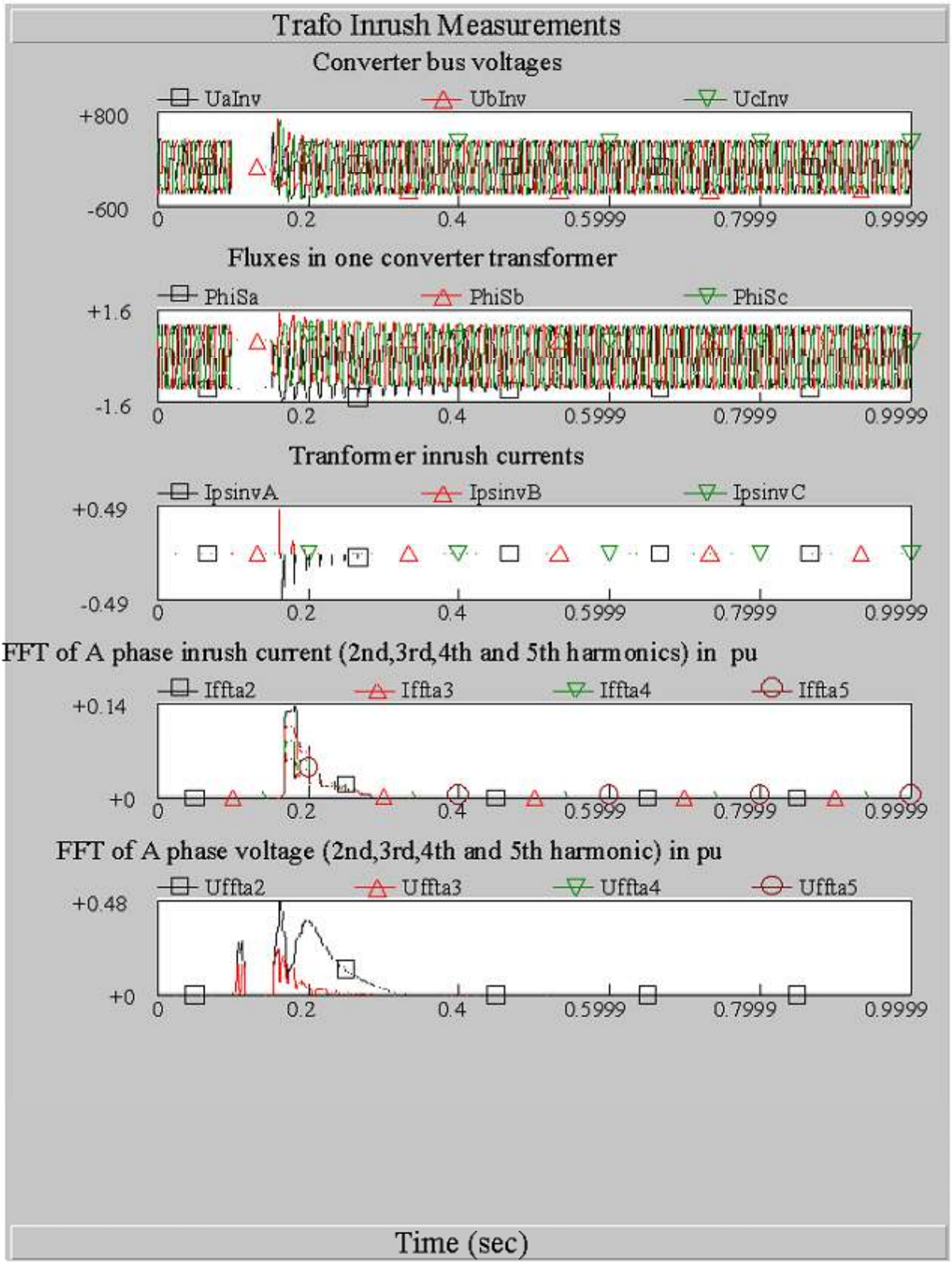


Figure E.7 - Currents and voltages after clearing a solid three-phase fault at the converter bus (converter blocked)

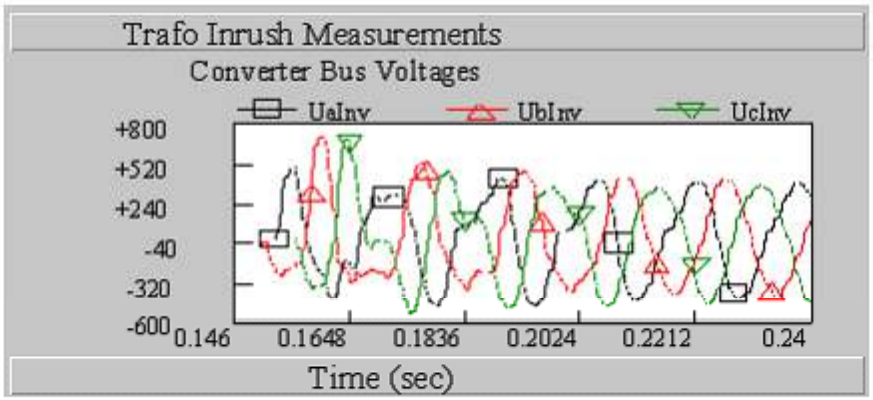


Figure E.8 - Expanded view of the first voltage cycles at the bus of the converter station, obtained from Figure E.7.

### E.3 Impact of the saturation characteristics of the converter transformer

Based on the observations made in the previous section, the inverter AC system utilized in the PSCAD model was altered in order to include a 254 km AC line (that is, the circuit shown on Figure E.5 was utilized from this point on). This network is more favorable (and almost certainly more realistic) that the equivalent circuit previously used.

As a result of what was noted and discussed above, the inverter AC circuit was used in the PSCAD model with the purpose to verify if the post-fault recovery showed itself very or little sensitive to the values used to define the saturation characteristics. As a reference, a solid three-phase fault at the inverter bus was chosen, with a 100 ms duration, and it was repeated while varying the transformer saturation parameters. The fault was always applied in the instant corresponding to a maximum flux in phase A, in order to obtain the maximum inrush current in phase A. In the cases 1 to 5, the control function which reduces the inverter firing angle, based on the saturation current, was disabled (this function, from now on, will be called “trafo mag current detector"). Table E.3 details the examined cases.

Table E.3 - Variation of the saturation parameters

| Case | Saturation parameters | | Commutation failure during recovery ? | Time to 90 % (ms) |
|---|---|---|---|---|
| | knee point V (pu) | leakage X (pu) | | |
| 1 | 1.25 (rated) | 0.288 (rated) | yes | Not available |
| 2 | Saturation removed | Saturation removed | no | 110 |
| 3 | 1.1 x (1.25) =1.375 | 0.288 | no | 110 |
| 4 | 1.25 | 1.4 x (0.288) = 0.3744 | no | 110 |
| 5 | 1.25 | 1.3 x (0.288) = 0.3456 | yes | Not available |
| 6 | 1.20 | 0.240 | no | 275 * |

* ”Trafo mag current detector” activated

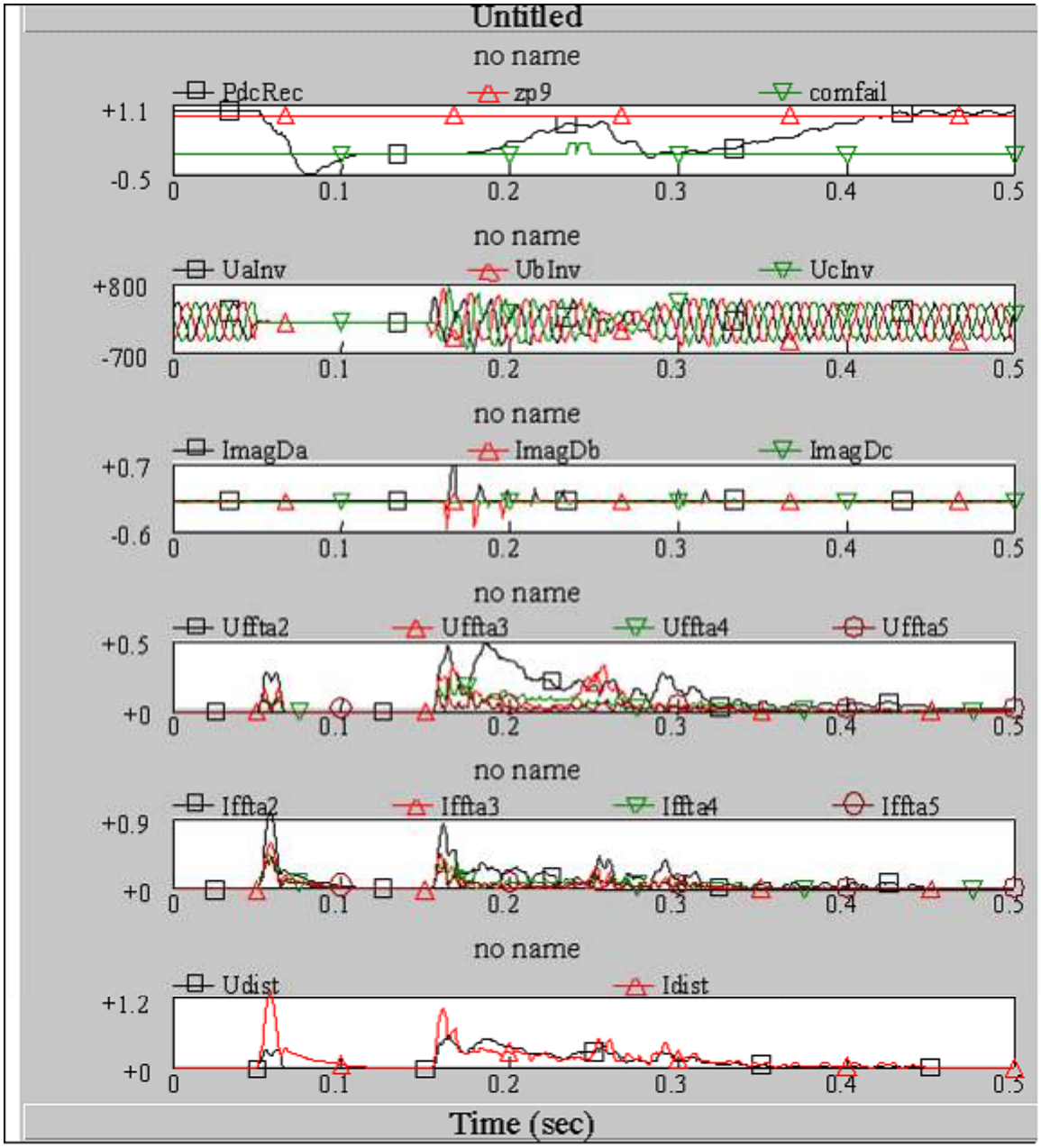


Figure E.9 - Case 1 results (rated saturation parameters, with “trafo mag current detector” disabled)

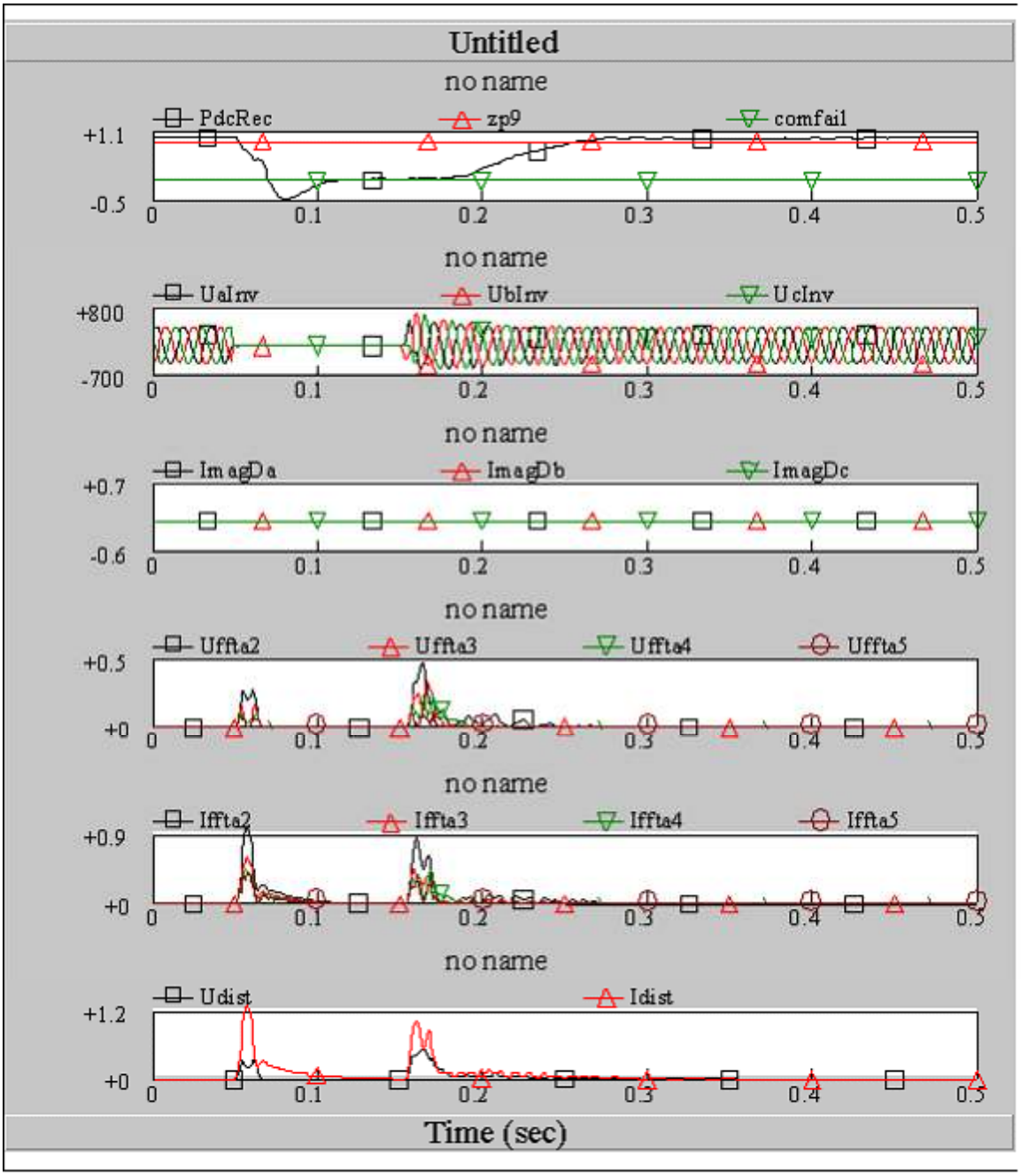


Figure E.10 - Case 2 results (transformer saturation disabled)

Case 1 (Figure E.9) shows that, with the rated saturation parameters, the "trafo mag current detector" becomes necessary in order to prevent commutation faults. Case 2 (Figure E.10) shows that, without the transformer saturation, it is possible to obtain 110 ms recovery times. Case 3 shows that a 10% increase in the saturation knee point voltage is sufficient to avoid commutation faults. No tracing of this case was reproduced, since it is essentially a repetition of case 2 (Figure E.10). Cases 4 and 5 show that, by increasing the leakage reactance up to 40% above the rated value, the commutation faults are also avoided.

The results shown above are not surprising. By selecting very high knee point saturation voltages or leakage reactances, the inrush currents are reduced substantially to values that do not cause disturbances during the post-fault recovery. More realistic levels result in severe voltage distortion, thus requiring the action of controls. In case 6, the function "trafo mag current detector" was activated and, also, slightly more realistic values for the saturation parameters were used ($V_{knee\ point}$ = 1.2 pu and $X_{leakage}$ = 0.24 pu). The recovery was satisfactory.

## E.4 Conclusions

- The transformer inrush currents may cause severe voltage distortion during the recovery after an AC fault. This way, the AC system impedance at the 2nd to the 5th harmonic frequencies is an important factor for the determination of the intensity of voltages distortion;

- At least in this case, the inclusion of transmission lines in the network representation improves the behavior during recovery, because it shifts the parallel resonance from almost exactly the 3rd harmonic to approximately the 2nd. In this case, there is also a greater damping of the inrush currents, and this is probably the most important factor. With sufficient damping, the distortion of voltages practically ceases before the inverter can reach firing angles sufficiently large (that is, gamma extinction angles sufficiently small) so that commutation faults may occur;

- It is possible to obtain smaller recovery times.

It should be noted that, in principle, these conclusions apply specifically to the values selected for our benchmark model (i.e., SCR = 1.3, filters with 140 Mvar capacity etc.)

## ANNEX F - ATP CASES: COMPARISON OF LINK PERFORMANCE AND MODELING WITH AND WITHOUT DC FILTERS

In long distance overhead line HVDC systems dc filters are not an option but a requirement basically due to telephone interference from the dc line. Generally, the dc filters impact on fault performance is small but operation without them is normally not allowed, except perhaps in contingency conditions. As valve firing controls operate within the dc filters frequency bandwidth they can be affected, especially in limit situations conducive to commutation failures. Hence, all 60 ATP cases previously analyzed were reprocessed including an explicit representation of filters in the DC line, and the results were compared with the same ATP cases without filters. The comparisons are shown in Figures F.1 to F.12.

Each of the following charts is associated to a type of fault (single-phase and three-phase, rectifier and inverter) and in each are superimposed the DC currents resulting from several values of impedances which, during the fault, produce voltages at the converter bus varying between 0% (solid fault) and 80% (remote fault). Each page shows the original cases without filters and the new cases considering the presence of DC filters.

The cases have been identified in the following manner, taking as an example the cases of Figure F.1: R1F0_100.pl or R1F0_100_F.pl4:

- R1 => Single-phase fault at rectifier
- F0 => Solid fault (0% residual voltage at the converter bus)
- 100 => CCC link power equal to 100% (1.0 pu)
- F => DC filters included

The results show that in the border conditions conducive to commutation failures the number of ATP cases showing the occurrence of commutation failures during fault recovery has increased from 4 without dc filter representation to 8 with dc filter representation.

From a modeling point of view it should be noted that the same original 4 cases without DC filters did not show the occurrence of commutation failures when run with the PSCAD program. This might be due to the fact that the ATP program does not use interpolation within integration steps through discontinuities and so is more prone to numerical imprecision in critical situations. We did not have an opportunity to reprocess all 60 cases with the PSCAD program with DC filters represented and so do not know if the same pattern of 8 cases with DC filter representation presenting commutation failures would also appear. In order to reach a more definite conclusion on this matter it is essential to effect the same reprocessing in the PSCAD program.

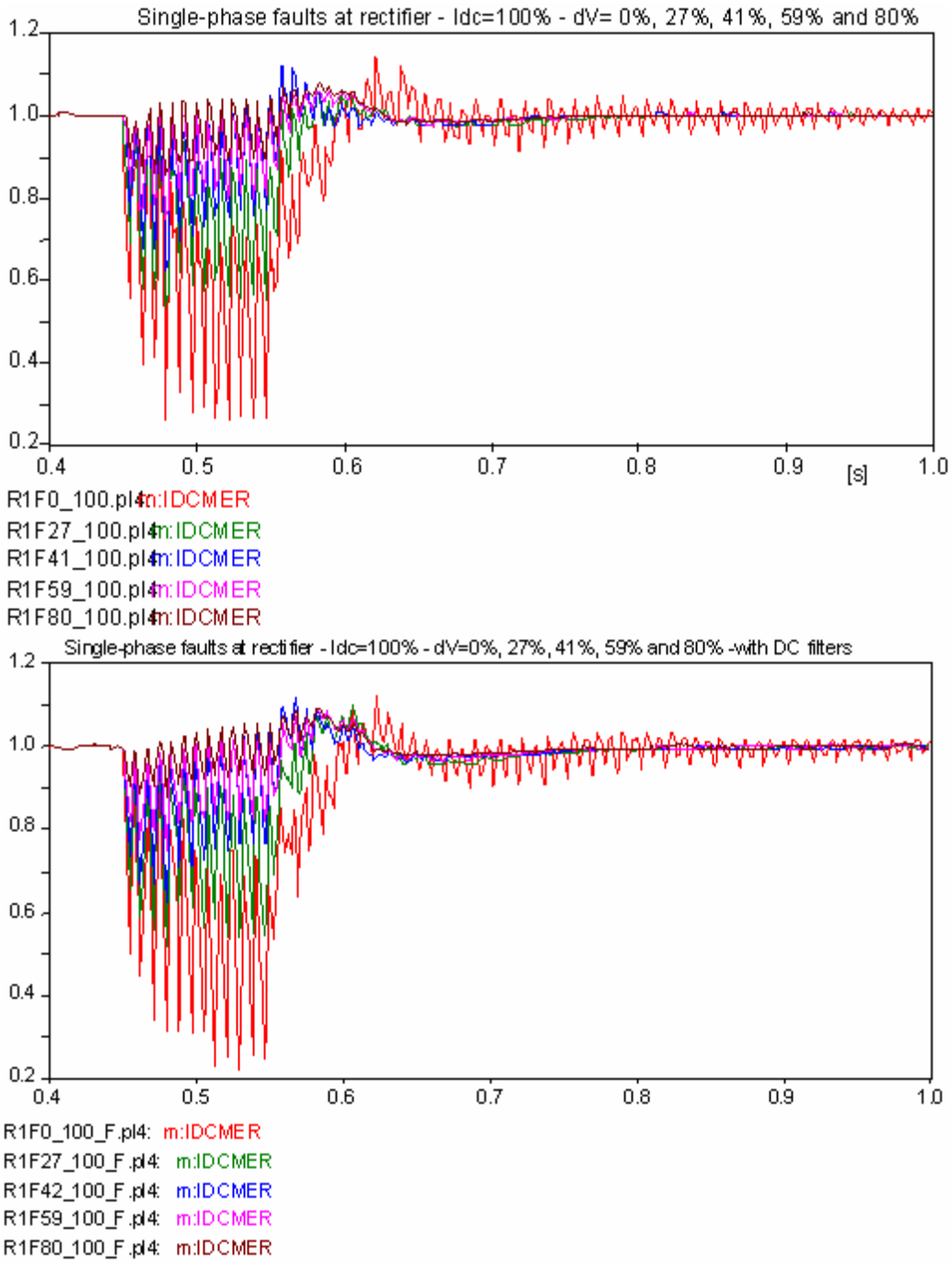


Figure F.1 – Single-phase faults at the rectifier for Pdc = 1.0 pu – with and without DC filters

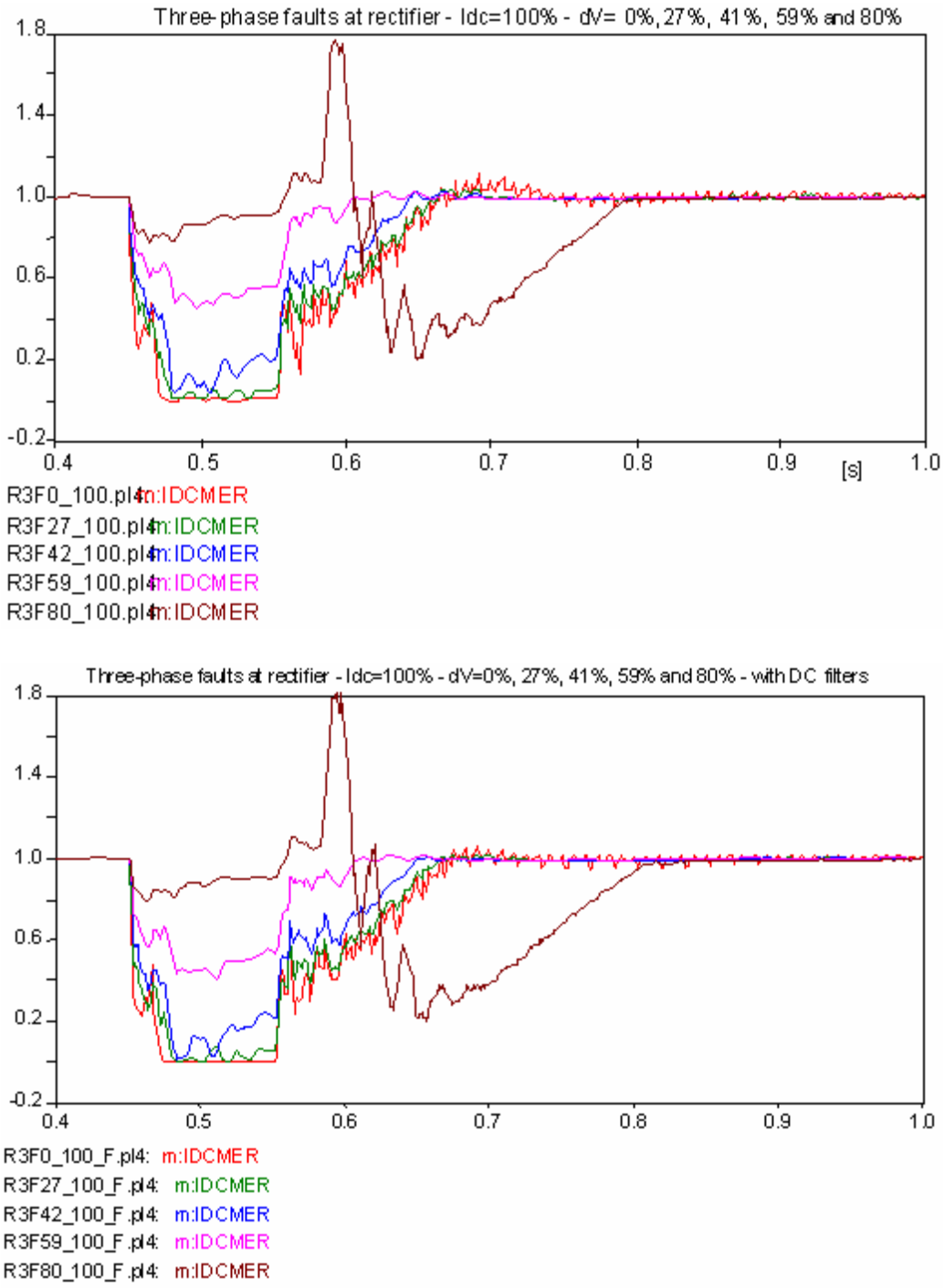


Figure F.2 – Three-phase faults at the rectifier for Pdc = 1.0 pu – with and without DC filters

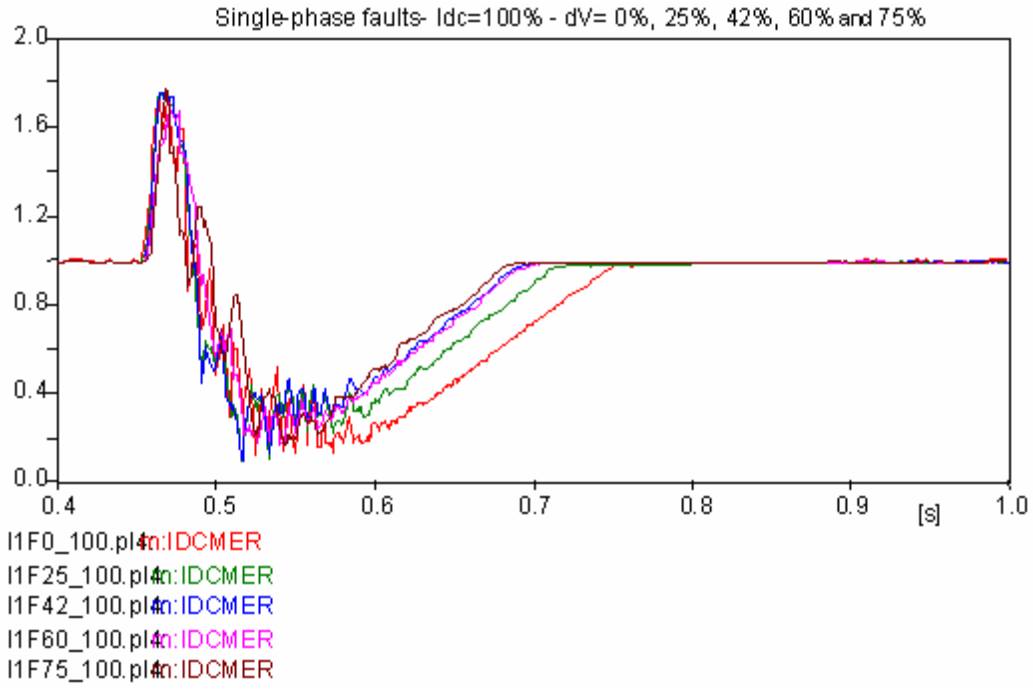


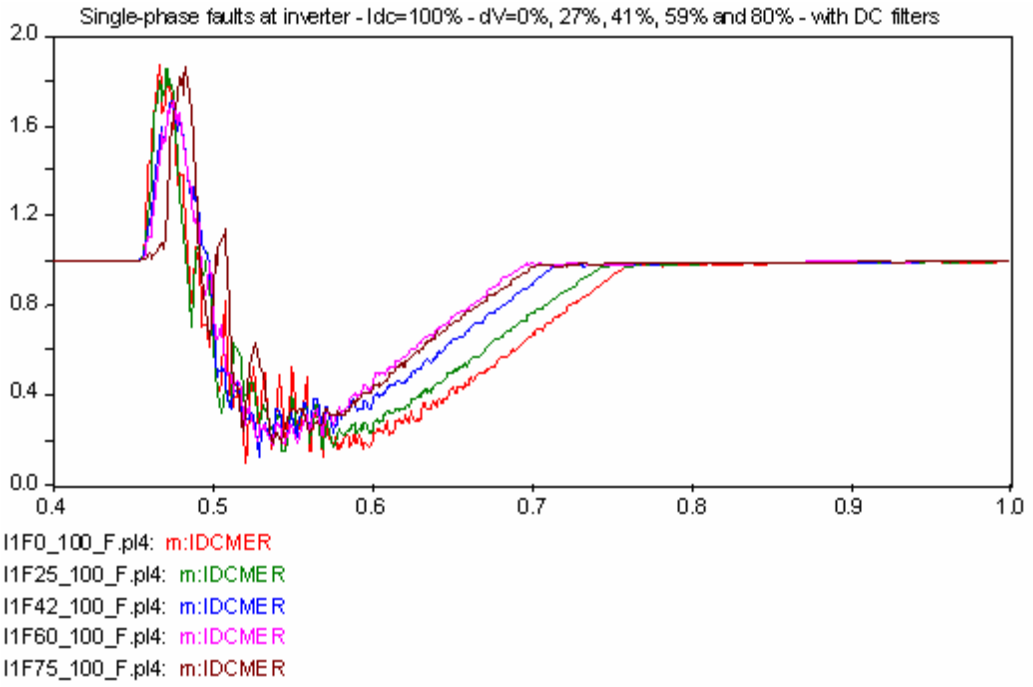


Figure F.3 – Single-phase faults at the inverter for Pdc = 1.0 pu – with and without DC filters

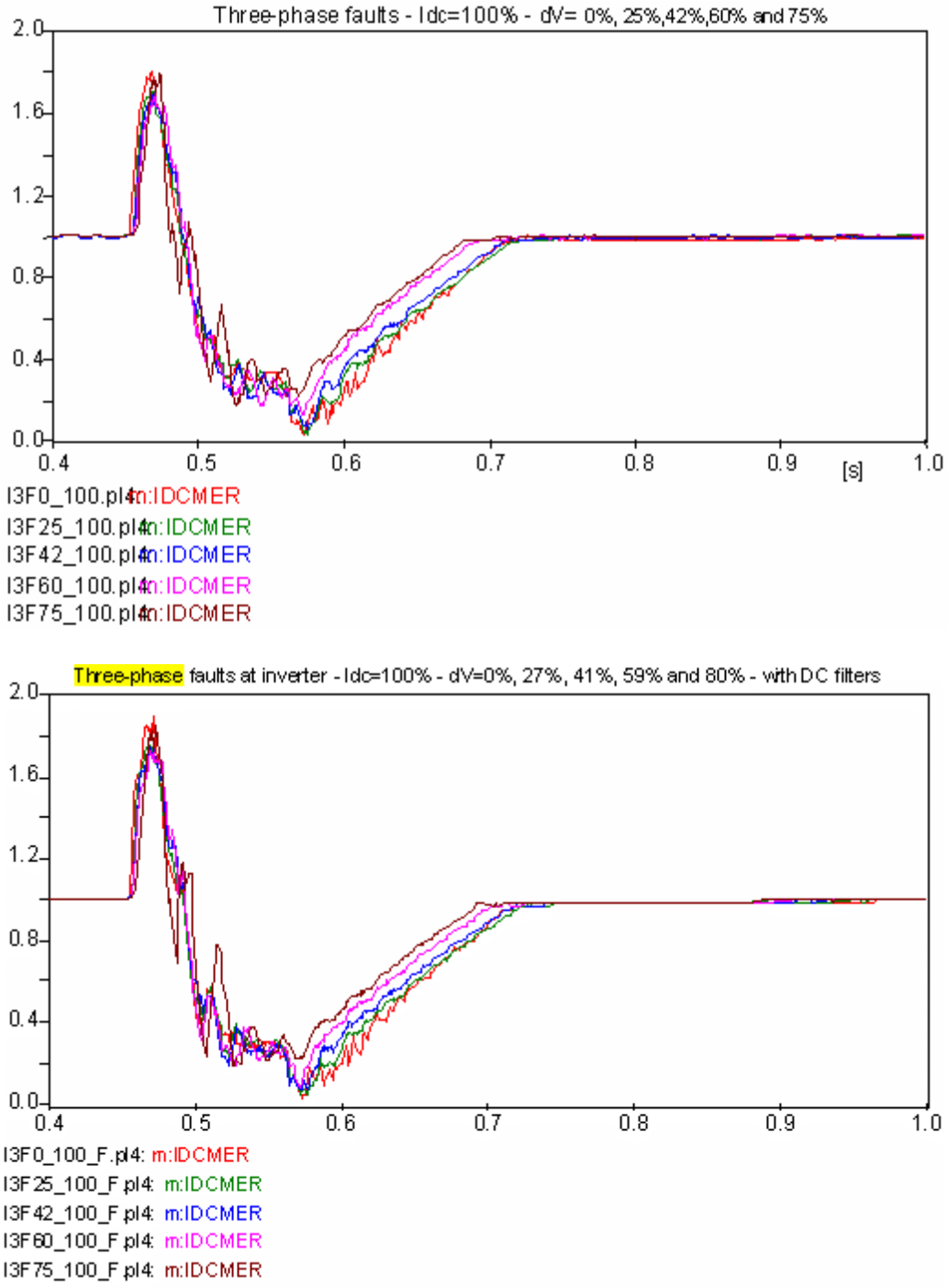


Figure F.4 – Three-phase faults at the inverter for Pdc = 1.0 pu– with and without DC filters

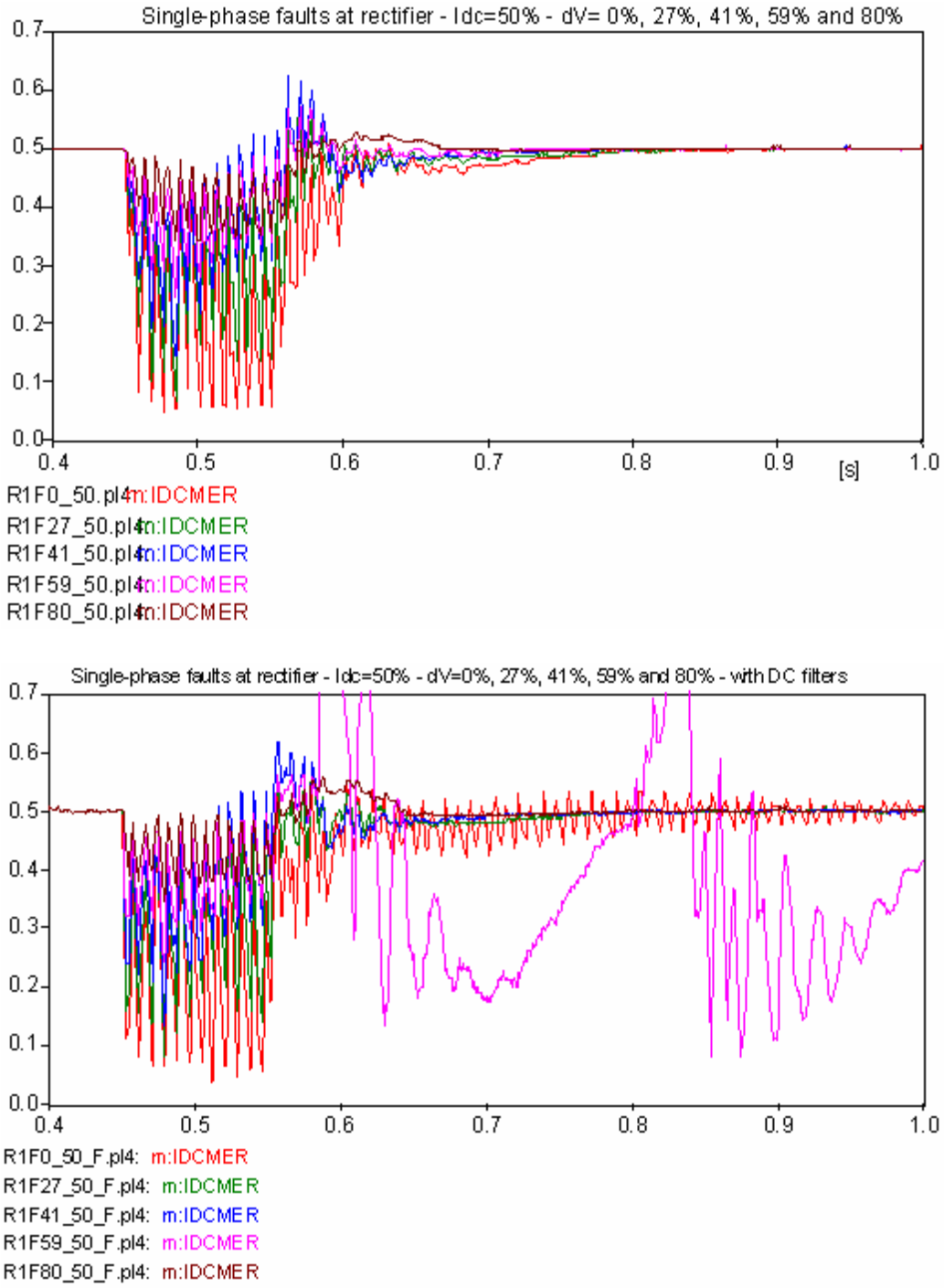


Figure F.5 – Single-phase faults at the rectifier for Pdc = 0.5 pu – with and without DC filters

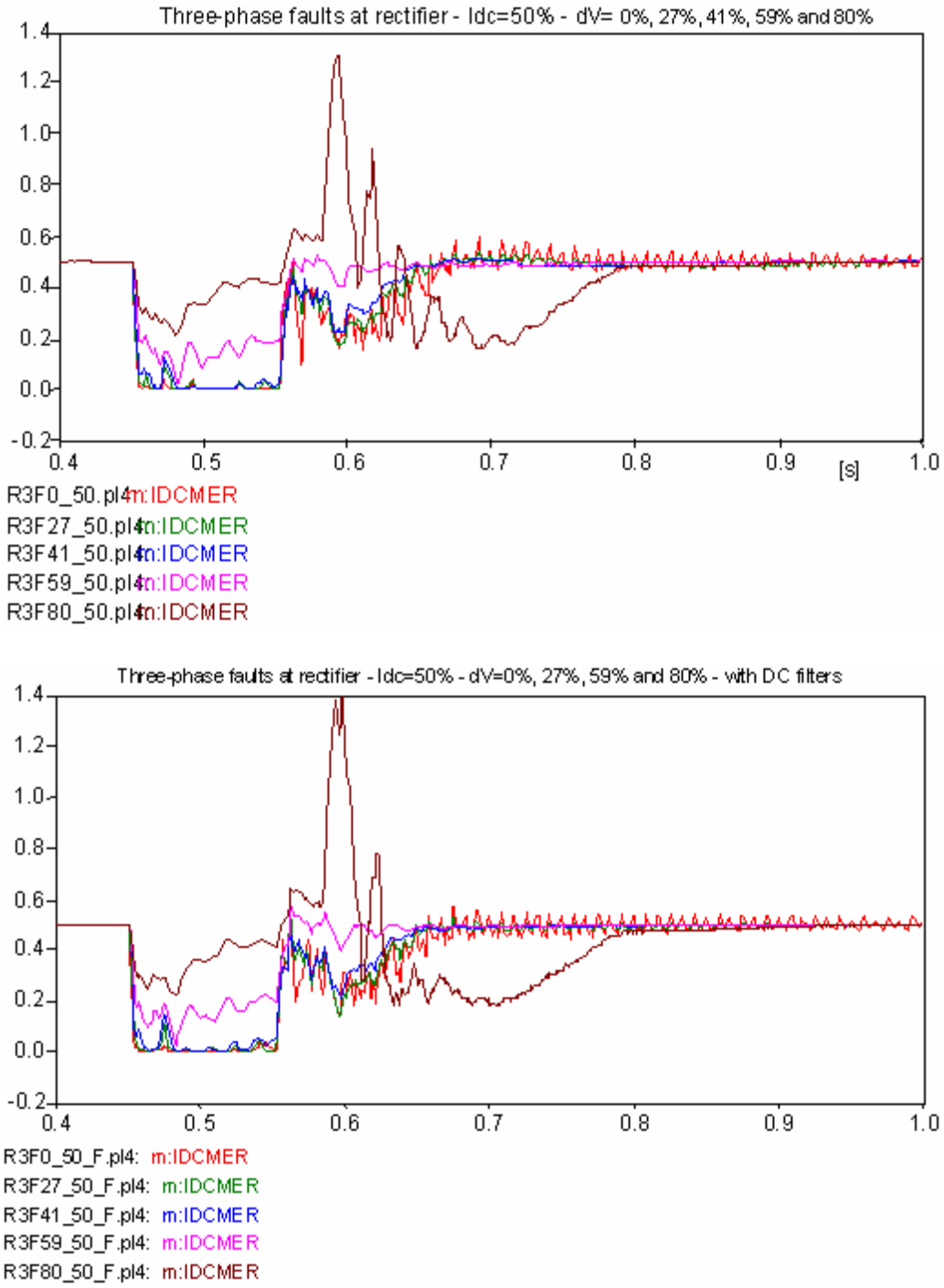


Figure F.6 – Three-phase faults at the rectifier for Pdc = 0.5 pu – with and without DC filters

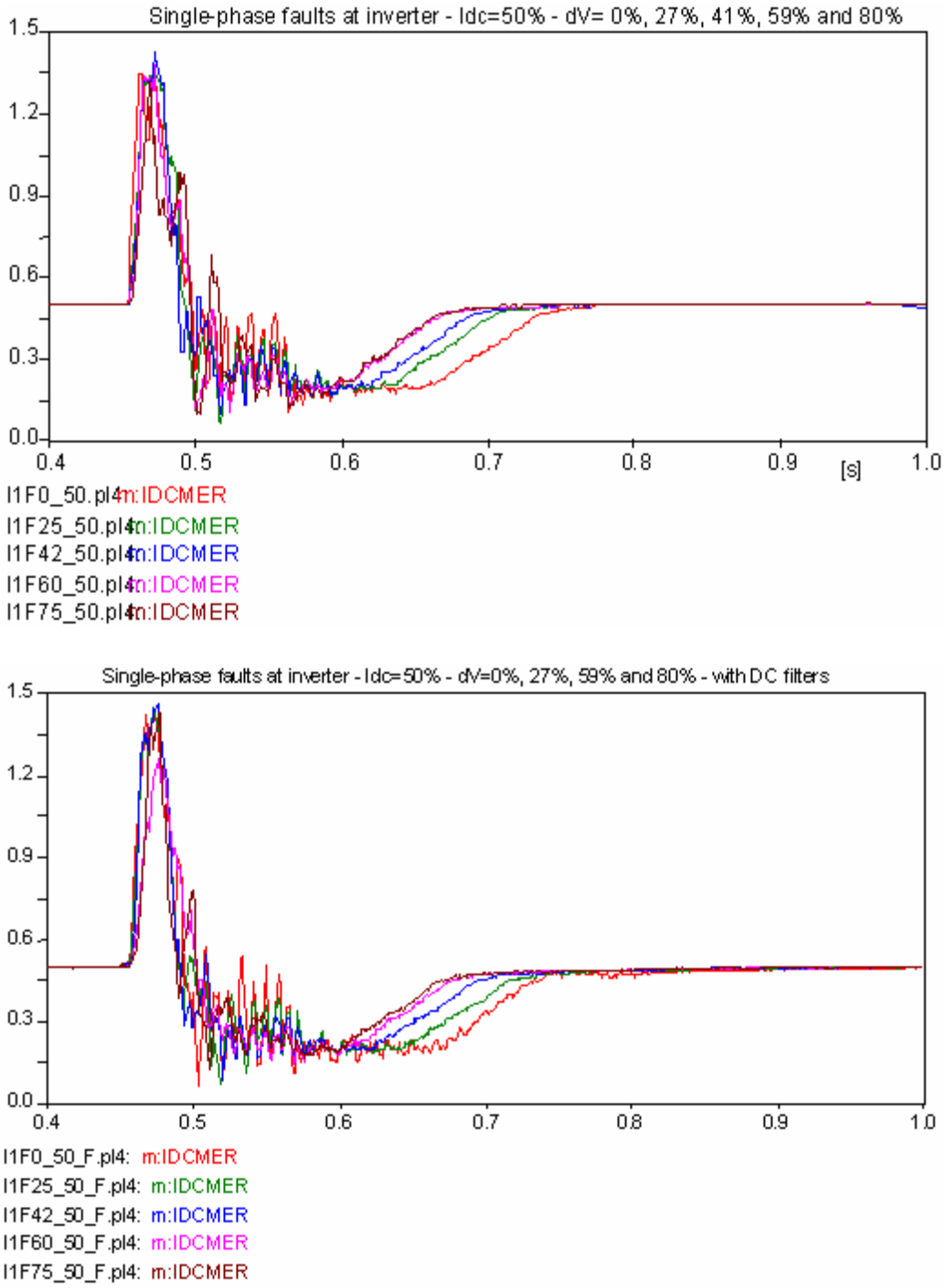


Figure F.7 – Single-phase faults at the inverter for Pdc = 0.5 pu – with and without DC filters

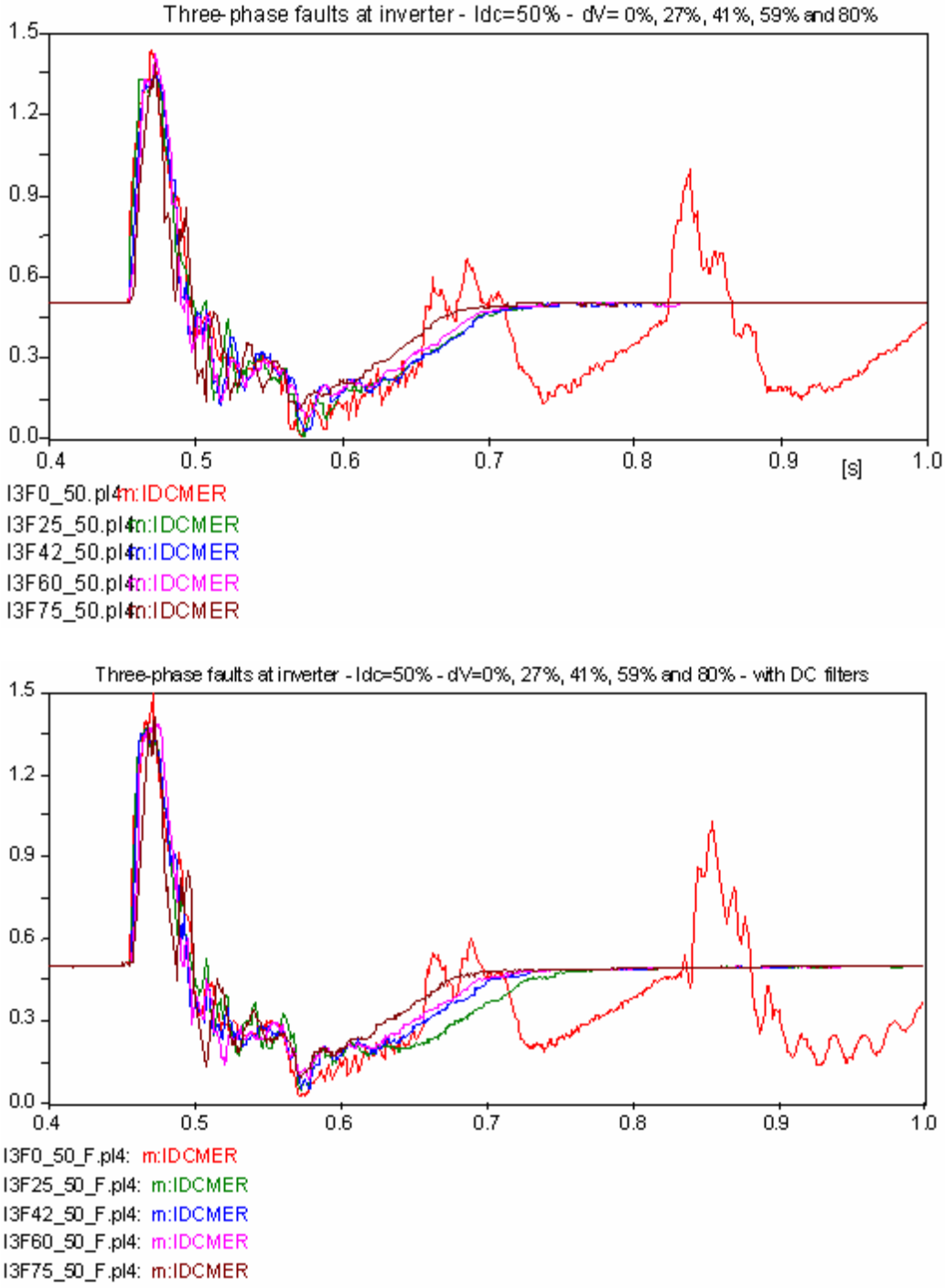


Figure F.8 – Three-phase faults at the inverter for Pdc = 0.5 pu – with and without DC filters

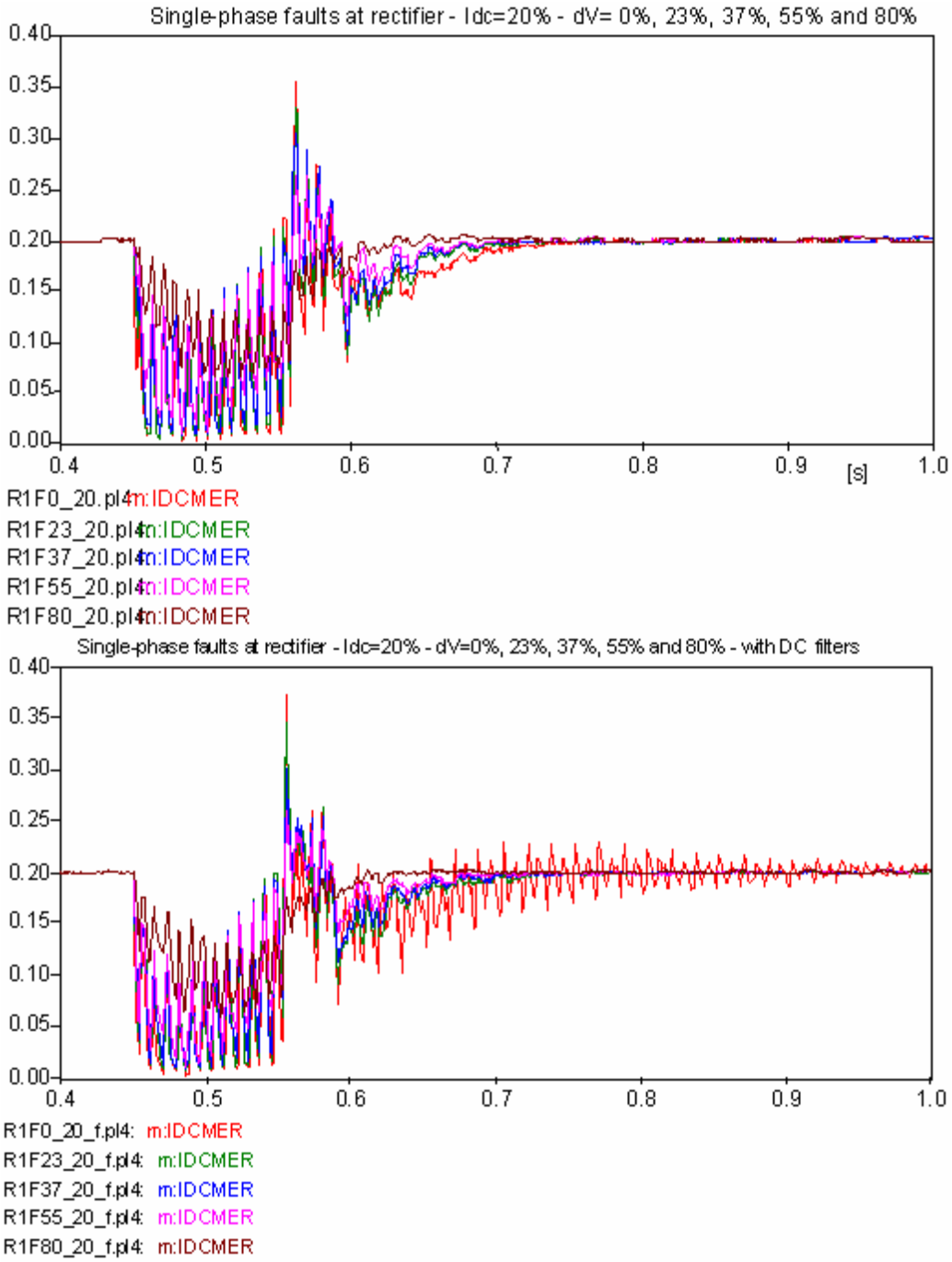


Figure F.9 – Single-phase faults at the rectifier for Pdc = 0.2 pu – with and without DC filters

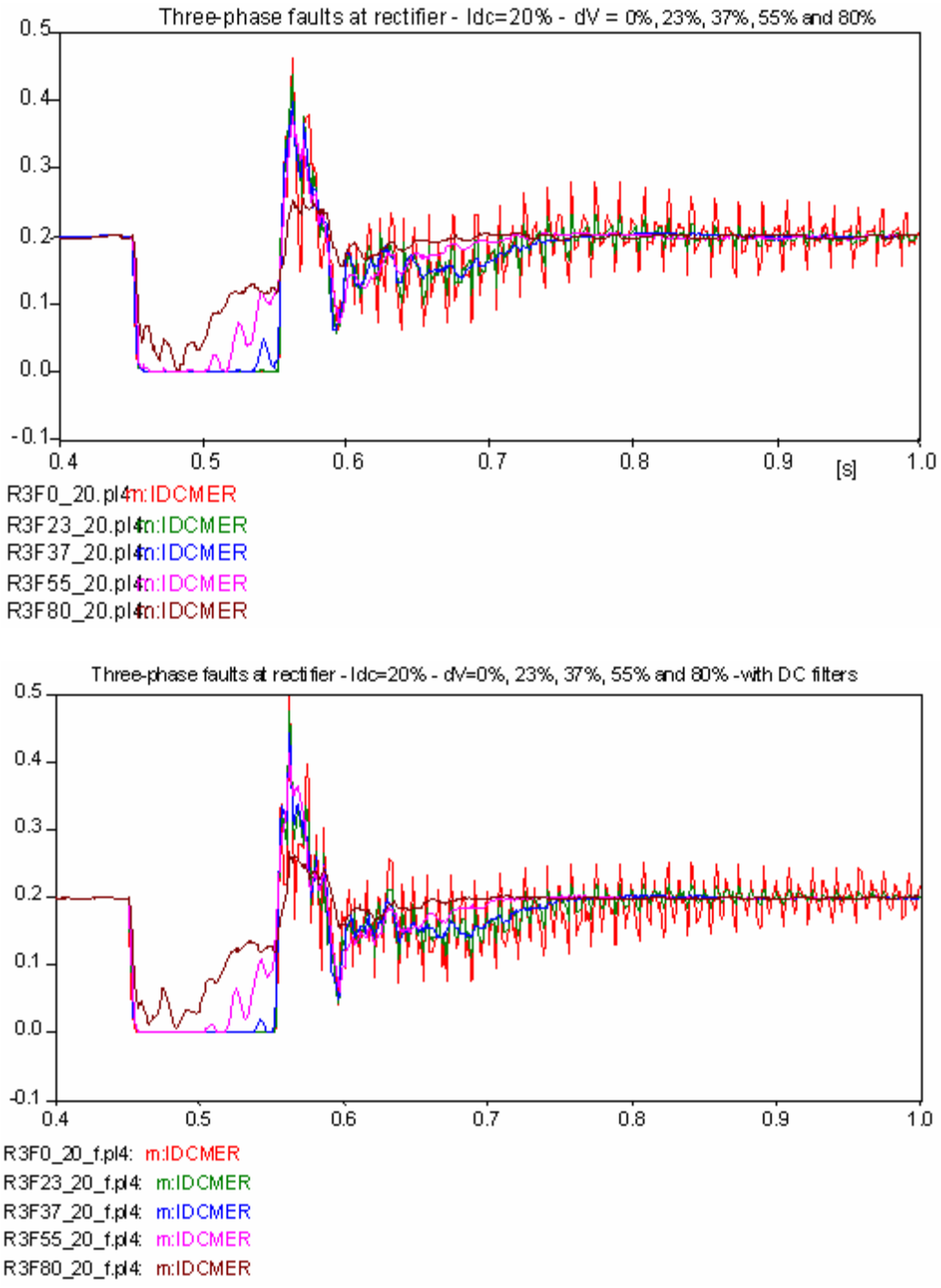


Figure F.10 – Three-phase faults at the rectifier for Pdc = 0.2 pu – with and without DC filters

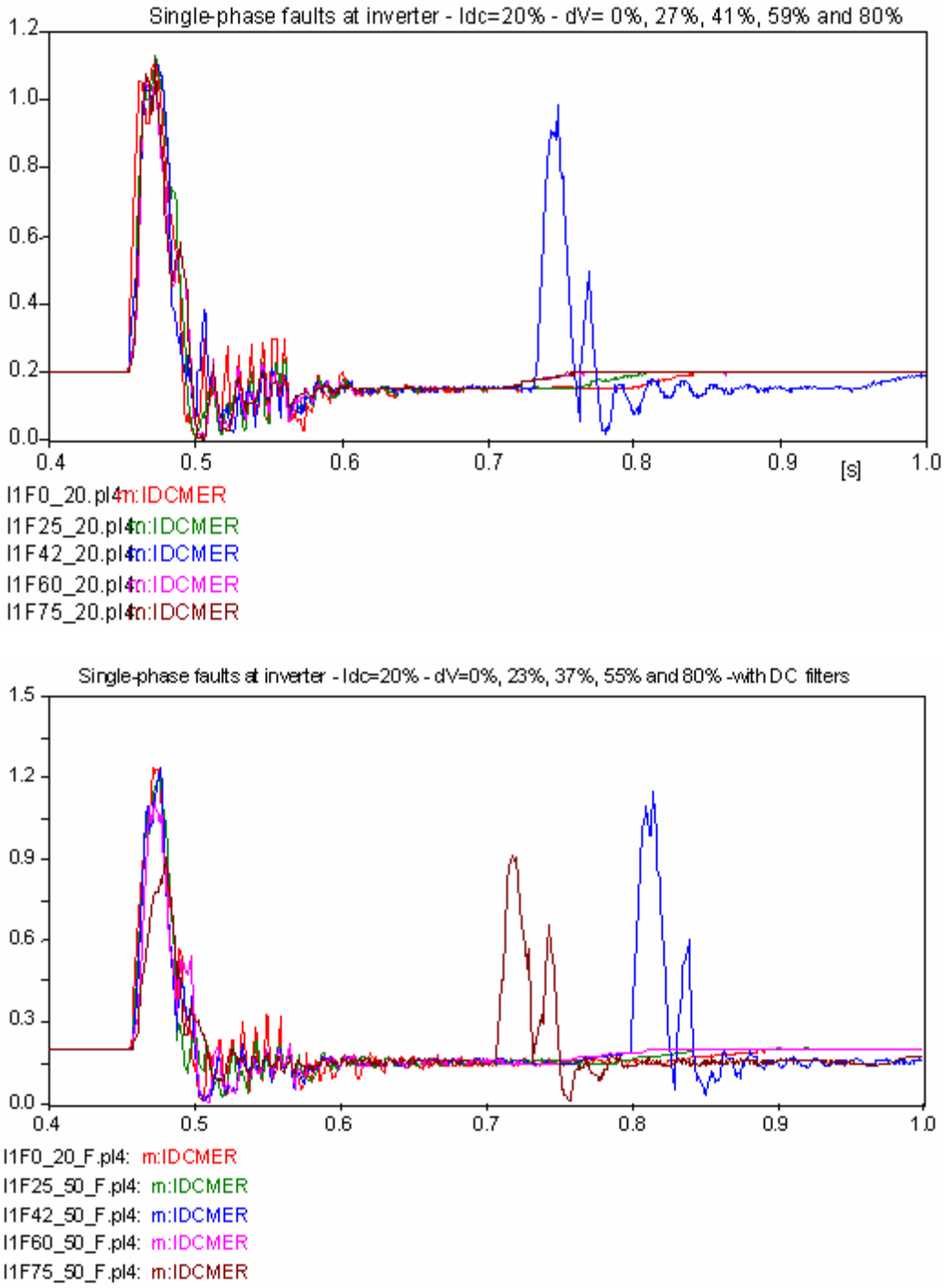


Figure F.11 – Single-phase faults at the inverter for Pdc = 0.2 pu – with and without DC filters

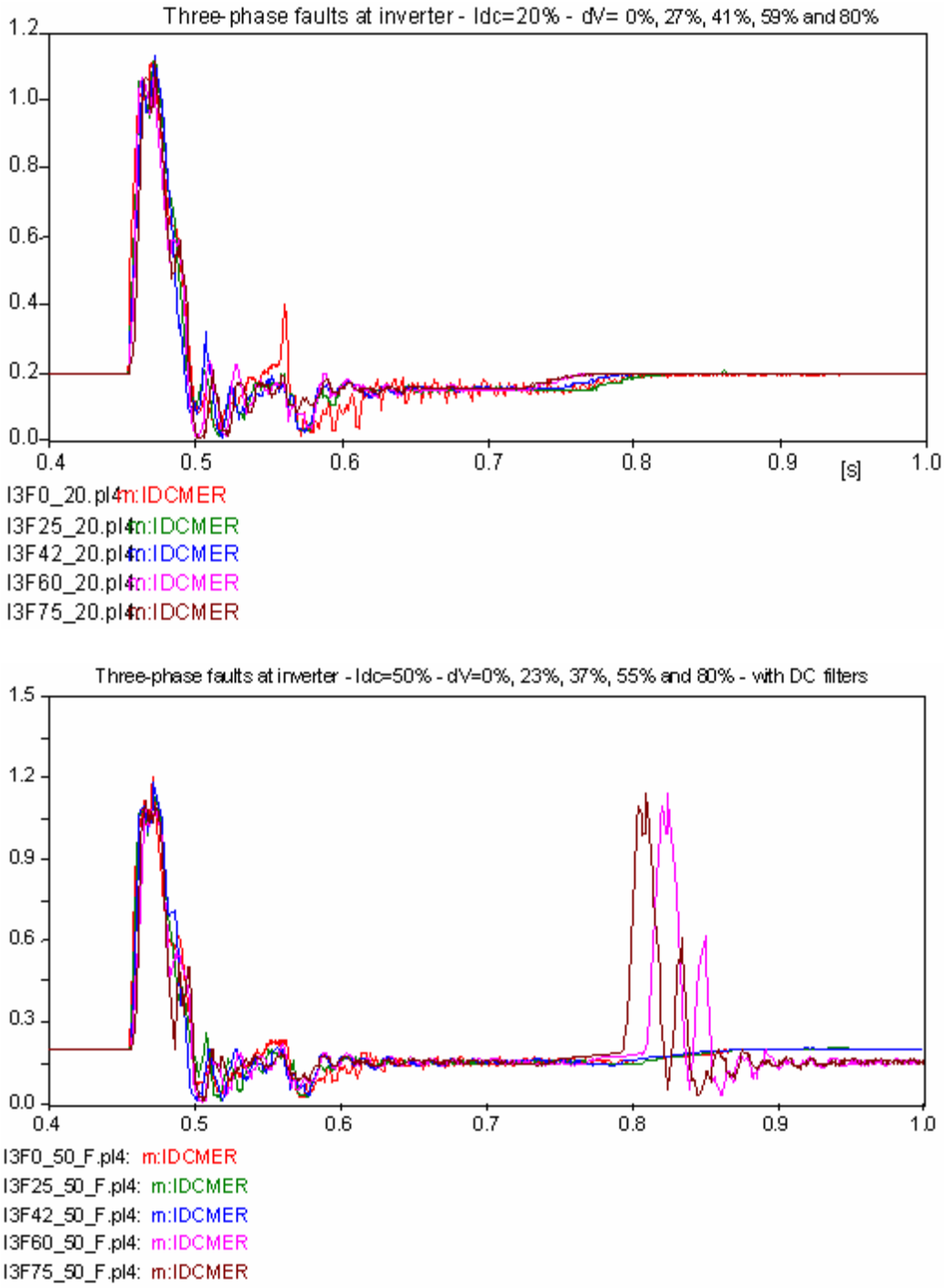


Figure F.12 – Three-phase faults at the inverter for Pdc = 0.2 pu – with and without DC filters

# ANNEX G - ELECTROMECHANICAL STABILITY STUDIES

## G.1 Comparison of the dynamic performance of the *Equivalent Network* and of the *Simplified Network,* employing the electromechanical stability program[1]

After the benchmark circuits were conceived, the focal point of the work was directed to the comparison of the dynamic response of the *Equivalent Network* to that of the *Simplified Network*. Although there was no concern to reach a full consistency between performances of the networks being analyzed – which would include the whole range of possible disturbances – it was attempted to preserve at least a minimum similarity for the less severe events, in order to avoid a significant discrepancy between results in case of an eventual migration, during the studies, from the *Simplified Network* to the *Equivalent Network*.

Before initiating the very comparison of performance between the networks, it should be kept in mind that the idea of a benchmark involves aspects that make performance tests of new HVDC/CCC converter projects feasible; for this reason, potential sources of problems should be preserved, in order to allow the evaluation of the capability of those projects to be able to overcome such problems. Under this focus, very diminished short-circuit ratios (SCR) were adopted, from the steady-state point of view. As for the dynamic aspects, a list of contingencies was identified, capable to be simulated in both networks, with increasing severity levels, in order to stimulate those sources of problems.

This way, at first a simulation was performed of a fast DC power reduction, down to half its steady-state value (*Case 1*), employing only the ANATEM electromechanical stability program, for the *Equivalent* and for the *Simplified Network*. The *Simplified Network* was simulated in that program with its machines represented by ideal constant voltage sources and, therefore, without associated dynamic representation. The *Equivalent Network*, however, was always studied with all its dynamics included.

[1] The CCC converters representation in the stability program (ANATEM) was based on the dc equations developed in Chapter 3 and control models made quite detailed, with closed loop primary loops also represented. This has certainly been quite helpful in assuring the similarity of results, but at a heavy computing cost: in most case time steps had to be substantially reduced to avoid imprecise simulation results.

### G.1.1 The Simplified Network with machines represented by ideal constant sources

Figure G.1 presents the voltages at buses of the rectifier AC network (buses #111 and #113) and of the inverter AC network (buses #11 and #26), of the *Equivalent* and of the *Simplified Network,* considering the simulation of a fast decrease of the power order down to 50%. The discrepancy between the two networks, in the dynamic behavior of the voltages, is clearly noticeable.

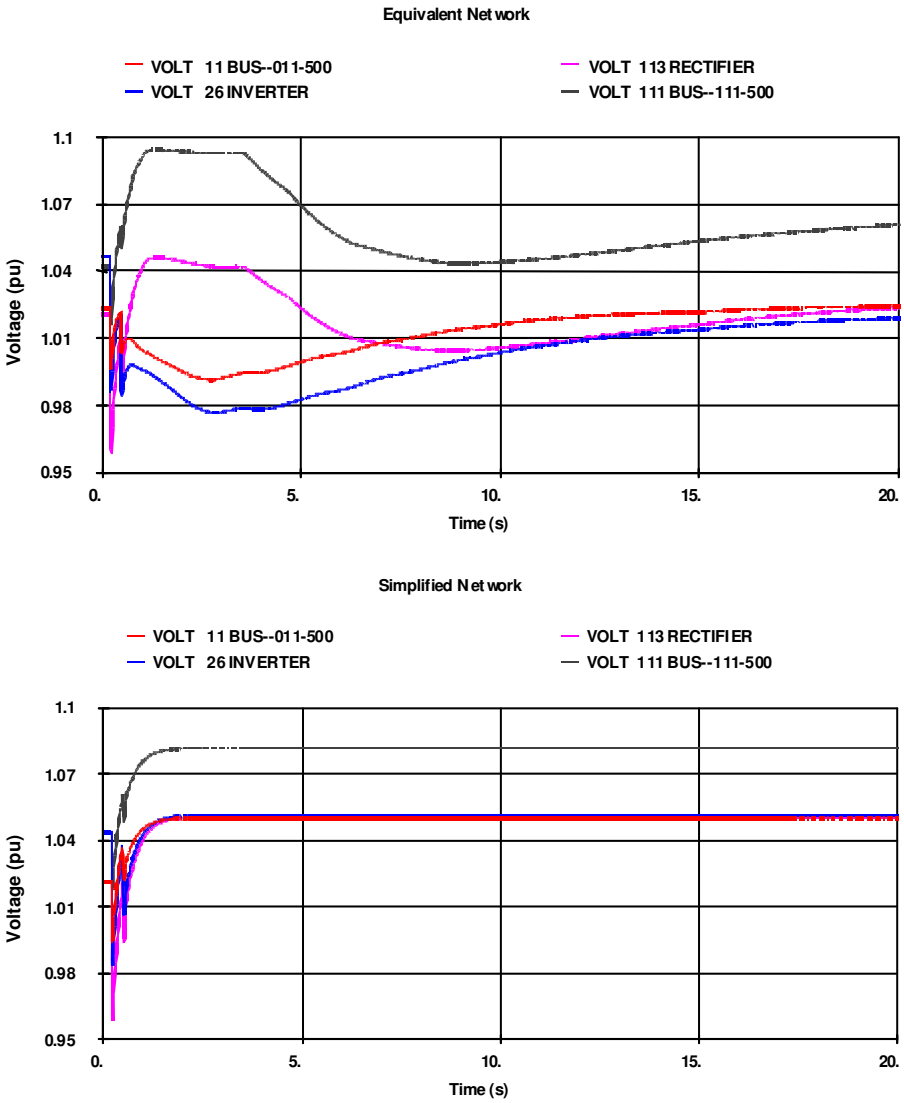


Figure G.1 – AC Voltages – Comparison between the *Equivalent Network* and the *Simplified Network (machines as infinite buses)*

### G.1.2 The Simplified Network with machines represented with equivalent dynamics

The discrepancy identified in the previous item (in dynamic behavior of the voltages, between the two networks) showed that it was necessary to improve the modeling of machines in the *Simplified Network*. Equivalent dynamics for its three generators were studied exhaustively, in order that the comparison with the results obtained from the *Equivalent Network* could present more consistency than what had been observed, considering the events previously defined.

Figure G.2 illustrates the results of the simulation of the 50% DC power reduction, including the dynamic representation of the equivalent machines. It is noted that the introduction of the machine equivalent models into the *Simplified Network* made voltages approach more closely the values obtained in the *Equivalent Network*. In addition, Figure G.2 (c) details the comparison between the two networks, in the simulation interval from 0 to 2 seconds.

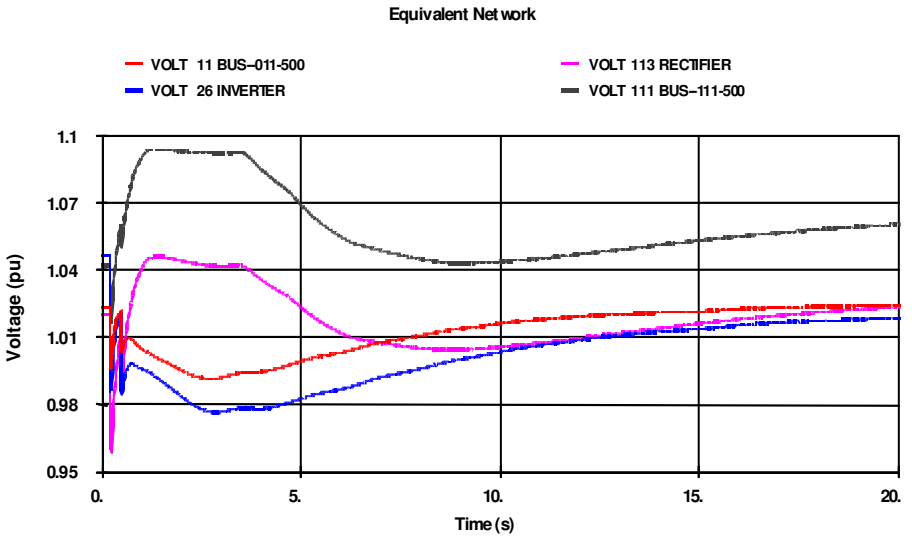


(a)

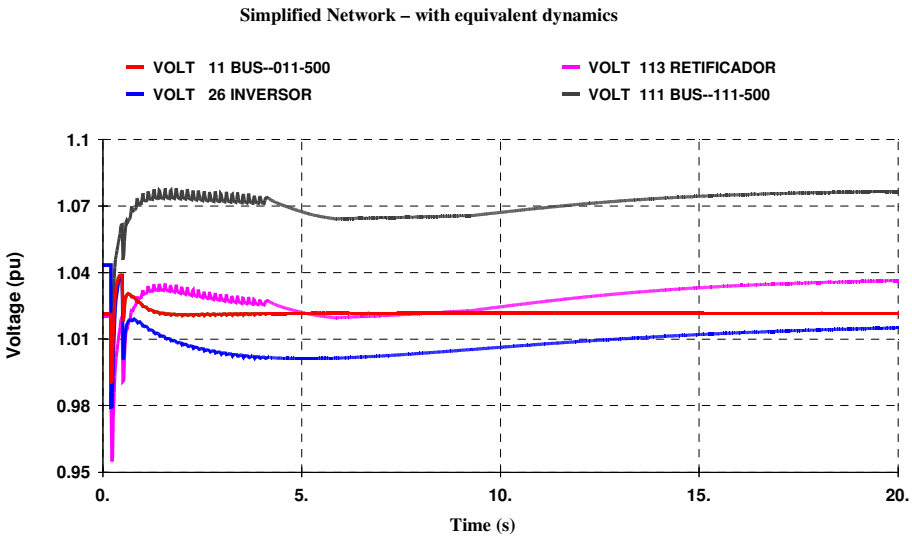


(b)

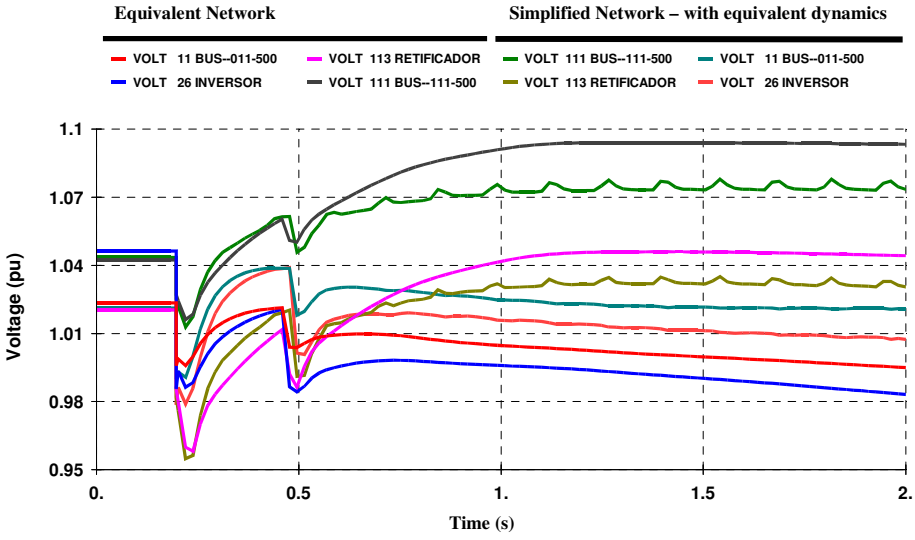


(c)

Figure G.2 – AC Voltages – Comparison between the *Equivalent* and the *Simplified Network.*
*(c) details the initial 2 seconds of (a) and (b).*

Tables H.12 to H.16 and Figures H.6 to H.8 present the equivalent dynamic models for the machines on the inverter and on the rectifier side of the *Simplified Network*, resulting from the evaluation performed. The remote voltage control at bus #11 of that AC network (see Figure 4.7 of Chapter 4) and the absence of PSS in the machine at the inverter side are underlined.

### G.1.3 Representation of commutation failures in electromechanical stability programs

Another fundamental point in adjusting the electromechanical stability programs is the representation of commutation failures in HVDC links. However, in order that the behavior may be reproduced in an adequate way in certain simulations, special procedures are required. It is important to observe that:

- Commutation failures are events of a probabilistic nature, and they may occur as a result of transient reductions in voltage magnitude, or of distortions in the waveform of AC voltage at the inverter terminal.
- Due to the limitations imposed by single-phase representation of the HVDC link in electromechanical stability programs, the algorithms that automatically represent a commutation failure in those programs are necessarily deterministic; they consider the occurrence of commutation failures when the magnitude of the AC voltage at the inverter side reaches values below a certain limit, or when the calculated value of the extinction angle gamma is lower than a preset reference value corresponding to a minimum extinction angle.
- In the specific case of the ANATEM program, the commutation failures occurring, at the instant when disturbances are applied to the AC network, may be represented automatically through the adjustment of parameters of a specific command (code DCFM). By means of this command, the commutation failure is automatically considered when the AC voltage drop reaches values below those of the parameter “Commutation failure voltage" (Vcf) or results in extinction angles below the value of the parameter “Commutation failure gamma angle” (Gfc). The commutation failure is simulated making DC voltage equal to zero for a preset time (Thd).
- In order to adjust these parameters, a sensitivity analysis is required, using tools for simulating electromagnetic transients with more precise three-phase models of the converter bridges, so as to verify from which AC voltage levels, or from which extinction angles, the commutation failure actually starts to occur, and which is its duration.
- For the hypothetical test systems in this work, the values employed in the present simulations were: Vcf = 0.50 pu; Gfc = 0 degrees, and Thd = 0.032 s. It is important to observe that these values apply to a CCC system and, in particular, to the system considered in this work.
- In addition to the automatic detection of commutation failures, it is also possible to cause a commutation failure at any desired instant, independent from the values of the AC voltage or of the extinction angle. In the ANATEM program, this may be done through the command APFC (application of commutation failures in AC-DC converters) of the DEVT execution code (event data). This makes possible to simulate, for instance, the dynamic consequences of faults in the firing circuits.
- In HVDC links employing the CCC configuration, commutation failures may also occur after fault clearing. The pronounced voltage unbalances upon the commutation capacitors – generated by the unbalanced currents derived from asymmetric faults – may originate commutation failures during the DC current recovery. On account of their algorithms being based on a single-phase representation of the system, electromechanical stability programs, such as ANATEM, cannot detect automatically this type of fault. In this case, it is necessary to verify the probability of fault occurrence for the specific faults to be studied, by means of analyses using electromagnetic transients programs, for a subsequent representation, through the APFC command, in simulations of electromechanical stability.

Figure G.3 shows an example where a commutation failure occurred at the instant of application of a single-phase solid fault at the inverter AC side (1), and another one after fault clearing (2), during recovery, in a simulation performed with ATP. In the simulation of the same event with the ANATEM program, the first commutation failure was automatically detected by the program, and the second one required to be forced through the APC command of the DEVT execution code.

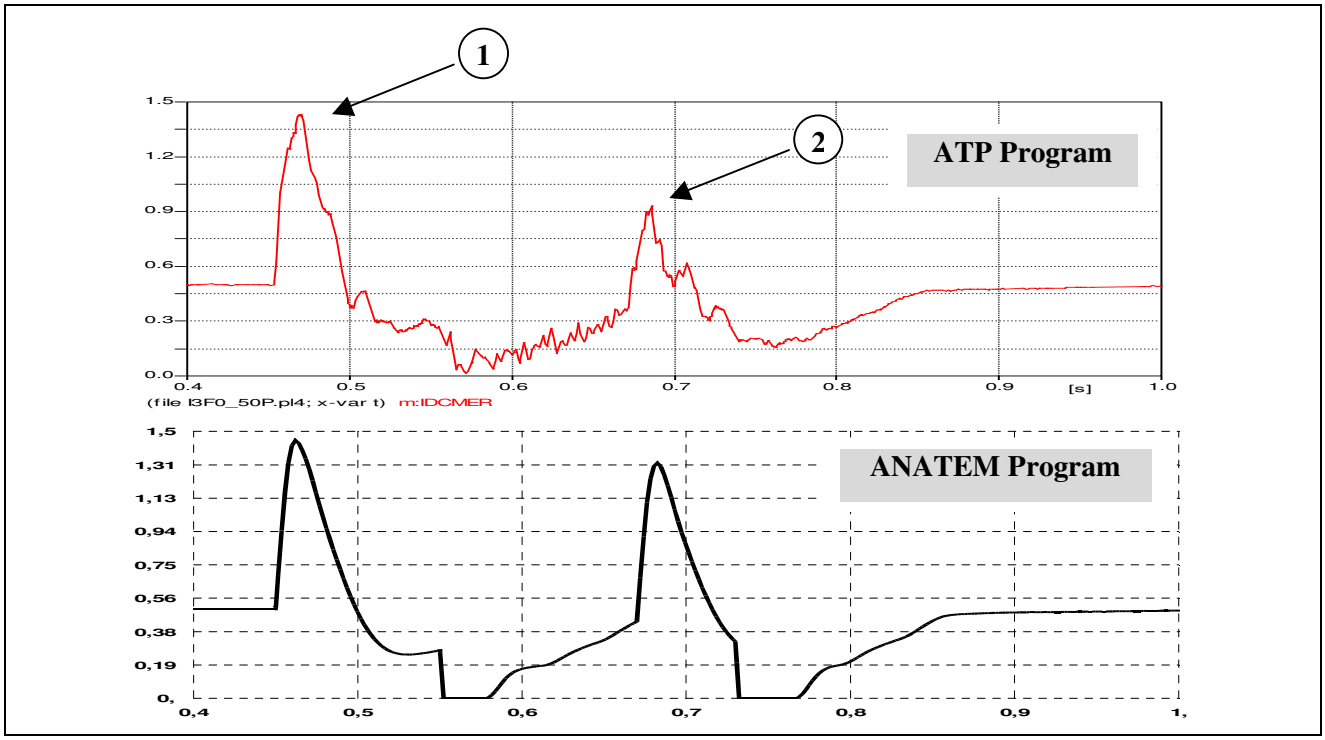


Figure G.3 - DC current variation – single-phase solid fault at the inverter.

### G.1.4 Fault Application

After equivalent dynamics were defined for the machines of the *Simplified Network*, based on Case 1 presented above – in which a fast reduction in the DC power order was simulated, with the purpose of evaluating the adequacy of this modeling for other disturbances – additional cases were simulated in sequence, involving the application of a three-phase solid fault, for 100 ms, to bus #11 of the inverter AC network, as summarized below.

- *Equivalent Network*: application of three-phase solid fault to bus #11 (inverter AC network), for 100ms, followed by:
  Case 2 - fault extinction (without topological alteration);
  Case 3 - circuit opening between buses #11 and #12;
  Case 4 - circuit opening between buses #11 and #12, and between buses #7 and #8.

- *Simplified Network*: application of three-phase solid fault to bus #11 (inverter AC network), for 100ms, followed by:
  Case 2- fault extinction (without topological alteration);
  Case 3- 20% impedance increase of the equivalent connected to bus #11, when fault is being cleared;
  Case 4- 20% impedance increase of the equivalent connected to bus #11, when fault is being cleared.

Some of these disturbances originate a reduction of the ESCR in the inverter AC network, when the fault is being cleared. Nevertheless, in terms of this reduction, the configurations resulting from such contingencies are equivalent, as summarized in Table G.1.

Table G.1 – Short-circuit ratios at the inverter commutation bus after fault clearing

| Case Description | | ESCR |
|---|---|---|
| 2 | Fault extinction (without topological alteration) | 1.28 |
| 3 | Circuit opening between buses #11 & #12, or<br>20% impedance increase of the equivalent | 1.13<br>1.07 |
| 4 | Circuit opening between buses #11 & #12, and #7 & #8, or<br>50% impedance increase of the equivalent | 0.99<br>0.95 |

The new features of the CCC converters main circuit, introduced by the series capacitors, provide them with an extremely favorable behavior when installed in AC systems having a very low ESCR. Table G.1 shows that Benchmark successful recovery from faults with an ESCR less than 1.0 after the clearing, is possible. Thus, it can be concluded that, as opposed to conventional arrangements, the CCC configuration is very robust, allowing, without commutation failures, considerably higher voltage drops at the converter bus on the occurrence of remote ac faults.

Before proceeding to the analysis of the results of these simulations – which are shown on Figures G.5 to G.13 – the control strategy adopted until then in the study should be pointed out. At first, Constant-Current Control in the HVDC link was chosen to be employed. In the cases presented next, where it was attempted to represent in more detail the link behavior, it was decided to adopt the Constant-Power Control, as being the strategy of wider use in the systems under commercial operation..

Figure G.4 presents the block diagram employed in the "Master Control". It was adopted a value of 300 ms for the time constant Tm, and of 0.95 pu and 1.05 pu, respectively, for the lower (Vmin) and upper (Vmax) limits.

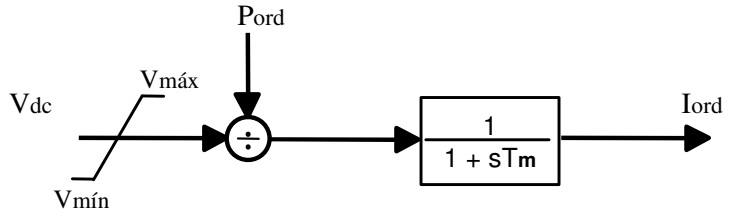


Figure G.4 – Block Diagram of the HVDC link Power Control

*Case 2 - Application of three-phase solid fault to bus #11, for 100ms, followed by its extinction*

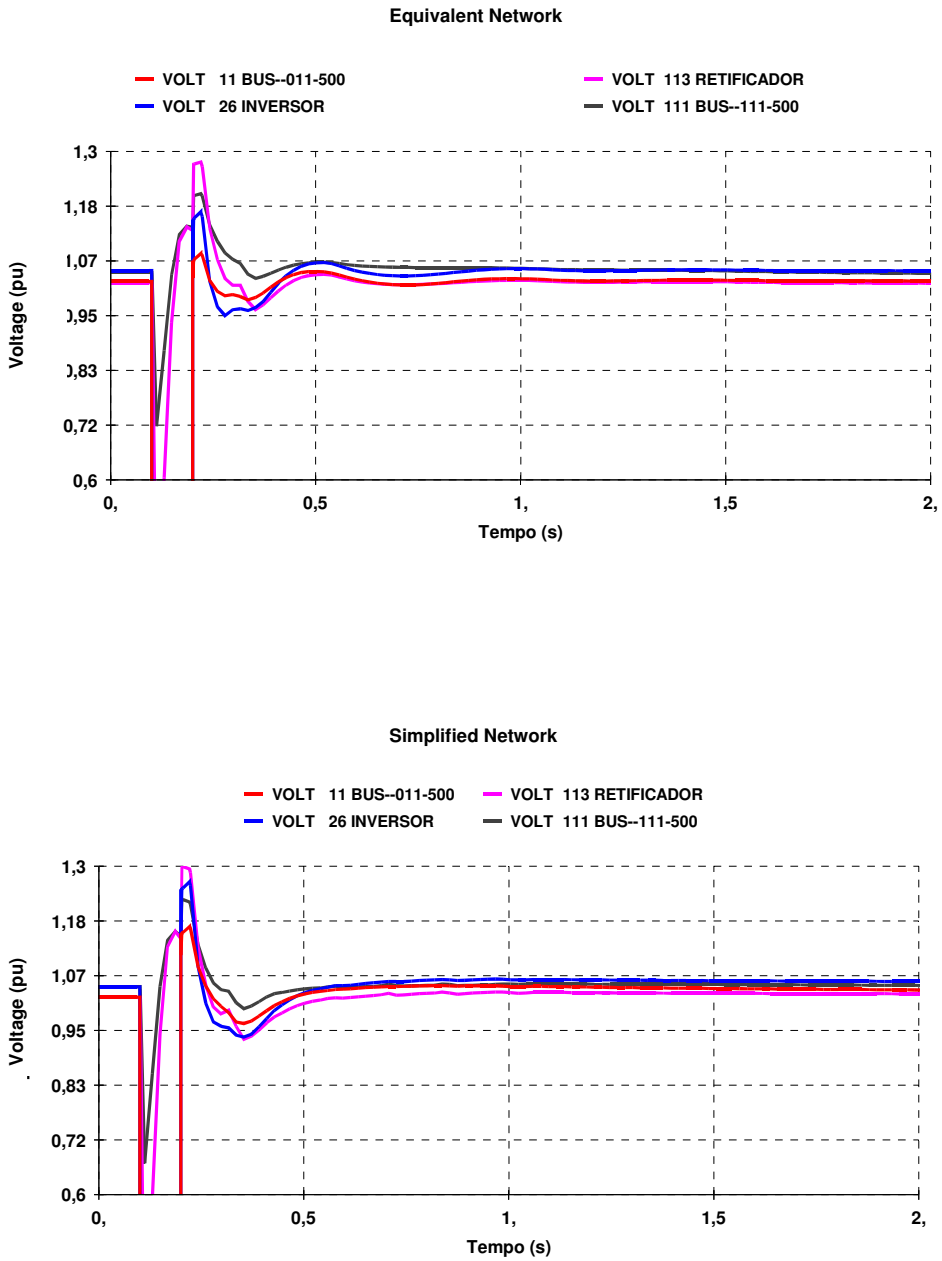


Figure G.5 – AC voltages - *Equivalent Network* and *Simplified Network*

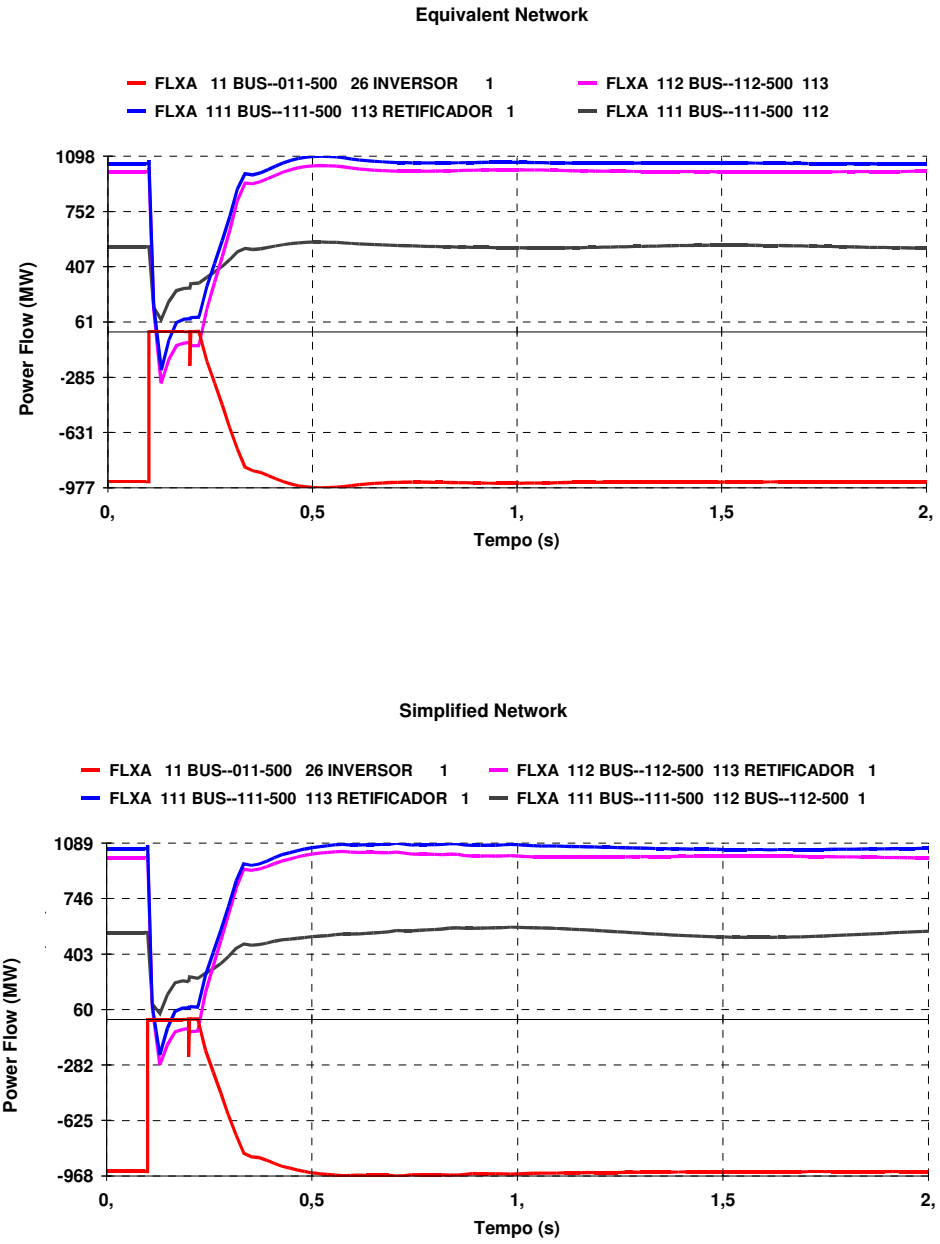


Figure G.6 – Power flow in the main AC transmission lines –
*Equivalent Network* and *Simplified Network*

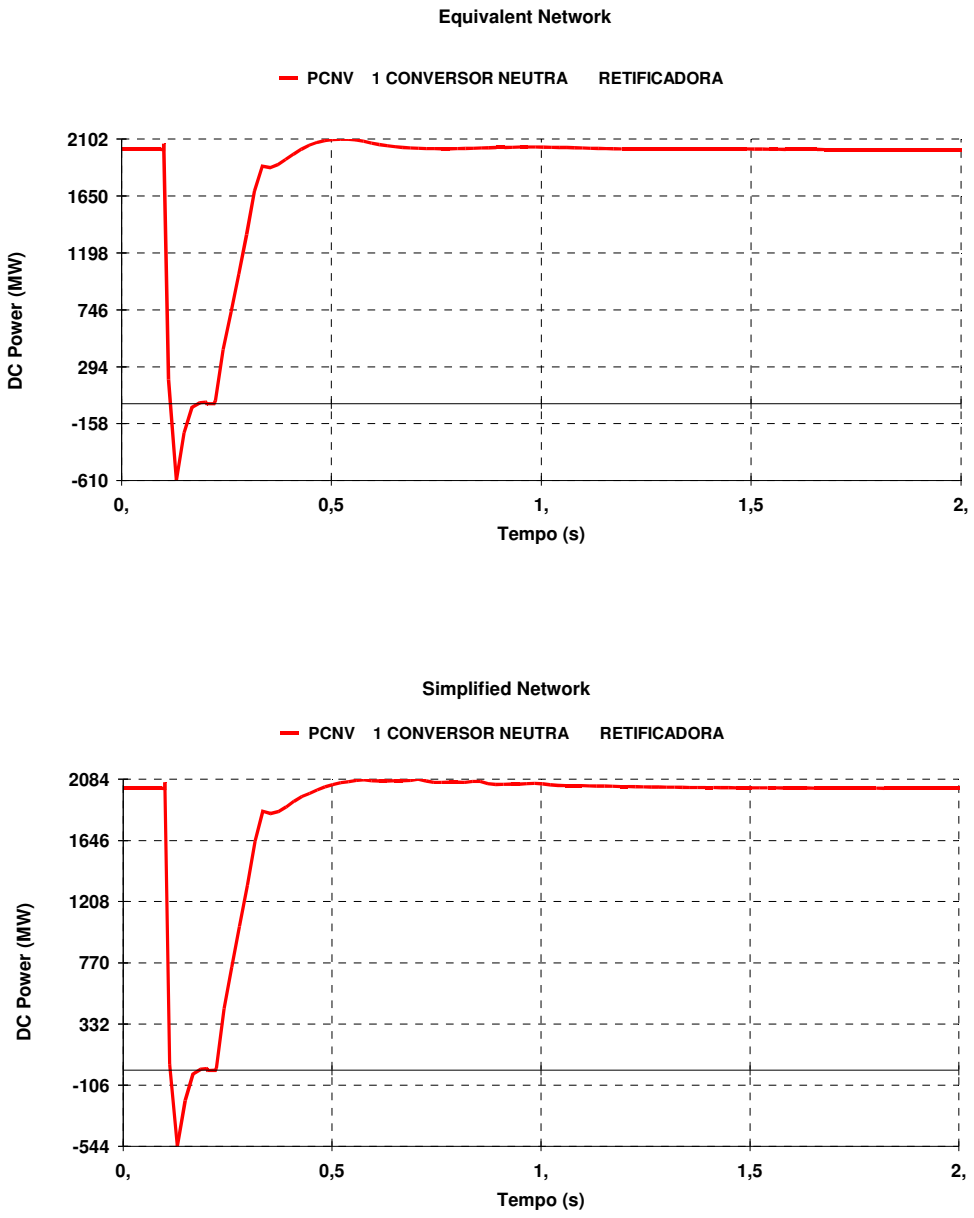


Figure G.7 – DC Power in the rectifier
*Equivalent Network* and *Simplified Network*

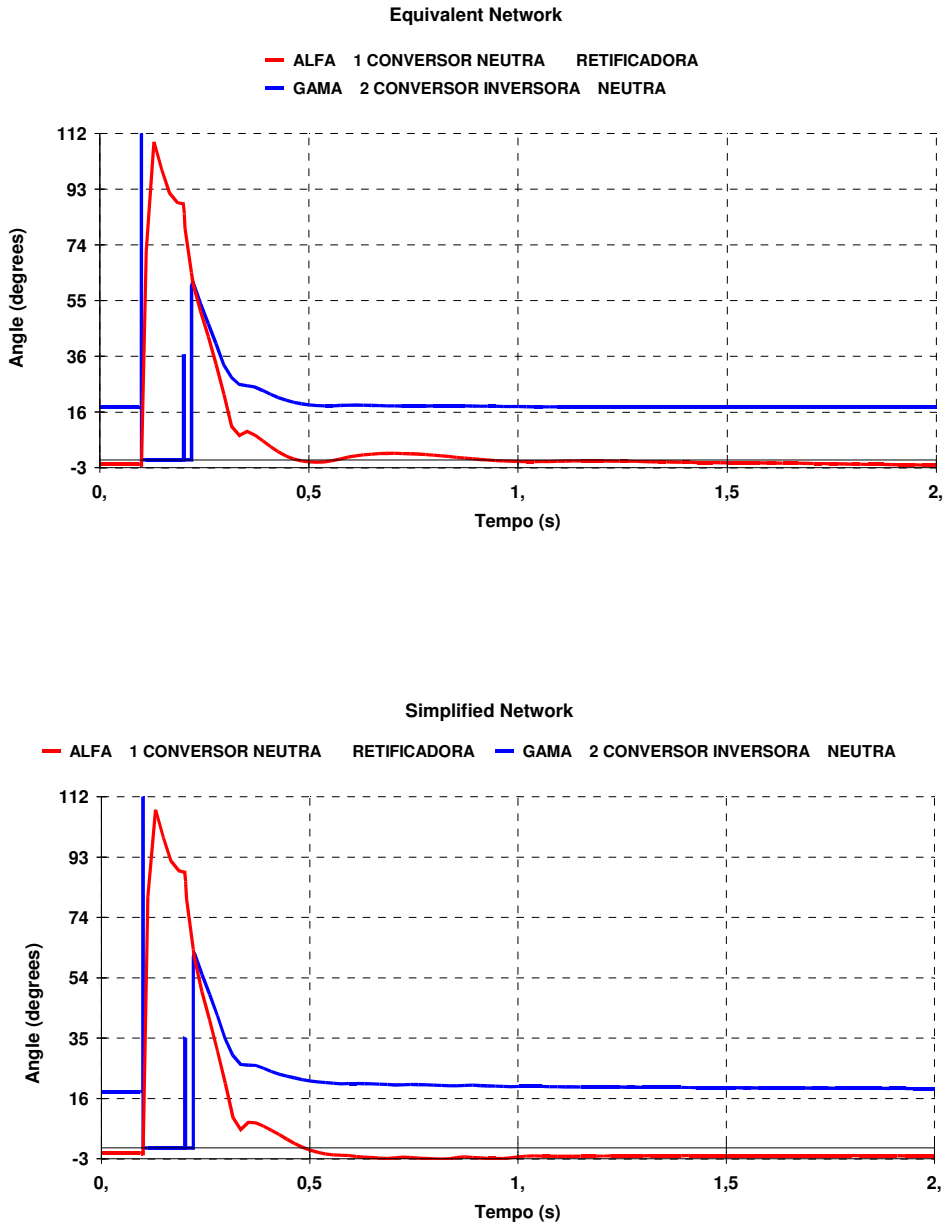


Figure G.8 – Firing angles (rectifier) and extinction angles (inverter)
*Equivalent Network* and *Simplified Network*

*Case 3- Application of three-phase solid fault to bus #11, for 100ms, followed by :*
*circuit opening between buses #11 and #12* *(Equivalent Network)*
*20% impedance increase of the equivalent connected to bus #11* *(Simplified Network)*

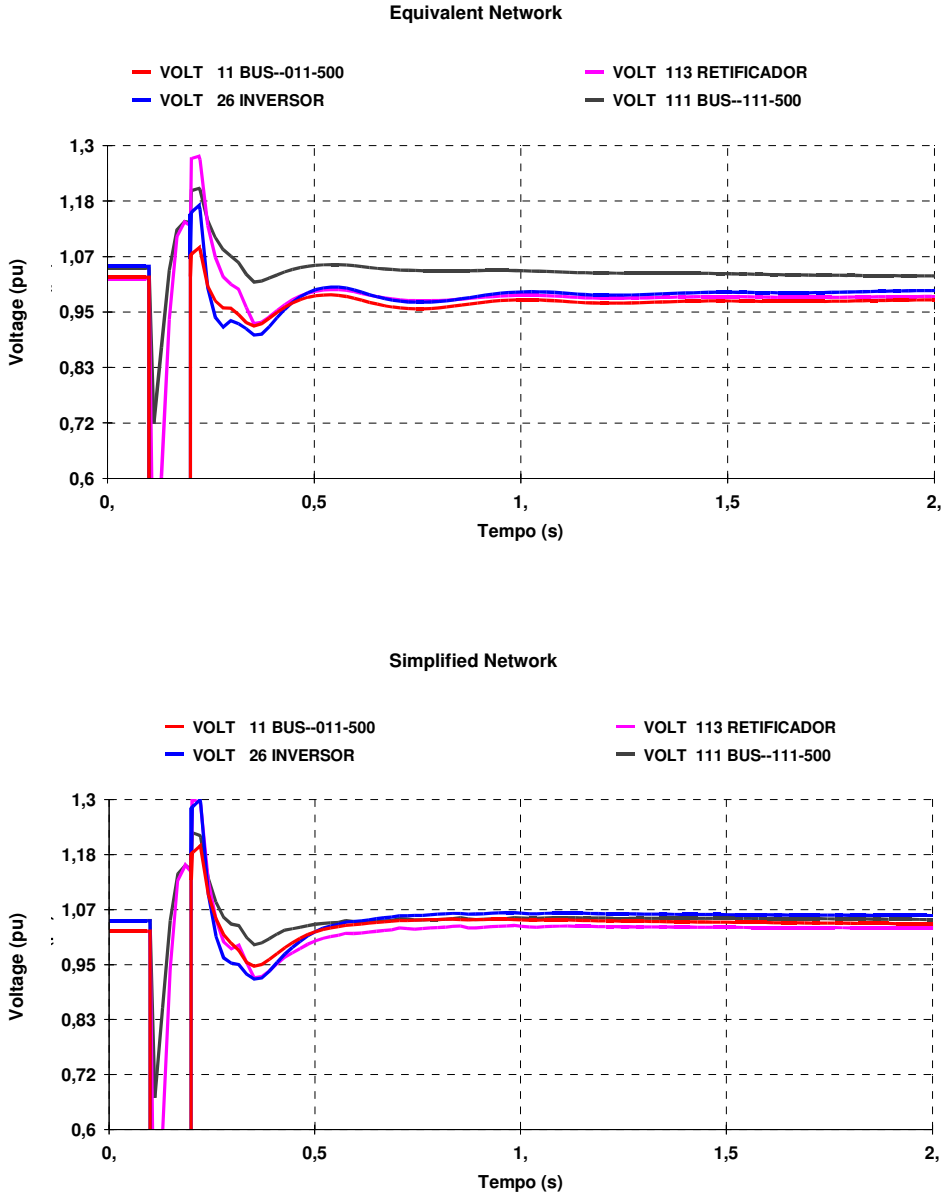


Figure G.9 – AC Voltages - *Equivalent Network* and *Simplified Network*

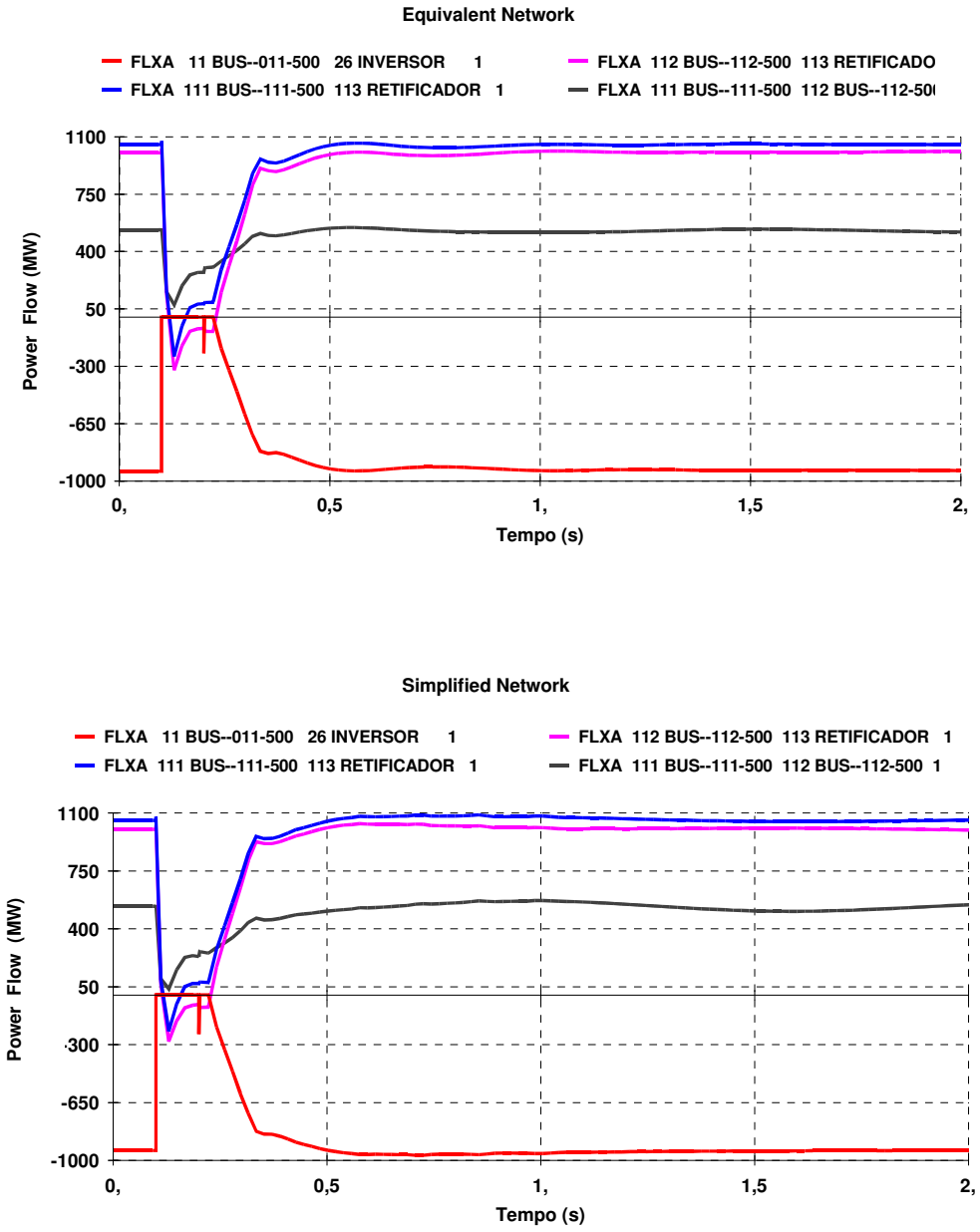


Figure G.10 – Power Flow in main AC transmission lines –
*Equivalent Network* and *Simplified Network*

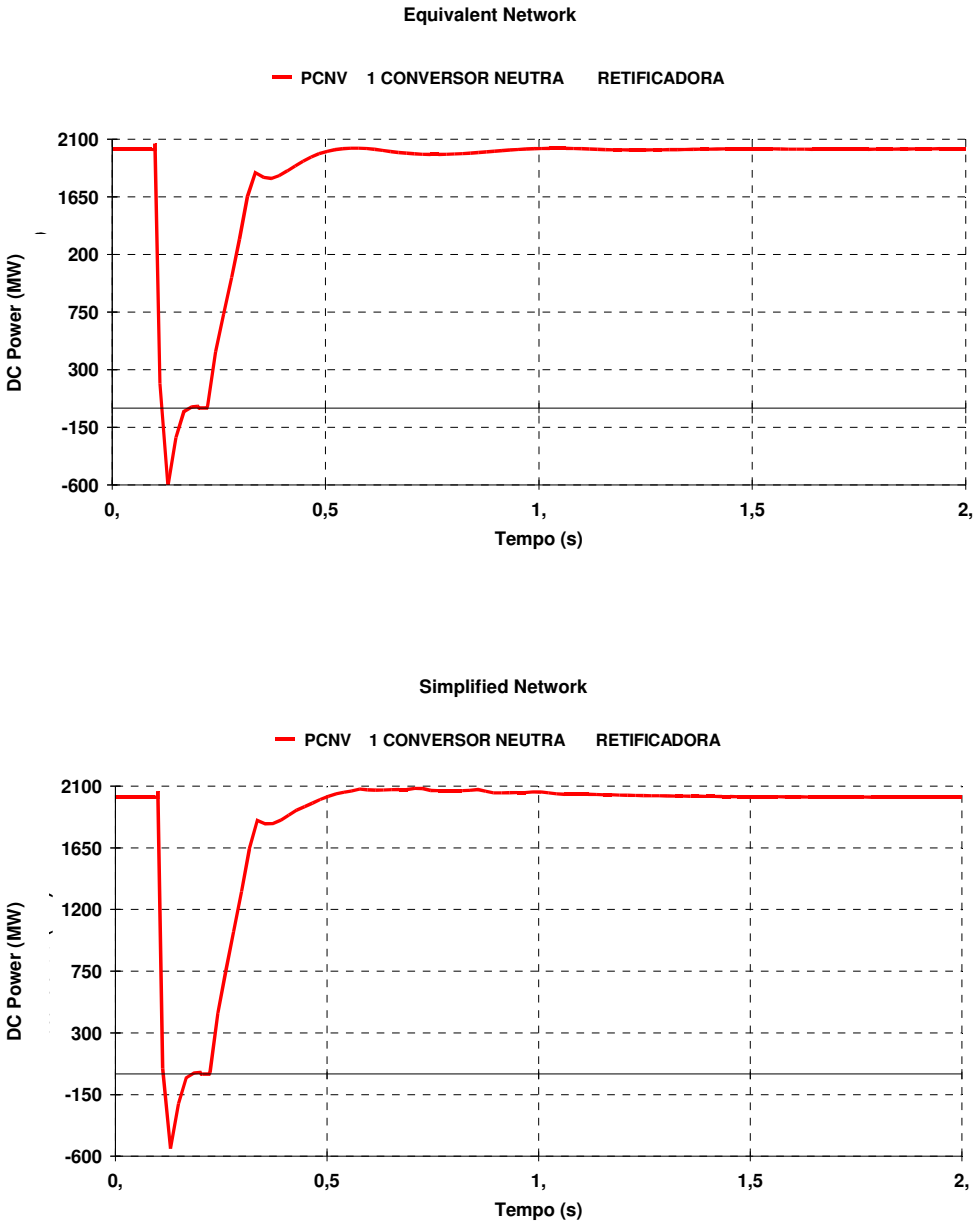


Figure G.11 – DC Power in rectifier
*Equivalent Network* and *Simplified Network*

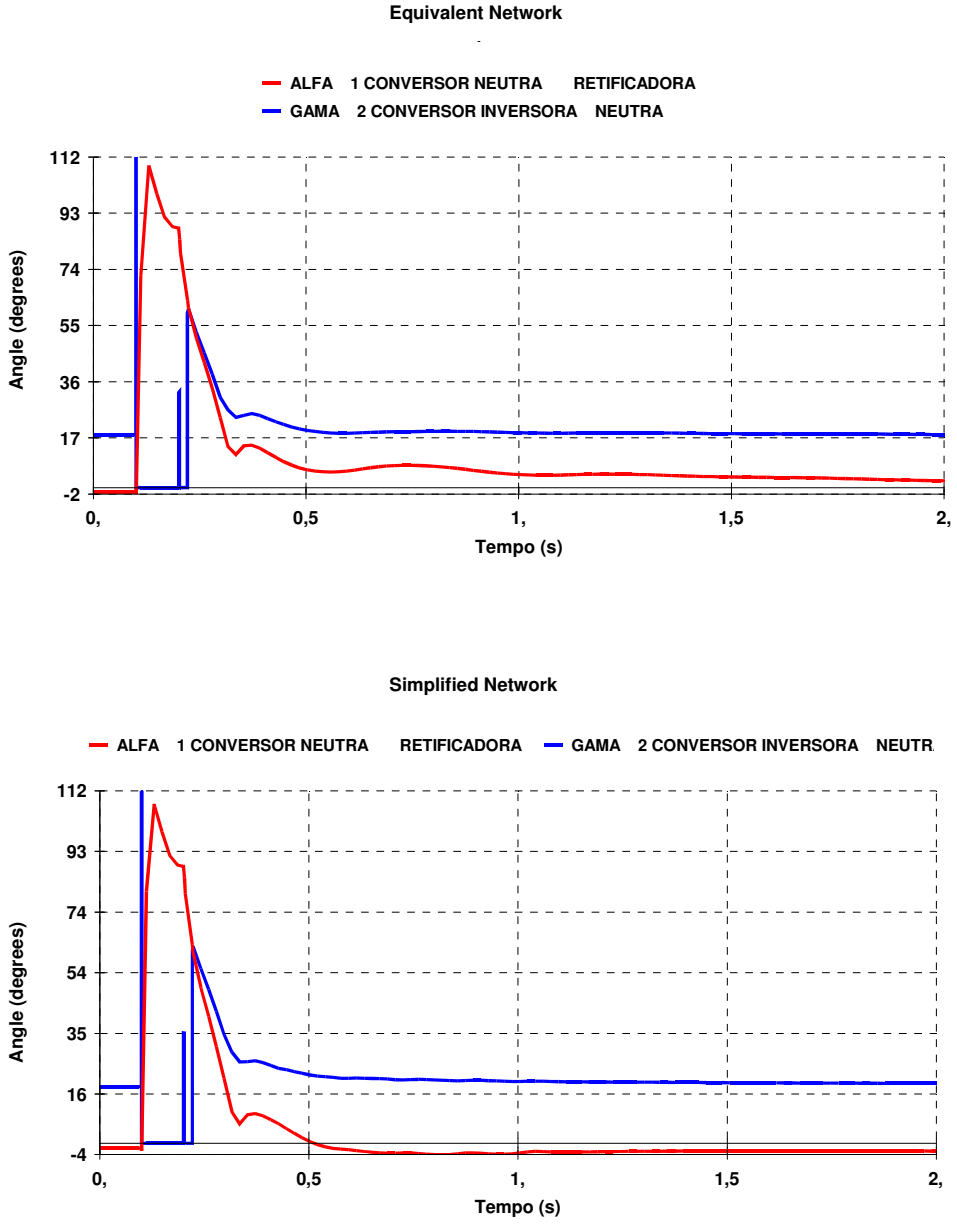


Figure G.12 – Firing angles (rectifier) and extinction angles (inverter)
*Equivalent Network* and *Simplified Network*

*Case 4- Application of three-phase solid short-circuit to bus #11, for 100ms, followed by:*
*circuit opening between buses #11 & #12, and #7 & #8* *(Equivalent Network)*
*50% impedance increase of the equivalent connected to bus #11* *(Simplified Network)*

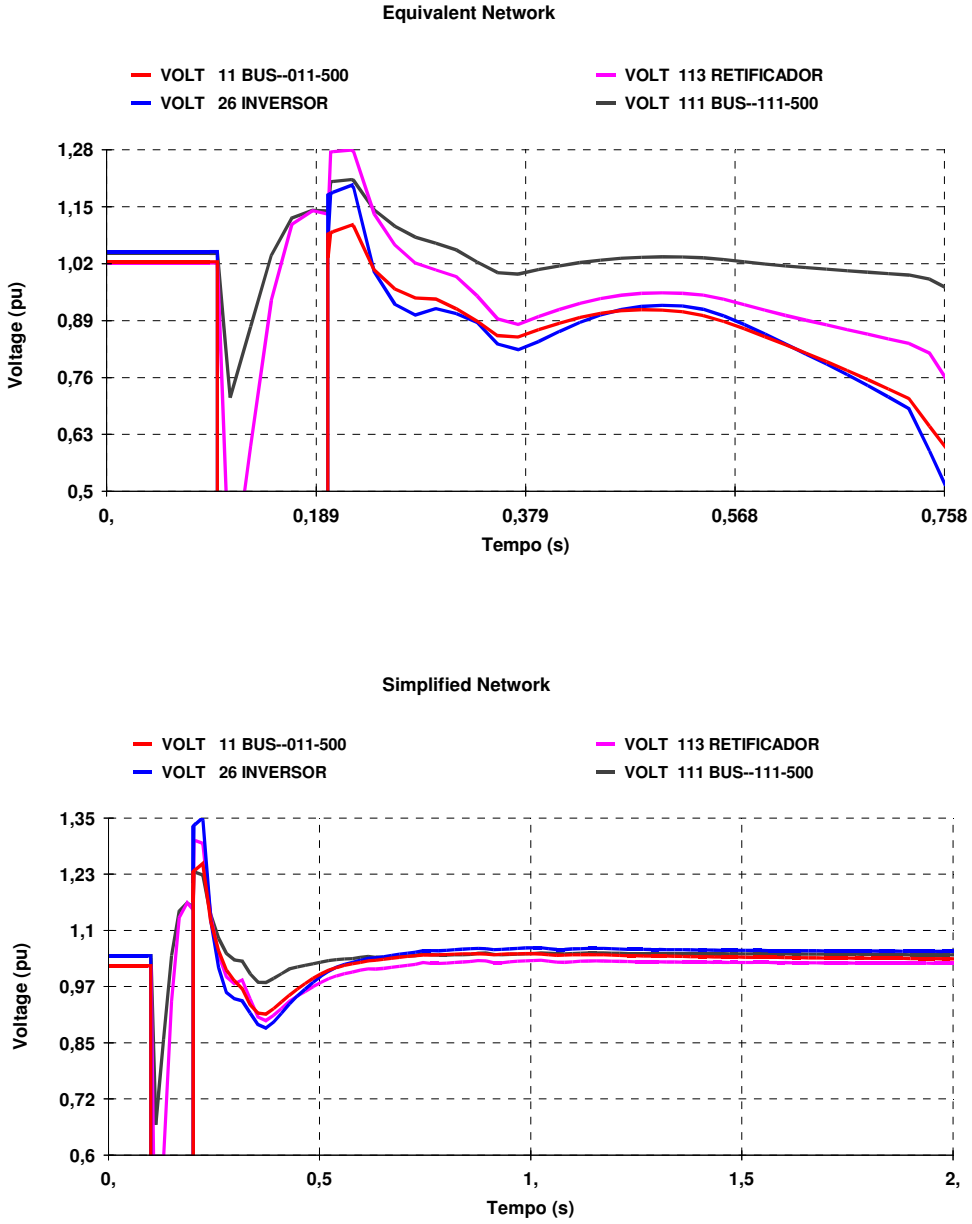


Figure G.13 – AC Voltages - *Equivalent Network* and *Simplified Network* - *(Vcf=0.5)*

For *Cases 2 and 3* a quite reasonable consistency is verified in the *Networks* behavior, for the quantities pointed out. Obviously, as some simplifications are involved, a few small differences may be observed. However, it may be noted the preservation of the main oscillation modes, with quite similar damping degrees. In *Case 4*, as it contemplates a more critical situation, such consistency was not verified. For the *Equivalent Network,* a collapse in the inverter voltage was verified, accompanied by commutation failures, whereas the *Simplified Network* presented system recovery after the disturbance.

Proceeding to a sensitivity analysis regarding parameter Vcf (*Commutation failure voltage* – see item G.1.3), when its value is changed to 0.30 pu – i.e., when the voltage above which commutation failures would occur is reduced – the *Equivalent Network* continues to present a significant reduction of the AC voltage, as it may be seen in Figure G.14. It is discerned, however, that it has been possible to avoid the occurrence of commutation failures, as a consequence of the voltage not having attained this new adjusted value (they occurred for Vcf = 0.5 pu).

On the other hand, a pronounced beat occurs, coinciding with the operation of the VDCOL, as it may be seen in Figures G.15 and G.16. This phenomenon may be explained as follows: after the DC power recovery (Figure G.17), AC voltage started to decrease, until it reached the value for VDCOL actuation which, in its turn, reduced the current order and, in consequence, the DC power. This made possible a recovery of the AC voltage, causing the VDCOL to return the current order to its initial value, increasing DC power, and so on, until the system managed to re-establish the operating conditions allowing reception of the initial power amount.

Even though the system had recovered, as mentioned above, a very impaired behavior is noted, which would not be acceptable under real conditions. Additional measures would evidently be required, in order to achieve a satisfactory dynamic performance and to make the rest of the system adequate for the new operating conditions. Other control adjustments could be tested, or even the adoption of a run-back procedure, reducing the DC power to be dispatched.

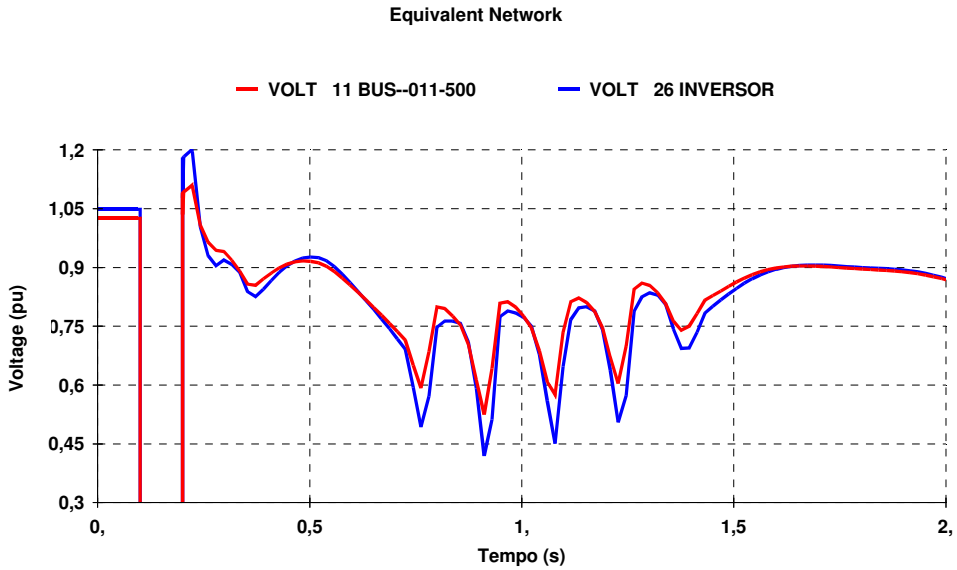


Figure G.14 – AC Voltages - *Equivalent Network - (Vcf=0.3)*

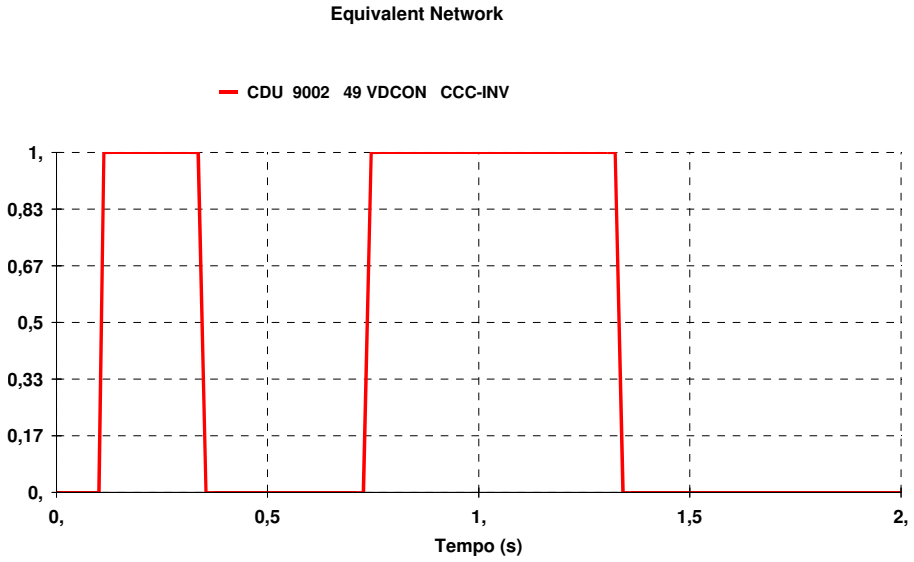


Figure G.15 – VDCOL actuation - *Equivalent Network - (Vcf=0.3)*

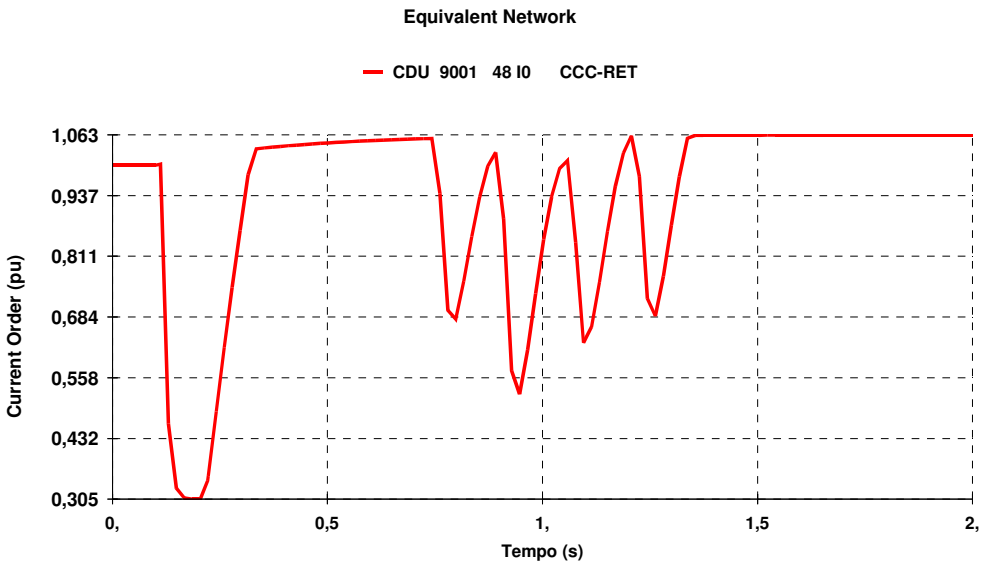


Figure G.16 –Current order of VDCOL - *Equivalent Network - (Vcf=0.3)*

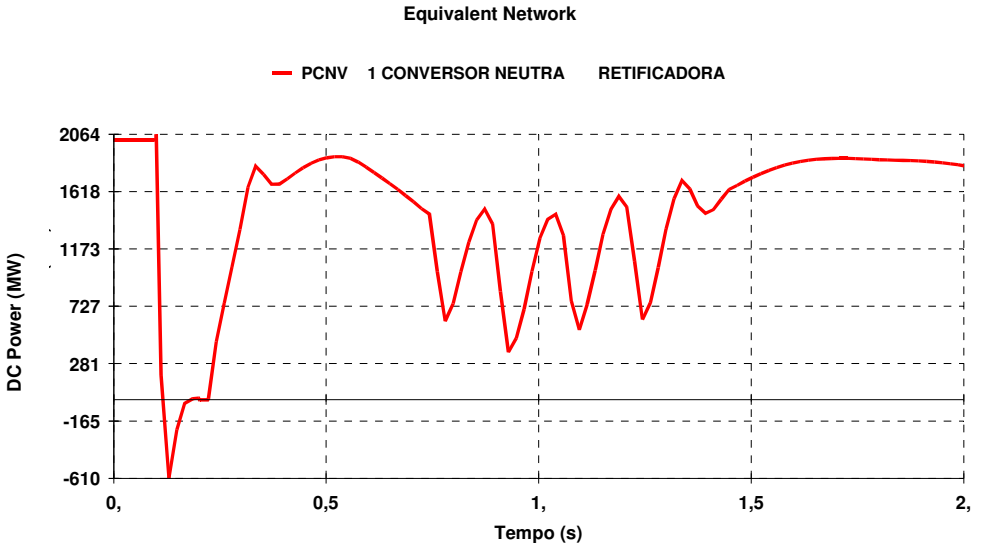


Figure G.17 – DC Power - *Equivalent Network - (Vcf=0.3)*

## G.2 Preliminary comparison of performance considering ANATEM and ATP programs

As presented above in item G.1, simulations with the ANATEM electromechanical stability program were initially performed, and the dynamic behaviors of the *Equivalent* and of the *Simplified Network* were compared. Hence it was found necessary to incorporate an equivalent dynamics into the machines of the latter network, in order that it should present a dynamic behavior consistent with that of the *Equivalent Network*.

In the programs aiming to study electromagnetic transients, the representation of all the system elements is detailed much further (among other features, the firing of each valve is specified, so as to make possible the representation of all the phase currents and voltages). Thus, it becomes possible to obtain a more representative and reliable behavior of the DC link by employing programs of the EMTP type, for the study of the more critical operating conditions, such as the recovery after faults, the sudden changes in the current or power orders, the border conditions where the risk of commutation failure inception appears etc. This way, a fundamental step for the validation of CCC link models developed for electromechanical stability programs – given the simplifications inherent to these tools (greater time constants, slow dynamics, single-phase single-line topology etc.) – is the utilization of simulations in electromagnetic transients programs.

For such validation, the *Simplified Network*, modeled in the ANATEM and ATP programs, was employed. At first, as a simplification, the machines were represented by infinite buses in both programs. Then, the equivalent dynamics of the machines in that network was considered, in both programs, on the basis of the model obtained in item G.1.

Figure G.18 shows the single-line diagram employed in the ATP program, comprising the configuration of the *Simplified Network* and the DC Network, where the presence of DC and AC filters and the AC circuits shunt reactors is underlined. The same configuration was used in the ANATEM program.

Simulations of disturbances in the system were made, for the evaluation of the HVDC/CCC link behavior, including the application of:

- Three-phase solid short-circuit at the rectifier side AC bus;
- Single-phase solid short-circuit at the rectifier side AC bus;
- Single-phase short-circuit, with V=59%, at the rectifier side AC bus;
- Three-phase solid short-circuit at the inverter side AC bus;
- Single-phase solid short-circuit at the inverter side AC bus;
- Single-phase short-circuit, with V=60%, at the inverter side AC bus;
- Single-phase short-circuit, with V=75%, at the inverter side AC bus.

The results of these simulations are shown from Figure G.19 onwards; it should be pointed out that:

- Without the representation of machine dynamics, the performance of the control for the HVDC/CCC link represented in the ANATEM program was, in general, quite close to that in the ATP program, for the majority of the events considered.
- In the simulations of single-phase solid short-circuit at the inverter, a difference was verified between the simulations with ATP and with ANATEM, of about 50 ms, in the time during which the HVDC/CCC link remains at zero power, as it may be seen in Figures G.19 and G.20, respectively. This difference is due to the additional control action introduced into the CCC link model for ATP, in order to reduce the influence of voltage unbalances upon the series capacitors in case of unbalanced faults, and to eliminate, or to reduce, the incidence of commutation failures during power recovery.
- In specific programs for the study of electromechanical stability, such as ANATEM, it is not possible to represent such additional control action based on voltage unbalance upon the capacitors, but it is possible to delay the CCC link recovery through the events command, by increasing the time during which the link remains at zero power, and correcting this difference for the specific type of fault. It should be pointed out, however, that such 50 ms difference should not affect significantly the results of analyses of electromechanical stability among AC system generators.

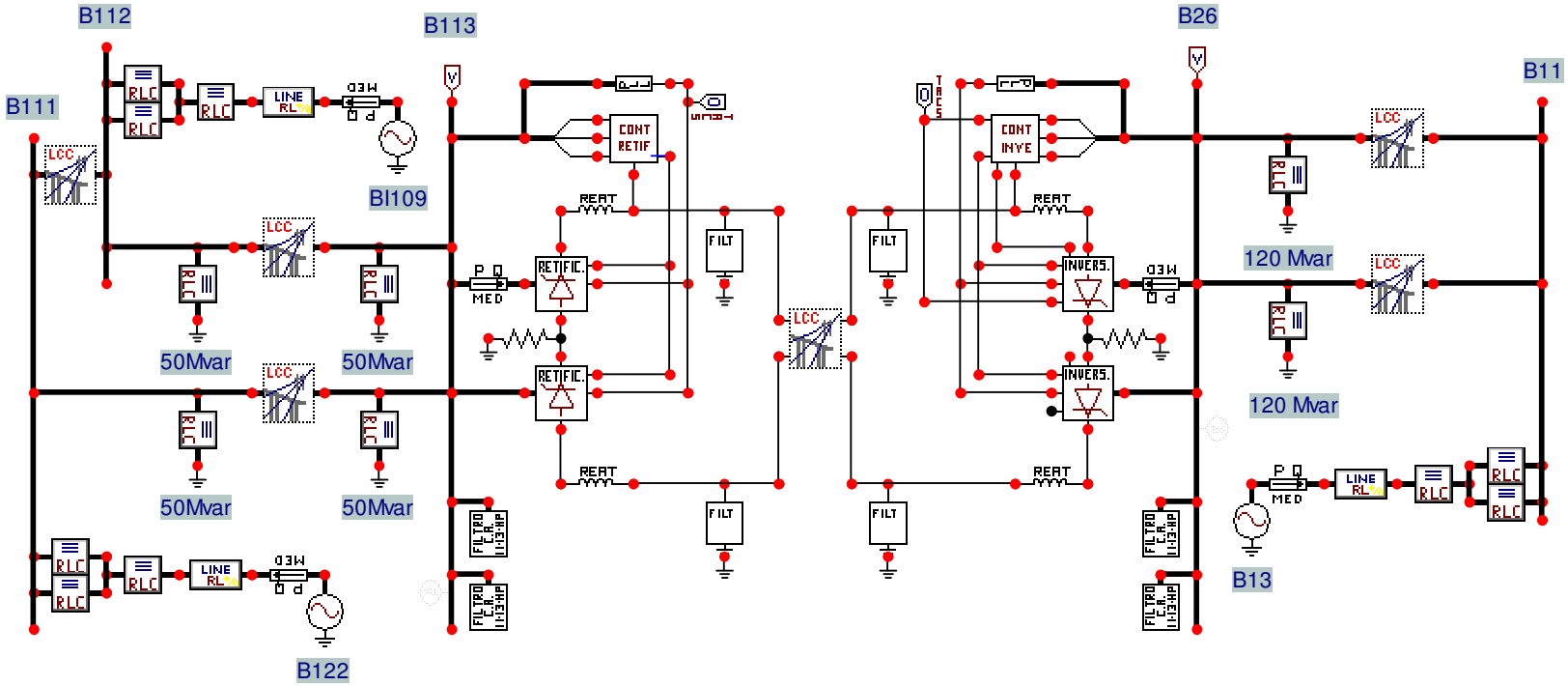


Figure G.18 – *Simplified Network* and DC Network – Model for ATP Program

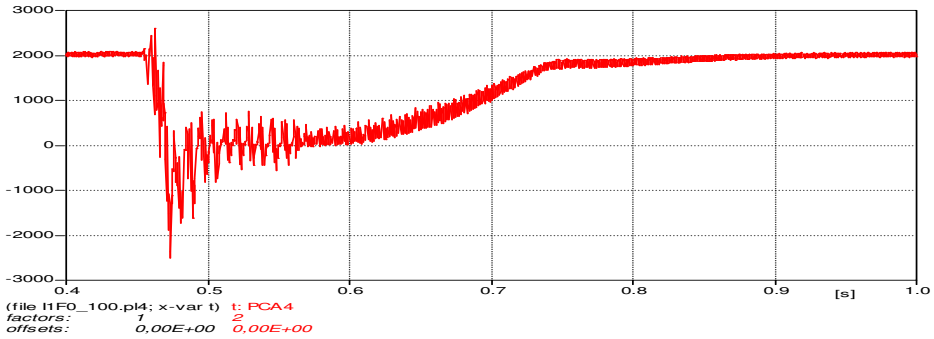


Figure G.19 - ATP - Variation of DC power – single-phase solid fault at the inverter

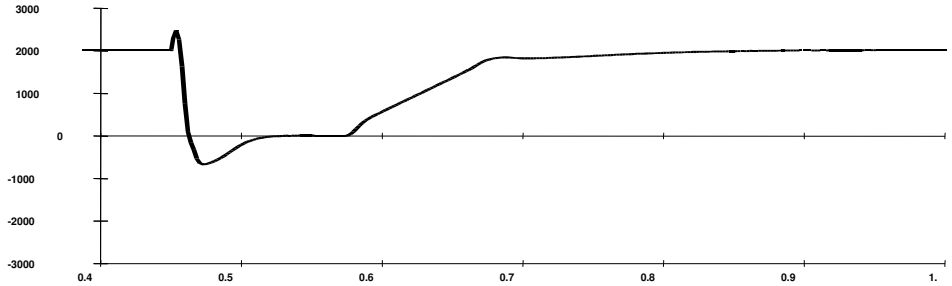


Figure G.20 - ANATEM - Variation of DC power – single-phase solid fault at the inverter

## Three-phase solid short-circuit at the rectifier AC bus

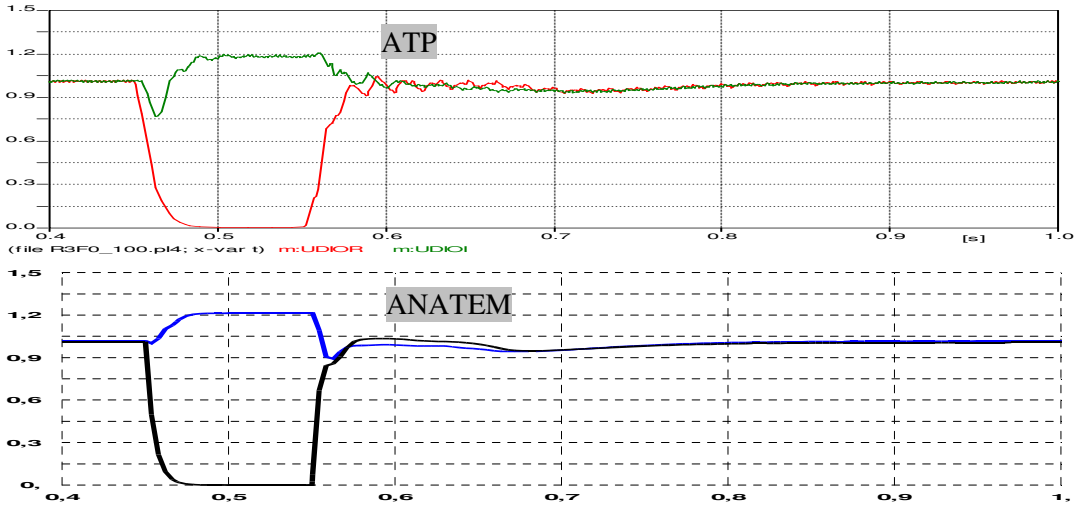


Figure G.21 - Udi0 voltages at rectifier and at inverter (pu)

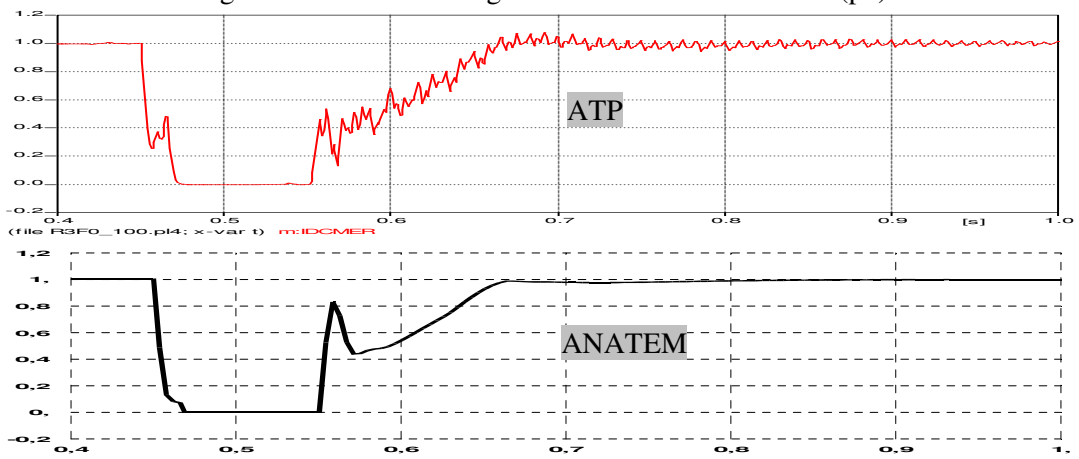


Figure G.22 - DC current (pu)

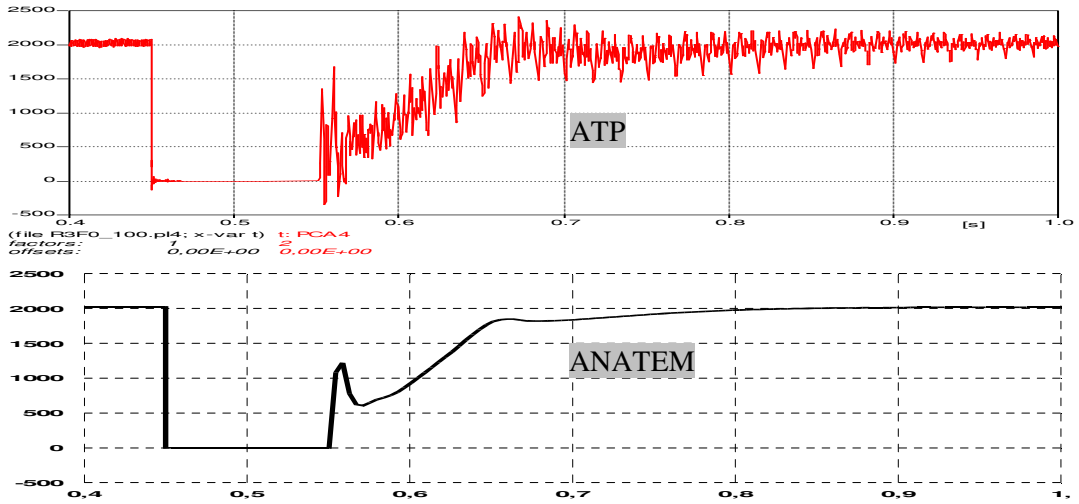


Figure G.23 - Inverter total Pcc (MW)

## Single-phase solid short-circuit at the rectifier AC bus

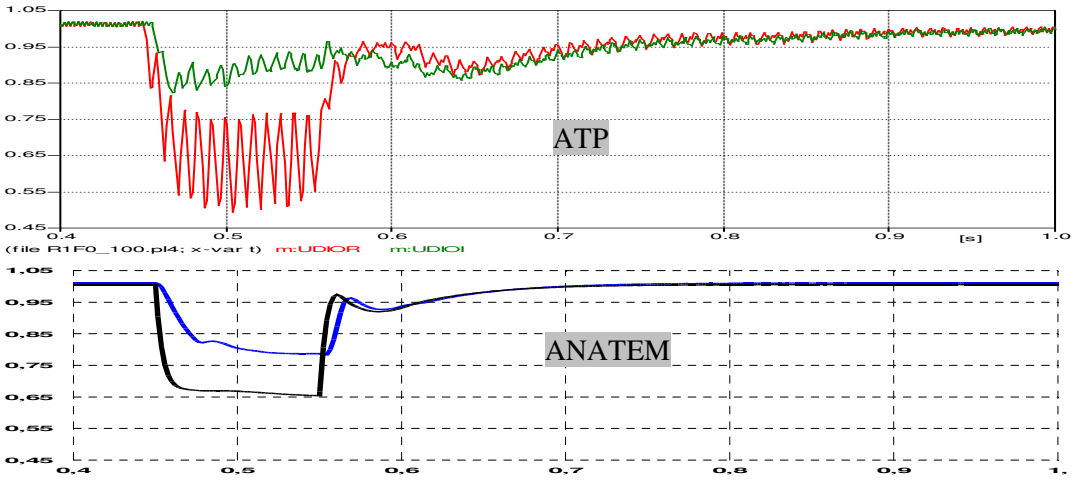


Figure G.24 - Udi0 voltages at rectifier and at inverter (pu)

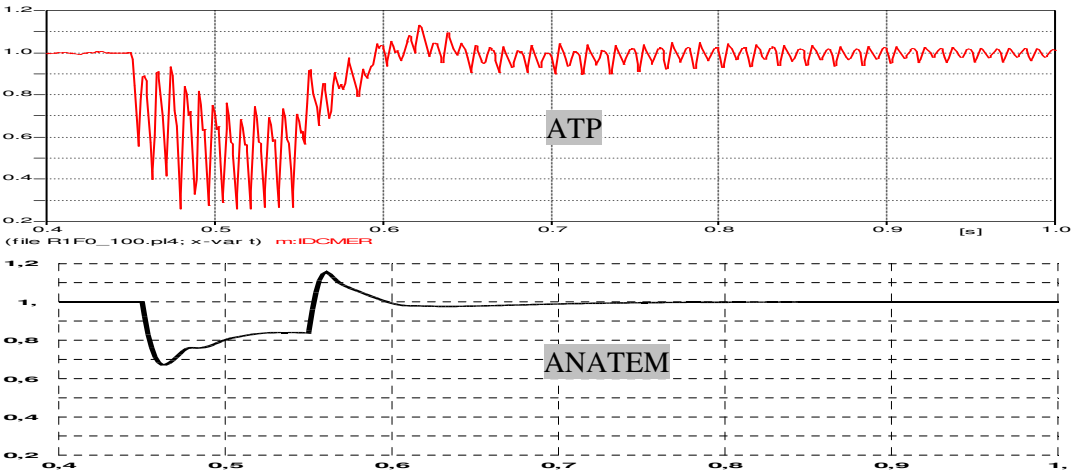


Figure G.25 - DC current (pu)

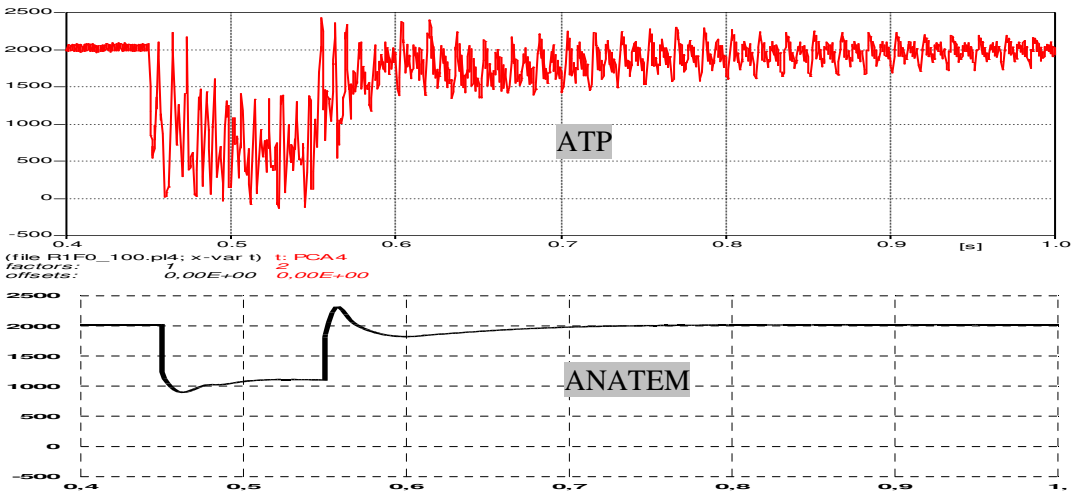


Figure G.26 - Inverter total Pcc (MW)

## Single-phase short-circuit, VAC=59%, at the rectifier side

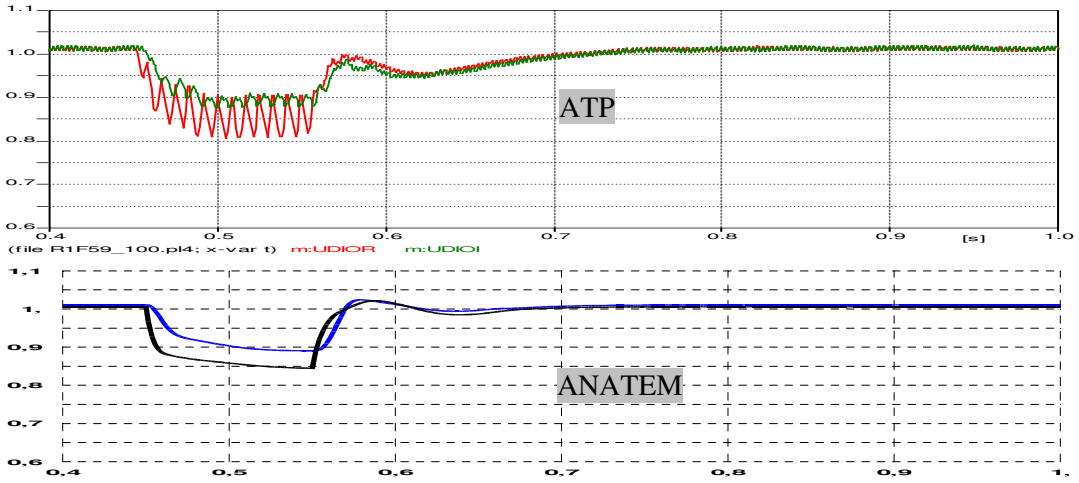


Figure G.27 - Udi0 voltages at rectifier and at inverter (pu)

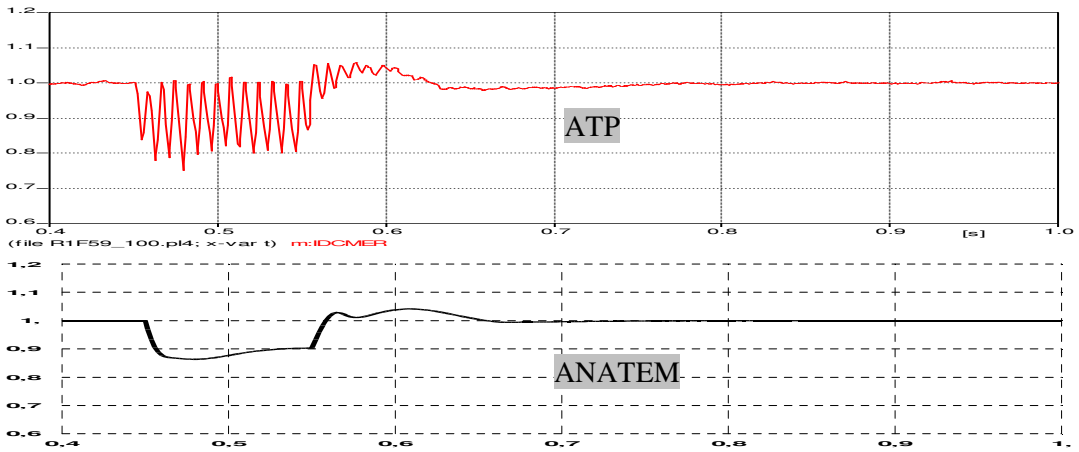


Figure G.28 - DC current (pu)

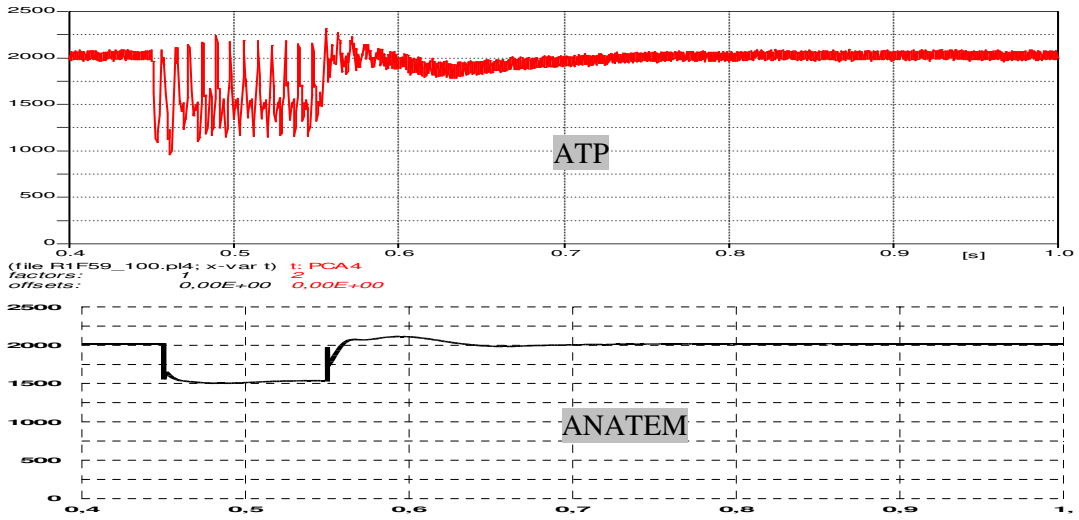


Figure G.29 - Inverter total Pcc (MW)

## Three-phase solid short-circuit at the inverter side

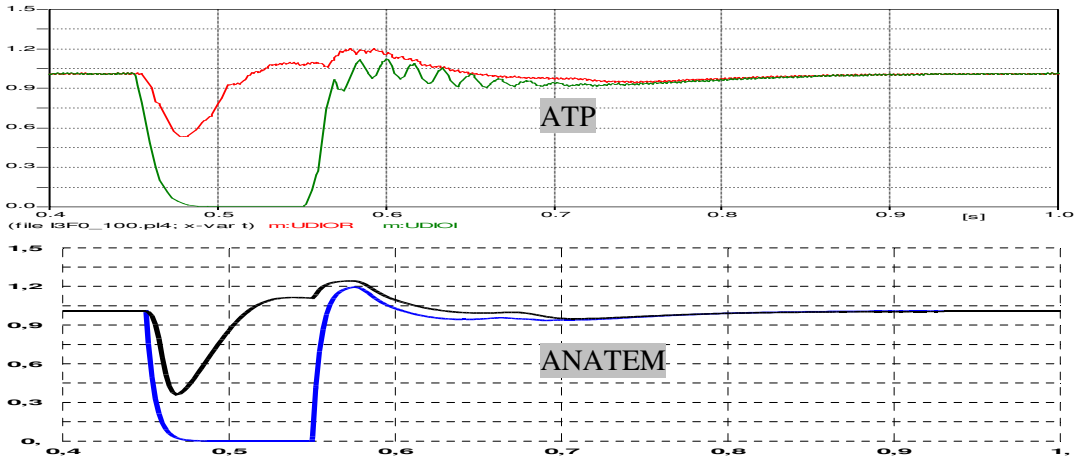


Figure G.30 - Udi0 voltages at rectifier and at inverter (pu)

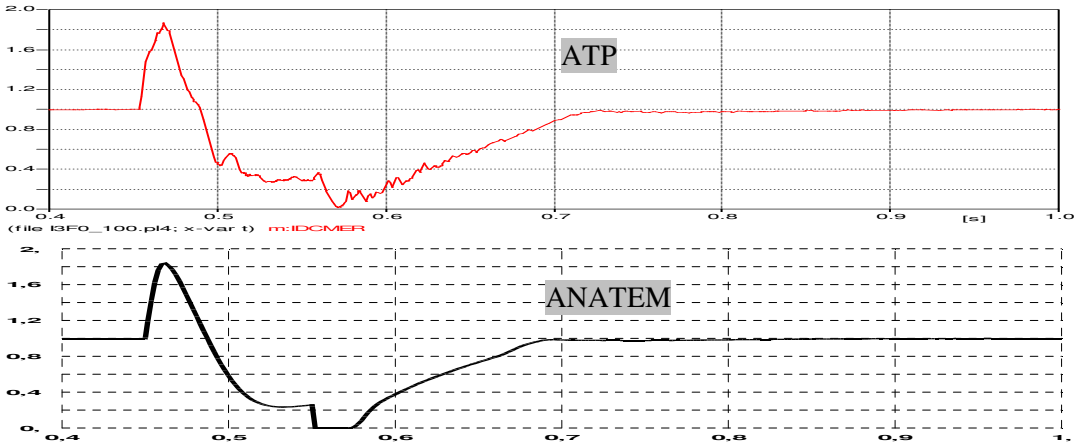


Figure G.31 - DC current (pu)

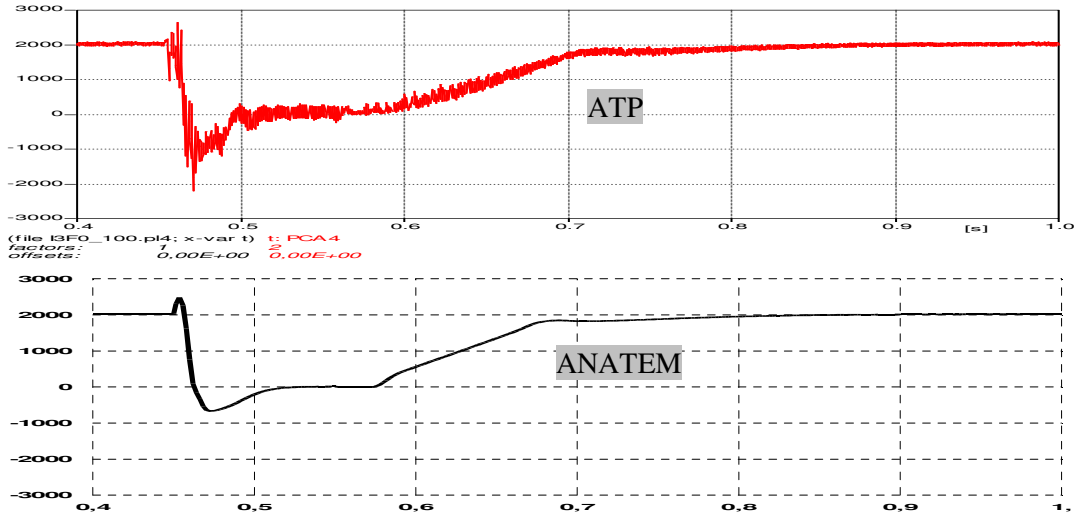


Figure G.32 - Inverter total Pcc (MW)

## Single-phase solid short-circuit at the inverter side

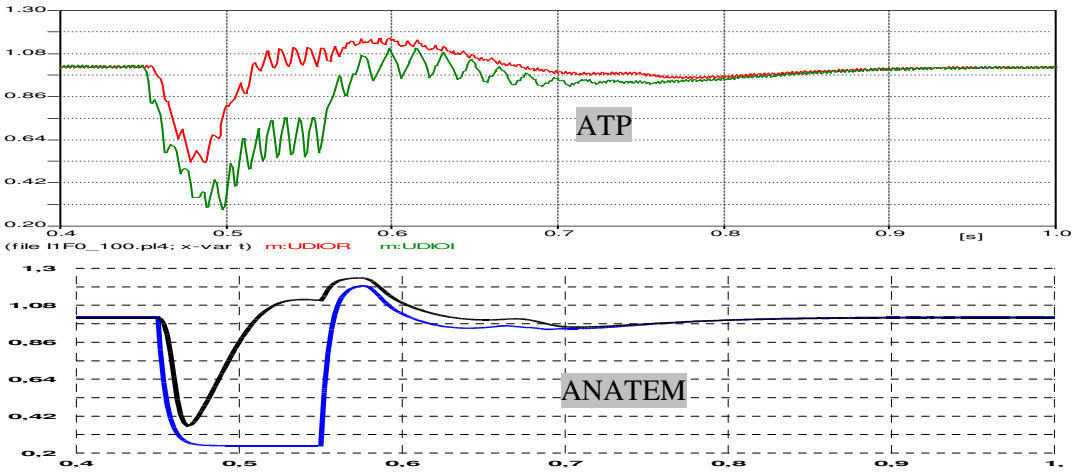


Figure G.33 - Udi0 voltages at rectifier and inverter (pu)

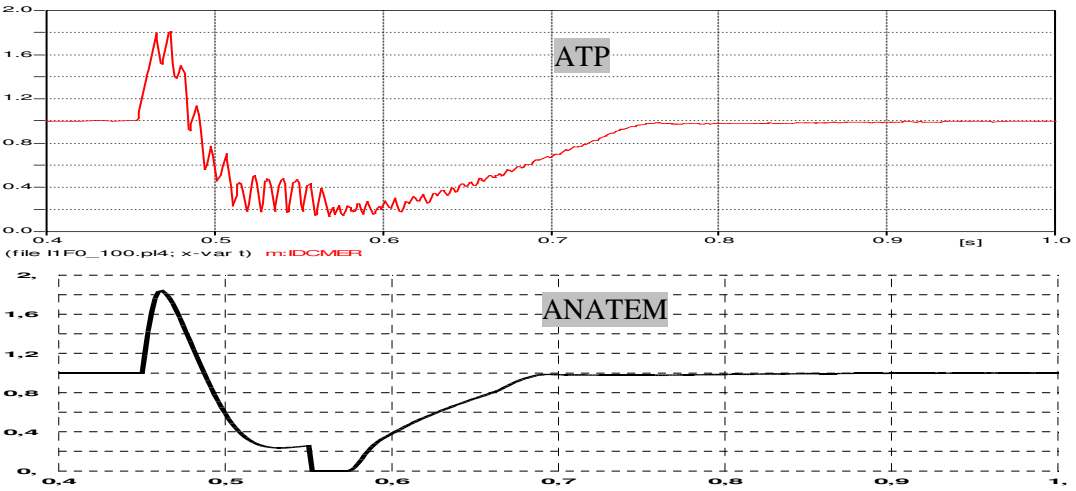


Figure G.34 - DC current (pu)

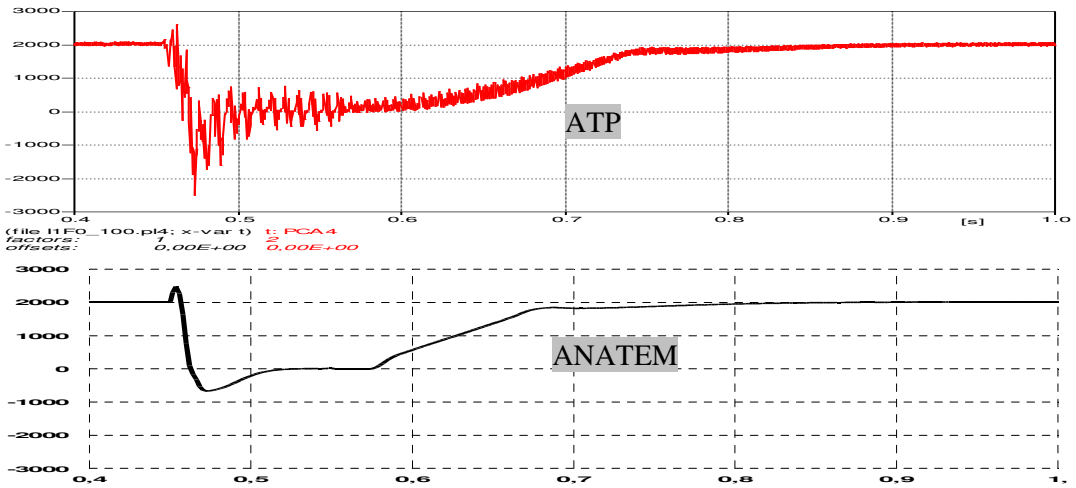


Figure G.35 - Inverter total Pcc (MW)

**Single-phase short-circuit, VAC= 60%, at the inverter side**

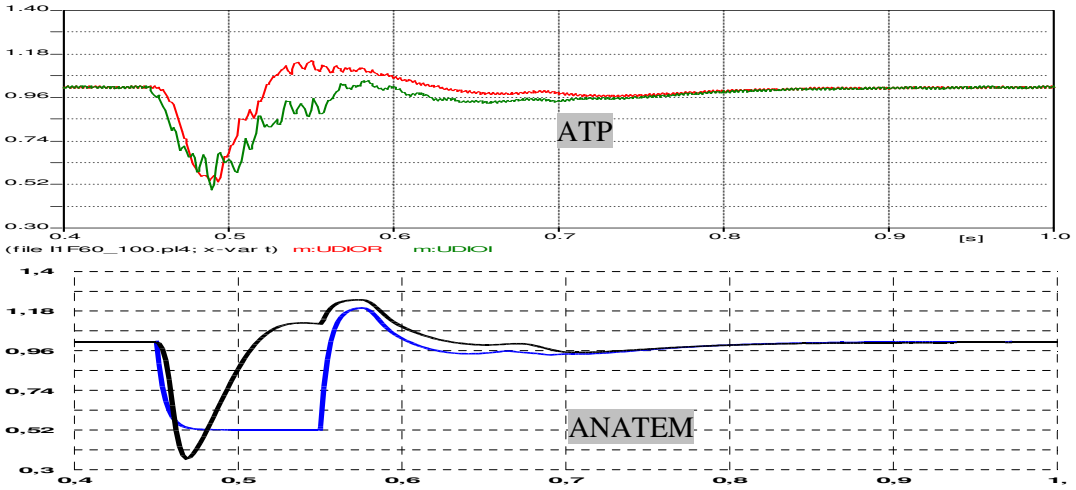


Figure G.36 - Udi0 voltages at rectifier and at inverter (pu)

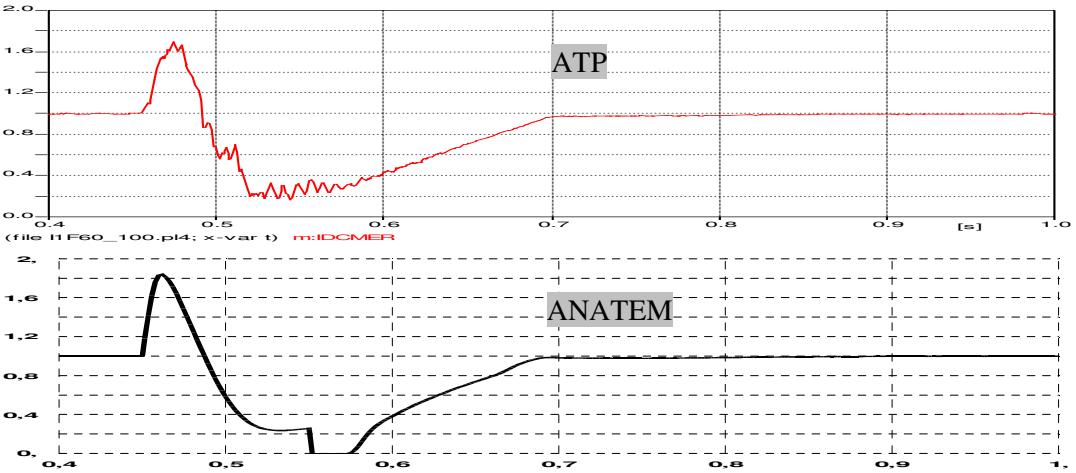


Figure G.37 - DC current (pu)

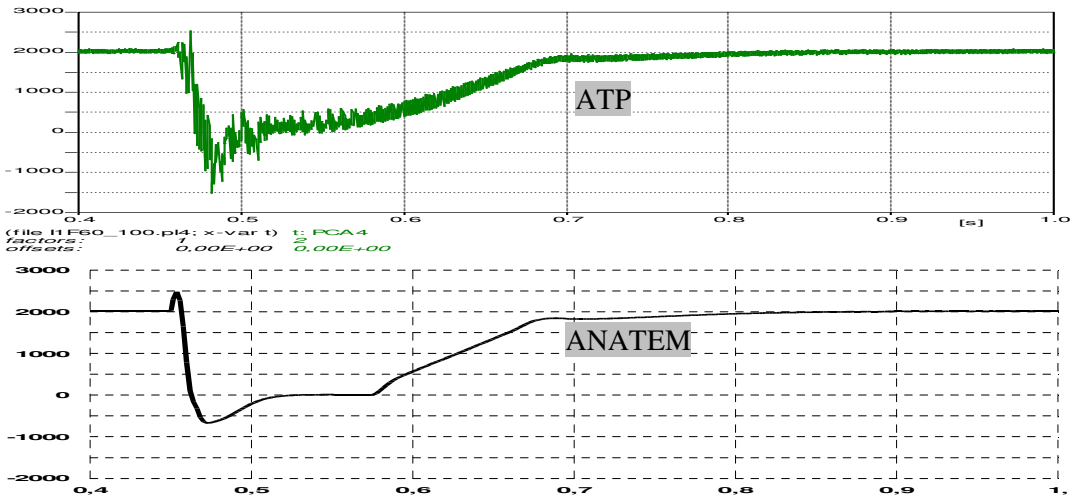


Figure G.38 - Inverter total Pcc (MW)

## Single-phase short-circuit, VAC= 75%, at the inverter side

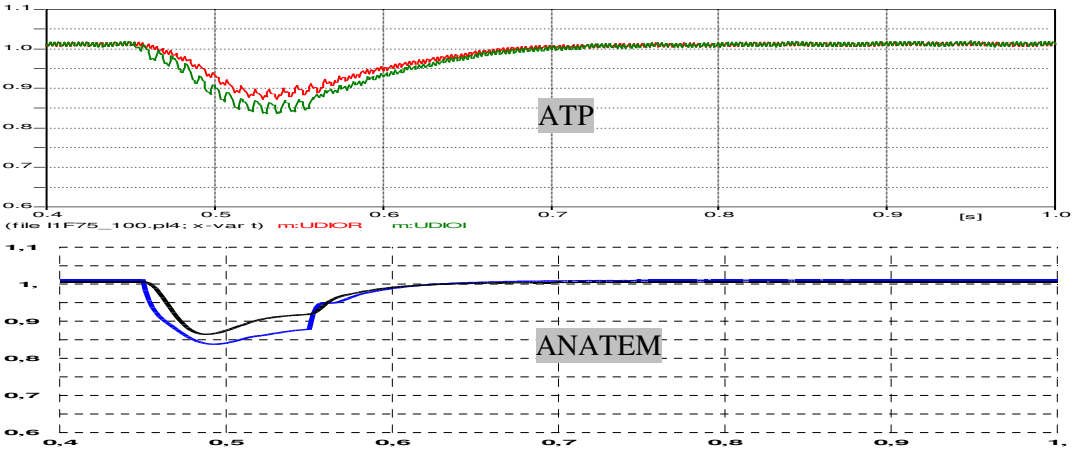


Figure G.39 - Udi0 voltages at rectifier and at inverter (pu)

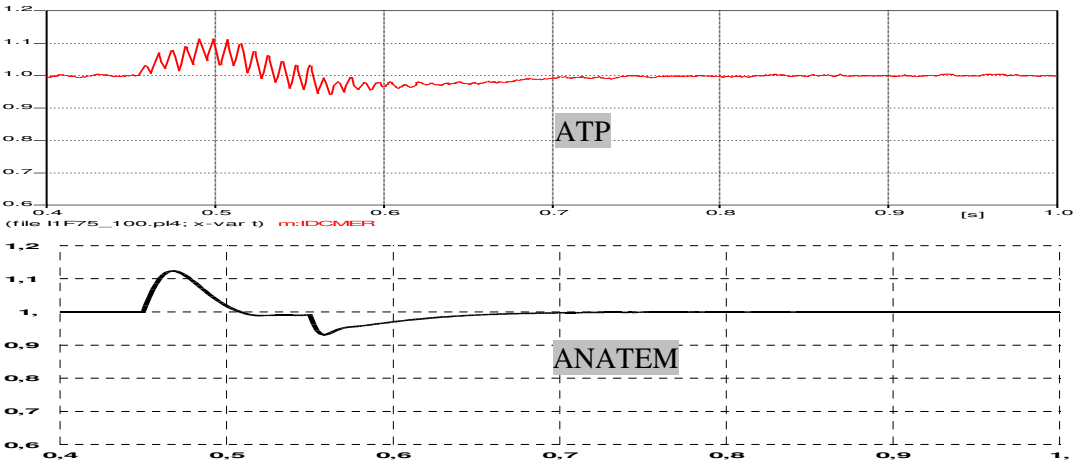


Figure G.40 - DC current (pu)

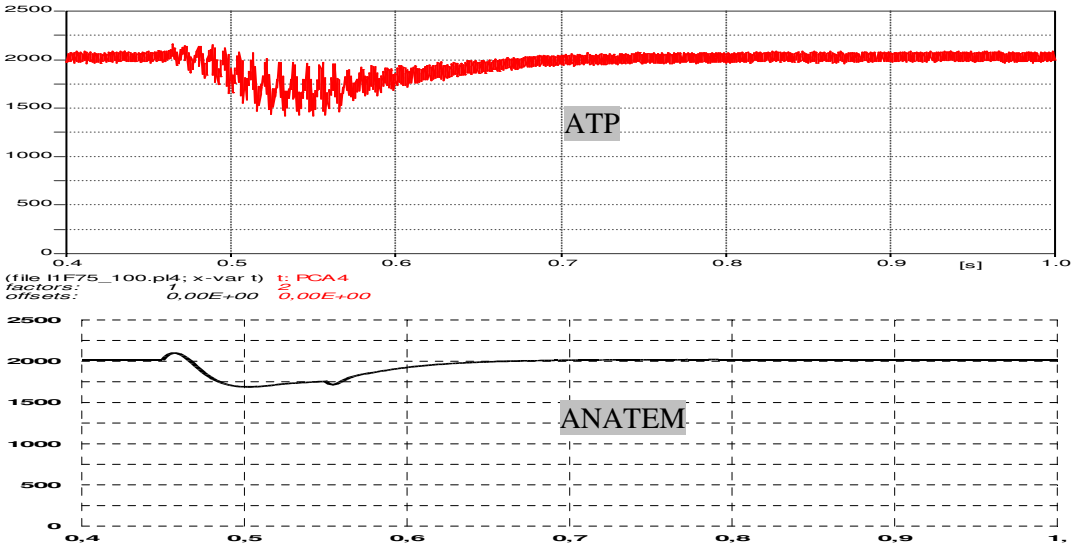


Figure G.41 - Inverter total Pcc (MW)

## G.3 Comparison between ANATEM and ATP programs, with the inclusion of the equivalent dynamics for the machines of the *Simplified Network*

In item G.2, a preliminary comparison of the performance of the CCC modeling in the ATP and ANATEM programs was presented, considering the *Simplified Network* with machines represented as infinite buses in both programs.

In item G.1 it had been shown that the representation of the equivalent dynamics in the *Simplified Network* makes the behaviors of *Simplified* and *Equivalent Networks* quite consistent in the ANATEM program.

Therefore, it was proceeded to model that equivalent dynamics in the ATP program. The machines were represented by the complete model, with their voltage regulators, and the results were compared with those previously presented for the ANATEM program.

As mentioned before, it was decided, in this work, to represent the *Simplified Network* in the ATP program. Nevertheless, the integral modeling of the *Equivalent Network*, with all its dynamics, may be performed, if required, in programs of the EMTP type, in a relatively easy way.

Among the simulations that were made for purposes of comparison between the programs involved, the most relevant are those which resulted in a reduction of the ESCR (*Cases 3 and 4* of item G.1). Figures G.42 to G.47 illustrate some of the results obtained. Those regarding the ANATEM program have been presented in item G.1, and are repeated here in order to make that comparison easier. As the system becomes more complex, with the inclusion of new dynamics, the differences tend to add, requiring then a specific validation of each component in the distinct tools, in order to achieve an acceptable consistency. Nonetheless, as a general conclusion, it is noted that the results obtained present a very significant consistency, thus permitting the utilization of both program types (stability and electromagnetic transients) in a complementary manner. Slow or long-duration phenomena are simulated more easily and inexpensively with the stability programs, while fast but critical phenomena, associated to faults, disturbances or control actions, should be studied with the assistance of electromagnetic transients simulation programs, with a detailed three-phase representation of the converter stations and, when required, of other parts of the system more directly affected.

*Case 3- Application of three-phase solid fault at bus #11, for 100ms, followed by a 20% impedance increase to the equivalent connected to bus #11*

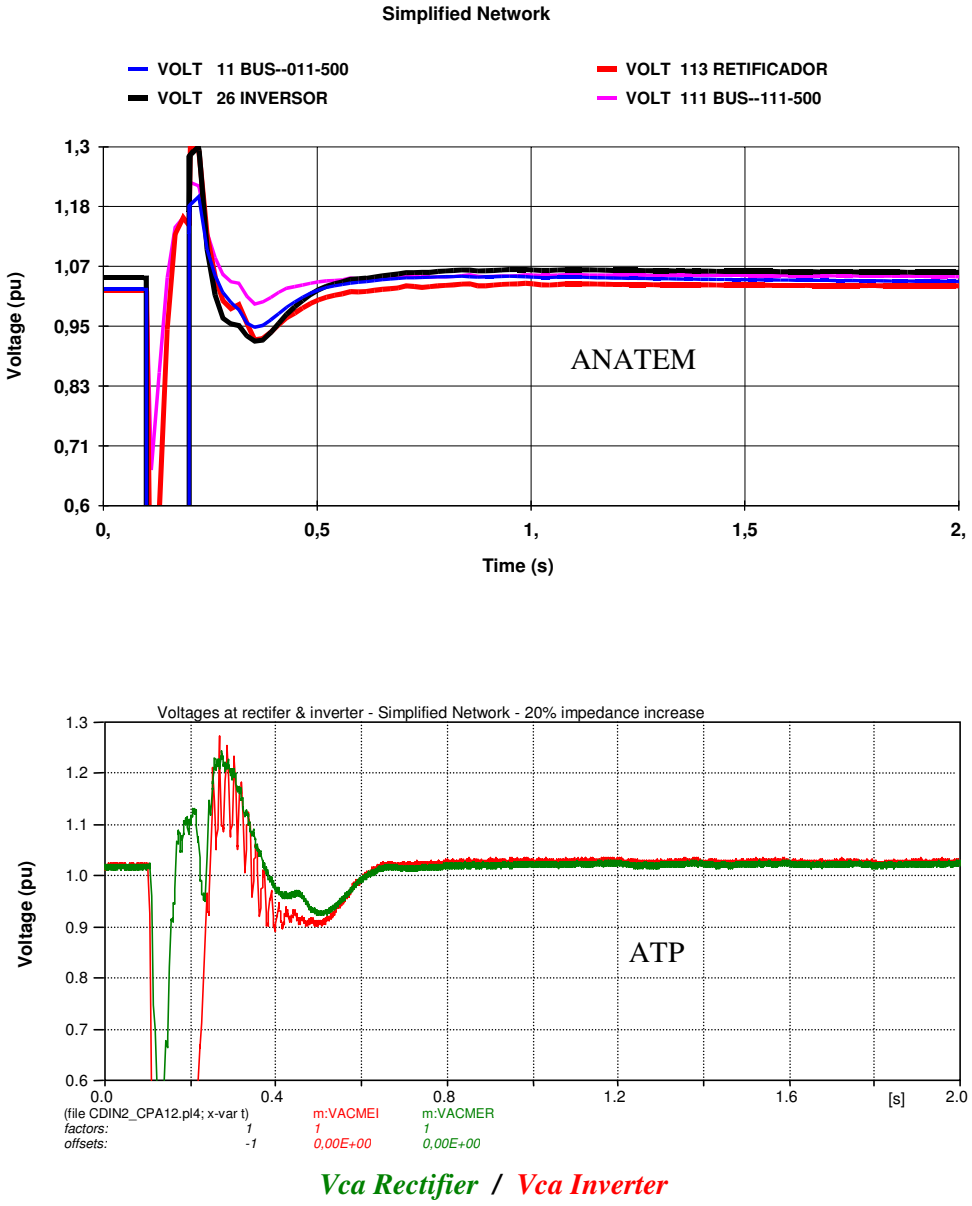


Figure G.42 – AC voltages - *Rectifier and Inverter*
*ANATEM and ATP Programs*

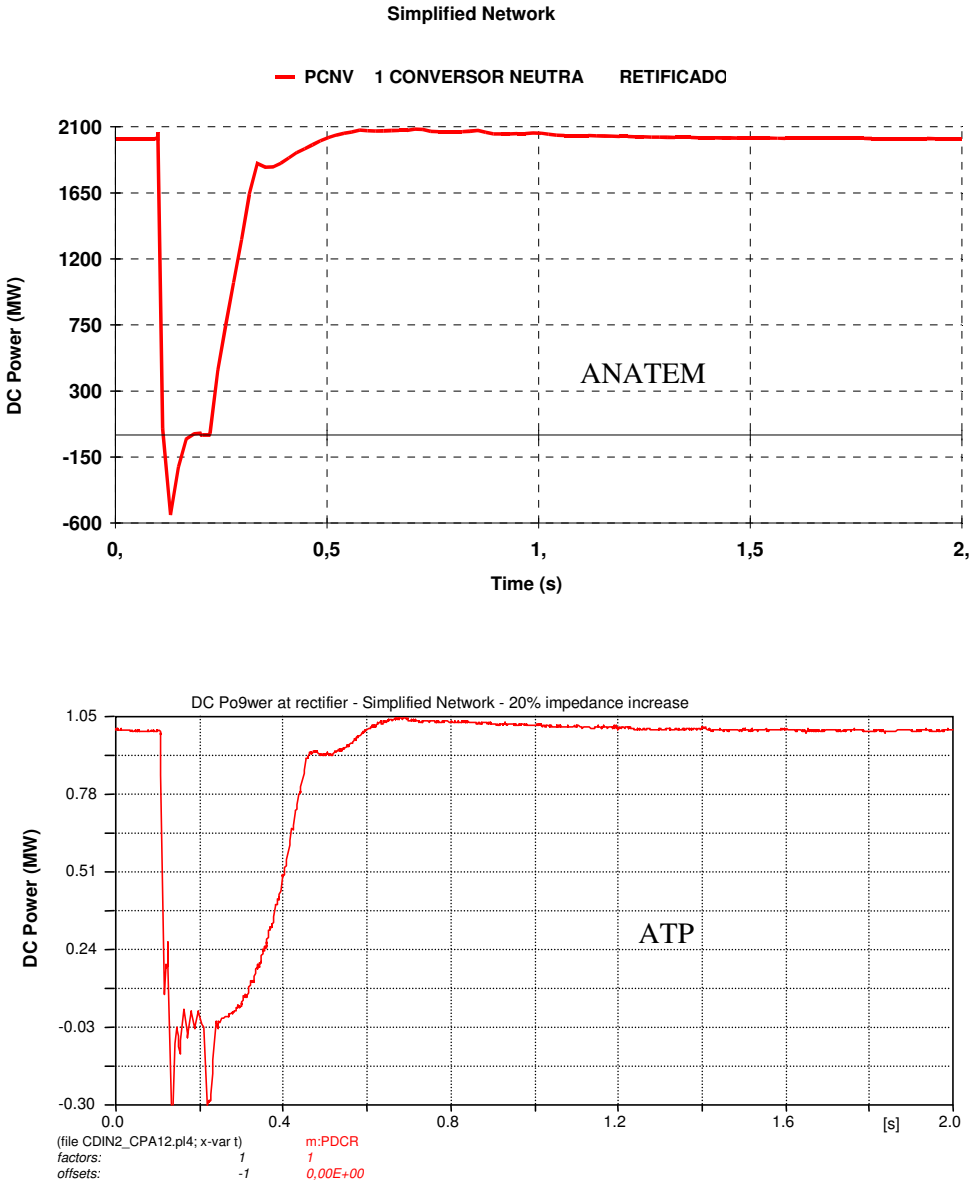


Figure G.43 – DC Power at rectifier
*ANATEM and ATP Programs*

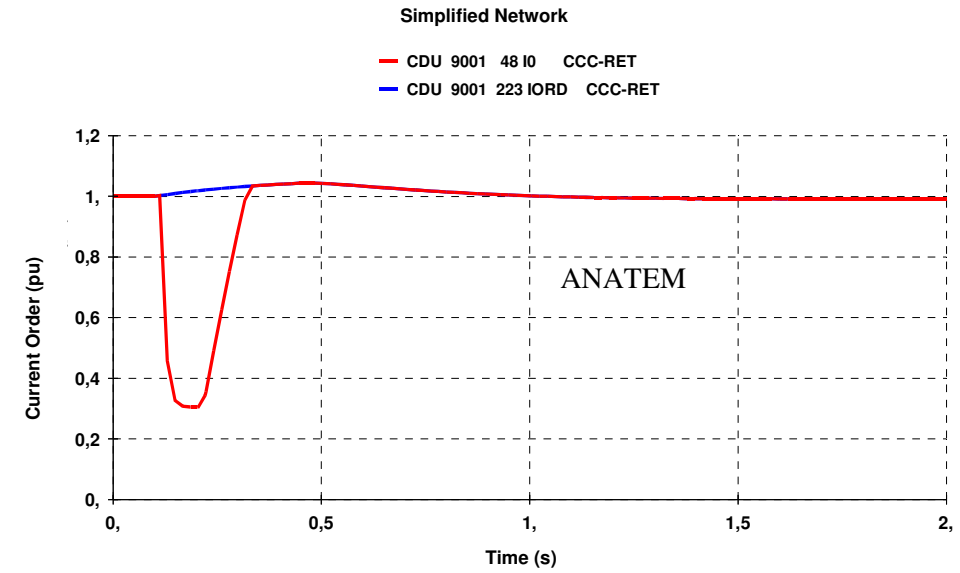


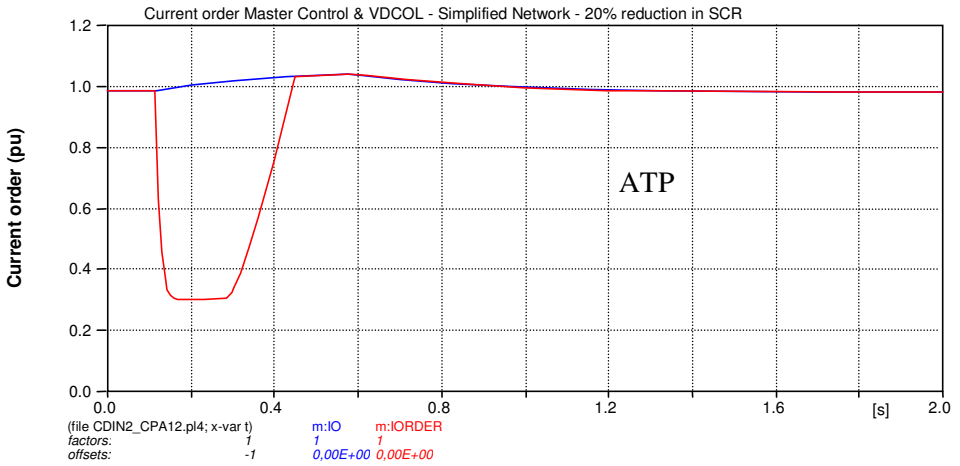


Figure G.44 – Current Orders ("Master Control" and VDCOL output)
*ANATEM and ATP Programs*

*Case 4- Application of three-phase solid fault to bus #11, for 100ms, followed by a 50% increase of the impedance of the equivalent connected to bus #11*

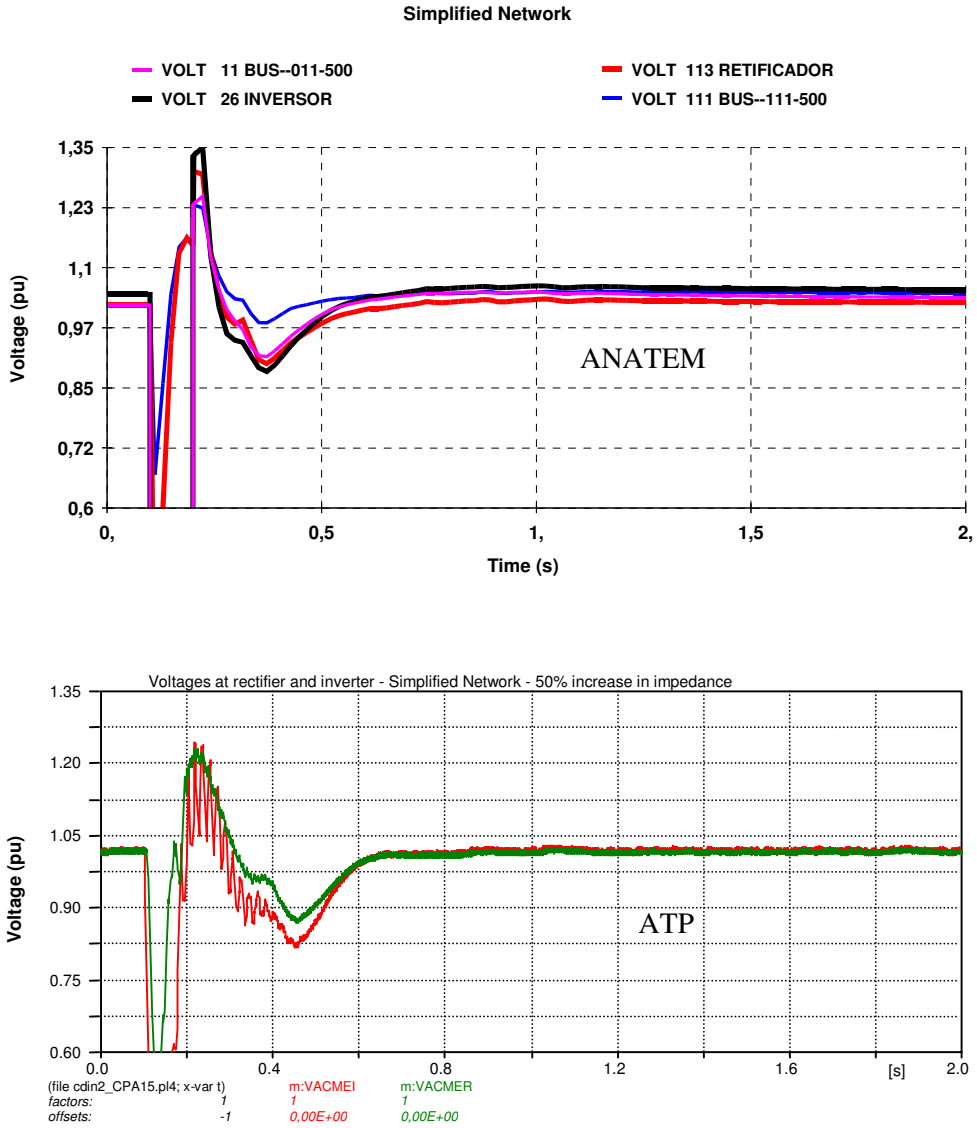


Figure G.45 – AC Voltages – *Rectifier and Inverter ANATEM and ATP Programs*

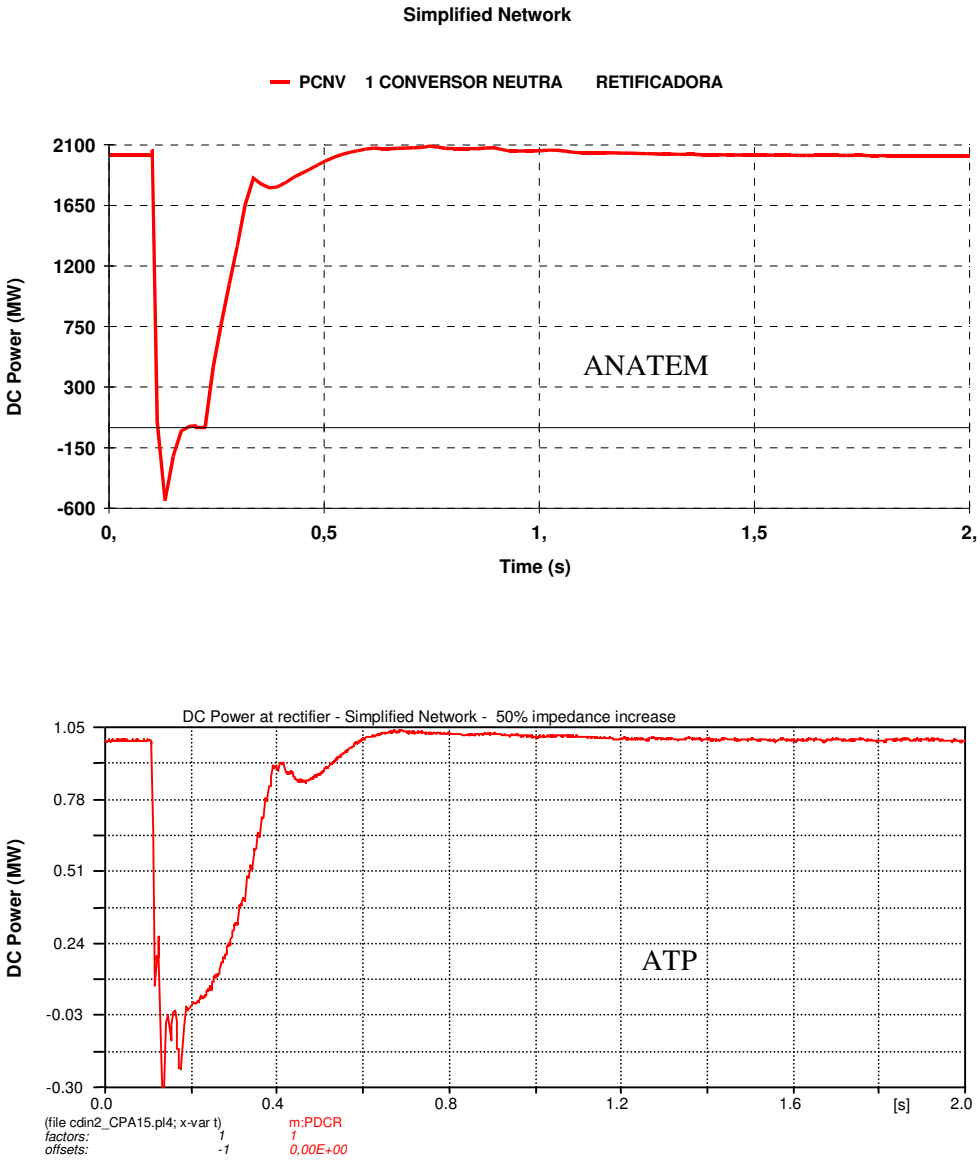


Figure G.46 – DC Power at rectifier
*ANATEM and ATP Programs*

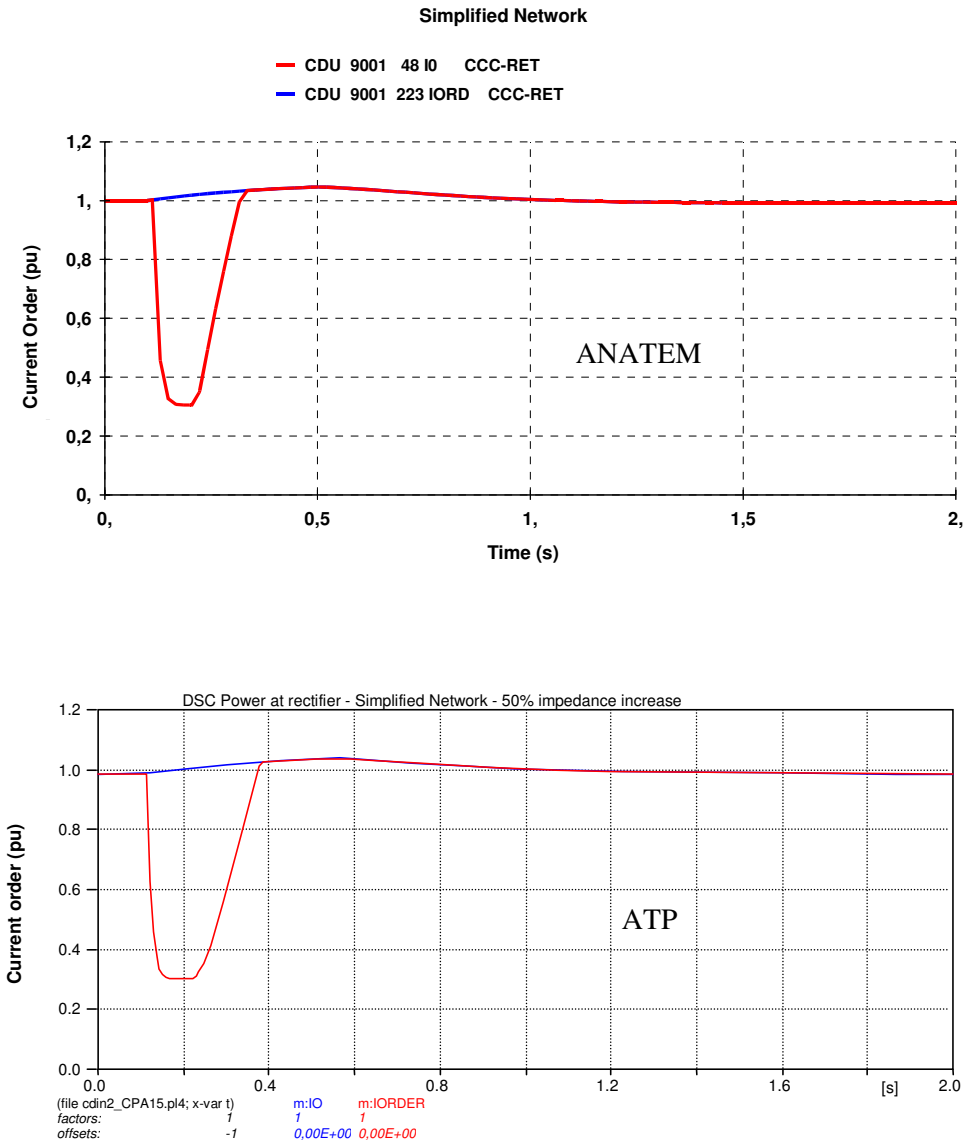


Figure G.47 – Current Orders (“Master Control” and VDCOL output)
*ANATEM and ATP Programs*

## ANNEX H - DATA USED FOR ELECTROMECHANICAL STABILITY STUDIES

Table H.1 – Equivalent Network Steady State Bus Data

| Bus | Type | Voltage | Pg [MW] | Qg [Mvar] | Pl[MW] | Ql[Mvar] | Shunt [Mvar] |
|---|---|---|---|---|---|---|---|
| 7 | PQ | - | - | - | 0.00 | 0.00 | 0.00 |
| 8 | PQ | - | - | - | 0.00 | 0.00 | 0.00 |
| 9 | PQ | - | - | - | 2174.00 | 250.00 | 0.00 |
| 10 | PQ | - | - | - | 0.00 | 0.00 | 0.00 |
| 11 | PQ | - | - | - | 0.00 | 0.00 | 0.00 |
| 12 | PQ | - | - | - | 0.00 | 0.00 | 0.00 |
| 13 | PQ | - | - | - | 0.00 | 0.00 | 0.00 |
| 14 | PV | 0.95 | 0.00 | 5.235 | 0.00 | 0.00 | 0.00 |
| 21 | PQ | - | - | - | 467.00 | 14.40 | 0.00 |
| 22 | PQ | - | - | - | 787.00 | 97.20 | 0.00 |
| 24 | PQ | - | - | - | 2100.00 | 0.00 | 0.00 |
| 26 | PQ | - | - | - | 0.00 | 0.00 | 40.00 |
| 37 | Vθ | 1.00 | 1266.42 | 151.75 | 0.00 | 0.00 | 0.00 |
| 38 | PV | 1.00 | 920.00 | 167.02 | 0.00 | 0.00 | 0.00 |
| 39 | PV | 0.95 | 670.00 | 37.07 | 0.00 | 0.00 | 0.00 |
| 40 | PV | 0.95 | 900.00 | 95.05 | 0.00 | 0.00 | 0.00 |
| 107 | PQ | - | - | - | 310.00 | -166.00 | 0.00 |
| 108 | PQ | - | - | - | 0.00 | 0.00 | 0.00 |
| 109 | PQ | - | - | - | 1200.00 | 1134.00 | 950.00 |
| 111 | PQ | - | - | - | 2.90 | 0.00 | -50.00 |
| 112 | PQ | - | - | - | 0.00 | 0.00 | -50.00 |
| 113 | PQ | - | - | - | 0.00 | 0.00 | 180.00 |
| 122 | PQ | - | - | - | 0.00 | 0.00 | 0.00 |
| 137 | Vθ | 1.00 | 1585.16 | 54.18 | 1.70 | 0.00 | 0.00 |
| 138 | PV | 1.03 | 1020.00 | 136.14 | 0.00 | 0.00 | 0.00 |
| 140 | PV | 1.02 | 1000.00 | 38.84 | 1.61 | 0.00 | 0.00 |

Table H.2 – Equivalent Network Steady State Line Data

| Bus From | Bus To | R (%) | X (%) | Shunt (Mvar) | Tap |
|---|---|---|---|---|---|
| 7 | 11 | 0.091 | 1.162 | 142.0 | - |
| 7 | 37 | 0.0273 | 1.612 | - | 1.024 |
| 8 | 7 | 0.056 | 0.697 | 85.746 | - |
| 8 | 9 | 0.052 | 0.654 | 80.493 | - |
| 8 | 38 | 0.00 | 1.4 | - | 1.024 |
| 9 | 7 | 0.31 | 3.95 | 120.26 | - |
| 9 | 12 | 0.162 | 2.048 | 250.17 | - |
| 10 | 9 | 0.005 | 0.062 | 30.632 | - |
| 10 | 39 | 0.00 | 1.088 | - | 1.048 |
| 11 | 12 | 0.12 | 1.64 | 220.0 | - |
| 12 | 13 | 0.225 | 3.033 | 381.5 | - |
| 13 | 11 | 0.282 | 3.852 | 493.7 | - |
| 13 | 14 | 0.01 | 2.0 | - | 1.000 |
| 21 | 9 | 0.031 | 1.207 | - | 1.038 |
| 21 | 22 | 1.521 | 7.864 | 54.212 | - |
| 22 | 40 | 0.1673 | 1.133 | 1.025 | - |
| 24 | 13 | 0.0087 | 0.330 | - | 1.054 |
| 26 | 11 | 0.2824 | 3.75 | 364.6 | - |
| 26 | 11 | 0.2824 | 3.75 | 364.6 | - |
| 107 | 109 | 0.129 | 1.593 | 48.42 | - |
| 107 | 111 | 0.086 | 1.108 | 134.7 | - |
| 107 | 137 | 0.0273 | 1.612 | - | 1.024 |
| 108 | 107 | 0.056 | 0.698 | 85.746 | - |
| 108 | 109 | 0.052 | 0.655 | 80.493 | - |
| 108 | 138 | 0.00 | 1.4 | - | 1.024 |
| 109 | 112 | 0.088 | 1.095 | 133.3 | - |
| 111 | 113 | 0.1988 | 2.654 | 254.0 | - |
| 112 | 111 | 0.1002 | 1.322 | 123.14 | - |
| 112 | 113 | 0.158 | 2.1 | 200.0 | - |
| 122 | 111 | 0.086 | 1.137 | 138.7 | - |
| 122 | 140 | 0.0167 | 0.133 | 0.00 | 1.025 |

Table H.3 – Machines and Regulators Association

| Bus | Units Number | Machine Model | Voltage Regulator | Speed Governor | Power System Stabilizer |
|---|---|---|---|---|---|
| 14 | 2 | 138 | 127 | - | - |
| 37 | 12 | 5037 | 6037 | 850 | 8037 |
| 38 | 10 | 5038 | 6038 | 744 | - |
| 39 | 9 | 5039 | 6039 | 740 | 8039 |
| 40 | 18 | 5040 | 6040 | 149 | 8040 |
| 137 | 12 | 5037 | 6137 | 851 | 8137 |
| 138 | 10 | 5038 | 6138 | 745 | - |
| 140 | 18 | 5040 | 6140 | 150 | 8140 |

Table H.4 – Machine Model Data

| Model Number | Xd | Xq | X'd | X"d | Xl | T'd | T"d | T"q | H | MVA |
|---|---|---|---|---|---|---|---|---|---|---|
| 138 | 170.000 | 100.000 | 37.000 | 22.000 | 15.400 | 9.000 | 0.060 | 0.200 | 1.600 | 300.000 |
| 5037 | 91.790 | 62.250 | 31.650 | 23.210 | 18.860 | 10.000 | 0.040 | 0.130 | 3.873 | 369.800 |
| 5038 | 87.850 | 56.610 | 24.510 | 19.860 | 10.350 | 7.590 | 0.070 | 0.170 | 4.071 | 333.000 |
| 5039 | 91.890 | 68.630 | 30.250 | 24.220 | 16.130 | 7.920 | 0.060 | 0.090 | 4.439 | 419.000 |
| 5040 | 116.800 | 64.380 | 33.040 | 27.370 | 13.220 | 8.520 | 0.045 | 0.072 | 3.530 | 186.200 |

**Voltage Regulator**
**127**

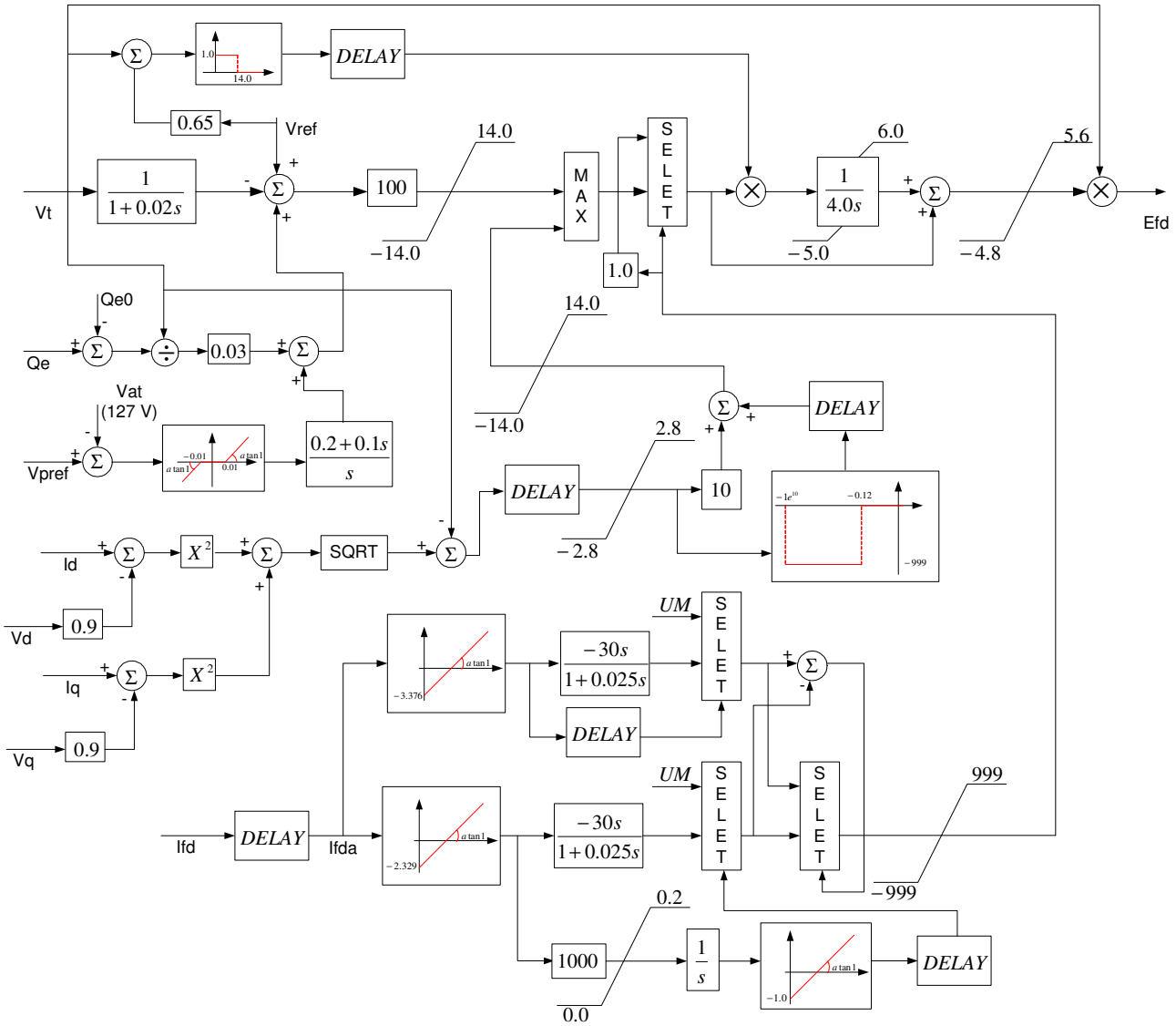

**Voltage Regulator**
**6037 and 6137**

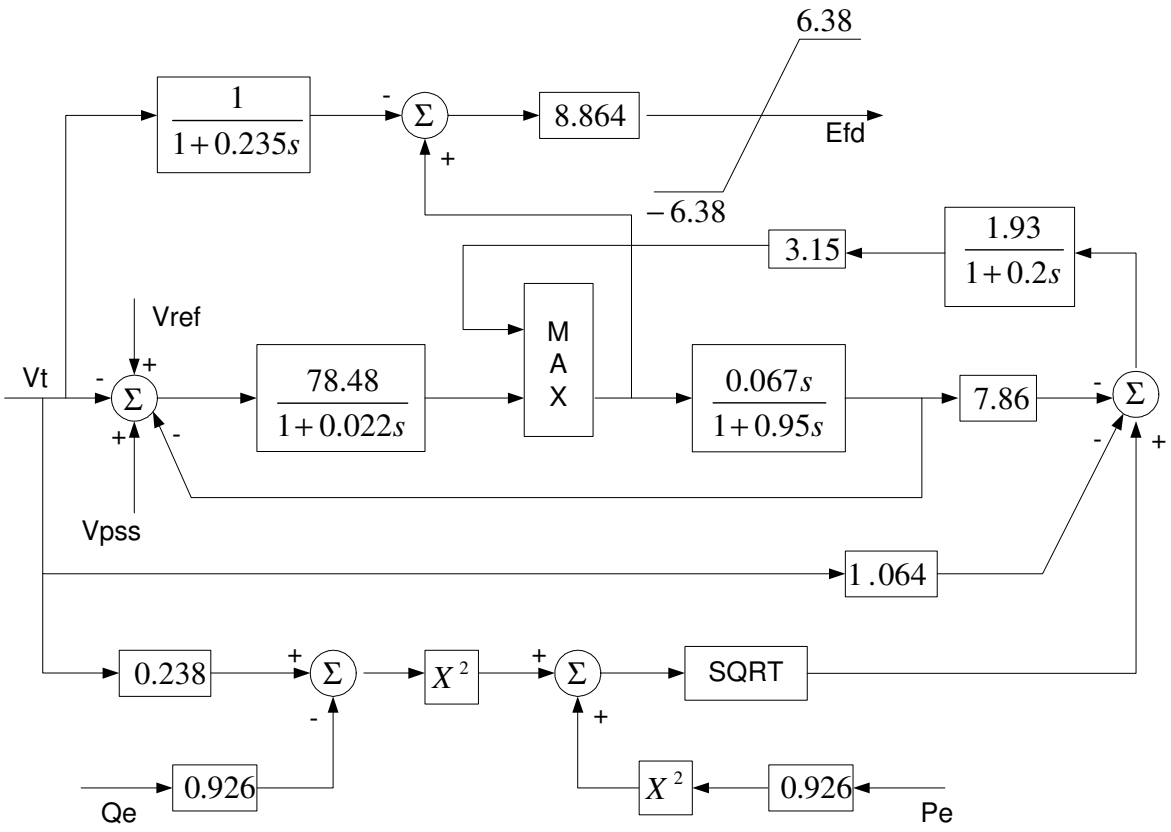


**Voltage Regulator**
**6038 and 6138**

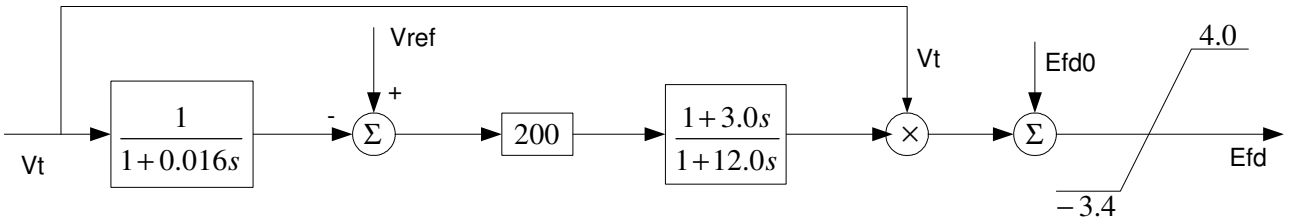


**Voltage Regulator**
**6039**

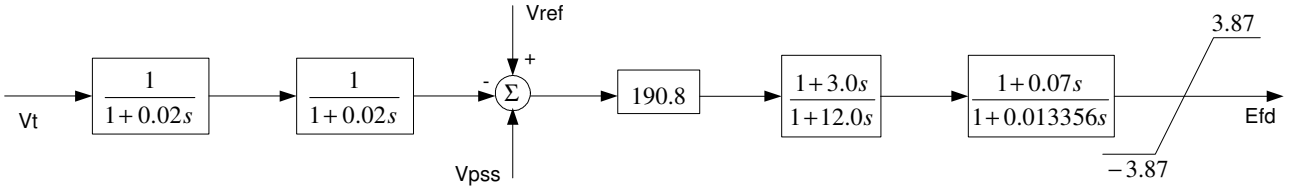

**Voltage Regulator 6040 and 6140**

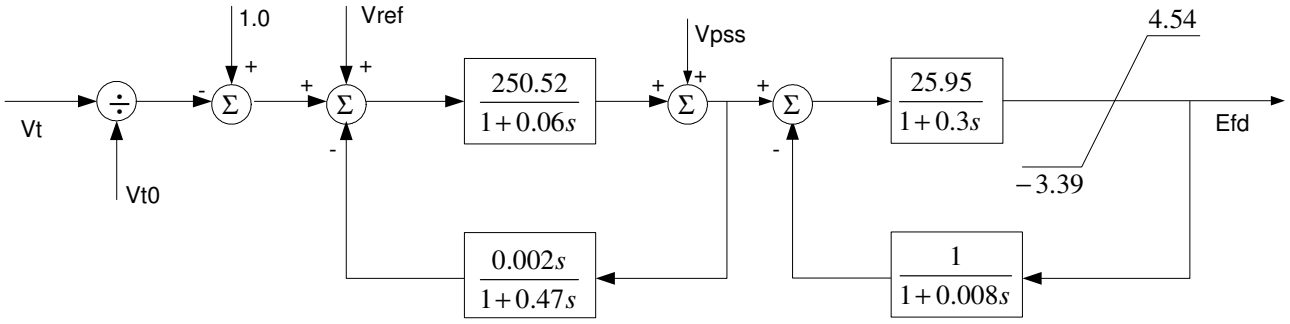


Figure H.1 – Automatic Voltage Regulators on the *Equivalent Network*

Table H. 5 – Voltage Regulator Parameters

AVR 127

| Parameter | Value | Parameter | Value | Parameter | Value | Parameter | Value |
|---|---|---|---|---|---|---|---|
| A1 | 999. | B1 | -0.12 | Ka | 100. | Kq1 | -14.0 |
| A2 | -999. | B4 | -14.0 | Keli | 3.376 | Kq2 | 14.0 |
| A3 | -2.8 | B5 | 14.0 | Kelt | 2.329 | LOCM | 127 |
| A4 | 2.8 | B7 | 0.9 | Kiaj | 0.20 | Ta | 0.02 |
| A6 | 10.0 | B8 | 1.8 | Kpaj | 0.10 | Te | 4.0 |
| Aex | -5.0 | B9 | 0.03 | Kpli | 30.0 | Tse | 0.0167 |
| | | Bex | 6.0 | Kplt | 30.0 | Vamax | 5.60 |
| | | BMN | -0.01 | | | Vamin | -4.8 |
| | | BMP | 0.01 | | | | |

AVR 6037 and 6137

| Parameter | Value | Parameter | Value |
|---|---|---|---|
| Cte | 0.926 | T | 0.2 |
| K | 3.15 | Ta | 0.022 |
| K1 | 7.86 | Tse | 0.95 |
| Ka | 78.48 | Us | 0.067 |
| Kc | 0.238 | VAmax | 6.38 |
| Ke | 8.864 | VAmin | -6.38 |
| Kr | 0.826 | | |

AVR 6038 and 6138

| Parameter | Value | Parameter | Value |
|---|---|---|---|
| A1 | 0.016 | VAmax | 4.0 |
| Ka | 200.0 | VAmin | -3.4 |
| Ke | 1.0 | | |
| Tse | 12.0 | | |
| Us | 3.0 | | |

AVR 6039 and 6139

| Parameter | Value | Parameter | Value |
|---|---|---|---|
| Ka | 190.8 | T2 | 12.0 |
| Lmax | 3.87 | T3 | 0.07 |
| Lmin | -3.87 | T4 | 0.013356 |
| | | Ta | 3.0 |
| | | Tse | 0.02 |

AVR 6040 and 6140

| Parameter | Value | Parameter | Value |
|---|---|---|---|
| Ka | 250.52 | Tse | 0.47 |
| Ke | 25.95 | us | 0.002 |
| Ta | 0.06 | VAmax | 4.54 |
| Te | 0.3 | VAmin | -3.39 |
| Tq | 0.008 | | |

Speed Governors
149 and 150

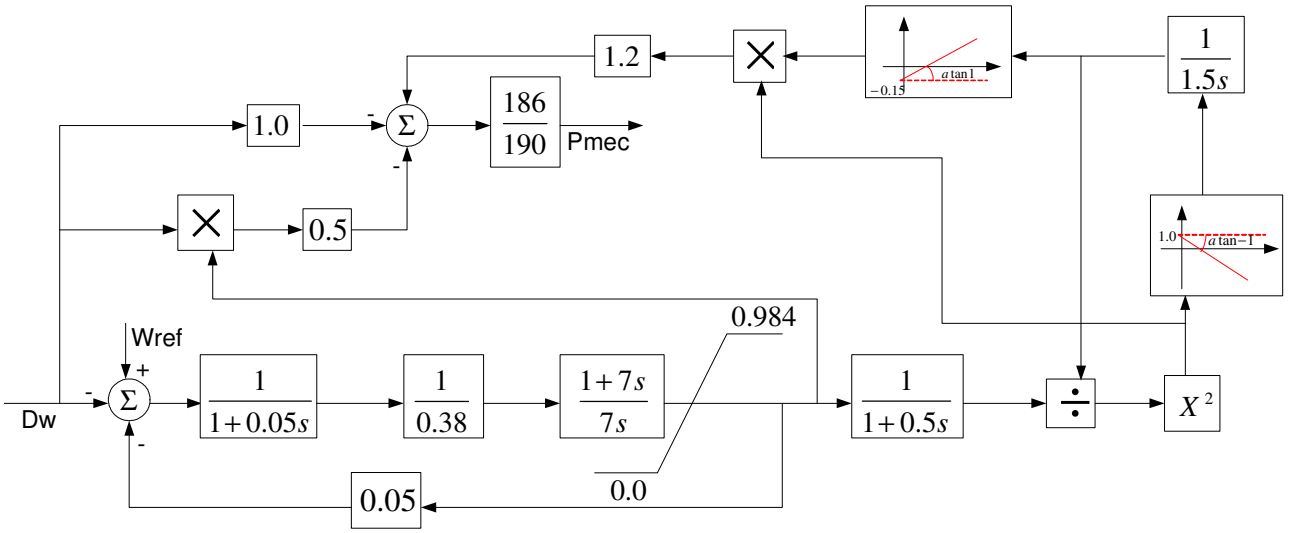


Speed Governor
740

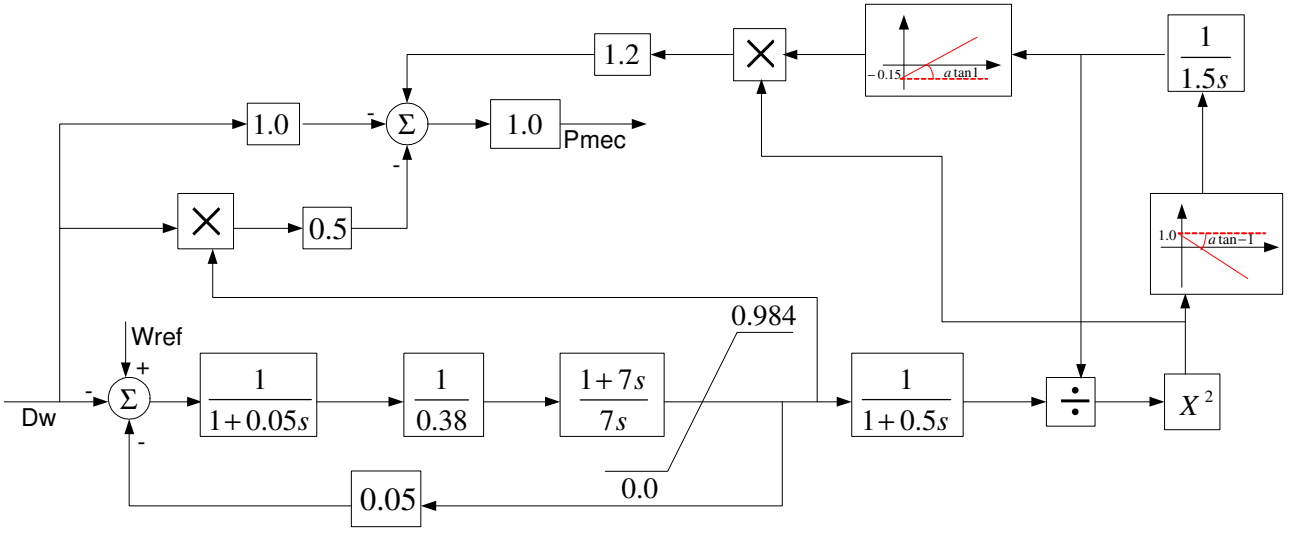

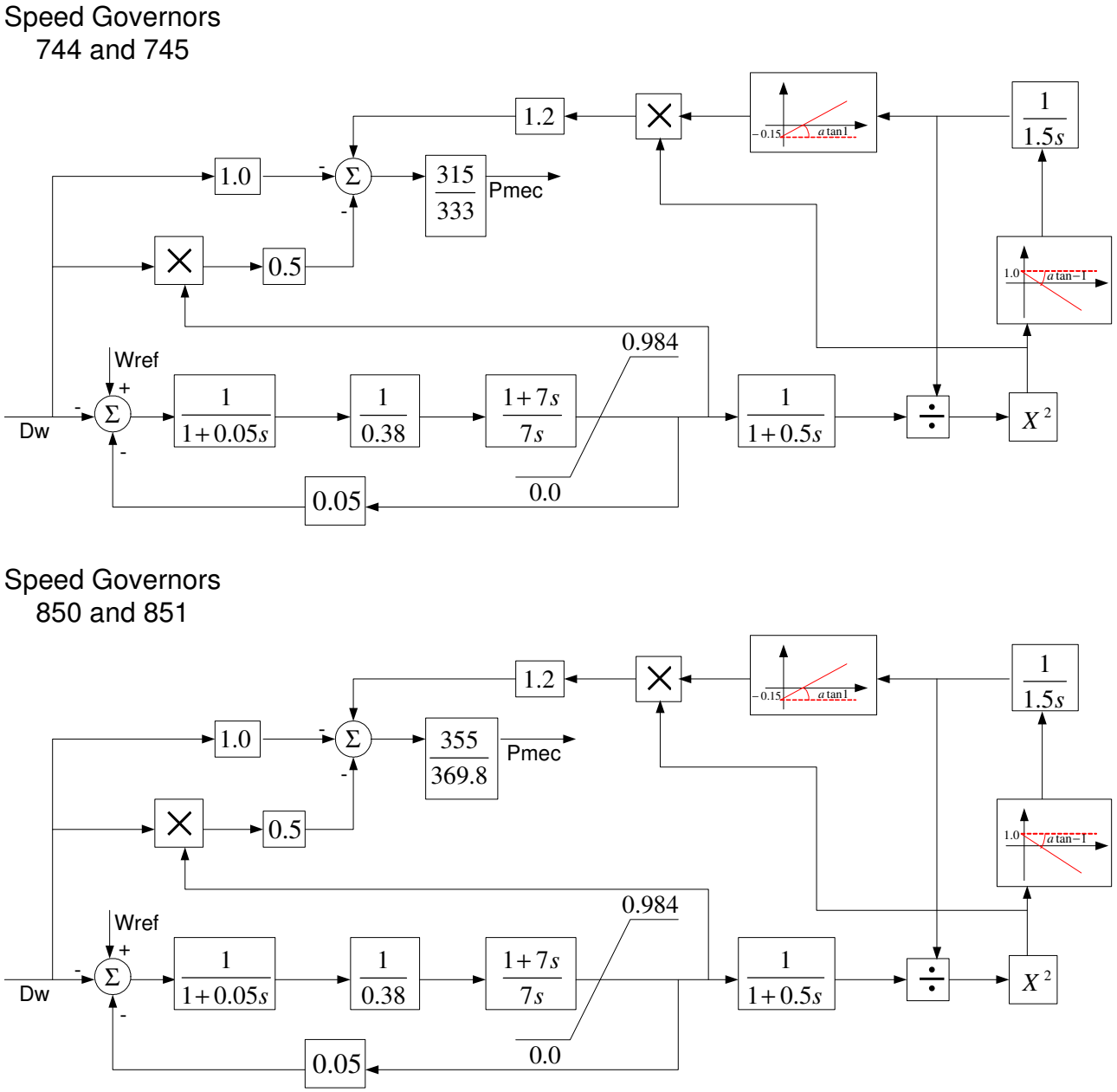


Figure H.2 – Speed Governors on the *Equivalent Network*

Table H.6 – Speed Governors Parameters

SG 149 and 150

| Parameter | Value | Parameter | Value |
|---|---|---|---|
| At | 1.2 | Qnl | 0.15 |
| D | 1.0 | R | 0.05 |
| Dt | 0.5 | rp | 0.38 |
| Lmax | 0.984 | Tf | 0.05 |
| Lmin | 0.0 | Tg | 0.5 |
| PBmaq | 190. | Tr | 7.0 |
| PBtur | 186. | Tw | 1.5 |

SG 740

| Parameter | Value | Parameter | Value |
|---|---|---|---|
| At | 1.2 | Qnl | 0.15 |
| D | 1.0 | R | 0.05 |
| Dt | 0.5 | rp | 0.38 |
| Lmax | 0.984 | Tf | 0.05 |
| Lmin | 0.0 | Tg | 0.5 |
| PBmaq | 419. | Tr | 7.0 |
| PBtur | 419. | Tw | 1.5 |

SG 744 and 745

| Parameter | Value | Parameter | Value |
|---|---|---|---|
| At | 1.2 | Qnl | 0.15 |
| D | 1.0 | R | 0.05 |
| Dt | 0.5 | rp | 0.38 |
| Lmax | 0.984 | Tf | 0.05 |
| Lmin | 0.0 | Tg | 0.5 |
| PBmaq | 333. | Tr | 7.0 |
| PBtur | 315. | Tw | 1.5 |

SG 850 and 851

| Parameter | Value | Parameter | Value |
|---|---|---|---|
| At | 1.2 | Qnl | 0.15 |
| D | 1.0 | R | 0.05 |
| Dt | 0.5 | rp | 0.38 |
| Lmax | 0.984 | Tf | 0.05 |
| Lmin | 0.0 | Tg | 0.5 |
| PBmaq | 369.8 | Tr | 7.0 |
| PBtur | 355.0 | Tw | 1.5 |

Power System Stabilizer
8037 and 8137

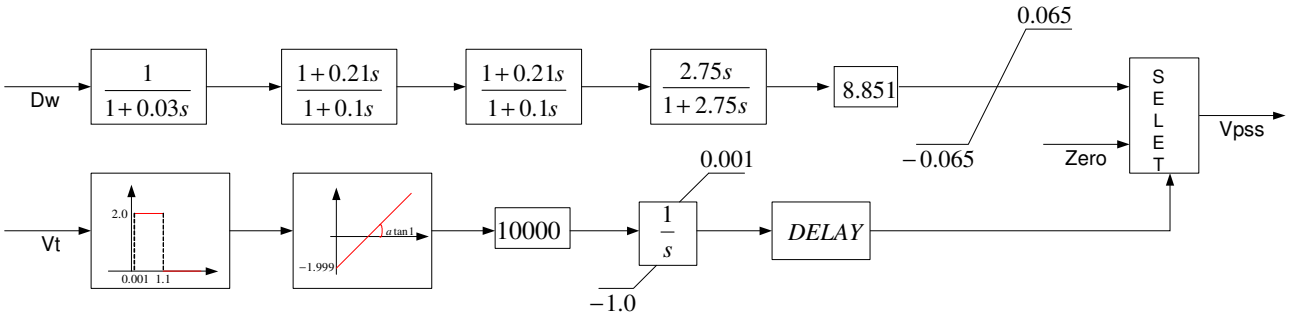

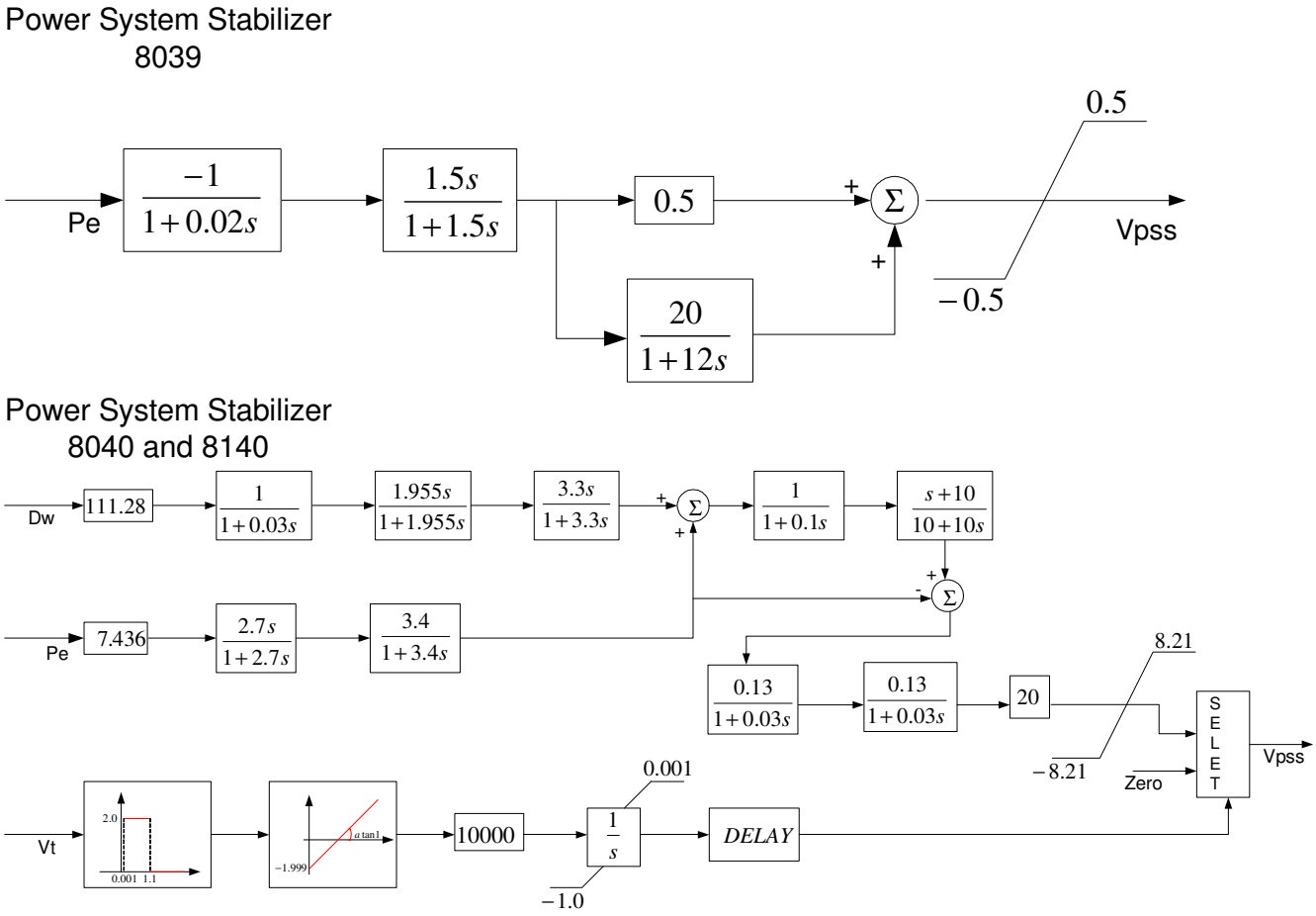


Figure H.3 – Power System Stabilizers on the *Equivalent Network*

Table H.7 – Power System Stabilizer Parameters

PSS 8037 and 8137

| Parameter | Value | Parameter | Value |
|---|---|---|---|
| A2 | 8.851 | Kp | 0.21 |
| B2 | 0.065 | Te | 0.1 |
| B3 | -0.065 | Tq | 2.75 |

PSS 8039

| Parameter | Value | Parameter | Value |
|---|---|---|---|
| B2 | 0.05 | Kq1 | 0.5 |
| B3 | -0.05 | Kq2 | 20.0 |
| Ki | 1.50 | Tse | 0.02 |
| Kp | 12.0 | | |

PSS 8040 and 8140

| Parameter | Value | Parameter | Value |
|---|---|---|---|
| A1 | 111.28 | KI | 3.4 |
| A2 | 7.436 | Kp | 2.7 |
| A3 | 20.0 | Kq1 | 1.955 |
| A4 | 0.03 | Kq2 | 3.3 |
| A5 | 0.1 | W0 | 10.0 |
| Aex | 0.13 | W02 | 100. |
| B2 | 8.21 | | |
| B3 | -8.21 | | |
| Bex | 0.03 | | |

Table H.8 – CCC Model Data

DC Lines

| DC Bus From | DC Bus To | R | L |
|---|---|---|---|
| 1 | 2 | 22.84 | 2730 |

Converters

| Converter Number | AC Bus | DC Bus | Type | Bridge Number | Rated Current | |
|---|---|---|---|---|---|---|
| 1 | 113 | 1 | Rectifier | 4 | 2000 | |
| 2 | 26 | 2 | Inverter | 4 | 2000 | |

| Converter Number | Commutation Reactance | Secondary Voltage | Transformer Power | Reactor Resistance | Reactor Reactance | Commutation Capacitor |
|---|---|---|---|---|---|---|
| 1 | 12. | 187.3 | 505 | 0.0016 | 540. | 93.84 |
| 2 | 12. | 177.4 | 483 | 0.0016 | 540. | 93.84 |

| Converter Number | Control Type | Current Order | Current Margin | Converter Angle | Minimum Converter Angle | Maximum Converter Angle | Minimum Tap | Maximum Tap | Tap in HIMVAr |
|---|---|---|---|---|---|---|---|---|---|
| 1 | Current | 2000 | - | -1.5 | -17. | 5. | 0.1 | 5.25 | |
| 2 | Current | 2000 | 10. | 18. | 15. | 36.7 | 0.1 | 5.25 | |

Rectifier:

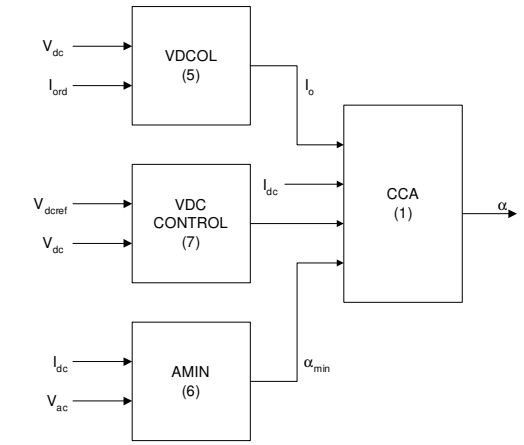


1 - CCA

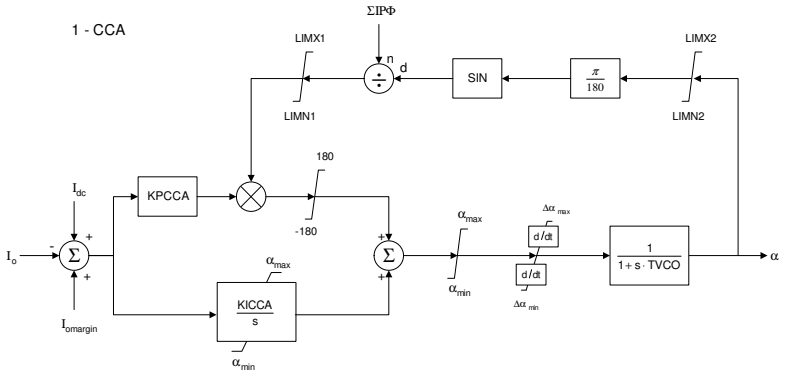


5 - VDCOL

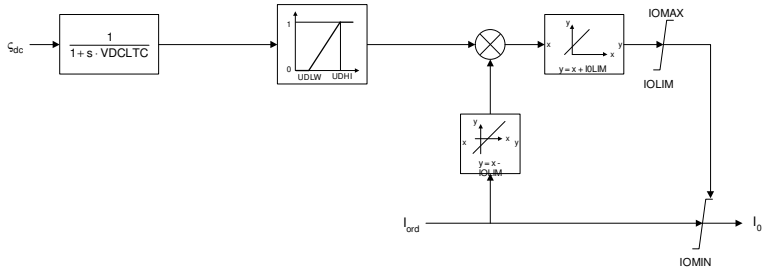


6 - AMIN

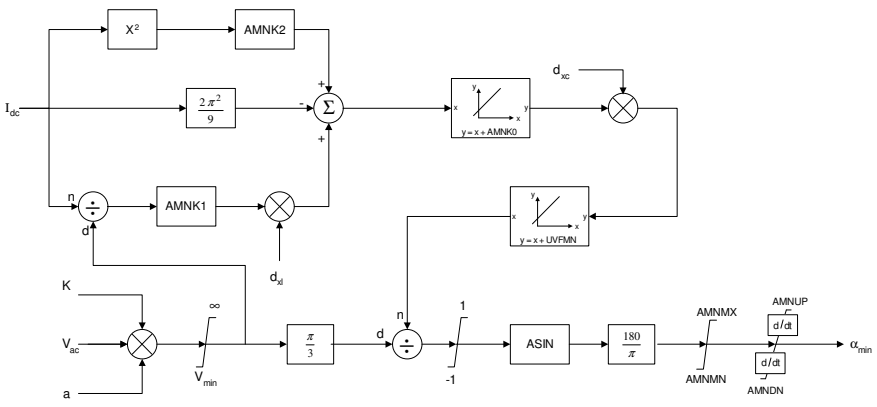

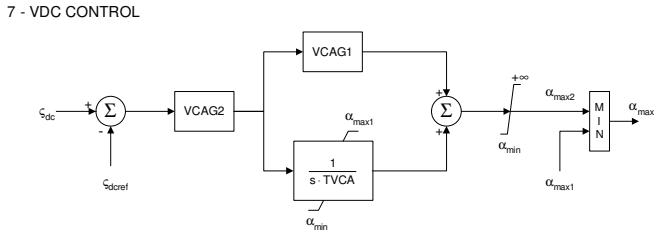


Figure H.4 – Rectifier CCC Controllers

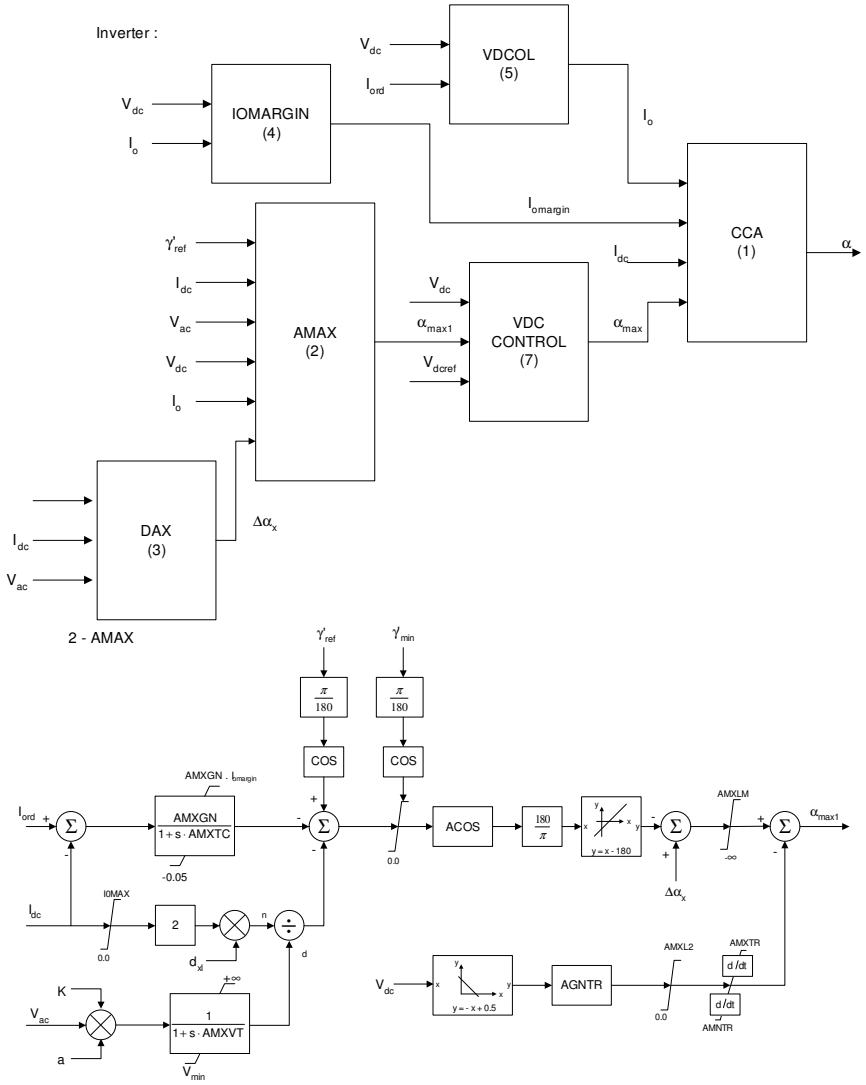

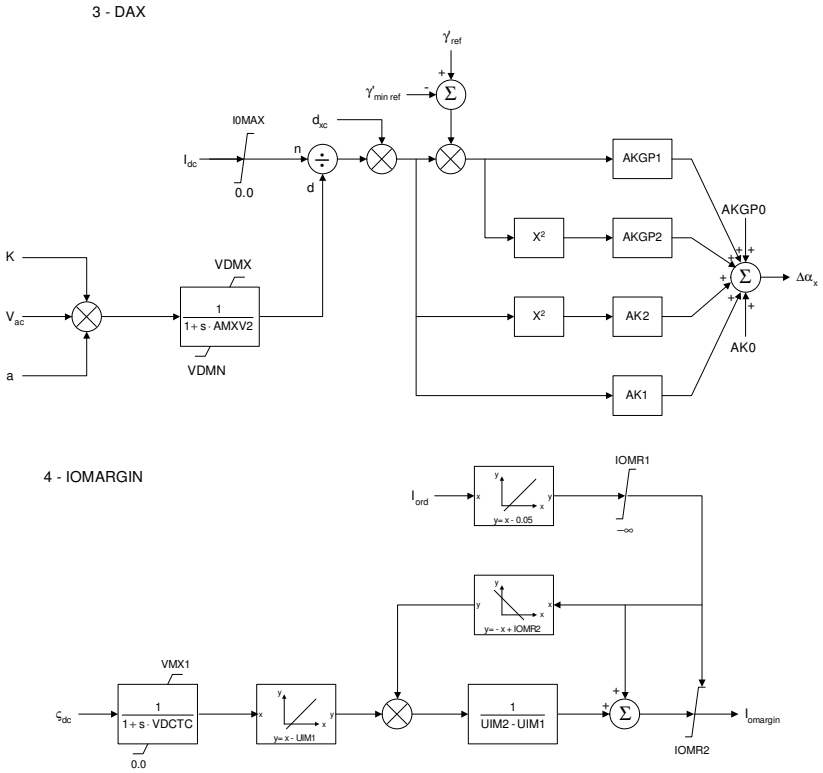


Figure H.5 – Inverter CCC Controllers

Table H.9 – CCC Controller Parameters

Rectifier

| | Parameter | Value | | Parameter | Value |
|---|---|---|---|---|---|
| CCA | ALFMX | 155. | Voltage Transient Detector | A | 0.001326 |
| | KICCA | 4000 | | A2 | 1.7590483e-6 |
| | KPCCA | 40 | | DAFMX | 70.0 |
| | Tmc | 0.001592 | Master Control | TM | 0.30 |
| VCO | TVCO | 0.00139 | | UMSMI | 0.950 |
| VDCOL | Tmv | 0.00531 | | UMSMA | 1.05 |
| | UDMIN | 0.2 | Asymmetrical Fault Detector | Tmvac | 0.005 |
| | UDMAX | 1.0 | | DAK1 | -127.7 |
| | TDWN1 | 0.01 | | DAK2 | 80.0 |
| | TUP1 | 0.075 | | DAMMN | -9.4 |
| | GVDCL | 1.5 | | DAMMX | 30. |
| | I0MIN | 0.3 | | | |
| | I0MAX | 1.2 | | | |
| | I0MN | 0.1 | | | |
| Minimum Firing Angle | CNVK | 1.0 | | | |
| | KI | 0.248 | | | |
| | VMIN | 0.5 | | | |
| | Tmud0 | 0.005 | | | |
| | Tamn | 0.02 | | | |
| | AMNMN | -9.4 | | | |
| | KU0 | -0.76 | | | |
| | KU1 | -21.971 | | | |
| | KU2 | 0.056 | | | |
| | TADWN | 0.05 | | | |
| | TAUP | 0.001 | | | |

Inverter

| | Parameter | Value | | Parameter | Value |
|---|---|---|---|---|---|
| CCA | ALFMN | 100. | Maximum Firing Angle | CNVK | 1.0 |
| | KICCA | 4000.0 | | VMIN | 0.25 |
| | KPCCA | 60.0 | | Tmud0 | 0.005 |
| | Tmc | 0.003184 | | Tamn | 0.005 |
| VCO | TVCO | 0.00139 | | AONMX | 170.25 |
| VDCOL | Tmv | 0.00531 | | AOFMX | 170.25 |
| | UDMIN | 0.2 | | KU0ON | 157. |
| | UDMAX | 1.1 | | KU1ON | 5.496 |
| | TDWN1 | 0.005 | | KU2ON | 3.672 |
| | TUP1 | 0.075 | | KU0OF | 162. |
| | GVDCL | 1.5 | | KU1OF | 3.422 |
| | I0MIN | 0.3 | | KU2OF | 4.828 |
| | I0MAX | 1.2 | Voltage Transient Detector | A | 0.001326 |
| | I0MN | 0.1 | | A2 | 1.7590483e-6 |
| Current Margin | Tdoff | 0.1 | | DAFMX | 70.0 |
| | IMRG1 | 0.1 | | DAMN1 | 110. |
| | IMRG2 | 0.2 | | DAMX1 | 180. |
| | Tmarg | 0.025 | | DAMN2 | 90. |
| | | | | DAMX2 | 200. |
| | | | | DAMN3 | 100. |

Table H.10 – *Simplified Network* Steady State Bus Data

| Bus | Type | Voltage | Pg [MW] | Qg [Mvar] | Pl[MW] | Ql[Mvar] | Shunt [Mvar] |
|---|---|---|---|---|---|---|---|
| 11 | PQ | - | - | - | 0.00 | 0.00 | 0.00 |
| 13 | Vθ | 0.995 | -1755 | 451.6 | 0.00 | 0.00 | 0.00 |
| 26 | PQ | - | - | - | 0.00 | 0.00 | 40.00 |
| 109 | PV | 1.095 | 485.0- | 84.13 | 0.00 | 0.00 | 0.00 |
| 111 | PQ | - | - | - | 0.00 | 0.00 | -50.00 |
| 112 | PQ | | | | | | -50.00 |
| 113 | PQ | | | | | | 180 |
| 112 | PQ | 1.095 | 1622 | 398.9 | | | |

Table H.11 – *Simplified Network* Steady State Line Data

| Bus From | Bus To | R (%) | X (%) | Shunt (Mvar) | Type |
|---|---|---|---|---|---|
| 11 | 13 | 0.3086 | 1.423 | 0.00 | Equivalent Circuit |
| 111 | 122 | 0.1298 | 1.635 | 0.00 | |
| 112 | 109 | 0.9078 | 3.912 | 0.00 | |
| 26 | 11 | 0.2824 | 3.750 | 364.60 | Transmission Lines |
| 26 | 11 | 0.2824 | 3.750 | 364.60 | |
| 112 | 111 | 0.1002 | 1.322 | 123.14 | |
| 112 | 113 | 0.158 | 2.100 | 200.00 | |

Table H.12 – Machines and Regulators Association

| Bus | Units Number | Machine Model | Voltage Regulator | Speed Governor | Power System Stabilizer |
|---|---|---|---|---|---|
| 13 | 30 | 5039 | 6039 | 740 | - |
| 109 | 10 | 5038 | 6138 | 745 | - |
| 122 | 44 | 5040 | 6141 | 150 | 8140 |

Table H.13 – Machine Model Data

| Model Number | Xd | Xq | X'd | X''d | Xl | T'd | T''d | T''q | H | MVA |
|---|---|---|---|---|---|---|---|---|---|---|
| 5038 | 87.850 | 56.610 | 24.510 | 19.860 | 10.350 | 7.590 | 0.070 | 0.170 | 4.071 | 333.000 |
| 5039 | 91.890 | 68.630 | 30.250 | 24.220 | 16.130 | 7.920 | 0.060 | 0.090 | 4.439 | 419.000 |
| 5040 | 116.800 | 64.380 | 33.040 | 27.370 | 13.220 | 8.520 | 0.045 | 0.072 | 3.530 | 186.200 |

**Voltage Regulator**
**6039**

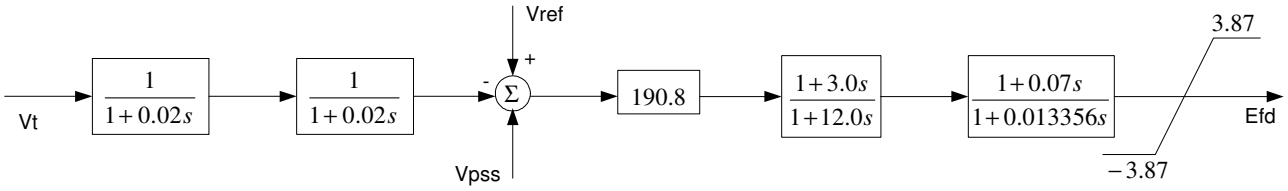

**Voltage Regulator 6038 and 6138**

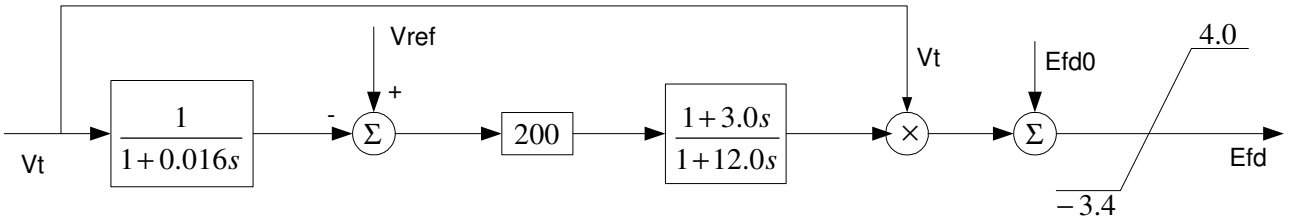


**Voltage Regulator 6141**

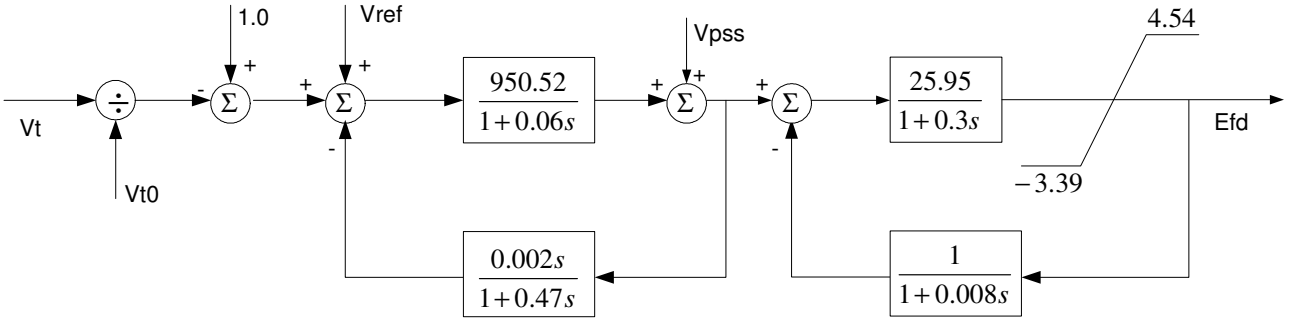


Figure H.6 – Voltage Regulators for the *Simplified Network*

Table H.14 – Voltage Regulator Parameters

AVR 6039

| Parameter | Value | Parameter | Value |
|---|---|---|---|
| Ka | 190.8 | T2 | 12.0 |
| Lmax | 3.87 | T3 | 0.07 |
| Lmin | -3.87 | T4 | 0.013356 |
| | | Ta | 3.0 |
| | | Tse | 0.02 |

AVR 6138

| Parameter | Value | Parameter | Value |
|---|---|---|---|
| A1 | 0.016 | VAmax | 4.0 |
| Ka | 200.0 | VAmin | -3.4 |
| Ke | 1.0 | | |
| Tse | 12.0 | | |
| us | 3.0 | | |

AVR 6141

| Parameter | Value | Parameter | Value |
|---|---|---|---|
| Ka | 950.52 | Tse | 0.47 |
| Ke | 25.95 | us | 0.002 |
| Ta | 0.06 | VAmax | 4.54 |
| Te | 0.3 | VAmin | -3.39 |
| Tq | 0.008 | | |

Speed Governor
740

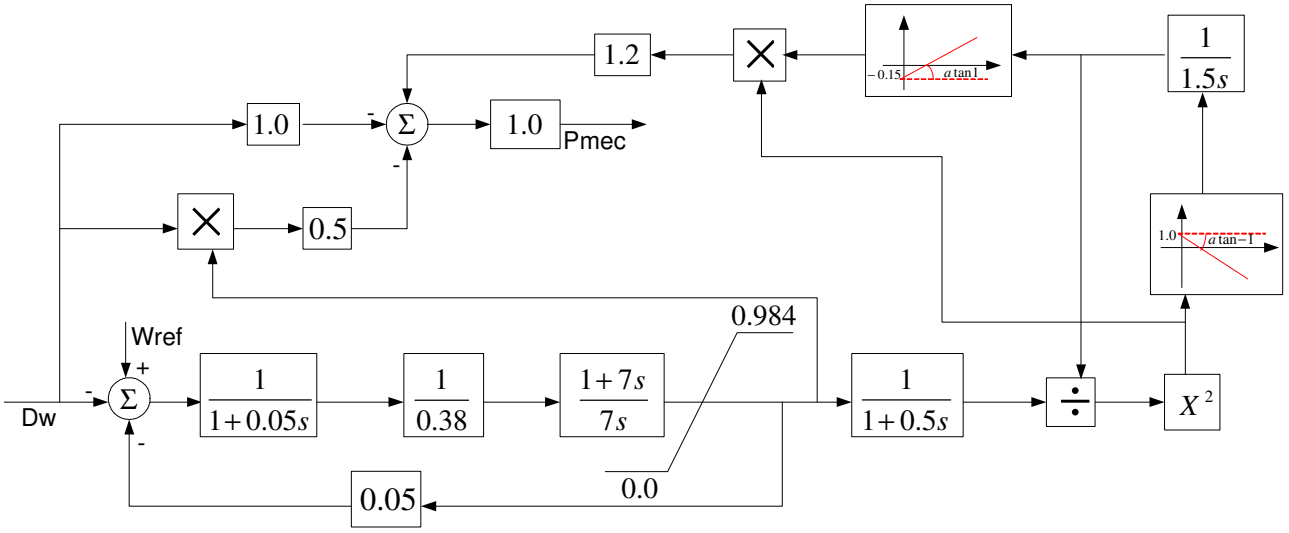


Speed Governors
744 and 745

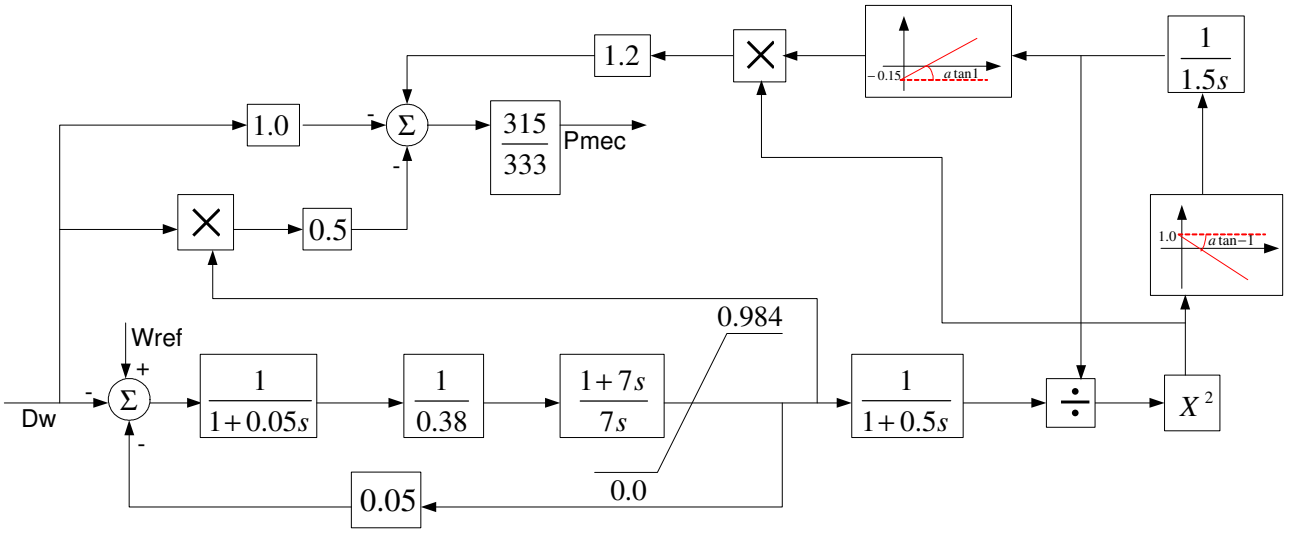

Speed Governors
149 and 150

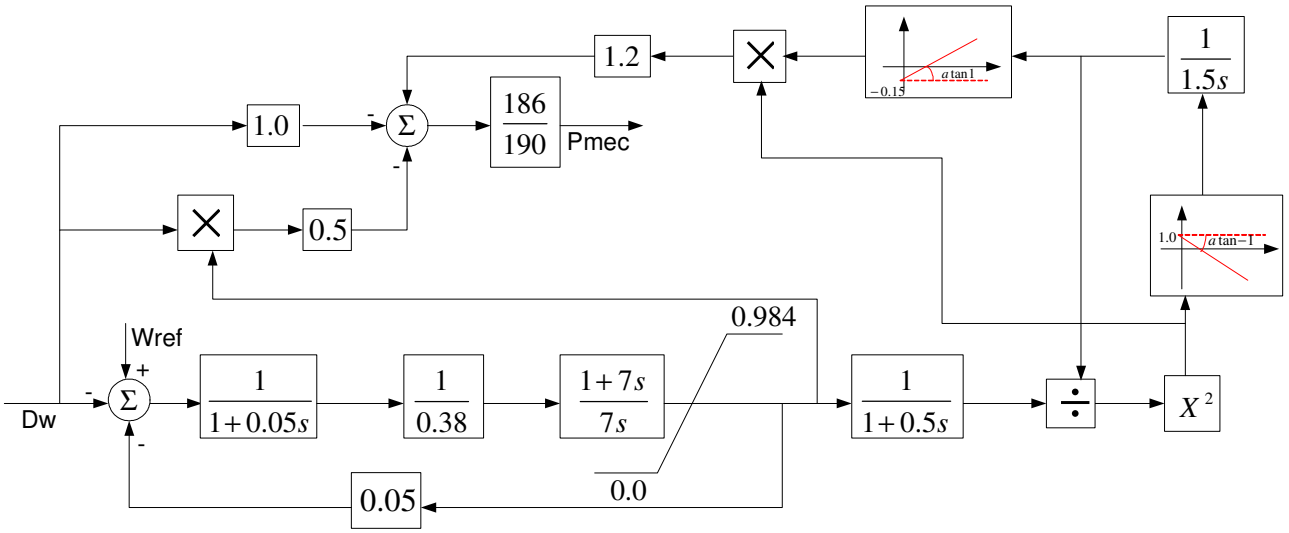


Speed Governor
740

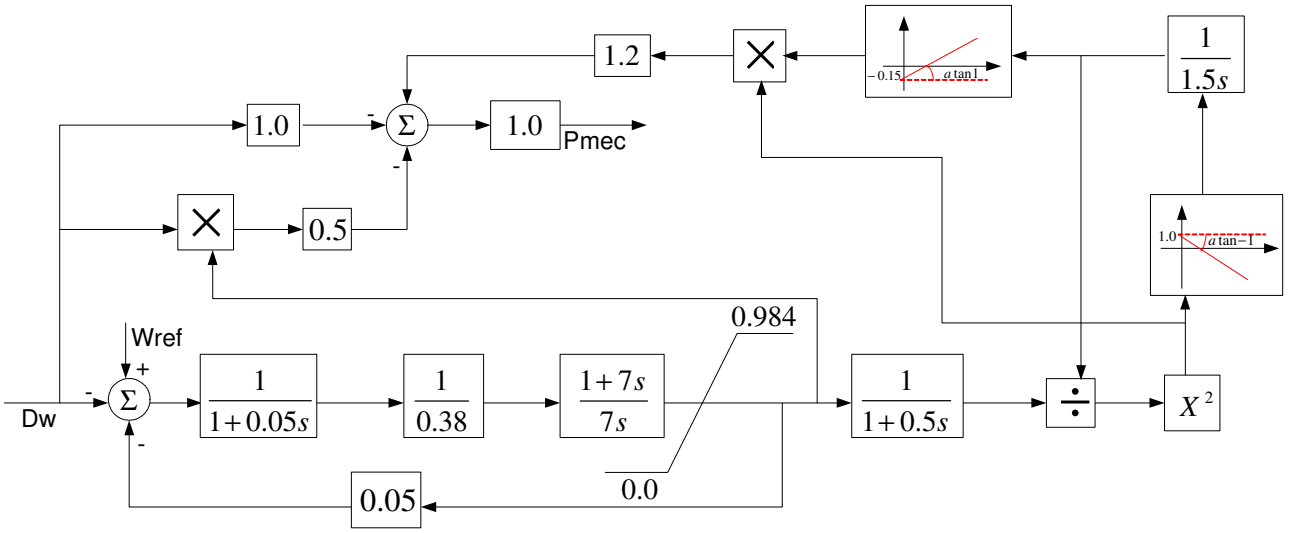

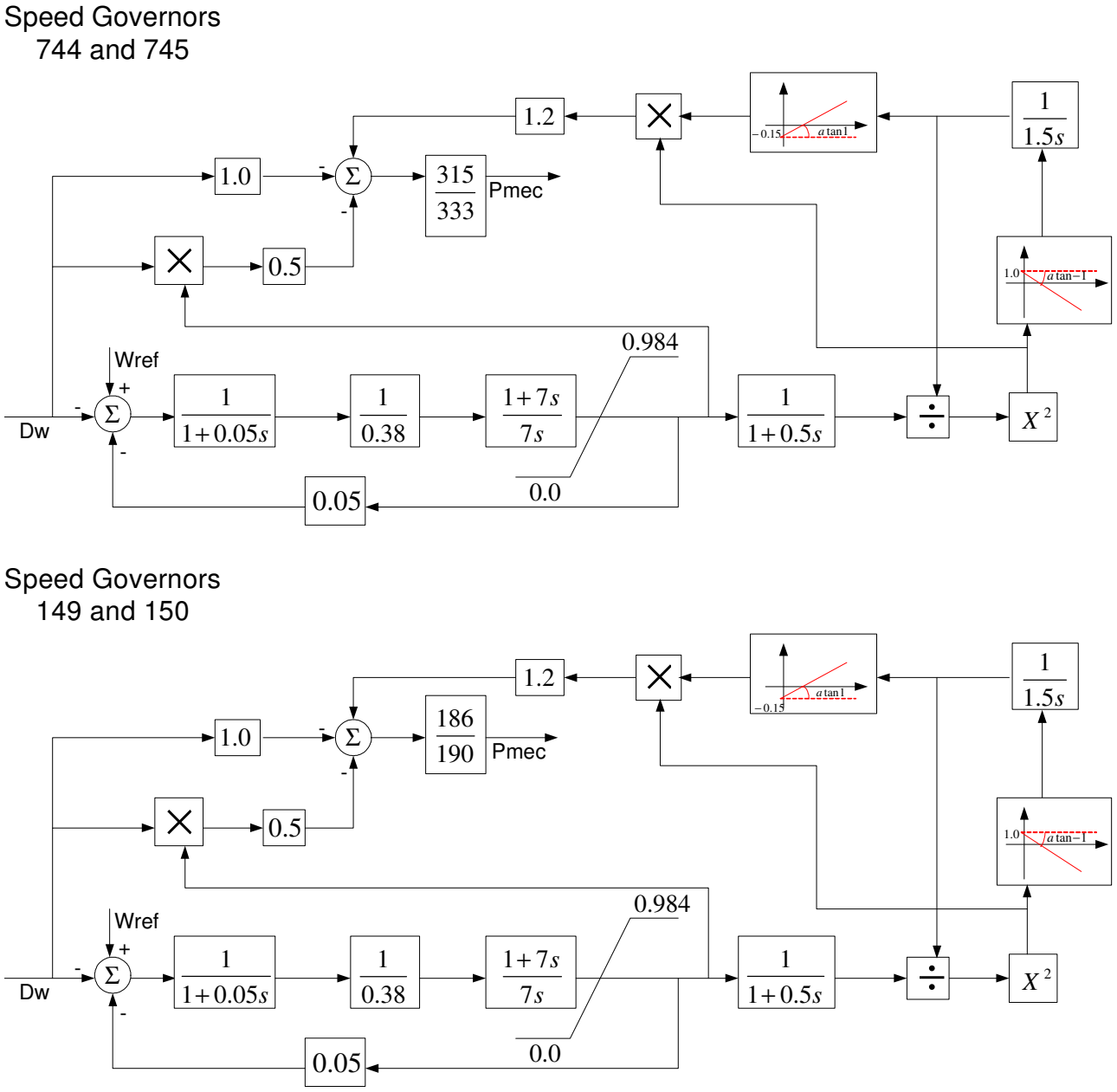


Figure H.7 – Speed Governors for the *Simplified Network*

Table H.15 – Speed Governors Parameters

SG 740

| Parameter | Value | Parameter | Value |
|---|---|---|---|
| At | 1.2 | Qnl | 0.15 |
| D | 1.0 | R | 0.05 |
| Dt | 0.5 | rp | 0.38 |
| Lmax | 0.984 | Tf | 0.05 |
| Lmin | 0.0 | Tg | 0.5 |
| PBmaq | 419. | Tr | 7.0 |
| PBtur | 419. | Tw | 1.5 |

SG 745

| Parameter | Value | Parameter | Value |
|---|---|---|---|
| At | 1.2 | Qnl | 0.15 |
| D | 1.0 | R | 0.05 |
| Dt | 0.5 | rp | 0.38 |
| Lmax | 0.984 | Tf | 0.05 |
| Lmin | 0.0 | Tg | 0.5 |
| PBmaq | 333. | Tr | 7.0 |
| PBtur | 315. | Tw | 1.5 |

SG 150

| Parameter | Value | Parameter | Value |
|---|---|---|---|
| At | 1.2 | Qnl | 0.15 |
| D | 1.0 | R | 0.05 |
| Dt | 0.5 | rp | 0.38 |
| Lmax | 0.984 | Tf | 0.05 |
| Lmin | 0.0 | Tg | 0.5 |
| PBmaq | 190. | Tr | 7.0 |
| PBtur | 186. | Tw | 1.5 |

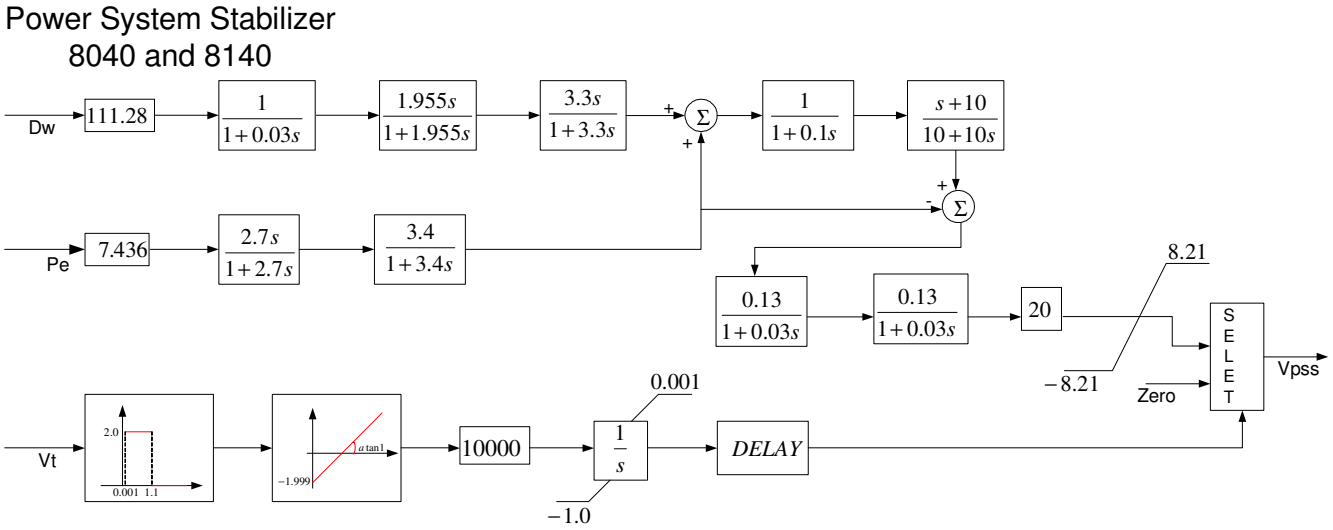


Figure H.8 – Power System Stabilizer for the *Simplified Network*

Table H.16 – Power System Stabilizer Parameters

| Parameter | Value | Parameter | Value |
|---|---|---|---|
| A1 | 111.28 | KI | 3.4 |
| A2 | 7.436 | Kp | 2.7 |
| A3 | 20.0 | Kq1 | 1.955 |
| A4 | 0.03 | Kq2 | 3.3 |
| A5 | 0.1 | W0 | 10.0 |
| Aex | 0.13 | W02 | 100. |
| B2 | 8.21 | | |
| B3 | -8.21 | | |
| Bex | 0.03 | | |

Table H.17 – DC Line Parameter

| Phase no. | Skin | Resis (ohm/mile) | IX | Diam (inch) | Horiz (feet) | VTower (feet) | VMid (feet) | Separ (inch) | Alpha (deg) | NB |
|---|---|---|---|---|---|---|---|---|---|---|
| 1 | 0.375 | 0.07340 | 4 | 1.3858 | +21. | 100. | 60. | 18. | 45 | 4 |
| 2 | 0.375 | 0.07340 | 4 | 1.3858 | -21. | 100. | 60. | 18. | 45 | 4 |
| 0 | 0.5 | 6.7020 | 4 | 0.374 | +12. | 130. | 90. | 0 | 0 | 1 |
| 0 | 0.5 | 6.7020 | 4 | 0.374 | -12. | 130. | 90. | 0 | 0 | 1 |

Phase no.: Phase number (0:ground wire)
Skin: skin effect flag
Resis: Conductor resistance at DC.
IX: self-inductance flag.
Diam: outside diameter of one conductor.
Horiz: Horizontal distance from the center of bundle to a user selectable reference line.
VTower: Vertical bundle height at tower.
VMid: Vertical bundle height at mid-span.
Separ: Distance between conductors in a bundle.
Alpha: Angular position of one of the conductors in a bundle, measured counter-clockwise from the horizontal line
NB: Number of conductors in a bundle

Table H.18 – AC Lines Parameter

| Phase no. | Skin | Resis (ohm/km) | IX | Diam (cm) | Horiz (m) | VTower (m) | VMid (m) | Separ (cm) | Alpha (deg) | NB |
|---|---|---|---|---|---|---|---|---|---|---|
| 1 | 0.333 | 0.0917 | 4 | 2.482 | -12.7 | 28.5 | 12.4 | 45. | 45. | 4 |
| 2 | 0.333 | 0.0917 | 4 | 2.482 | 0.0 | 28.5 | 12.4 | 45. | 45. | 4 |
| 3 | 0.333 | 0.0917 | 4 | 2.482 | +12.7 | 28.5 | 12.4 | 45. | 45. | 4 |
| 0 | 0.5 | 4.1889 | 4 | 0.914 | -11. | 37.5 | 23. | 0.0 | 0.0 | 1 |
| 0 | 0.5 | 4.1889 | 4 | 0.914 | +11. | 37.5 | 23. | 0.0 | 0.0 | 1 |

Table H.19 – AC Lines Length

| Bus from | Bus to | R (Ω/km) | X (Ω/km) | Mvar | Length (km) |
|---|---|---|---|---|---|
| 26 | 11 | 0.025214285 | 0.334821428 | 364.6 | 280. |
| 112 | 113 | 0.024687500 | 0.321250000 | 200.0 | 160. |
| 113 | 111 | 0.024482758 | 0.326847290 | 254.0 | 203. |
| 113 | 111 | 0.025050000 | 0.330500000 | 123.1 | 100. |

DC filters for 12th harmonic

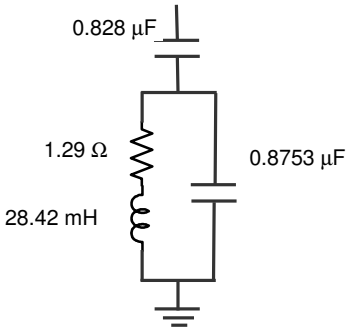


DC filter for 24th harmonic

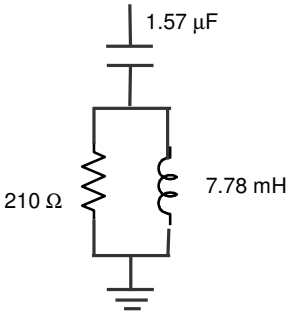


AC filter for 11th harmonic

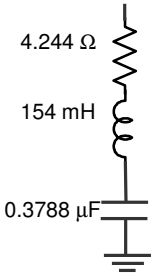


AC filter for 13th harmonic

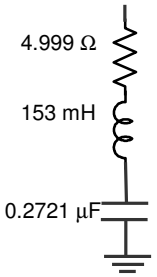


AC filter for 24th harmonic

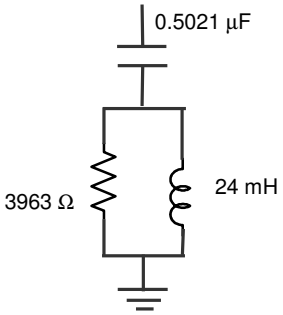


AC filter for 36th harmonic

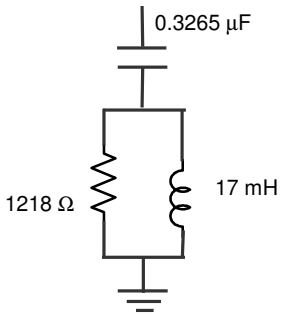


Figure H.9 - Structures and Parameters of Filters